ISSN 0021-9673

VOL. 683 NO. 2 OCTOBER 21, 1994

THIS ISSUE COMPLETES VOL. 683

JOURNAL OF CHROMATOGRAPHY A

INCLUDING ELECTROPHORESIS AND OTHER SEPARATION METHODS

ELSEVIER

JOURNAL OF CHROMATOGRAPHY A

INCLUDING ELECTROPHORESIS AND OTHER SEPARATION METHODS

Scope. The *Journal of Chromatography A* publishes papers on all aspects of **chromatography, electrophoresis** and related methods. Contributions consist mainly of research papers dealing with chromatographic theory, instrumental developments and their applications. In the *Symposium volumes*, which are under separate editorship, proceedings of symposia on chromatography, electrophoresis and related methods are published. *Journal of Chromatography B: Biomedical Applications* —This journal, which is under separate editorship, deals with the following aspects: developments in and applications of chromatographic and electrophoretic techniques related to clinical diagnosis or alterations during medical treatment; screening and profiling of body fluids or tissues related to the analysis of active substances and to metabolic disorders; drug level monitoring and pharmacokinetic studies; clinical toxicology; forensic medicine; veterinary medicine; occupational medicine; results from basic medical research with direct consequences in clinical practice.

Submission of Papers. The preferred medium of submission is on disk with accompanying manuscript (see *Electronic manuscripts* in the Instructions to Authors, which can be obtained from the publisher, Elsevier Science B.V., P.O. Box 330, 1000 AH Amsterdam, Netherlands). Manuscripts (in English; *four* copies are required) should be submitted to: Editorial Office of *Journal of Chromatography A*, P.O. Box 681, 1000 AR Amsterdam, Netherlands, Telefax (+31-20) 5862 304, or to: The Editor of *Journal of Chromatography B: Biomedical Applications*, P.O. Box 681, 1000 AR Amsterdam, Netherlands. Review articles are invited or proposed in writing to the Editors who welcome suggestions for subjects. An outline of the proposed review should first be forwarded to the Editors for preliminary discussion prior to preparation. Submission of an article is understood to imply that the article is original and unpublished and is not being considered for publication elsewhere. For copyright regulations, see below.

Publication information. *Journal of Chromatography A* (ISSN 0021-9673): for 1995 Vols. 683–714 are scheduled for publication. *Journal of Chromatography B: Biomedical Applications* (ISSN 0378-4347): for 1995 Vols. 663–674 are scheduled for publication. Subscription prices for *Journal of Chromatography A*, *Journal of Chromatography B: Biomedical Applications* or a combined subscription are available upon request from the publisher. Subscriptions are accepted on a prepaid basis only and are entered on a calendar year basis. Issues are sent by surface mail except to the following countries where air delivery via SAL is ensured: Argentina, Australia, Brazil, Canada, China, Hong Kong, India, Israel, Japan, Malaysia, Mexico, New Zealand, Pakistan, Singapore, South Africa, South Korea, Taiwan, Thailand, USA. For all other countries airmail rates are available upon request. Claims for missing issues must be made within six months of our publication (mailing) date. Please address all your requests regarding orders and subscription queries to: Elsevier Science B.V., Journal Department, P.O. Box 211, 1000 AE Amsterdam, Netherlands. Tel.: (+31-20) 5803 642; Fax: (+31-20) 5803 598. Customers in the USA and Canada wishing information on this and other Elsevier journals, please contact Journal Information Center, Elsevier Science Inc., 655 Avenue of the Americas, New York, NY 10010, USA, Tel. (+1-212) 633 3750, Telefax (+1-212) 633 3764.

Abstracts/Contents Lists published in Analytical Abstracts, Biochemical Abstracts, Biological Abstracts, Chemical Abstracts, Chemical Titles, Chromatography Abstracts, Current Awareness in Biological Sciences (CABS), Current Contents/Life Sciences, Current Contents/Physical, Chemical & Earth Sciences, Deep-Sea Research/Part B: Oceanographic Literature Review, Excerpta Medica, Index Medicus, Mass Spectrometry Bulletin, PASCAL-CNRS, Referativnyi Zhurnal, Research Alert and Science Citation Index.

US Mailing Notice. *Journal of Chromatography A* (ISSN 0021-9673) is published weekly (total 52 issues) by Elsevier Science B.V., (Sara Burgerhartstraat 25, P.O. Box 211, 1000 AE Amsterdam, Netherlands). Annual subscription price in the USA US$ 5389.00 (US$ price valid in North, Central and South America only) including air speed delivery. Second class postage paid at Jamaica, NY 11431. **USA POSTMASTERS**: Send address changes to *Journal of Chromatography A*, Publications Expediting, Inc., 200 Meacham Avenue, Elmont, NY 11003. Airfreight and mailing in the USA by Publications Expediting.

See inside back cover for Publication Schedule, Information for Authors and information on Advertisements.

0021-9673/94 $07.00

Printed in the Netherlands

VOL. 683, NO. 2 JOURNAL OF CHROMATOGRAPHY A OCTOBER 21, 1994

CONTENTS

(Abstracts/Contents Lists published in Analytical Abstracts, Biochemical Abstracts, Biological Abstracts, Chemical Abstracts, Chemical Titles, Chromatography Abstracts, Current Awareness in Biological Sciences (CABS), Current Contents/Life Sciences, Current Contents/Physical, Chemical & Earth Sciences, Deep-Sea Research/Part B: Oceanographic Literature Review, Excerpta Medica, Index Medicus, Mass Spectrometry Bulletin, PASCAL-CNRS, Referativnyi Zhurnal, Research Alert and Science Citation Index)

REGULAR PAPERS

Column Liquid Chromatography

Gas Chromatography

SHORT COMMUNICATIONS

Gas Chromatography

Supercritical Fluid Chromatography and Extraction

(Continued overleaf)

Contents (continued)

ELSEVIER

Journal of Chromatography A, 683 (1994) 279–291

JOURNAL OF CHROMATOGRAPHY A

Second-order kinetics in the liquid chromatographic reactor

Richard Thede[a], Detlef Haberland[a], Zengqun Deng[b], Stanley H. Langer[b,*]

[a]*Department of Chemistry, University of Greifswald, Soldtmannstrasse 23, D-17489 Greifswald, Germany*

[b]*Department of Chemical Engineering, University of Wisconsin, 1415 Johnson Drive, Madison, WI 53706-1691, USA*

First received 31 March 1994; revised manuscript received 31 May 1994

Abstract

Equations for the determination of second order rate constants with the pulse overlay method, based on the application of empirical peak shape equations are derived. This approach was then applied in an experimental study of the rection of pyridine with tetrachloroterephthaloyl chloride in a reversed-phase HPLC system. Rate constants evaluated from reaction chromatograms were found to be in good agreement with those obtained earlier for this reaction by Chu and Langer in chromatographic reactor experiments under pseudo-first order conditions.

1. Introduction

Chromatographic reactors can provide a number of advantages for carrying out and studying chemical reactions [1–5]. The determination of rate constants through analysis of typical reaction chromatograms from chemical reactions in chromatographic columns has been described by many workers over the last three decades for gas chromatographic systems and, more recently, for liquid chromatographic systems. A number of reviews and references to other reviews on these subjects are available [1–5]. However, almost all the published applications and theoretical work have been devoted to first-order or pseudo-first-order reactions which were either reversible or irreversible.

Up to the end of the last decade there were only two papers [6,7] describing second-order reaction studies on gas chromatographic columns; in both instances numerical evaluations of the rate constant were used. More recently, the concept of the "extended ideal chromatographic reactor (EICR)" [8,9] was proposed and applied to second-order reactions on gas chromatographic columns, simplifying the calculations for obtaining rate constants to a considerable extent. For the EICR development the following assumptions are used: (1) isothermal column, negligible temperature and pressure gradients neglected, (2) linear sorption isotherms, (3) rate of mass transfer does not limit the chemical reaction, (4) the reactant peak shape is a Gaussian function, (5) the first absolute moment and the second central moment depend linearly on the local coordinate.

Assumptions 1–3 coincide with those of the "ideal chromatographic reactor" model introduced by Langer and co-workers [4,5]. Assumptions 4 and 5 which extend this model with respect to peak shape and peak spreading are necessary for treating second-order reactions.

The EICR model, however, has the character of an "ad hoc hypothesis", and it was somewhat

* Corresponding author.

0021-9673/94/$07.00
SSDI 0021-9673(94)00512-8

unclear, how it might fit within the framework of the original balance equations of the chromatographic reactor. The purpose of this work is to explore the connection between these models and, moreover, to report some results from an initial experimental investigation of a second-order reaction in a liquid chromatographic reactor.

2. Mathematical modeling

2.1. Balance equations

We can start the theoretical treatment with the balance equations of isothermal linear chromatographic systems, which are commonly considered sufficient [10] for modeling the chromatographic process, and extend them with general reaction terms. (More sophisticated models which have been discussed, i.e. [11], are more suitable for the elucidation of partition kinetics than for our purposes.)

For concentration in the mobile (m) phase:

$$D_i \cdot \frac{\partial^2 c_i}{\partial x^2} - \frac{\partial c_i u}{\partial x} - k_{fi} q_i c_i + k_{fi} a_{si} + r_{mi} = \frac{\partial c_i}{\partial t} \tag{1a}$$

For concentration in the stationary (s) phase:

$$k_{fi} q_i c_i - k_{fi} a_{si} + r_{si} = \frac{\partial a_{si}}{\partial t} \tag{1b}$$

These balance equations can be simplified further by neglecting diffusional effects (which is justified for liquid chromatography in general and for gas chromatography with adequate flow-rates) and addressing situations where mass transfer rates do not limit reaction kinetics. Then,

$$-\frac{\partial c_i u}{\partial x} - k_{fi} q_i c_i + k_{fi} a_{si} - r_i = \frac{\partial c_i}{\partial t} \tag{2a}$$

$$k_{fi} q_i c_i - k_{fi} a_{si} = \frac{\partial a_{si}}{\partial t} \tag{2b}$$

The "lumped" reaction term r_i is the sum of the reaction terms r_{mi} and r_{si} considering the effective phase volume ratios of the mobile phase and the stationary phase with the kinetic time variable. The latter can be the void time or the reactant retention time or, where more than one reactant is involved, each of the reactant retention times. With first-order reactions the retention time of the reactant is generally used. For second-order reactions we can reference with respect to the void time, since then results can be interrelated where more than one reactant with different retentions are involved. The general reaction term, r_i, is then

$$r_i = \sum_{j=1}^{m} \nu_{ij} k_{aj} \prod_{i=1}^{l} c_i^{\alpha_{ij}} \tag{3}$$

with the apparent rate constant of the jth reaction:

$$k_{aj} = k_{mj} + \frac{V_s}{V_m} \cdot k_{sj} \prod_{i=1}^{l} K_i^{\alpha_{ij}} \tag{4}$$

Now, the partial differential equation system (2) can be transformed into a system of ordinary differential equations of the statistical moments of the reactants through multiplication of the whole system (2) by t^0 for the zeroth moment, t^1 for the first moment, t^2 for the second moment and so on, followed by integrating the system over time from zero to infinity. Using the defining equations for the moments, a tedious but straightforward rearrangement leads to the following set of ordinary differential equations for the zeroth absolute and the first four moments:

$$\left.\begin{aligned}
&-u \cdot \frac{\mathrm{d} \ln \bar{m}_{0i}}{\mathrm{d}x} = m_{R0i} \\
&-u \cdot \frac{\mathrm{d}\mu_{1i}}{\mathrm{d}x} + (q_i + 1) = u \cdot \frac{\mathrm{d} \ln \bar{m}_{0i}}{\mathrm{d}x} \cdot (\mu_{1i} - \mu_{R1i}) \\
&-u \cdot \frac{\mathrm{d}\mu_{2i}}{\mathrm{d}x} + 2\left[\mu_{1i}(q_i + 1) + \frac{q_i}{k_{fi}}\right] \\
&\quad = u \cdot \frac{\mathrm{d} \ln \bar{m}_{0i}}{\mathrm{d}x} \cdot (\mu_{2i} - \mu_{R2i}) \\
&-u \cdot \frac{\mathrm{d}\mu_{3i}}{\mathrm{d}x} + 3\left[\mu_{2i}(q_i + 1) + 2 \cdot \frac{q_i \mu_{1i}}{k_{fi}} + 2 \cdot \frac{q_i}{k_{fi}^2}\right] \\
&\quad = \frac{\mathrm{d} \ln \bar{m}_{0i}}{\mathrm{d}x} \cdot (\mu_{3i} - \mu_{R3i}) \\
&-u \cdot \frac{\mathrm{d}\mu_{4i}}{\mathrm{d}x}
\end{aligned}\right\} \tag{5}$$

$$+4\left[\mu_{3i}(q_i+1)+3\cdot\frac{q_i\mu_{2i}}{k_{fi}}+6\cdot\frac{q_i\mu_{1i}}{k_{fi}^2}+6\cdot\frac{q_i}{k_{fi}^3}\right]$$

$$=u\cdot\frac{\mathrm{d}\ln\bar{m}_{0i}}{\mathrm{d}x}\cdot(\mu_{4i}-\mu_{R4i})$$

An arbitrary formulation for any moment is found to be:

$$-u\cdot\frac{\mathrm{d}\mu_{ni}}{\mathrm{d}x}+n\left[\mu_{(n-1)i}(q_i+1)+\sum_{j=2}^{n}\frac{(n-1)!}{(j-2)!}\frac{q_i\mu_{(j-2)i}}{k_{fi}^{n+1-j}}\right]=u\cdot\frac{\mathrm{d}\ln\bar{m}_{0i}}{\mathrm{d}x}\cdot(\mu_{ni}-\mu_{Rni}) \quad (6)$$

It can be noted that the derivation of Eq. 5 does not require the introduction of any simplifications. Furthermore, in these formulae the linear flow-rate, u, is still a function of the local coordinate, x. Therefore, a zeroth moment was introduced, which is related to the average flow-rate in a chromatographic column. For a gas chromatographic column the flow-rate, u, is usually obtained from the relation

$$u=\frac{l}{t_0}\cdot\frac{p^3-1}{p^2-1}\cdot\frac{1}{\sqrt{p^2-(p^2-1)\frac{x}{l}}} \quad (7)$$

For a liquid chromatographic system, however, with negligible mobile phase compressibility and constant linear flow-rate, the zeroth moment itself can be used.

2.2. Introduction of empirical peak shape equations

Eq. 5 contains terms of the form, μ_{Rni}, designated as "moments of reaction". Those are abbreviations of the following:

$$\mu_{Rni}=\frac{\int_0^\infty r_i t^n\,\mathrm{d}t}{\int_0^\infty r_i\,\mathrm{d}t} \quad (8)$$

For irreversible reactions following simple power law kinetics, Eq. 8 in terms of concentrations becomes

$$\mu_{R_{ni}}=\frac{\int_0^\infty t^n\prod_{i=1}^{l}c_i^{\alpha_i}\,\mathrm{d}t}{\int_0^\infty\prod_{i=1}^{l}c_i^{\alpha_i}\,\mathrm{d}t} \quad (9)$$

Furthermore, these concentrations can be expressed in terms of a product of concentration–time (peak-) areas and distribution density (peak shape) functions:

$$c_i=m_{0i}\Psi_i \quad (10)$$

For such irreversible reactions, the moments of the reactions are the moments of the reaction order power of the peak shape functions:

$$\mu_{Rni}=\frac{\int_0^\infty t^n\prod_{i=1}^{l}\Psi_i^{\alpha_i}\,\mathrm{d}t}{\int_0^\infty\prod_{i=1}^{l}\Psi_i^{\alpha_i}\,\mathrm{d}t} \quad (11)$$

For first-order reactions, it can be seen that there is no difference between the moments of reaction and the common moments. Therefore, the differences in Eq. 5 become zero to give a linear differential equation system. However, to evaluate the reaction moments for a second order reaction the peak shapes which are solutions of Eq. 2 appear to be necessary. Fortunately there are empirical and plausible peak shape functions, which might be used in place of the unknown solutions. Of these, the Gaussian function is the simplest and most frequently encountered.

2.3. Reaction Type, $2A_1 \rightarrow P$

For simplicity, a dimerization reaction can be considered first. For this reaction type we examine besides the Gaussian, the EMG function [12], the Gram–Charlier series (GCS) [13] and the GEX function [14] as well. (Function representations are given in the list of symbols.)

Analytical solutions are available for GCS and for the Gaussian, of course, with the framework of Eq. 11. They are presented here in terms of central moments, beginning with the second, because of simpler formulations. (Any set of

central moments can be converted into a set of absolute moments and vice versa.)

For the Gaussian function (with only one reactant, the index i can be omitted):

$$\left.\begin{aligned} m_{R0} &= \frac{m_0^2}{2\sqrt{\pi\mu_2'}} \\ \mu_{R1} &= \mu_1 \\ \mu_{R2}' &= \frac{\mu_2'}{2} \\ \mu_{R3}' &= 0 \\ \mu_{R4}' &= \frac{3}{4}\cdot\mu_2'^2 \end{aligned}\right\} \qquad (12)$$

For the GCS (Note that the μ_{Rn}' are central moments over μ_1, not over μ_{R1}):

$$\left.\begin{aligned} m_{R0} &= \frac{m_0}{2\sqrt{\pi\mu_2'}}\left[1+\frac{5S^2}{96}+\frac{E}{16}+\frac{35E^2}{3072}\right] \\ \mu_{R1} &= \mu_1 + \frac{\frac{5ES}{384}-\frac{S}{4}}{\frac{35E^2}{3072}+\frac{E}{16}+\frac{5S^2}{96}+1} \\ \mu_{R2}' &= \frac{\mu_2'}{2}\left[\frac{\frac{25E^2}{1024}-\frac{3E}{16}+\frac{11S^2}{96}+1}{\frac{35E^2}{3072}+\frac{E}{16}+\frac{5S^2}{96}+1}\right] \\ \mu_{R3}' &= \frac{\frac{11ES}{256}-\frac{S}{8}}{\frac{35E^2}{3072}+\frac{E}{16}+\frac{5S^2}{96}+1} \\ \mu_{R4}' &= \frac{3\mu_2^2}{4}\cdot\left[\frac{1+\frac{163E^2}{3072}-\frac{13E}{48}+\frac{25S^2}{96}+1}{\frac{35E^2}{3072}+\frac{E}{16}+\frac{5S^2}{96}+1}\right] \end{aligned}\right\} \qquad (13)$$

The other peak shape equations apparently do not permit an analytical solution with respect to Eq. 11. However, the possibility of fitting a linear regression model to the numerical results of Eq. 11 remains. Using the Gaussian shape as an ideal model, the differences between the moments of the reaction for the Gaussian and for the other peak shape equations can be considered:

$$\left.\begin{aligned} F_0(\mu_{R0}, \mu_i, \mu_2') &= \frac{2\sqrt{\pi\mu_2'}m_{R0}}{m_0^2} - 1 \\ F_1(\mu_{R1}, \mu_i, \mu_2') &= \frac{\mu_{R1}-\mu_1}{\sqrt{\mu_2'}} \\ F_3(\mu_{R3}, \mu_i, \mu_2') &= \frac{\mu_{R3}'}{\sqrt{\mu_2'^3}} \\ F_4(\mu_{R4}, \mu_i, \mu_2') &= \frac{4\mu_{R4}'}{3\mu_2'^2} - 1 \end{aligned}\right\} \qquad (14)$$

Using results from Eq. 12 in the equations above it can be seen that all F_i values become zero for Gaussian shapes. To match the deviations of the other functions from the Gaussian the following regression model can be used:

$$F_i(\mu_{Ri}, \mu_i, \mu_2') = a_{1i}S + a_{2i}E + a_{3i}S^2 + a_{4i}E^2 + a_{5i}SE \qquad (15)$$

Results from those regressions are summarized in Table 1. Eq. 5 was solved using a fourth-order Runge–Kutta method. All of the empirical peak shape equations give fairly similar plots when this is done for moments vs. the local coordinate (see Fig. 1). Table 2 shows that the results for the GCS are in increasing accord with the solution of Eq. 2 by an explicit finite difference method as the number of grid points in the length coordinate increases.

Table 3 illustrates some results for a com-

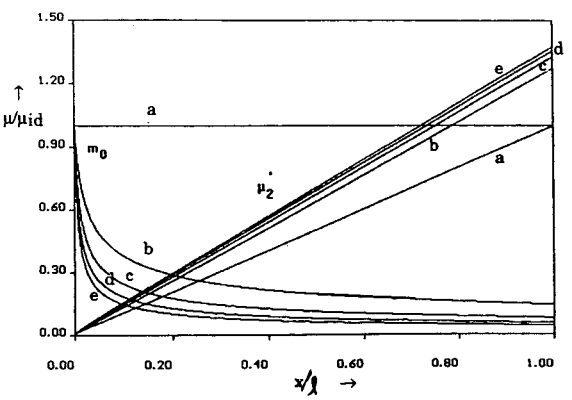

Fig. 1. Increase of the second central moment of the reactant with increasing conversion (reduced moments referenced to values without reaction) and advancement through the column. Conversions: a = 0%; b = 85%; c = 90%; d = 93%; e = 96%.

Table 1
Coefficients for deviations from Gaussian function for empirical peak shape equations calculated from Eq. 15

F (EMG)	a_1	a_2	a_3	a_4	a_5
m_0	0.0387	0	0.0952	0	0
μ_1	−0.137	0	−0.0851	0	0
μ_2	−0.209	0	−0.0169	0	0
μ_3	0.0957	0	0.0897	0	0
F (GEX)	a_1	a_2	a_3	a_4	a_5
m_0	0	0.0444	0.0745	−0.0138	0
μ_1	−0.291	−0.0457	0.0703	0	0.0630
μ_2	0.0291	−0.246	0.147	0.193	0.114
μ_3	0.315	0.0922	−0.136	−0.0827	−0.186
μ_4	0	−0.395	0.565	0.264	0.298

Table 2
Comparison between the moments obtained from Eq. 11 with the GCS function and the results from a finite difference solution (FD) of Eq. 3 with increasing grid points ($q = 1$, $k_a = 1$, $m_0(0) = 1$, $k_f = 100$, $\mu_2'(0) = 0.001$, $x = 1$)

Number of points in x-direction	$\frac{m_0(\text{GCS})}{m_0(\text{FD})}$	$\frac{\mu_1(\text{GCS})}{\mu_1(\text{FD})}$	$\frac{\mu_2(\text{CS})}{\mu_2(\text{FD})}$	$\frac{\mu_3(\text{GCS})}{\mu_3(\text{FD})}$	$\frac{\mu_4(\text{GCS})}{\mu_4(\text{FD})}$
100	0.812	1.00	0.550	0.219	0.304
500	0.951	1.00	0.867	0.661	0.801
1000	0.977	1.00	0.936	0.830	0.914
7500	0.998	1	0.9997	0.963	0.975

parison between the empirical peak shape equations. The EMG function deviates most from results with the others. Results from use of the GEX function do not differ much from those using the GCS function. Therefore, from those considered here the GCS function is the next best approximation relative to the Gaussian.

The following conclusions results from this numerical investigation:

(1) The first absolute moment does not depend significantly on conversion.

(2) The second central moment increases with conversion, however its linear dependence on the locale coordinate is maintained.

(3) The deviation of the fourth central moment, or in other words of the excess, has the largest influence on non-ideal deviations with conversion.

Table 3
Comparison between the moments from the GCS and the other empirical functions using Eq. 11 (parameters: see Table 2, GAU = Gaussian)

Peak shape function (PSF)	$\frac{m_0(\text{GCS})}{m_0(\text{PSF})}$	$\frac{\mu_1(\text{GCS})}{\mu_1(\text{PSF})}$	$\frac{\mu_2(\text{GCS})}{\mu_2(\text{PSF})}$	$\frac{\mu_3(\text{GCS})}{\mu_3(\text{PSF})}$	$\frac{\mu_4(\text{GCS})}{\mu_4(\text{PSF})}$
GAU	1.001	1.004	0.986	–	–
EMG	1.007	1.001	0.971	0.848	–
GEX	1.003	1.0	0.996	0.978	1.005

The first conclusion above enables us now to derive the equations of the EICR from Eq. 5, i.e. from the balance equations, since in this case it becomes possible to rewrite Eq. 5 to yield:

$$\left.\begin{aligned}
&-\frac{1}{u}\cdot m_{R0}=\frac{d\ln m_0}{dx}\\
&\frac{d\Delta\mu_1}{dx}=0\\
&\frac{d\Delta\mu_2'}{dx}=\frac{d\ln m_0}{dx}\cdot(\mu_{R2}'-\mu_2')\\
&\frac{d\Delta\mu_3'}{dx}=\frac{d\ln m_0}{dx}\cdot(\mu_{R3}'-\mu_3')\\
&\frac{d\Delta\mu_z'}{dx}+6\mu_2'\cdot\frac{d\Delta\mu_2'}{dx}=\frac{d\ln m_0}{dx}\cdot(\mu_{R4}'-\mu_4')
\end{aligned}\right\}\quad(16)$$

The first three equations of Eq. 16 —together with the Gaussian assumption for the peak shape equation— are the very equations of the EICR, and for the case of a Gaussian model the other equations become non-relevant. The solution for this situation was presented in [15].

For the zeroth moment we find:

$$\frac{1}{m_0}=\frac{1}{m_0(0)}+\frac{2k_at_0}{\sqrt{\pi\mu_2'}}\quad(17)$$

We can also find an equation for the zeroth moment using the GCS model, the first equation of the system (5), and a linear dependence of the second central moment on the local coordinate. However, the use of the GCS model results in realistic chromatographic peaks only in a limited range, for the skew and for the excess. If the second central moment of the injected peak becomes very small, as assumed for the EICR, the skew and the excess produced by Eq. 2 become very large. Therefore, the introduction of the GCS model as the "next best approximation" to the real chromatographic peak demands well defined initial conditions. Fortunately, the availability of injection valves with a well defined geometry with liquid chromatography makes this problem less challenging than with gas chromatography.

2.4. *Reactions of the type, $A_1 + A_2 \rightarrow P$*

This reaction type is at first glance considerable more complicated, since one has to deal with the moments of both reactants and the distance between them in space and in time, since in most instances the chromatographic process will give separation because of the differences in the rate of travel of these peaks through the column. Thus, no simple regression model could be found, and the theoretical investigation of peak shape equations had to be confined to these cases of analytical solution of Eq. 11 where Gaussian and GCS peak shapes were involved. The analytical solutions of the moments of the reaction with the GCS could only be obtained in a compact form using the following terms:

$$\left.\begin{aligned}
&\int_0^\infty \Psi_1\Psi_2 t^n\,dt\\
&\quad=\int_{-\infty}^{\infty}\frac{1}{\sqrt{2\pi(\mu_{21}'+\mu_{22}')}}\cdot e^{-\frac{(\mu_{11}-\mu_{12})^2}{2(\mu_{21}'+\mu_{22}')}}\\
&\quad\cdot\frac{1}{\sqrt{2\pi}\sigma_0}\cdot e^{-\frac{1}{2}\frac{\xi^2}{\sigma_0^2}}f_1(\xi-\mu)\cdot f_2\left(\frac{\xi+\sigma^2\mu}{\sigma}\right)\\
&\quad\cdot\sqrt{\mu_{21}'^n}\xi^n\,d\xi\\
&\sigma^2=\frac{\mu_{22}'}{\mu_{21}'}\\
&\mu=\frac{\mu_{id}-\mu_{11}}{\sqrt{\mu_{21}'}}\\
&\mu_{id}=\frac{\mu_{22}'\mu_{11}+\mu_{12}'\mu_{21}}{\mu_{21}'+\mu_{22}'}\\
&\sigma_0^2=\left(\frac{\mu_{21}'\mu_{22}'}{\mu_{21}'+\mu_{22}'}\right)\cdot\frac{1}{\mu_{21}'}\\
&f_i(z)=\frac{S_i}{6}(z^3-3z)+\frac{E_i}{24}\cdot(z^4-6z^2+3)
\end{aligned}\right\}\quad(18)$$

Since these solutions require several pages they are not presented here. Now, we are again able to apply the Runge–Kutta method to the solution of system 11 and thereby investigate the moments as functions of the local coordinate.

As illustrated in Figs. 2 and 3 the use of GCS as the "next best approximation" relative to a Gaussian model results in a considerable deviation from the linear dependence of the second central moment on the local coordinate starting at conversions close to 50%. The initial conditions are of less importance for reaction type, since reaction can be initiated deeper into the

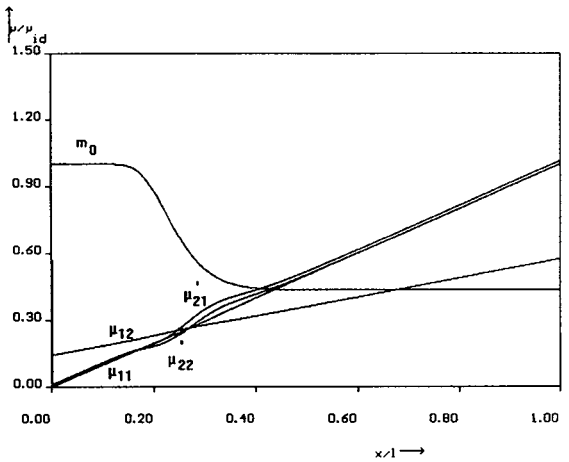

Fig. 2. Slight non-linearity in the second central moments in the case of a pulse overlay reaction with ca. 60% conversion (stoichiometric case, reduced moments referenced to values without reaction).

column, where well defined peak shapes are formed as a result of the chromatographic process with unreacted materials.

As shown before [16] for a linear dependence of the second central moments on the local coordinate, the following equations for the zeroth moment can be derived:

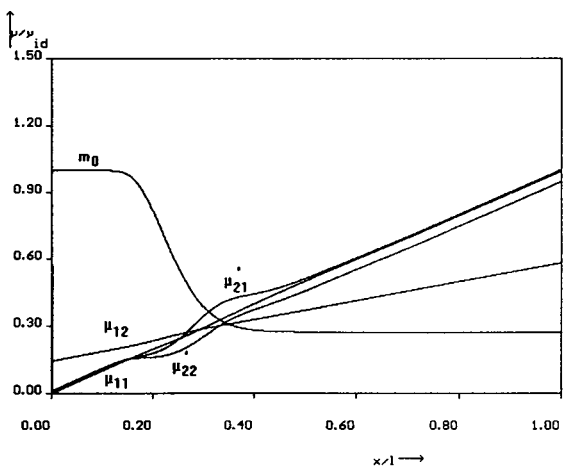

Fig. 3. Strong deviation from linearity in the second central moments in the case of a pulse overlay reaction with ca. 80% conversion (stoichiometric case, reduced moments referenced to values without reaction).

Non-stoichiometric case:

$$\ln\left(\frac{m_{01}}{m_{02}}\right) = \ln\left(\frac{m_{01}(0)}{m_{02}(0)}\right) + (m_{01}(0) - m_{02}(0))k_a t_0 \cdot \int_0^1 \frac{1}{\sqrt{2\pi(\mu'_{21} + \mu'_{22})}} \cdot \exp - \frac{(\mu_{11} - \mu_{12})^2}{2(\mu'_{21} + \mu'_{22})} \cdot \mathrm{d}\frac{x}{l} \tag{19}$$

Stoichiometric case:

$$\frac{1}{m_{01}} = \frac{1}{m_{01}}(0) + k_a t_0 \cdot \int_0^1 \frac{1}{\sqrt{2\pi(\mu'_{21} + \mu'_{22})}} \cdot \exp - \frac{(\mu_{11} - \mu_{12})^2}{2(\mu'_{21} + \mu'_{22})} \cdot \mathrm{d}\frac{x}{l} \tag{20}$$

The integral appearing in Eqs. 19 and 20 can be separated in the following way:

$$\left.\begin{aligned} &\int_0^1 \frac{1}{\sqrt{2\pi(\mu'_{21} + \mu'_{22})}} \cdot \exp - \frac{(\mu_{11} - \mu_{12})^2}{2(\mu'_{21} + \mu'_{22})} \cdot \mathrm{d}\frac{x}{l} \\ &= \frac{1}{\sqrt{(\mu_{11}(l) - \mu_{12}(l))^2}} \\ &\cdot \int_{-\infty}^{1-\Delta t' \cdot \sqrt{\frac{(\mu_{11}(l)+\mu_{12}(l))^2}{\mu'_{21}(l)+\mu'_{22}(l)}}} \frac{1}{\sqrt{(2\pi)}} \cdot \mathrm{e}^{-\frac{\xi^2}{2}} \mathrm{d}\xi \\ &+ \frac{1}{2} \cdot \int_0^1 \frac{1}{\sqrt{2\pi(\mu'_{21}(l) + \mu'_{22}(l))}} \cdot \frac{x - \Delta t'}{x} \\ &\cdot \mathrm{e}^{-\frac{(\mu_{11}(l)-\mu_{12}(l))^2}{\mu'_{21}(l)+\mu'_{22}(l)} \frac{(x-\Delta t')^2}{2x}} \mathrm{d}\frac{x}{l} \end{aligned}\right\} \tag{21}$$

where

$$\Delta t' = \frac{\Delta t}{|\mu_{11}(l) - \mu_{12}(l)|}$$

In those situations where the faster peak completely overtakes the slower one in the column, the first integral in Eq. 21 obviously will become unity and the second approach zero. Therefore, fairly simple equations become available for the zeroth moment:

Non-stoichiometric case:

$$\ln\left(\frac{m_{01}}{m_{02}}\right) = \ln\left(\frac{m_{01}(0)}{m_{02}(0)}\right) + (m_{01}(0) - m_{02}(0))k_a \cdot \frac{t_0}{|\mu_{11} - \mu_{12}|} \tag{22}$$

Stoichiometric case:

$$\frac{1}{m_{01}} = \frac{1}{m_{01}(0)} + k_a \cdot \frac{t_0}{|\mu_{11} - \mu_{12}|} \qquad (23)$$

2.5. Evaluation of rate constants from experimental results

The calculation of rate constants from experiments minimally requires a knowledge of the following parameters: (a) flow-rate, (b) molar inlet amounts of reactants, (c) retention times of reactants and (recommended) void time, (d) standard deviation of reactant peak for the case $2A \rightarrow P$, (e) ratio of the outlet pulse area to the inlet pulse area for at least one of the reactants as measured for several different injection amounts (recommended) and/or flow-rates.

The last parameter is the most crucial, because chromatographic equipment generally does not allow a direct measurement of the inlet pulse area without an additional detector. However, the use of the following approaches makes it possible to proceed without the reactant area at the column inlet [4]:

(a) Internal standard method: an inert substance is mixed with one of the reactants, and the ratio of the pulse areas of both substances is measured in a non-reactive system. Then, for the reactive system this known ratio can be used to substitute for the inlet pulse area.

(b) Product-reactant method: where the ratio of the molar detector responses for the reactant and the product are known, then the loss of reactant area can be evaluated from the product area.

(c) External standard method: the difference between the external and the internal standard method is that the inert standard is not mixed with the reactant but introduced with a precision injector between reaction experiments. For the case of a reaction of the type $A_1 + A_2 \rightarrow P$, one of the reactants can serve as an external standard. This simplifies the calculations considerably.

Now, with the experimental parameters mentioned above rate constants can be obtained through: (I) numerical analysis from Eq. 2, (II) numerical analysis from Eq. 5, (III) analytically from Eqs. 17, and 22 or 23, respectively. As shown before, the results of method II will not differ significantly from method I, if a GCS function and appropriate initial conditions are applied. The time for the calculations however is considerably shorter with method II. In those situations where only moderate (up to 50–60%) conversions are achieved with equipment which is not particularly sophisticated, experimental error most probably will exceed the systematic error from use of the analytical equations.

The experimental system which was used to test the application of the equations above was the first step in the reaction of pyridine with tetrachloroterephthaloyl chloride ($TCTPCl_2$) shown below [17].

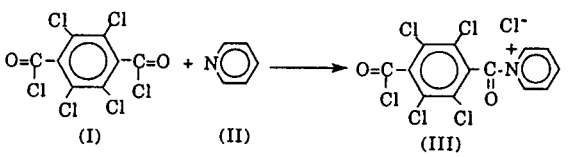

Addition of pyridine to tetrachloroterephthaloyl chloride: This well studied addition reaction to form a quaternary ammonium salt has been used earlier on a number of occasions as a model pseudo-first-order reaction [17,18] in the liquid chromatographic reactor. In the earlier experiments, pyridine was maintained in large excess in the mobile phase with pulses of $TCTPCl_2$ introduced into the liquid phase so that reaction could proceed as shown in Eq. 24. For testing the approach to the pulse overlay technique developed here, the reaction was carried out under conditions which made it truly second order.

3. Experimental

The array consisted of a Waters 590 HPLC pump, Beckman Model 210 sample injection valve with a 20-μl sample loop column, a Perkin-Elmer LC 55 variable-wavelength UV detector set at 275 nm and an SP 4050 Spectra-Physics

integrator. The column was Altex Ultrasphere ODS 250 mm × 4.6 mm I.D. Methanol (in glass-distilled grade) was the mobile phase.

A series of preliminary experiments was used to match the concentration conditions of a true second order reaction and to accommodate the limited solubility of $TCTPCl_2$ in methanol while achieving a reasonable conversion. With the wavelength and conditions used here a useful reaction chromatogram for both reactants (which have considerably different absorption characteristics in the UV range) and product was obtained.

Useful results were achieved using constant injections of $TCTPCl_2$ (0.05 *M* dissolved in tetrahydrofuran). Pyridine pulse concentrations were varied in the range from 0.4 to 0.1 *M* in steps of 0.1 *M* with a 0.2 ml/min flow-rate of methanol mobile phase. The flow-rate was also varied in the range from 0.2 to 0.5 ml/min in steps of 0.1 ml/min. The reaction was carried out at ambient temperature in a controlled-temperature room (about 298 K).

The $TCTPCl_2$ pulse as the slower moving reactant was introduced first, at which time the integrator was started. After about 1 min the pyridine pulse was introduced. To obtain the conversion with respect to the initial $TCTPCl_2$ pulse, separate $TCTPCl_2$ pulses were introduced to the column periodically as an external standard. This was done before each reaction experiment. Pyridine pulses were also introduced separately in a non-reacting mode in order to obtain the characteristic retention time.

4. Results and discussion

Figs. 4–6 show a series of typical reaction chromatograms with increasing pyridine concentrations. In these chromatograms the pyridine (II), the product quaternary ammonium salt (III) and $TCTPCl_2$ (I) are eluted consecutively. Now, in order to be comparable with earlier work [17] an apparent rate constant for the column with respect to $TCTPCl_2$ was evaluated, using Eq. 22 in the following formulation:

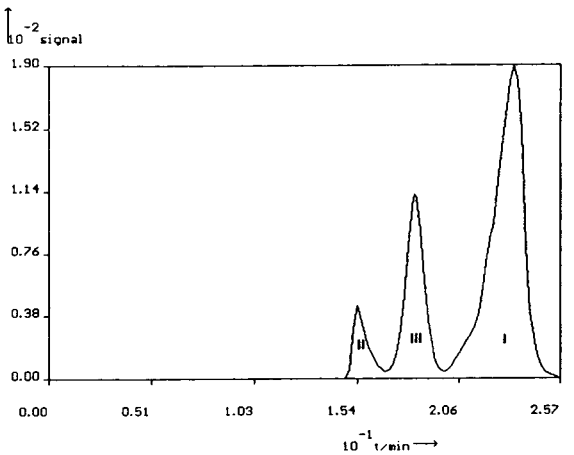

Fig. 4. Reaction chromatogram resulting from successive injections of $TCTPCl_2$ and pyridine (0.1 *M* pyridine). Peaks: II = pyridine; III = quaternary pyridinium salt; I = $TCTPCl_2$.

$$\left.\begin{aligned} X &= (c_{10} - c_{20}) \cdot \frac{20 \cdot 10^{-6} l}{\dot{v}} \\ Y &= \ln\left(\frac{A_1}{A_1(0)}\right) - \ln\left(1 + \frac{c_{10}}{c_{20}}\left(1 - \frac{A_1}{A_1(0)}\right)\right) \\ &\text{and} \\ Y &= aX \end{aligned}\right\} \quad (24)$$

Index 1 refers to $TCTPCl_2$, with *A* representing

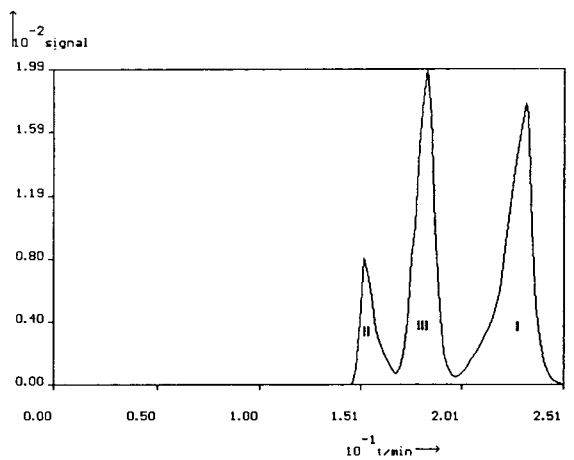

Fig. 5. Reaction chromatogram resulting from successive injections of $TCTPCl_2$ and pyridine (0.3 *M* pyridine). Peaks: II = pyridine; III = quaternary salt intermediate; I = $TCTPCl_2$.

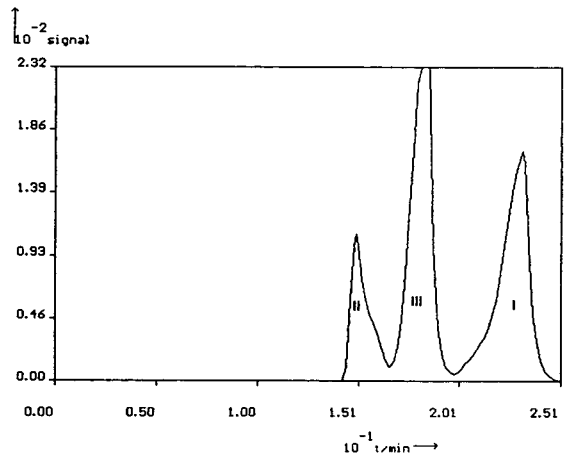

Fig. 6. Reaction chromatogram resulting from successive injections of $TCTPCl_2$ and pyridine (0.5 *M* pyridine). Peaks as in Fig. 5.

peak areas. The c_{10} and c_{20} are the concentrations of the pulsed solutions. The slope is then the product of the apparent rate constant for the column under our conditions and the corresponding time divided by the difference between reactant retention times. The intercept should be zero. Table 4 summarizes our results.

As can be seen, there is no significant difference between the slopes, and the intercepts do not significantly deviate from zero. Fig. 7 presents all the data of Table 4 in a single plot so that comparisons can be made.

From the slope of 2.78 ± 0.12 l/(mol · min) and the average ratio of the retention time difference 0.37 to the retention time of $TCTPCl_2$ we obtain an apparent second order rate constant of the reaction $k_a = 0.0171 \pm 0.0007$ l/(mol · s), which is in very good agreement with the rate constants, recalculated from our earlier pseudo-first order reaction constant measurements [17]: 0.019 l/(mol · s) (with 0.005 *M* pyridine) and 0.0177 l/(mol · s) (with 0.0075 *M* pyridine).

Moreover, it was possible to calculate a reaction chromatogram from Eq. 3. The molar detector responses could be calculated on the basis of material introduced to the column and measured chromatographic areas. The partial differential equation system was solved by an explicit finite difference method, using a grid of 1000 steps in space and time. The mass transfer coefficients were adjusted to meet the standard deviations of the pulses in a manner similar to the method used by Czok and Guiochon [19]. The resulting, calculated chromatogram is compared to an experimental one as shown in Fig. 8. Though there is some nonideality evident particularly for the $TCTPCl_2$-peak and there appears to be some interaction between the pyridine and the quaternary ammonium product, the agreement between these two chromatograms is quite satisfactory.

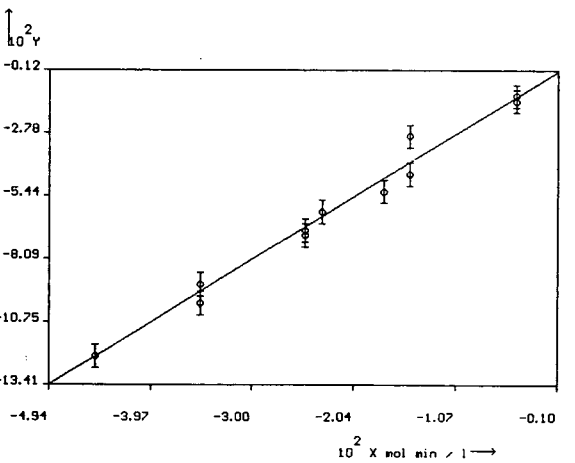

Fig. 7. Plot of *X* and *Y* of Eq. 24 for the $TCTPCl_2$–pyridine reaction.

5. Conclusions

The peak overlay method offers the possibility of studying second-order reactions in the liquid chromatographic reactor even where retentions of the two reactants differ. In comparison to pseudo-first-order methods, it can offer advantages especially for fast reactions and also because there is the possibility of separating products and reactants completely.

To calculate the column rate constant, measurements of both reactant retention times and the peak area of one reactant is necessary. The Gram–Charlier series proved to be suitable for use as an empirical peak shape equation, how-

Table 4
Results from regressions of experimental values with respect to Eq. 24

Experiment (see Experimental section)	Slope $\left(\frac{\text{mol} \cdot \text{min}}{\text{l}}\right)$	Intercept
(1) Pyridine concentration varied	2.78 ± 0.19	$4.25 \cdot 10^{-3} \pm 5.41 \cdot 10^{-3}$
(2) Pyridine concentration varied	2.88 ± 0.09	$6.85 \cdot 10^{-3} \pm 2.20 \cdot 10^{-3}$
(3) Mobile phase flow-rate varied	2.79 ± 0.48	$-5.17 \cdot 10^{-4} \pm 1.26 \cdot 10^{-2}$

ever with moderate conversions the assumption of a Gaussian distribution is sufficient and leads to analytical terms for the evaluation of the rate constant. Experimental and numerical analysis showed that the rate constants found with this approach do not differ from those found by previously employed pseudo-first-order methods.

Since all the substances involved in reaction here can be —at least in principle— completely separated, a comparison of experimental with recalculated chromatograms is quite feasible, the latter requiring only experimentally observed rate constants and mass transfer coefficients. Further development of the approach described here should make it possible to broaden the application of the liquid chromatographic reactor in the study of reaction kinetics.

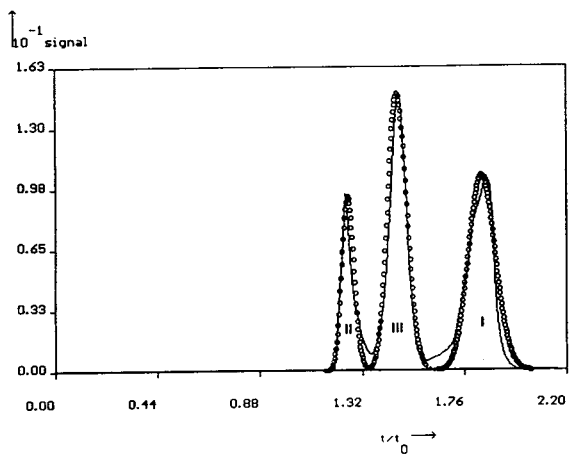

Fig. 8. Comparison of observed chromatogram with a numerically calculated chromatogram using a finite difference method (reduced time referenced to the column void time).

Symbols

A	Peak area
a_s	effective concentration in the stationary phase
c	concentration in the mobile phase
D	diffusion coefficient
E	excess of peak shape: $E = \frac{\mu_4' - 3\mu_2'^2}{\mu_2'^2}$
F_i	see Eq. 14
K	partition coefficient
k_f	mass transfer coefficient
k_a	apparent rate constant
k_s	rate constant (stationary phase)
k_m	rate constant (mobile phase)
l	length of the column
m_0	zeroth moment: $m_0 = \int_0^\infty c \, dt$
$m_0(0)$	zeroth moment at the column inlet
m_{R0}	zeroth moment of the reaction: $m_{R0} = \int_0^\infty r \, dt$
p	pressure
q	retention capacity
r	reaction terms
S	skew of peak shape: $S = \frac{\mu_3'}{\mu_2'^{3/2}}$
t	time
t_0	void time
u	linear flow-rate
v	volume or effective volume
$\dot{v}$	volume flow-rate
x	length coordinate
z	argument of the GCS (see Eq. 18)
α	partial reaction order

Δt time delay from the beginning of the measurements

$\Delta\mu$ difference between moment in reaction and without reaction

μ_n absolute nth moments:

$$\mu_n = \frac{\int_0^\infty t^n c \, dt}{m_0}$$

μ_n' absolute central moments:

$$\mu_n' = \frac{\int_0^\infty (t-\mu_1)^n c \, dt}{m_0}$$

μ_{id} absolute moments in case that no reaction occurs

μ_z' fourth semi-invariant: $\mu_z' = \mu_4' - 3\mu_2'^2$

μ_{Rn} nth moment of the reaction (Eq. 8)

$\mu(l)$ moment at the column outlet

ν stoichiomeric coefficient

ξ integration variable in Eq. 18 defined as

$$\xi = \frac{t-\mu_{id}}{\sqrt{\mu_{21}'}}$$

Ψ peak shape equation

GAU $$\Psi = \frac{1}{\sqrt{2\pi\mu_2'}} e^{-\frac{(t-\mu_1)^2}{2\mu_2'}}$$

GCS $$\Psi = \frac{1}{\sqrt{2\pi\mu_2'}} e^{-\frac{z^2}{2}}\left(1 + \frac{S}{6}(z^3 - 3z) + \frac{E}{24}(z^4 - 6z^2 + 3)\right)$$

$$z = \frac{t-\mu_1}{\sqrt{\mu_2'}}$$

EMG $$\Psi = \frac{1}{\tau}\exp\left(\frac{1}{2}\cdot\frac{\sigma_g^2}{\tau^2} - \frac{t-t_g}{\tau}\right)\int_{-\infty}^{\frac{t-t_g}{t\sqrt{2}}} e^{-\xi^2} d\xi$$

t_g breakthrough time of pulse maximum

σ_g width parameter

τ skew parameter

GEX $$\Psi = \frac{h_m}{m_0}\cdot\left(\frac{t-t_1}{t_g-t_1}\right)^{b-1} \cdot \exp\left(\frac{b-1}{a}\cdot\left[1 - \left(\frac{t-t_1}{t_g-t_1}\right)^a\right]\right)$$

h_m maximum peak height

t_1 break through time of pulse beginning

a, b shape parameters

Subscripts

i number of the substance

j number of the reaction

n number of the moment

m mobile phase

s stationary phase

Acknowledgement

We are grateful to the German Academic Exchange Service (DAAD) for their support of this work through a travel grant (to R.T.). We also appreciate support through the University of Wisconsin and help from Hazelton Laboratories of Madison through Mr. Robert L. Pesselman.

References

[1] R.J. Laub and R.L. Pecsok, *Physicochemical Applications of Gas Chromatography*, Wiley, New York, 1978.
[2] J.R. Conder and C.L. Young, *Physicochemical Measurements by Gas Chromatography*, Wiley, New York, 1979.
[3] G. Ganetsos and P.E. Barker (Editors), *Preparative and Process Scale Chromatographic Processes and Applications*, Marcel Dekker, New York, 1993.
[4] S.H. Langer and J.E. Patton, in J.H. Purnell (Editor), *New Developments in Gas Chromatography*, Wiley, New York, 1973, p. 293.
[5] C.Y. Jeng and S.H. Langer, *J. Chromatogr.*, 589 (1992) 1.
[6] L.G. Harrison and Y. Koga, *J. Chromatogr.*, 52 (1970) 39.
[7] P. Schulz, *Anal. Chem.*, 47 (1975) 1979.
[8] R. Thede, E. Below, D. Haberland and H. Pscheidl, *J. Chromatogr.*, 520 (1990) 109.
[9] R. Thede, H. Pscheidl and D. Haberland, *Z. Phys. Chem. (Leipzig)*, 271 (1990) 471.
[10] J.A. Jönsson, *Chromatography: Theory and Basic Principles*, Marcel Dekker, New York, 1985.
[11] A. Jaulmes and C. Vidal-Madjar, *Adv. Chromatogr.*, 28 (1989) 1.
[12] M.S. Jeansonne and J.P. Foley, *J. Chromatogr. Sci.*, 29 (1991) 258.
[13] F. Dondi, A. Betti, G. Blo and C. Bighi, *Anal. Chem.*, 53 (1981) 496.
[14] R.A. Vaidya and R.D. Hester, *J. Chromatogr.*, 287 (1984) 231.
[15] R. Thede, E. Möller, H. Pscheidl and D. Haberland, *Z. Phys. Chem. (Leipzig)*, 271 (1990) 891.

[16] R. Thede, F. Nohmie, H. Pscheidl and D. Haberland, *Z. Phys. Chem. (Munich)*, 173 (1991) 87.
[17] A.H.T. Chu and S.H. Langer, *Anal. Chem.*, 58 (1986) 1617.
[18] M.W. Bolme and S.H. Langer, *J. Phys. Chem.*, 87 (1983) 3363.
[19] M. Czok and G. Guiochon, *Anal. Chem.*, 62 (1990) 189.

ELSEVIER

Journal of Chromatography A, 683 (1994) 293–309

JOURNAL OF CHROMATOGRAPHY A

Study of the packing behavior of radial compression columns for preparative chromatography

Matilal Sarker, Georges Guiochon*

Department of Chemistry, University of Tennessee, Knoxville, TN 37996-1600, USA, and Division of Chemical and Analytical Sciences, Oak Ridge National Laboratory, Oak Ridge, TN 37831, USA

First received 22 February 1994; revised manuscript received 18 May 1994

Abstract

The behavior of the packing of radial compression preparative columns (17.5 × 7.5 cm) was studied using C_{18} silica IMPAQ as the stationary phase and water–methanol solutions as the mobile phase. The retention volumes of phenol and cresol and the efficiency of their peaks were repeatedly measured on three different columns, over several hundred hours, during which repeated water–methanol gradient runs were conducted. No significant changes in the retention factors and the column efficiency were observed during the testing period. The effects of the mobile phase temperature and of the radial compression pressure on the column efficiency were also studied. The external porosity and the permeability of the packing were found to decrease slowly with increasing compression pressure. Finally, a set of experiments were performed to trigger the formation of channels and to show their possible repair by applying elevated radial compression pressures.

1. Introduction

Preparative high-performance liquid chromatography (HPLC) is now routinely used by production chemists for the purification of fine chemicals [1]. Although there is an abundant literature on the theory of preparative, e.g., non-linear, chromatography [2,3], and on the optimization of the experimental conditions of this process for laboratory or industrial applications [3–9], there is a paucity of technical reports investigating the structure, the performance and the stability of column packings.

Most studies made on column packing have focussed on the packing technology in view of the achievement of small plate heights. Admittedly, this is one of the basic goals of chromatographers. However, the problem is too complex to be examined by considering a mere number, and especially one which is difficult to measure with great precision. Furthermore, if a poor column efficiency can often be ascribed to an inhomogeneous packing, other important factors, such as the distribution of the mobile phase stream at the column inlet, can explain why poor separations can be achieved with efficient columns. Packing homogeneity and

* Corresponding author. Address for correspondence: Department of Chemistry, University of Tennessee, Knoxville, TN 37996-1600, USA.

0021-9673/94/$07.00
SSDI 0021-9673(94)00503-2

stability are important properties which need to be investigated in detail to understand the behavior of preparative columns. The importance of the contribution of large-scale fluctuations of the mobile phase velocity (i.e., of fluctuations at the column radius scale) to the apparent column efficiency has already been pointed out by Giddings, 30 years ago [10].

Nicoud and Perrut [11] have proposed a model of inhomogeneous preparative columns based on the theory of transfer functions in the Laplace domain and shown some limited experimental data supporting the conclusions of their model. Kaminski [12] has proposed a method to test for possible distortions of the flow profile across the column cross-section. Ideally, the flow profile should be piston-like. However, fluctuations of the packing density promote fluctuations of the local velocity, which, in turn and if these fluctuations take place over significant distances, may result in severe warping of the isoconcentration surfaces, which should be flat, and in serious band broadening. Although the test described by Kaminski [12] is useful, it demonstrates an unacceptable situation, but does not supply any course of action for possible remediation.

Recently, Marme et al. [13] investigated the structure and homogeneity of the bed of stationary phase in an axially compressed column by NMR imaging. Because of the constraints of NMR which uses a very intense and homogeneous magnetic field, only plastic materials could be used in the column design, and the compression achieved was necessarily imperfect. The bed was found to be inhomogeneous, with regions containing ca. 10–20% more mobile phase than others. There are no doubts that NMR imaging can give much valuable information regarding the dynamics of flow in column packings, and will provide a better understanding of the phenomena which take place in all columns, but are enhanced in large-diameter columns. This, however, requires some adjustments in the column technology to permit the investigation of columns representative of those in current use. In the same study, an unexpected enrichment in fine particles was found towards the end of an axial compression column after only 30 h of column use.

Most of the earlier work in preparative chromatography was performed with columns obtained by packing empty steel tubings. Many operators have reported that voids or empty pockets appear frequently and unexpectedly at the top of the column bed, and result in a drastic and rapid loss of separation performance. A general agreement has now been reached that dynamic compression is necessary for long-term stable operation of preparative columns and permits a significant improvement of column performance. This has been related to the loss of wall support that the stationary phase experiences at distances from the wall exceeding the radius of typical analytical columns.

This phenomenon could be explained either by a loss of stationary phase or by a local or general increase of its apparent density. It does not seem that slow dissolution of the adsorbent in the mobile phase or the loss of its very fine particles in the exit stream could account for the volume of the voids formed. The silica content of even water-rich eluents is insufficient to account for the whole loss observed [14], although, under the proper set of circumstances, this could be a contributing factor. A change in apparent density could be related to a change in the surface tension of the liquid impregnating the bed [15]. Such a rapid change occurs when the packing solvent is replaced by the mobile phase, when the separation is carried out in gradient elution, or when the high concentration bands of the major components of large size samples migrate along the column. More attention should probably be paid to the subtle but far-reaching effects of such changes in the mobile phase surface tension, even though they are probably not the unique cause of an apparently most complex phenomenon.

Be like as it may, dynamic compression can oppose the formation of voids at the top of all columns and of channels in large diameter columns, if applied permanently, and possibly heal them if applied after the damage has appeared. There are three different bed compression technologies available for large-size columns; annular, axial and radial compression [16–18]. In principle, each of these compression modes could be implemented under static or dynamic

conditions. However, for practical reasons, the proper instrumentation has been developed only for axial and radial dynamic compression. Static compression cannot, by principle, correct automatically for the formation of voids. Thus, columns using static compression are at an intrinsic disadvantage when compared with dynamic compression columns. In a forthcoming paper, we discuss the behavior of the packing beds in axial compression columns [19]. The goal of the present paper is a study of packing performance in radial compression columns.

The first report on the dynamic radial compression was published by Little et al. [17]. The technology was patented by Waters Millipore Division for analytical and preparative applications [20–22]. The column packing is contained in a flexible-wall prepacked cartridge which is placed inside a stainless-steel chamber. The cartridge is compressed by injecting a pressurized liquid between the steel and the plastic walls. Suitable fittings ensure leak proof insulation between the pressurizing fluid and the mobile phase. Typical compression pressures are between 6.9 and 13.8 bar. In this work we present the results of experimental investigations carried out with a 7.5 cm internal diameter radial compression column. We studied the performance, the long-term stability and the reproducibility of the performance of this column, using an octadecyl bonded silica column, a standard methanol–water mobile phase and conventional samples. At the end of the study, a set of experiments were performed on one cartridge to demonstrate the formation of channels and their repair in a radial compression column.

2. Experimental

2.1. Chemicals

All chemicals used in this work were 99.9% pure or better. Acetone, *m*-cresol, phenol and methanol were purchased from Baxter (Atlanta, GA, USA). Distilled water was from the still of the Chemistry Department. It was filtered before use.

2.2. Column

Three 17.5 × 7.5 cm radial compression cartridges were supplied by Biotage (Charlottesville, VA, USA). The cartridges were packed with IMPAQ RG1020C18 irregular reversed-phase C_{18} bonded silica (BTR Separations, Wilmington, DE, USA; formerly The PQ Corporation). The product specifications provide for an average particle size of 16.7 μm and an average pore size of 100 Å. A 25 × 0.46 cm analytical column was packed in this laboratory with the same stationary phase, using a conventional slurry packing method at 345 bar [23]. The characteristics of these columns are summarized in Table 1.

2.3. Instrument

A Kiloprep 100 HPLC pump and a Kiloprep 100 radial compression module were obtained from Biotage. The pump is capable of delivering up to 500 ml/min at a maximum pressure of 138 bar. The radial compression module is capable of compressing either 30 cm or 17.5 cm long cartridges. It is rated at 207 bar. For monitoring the

Table 1
Column characteristics

Column properties	Column 1	Column 2	Column 3	Column 4
Dimensions (cm)	17.5 × 7.5	17.5 × 7.5	17.5 × 7.5	25 × 0.46
Dead volume (ml)	531 ± 8	532 ± 7	554 ± 5	2.89 ± 0.08
Total porosity	0.69	0.69	0.71	0.70
Phase ratio	0.46	0.45	0.40	0.44
k' (acetone)	0.32 ± 0.02	0.33 ± 0.02	0.30 ± 0.01	0.28 ± 0.01
k' (phenol)	2.58 ± 0.04	2.67 ± 0.3	2.66 ± 0.07	2.55 ± 0.10
k' (*m*-cresol)	5.89 ± 0.09	6.20 ± 0.09	6.16 ± 0.18	5.79 ± 0.17

Values measured with methanol–water (40:60, v/v) as eluent.

column inlet pressure a Model PX603-2KG5V pressure transducer from Omega (Stamford, CT, USA) was used. This transducer gives a 1 to 5 V (d.c.) output. After proper attenuation, the pressure was recorded with the data acquisition system between 0 and 138 bar. The dead volume of the transducer was decreased by adding PTFE packing inside the sensor head connector. The analytical system consisted of a Waters HPLC pump Model 510 (Waters, Milford, MA, USA) and a Spectraflow Model 757 detector (Kratos).

2.4. Detector

Two Model 204 UV–visible detectors (Linear Scientific, Reno, NV, USA), equipped with a variable path length preparative cell were used in this work. Because short path lengths can be used, the response of the detector remains linear up to much higher concentrations than that of conventional HPLC detectors. The cell is rated up to 500 ml/min and 138 bar pressure.

2.5. Data acquisition

The data system consisted of a Waters System Interface Module with two A/D convertor boards (Milford, MA, USA). These boards permit the simultaneous monitoring of four detectors. A Waters Maxima 820 version 3.3 software was used to collect the data. The data files were uploaded to the computer network of the University of Tennessee Computer Center. For further manipulation of these data, several DOS- and VMS-based softwares in BASIC and FORTRAN were developed in our laboratory.

2.6. Solvent

Methanol (99.9% pure) was used as solvent in some experiments, and in others a mixture of methanol–water (40:60, v/v). In the following, we refer to pure methanol as solvent A and to the methanol–water (40:60, v/v) mixture as solvent B. For economical reasons, none of these solvents were HPLC grade. For the same, obvious reasons and for better waste management, the mobile phase was pumped in closed circuit with a 15–20-l buffer tank on the line. Large elution bands were collected separately and wasted. The solvent was changed and wasted whenever the baseline absorption exceeded a certain threshold.

2.7. Methods

In most experiments, the compression pressure is set at 6.9 bar while there is no mobile phase flow-rate through the column, and the compression chamber is sealed by closing a valve. In some experiments (e.g., influence of compression pressure on the flow-rate, study of channel healing), the compression pressure is set independently and controlled.

For the low-concentration experiments [e.g., height equivalent to a theoretical plate (HETP) determinations], solvents A and B were used successively as eluent. During all experiments, the mobile phase flow-rate was measured with appropriate graduated measuring cylinders. The samples for these experiments consisted of a 3% solution of acetone, phenol and *m*-cresol dissolved in the eluent. The sample loop volume for the analytical injections was 1.5 ml on the preparative column and 20 μl on the analytical column.

The data collected by the Maxima 820 software were translated to ASCII format for further use. All detector outputs digitized and recorded by Maxima were in terms of volts. These voltages were then converted to the specific units by calibrated correlations, as indicated above. Several programs were written in BASIC to convert data. One of these programs calculates the column efficiency, using different equations among those suggested in the literature. In this work, however, the efficiency data were derived from the peak width at half-height. In all sets of experiments the reduced velocities and reduced plate heights were calculated. The classical Wilke and Chang [24] equation was used to estimate the diffusion coefficients. These data were fitted to the Van Deemter equation [25] by a non-linear regression and the parameters are reported in Table 2.

Table 2
Van Deemter parameters for the columns studied

Column	Solvent	Sample	a	b	c	h_{min}	ν_{opt}	Hours used
1	A	Acetone	2.595	4.411	0.0982	3.90	6.62	15
1	A	Acetone	1.999	5.273	0.1382	3.70	6.18	25
1[a]	A	Acetone	1.989	4.701	0.1397	3.61	5.58	35
1	B	Acetone	4.304	0.774	0.0397	4.65	4.15	50
		Phenol	2.980	2.988	0.0956	4.05	5.44	
		m-Cresol	3.134	1.401	0.0815	3.81	4.15	
1	B	Acetone	1.490	16.14	0.1177	4.25	11.6	65
		Phenol	1.388	11.78	0.1315	3.87	9.30	
		m-Cresol	0.641	20.48	0.1319	3.93	12.5	
1	B	Acetone	3.594	13.83	0.0720	5.59	13.8	90
		Phenol	0.999	22.62	0.1462	4.64	12.5	
		m-Cresol	0.782	21.42	0.1210	4.40	13.4	
2	A	Acetone	7.030	4.285	0.0628	8.07	8.27	6
2	B	Acetone	6.629	7.533	0.0591	7.96	8.27	26
		Phenol	8.005	15.09	0.0606	9.92	11.2	
		m-Cresol	7.355	28.82	0.0837	10.5	15.8	
2	B	Acetone	4.474	36.27	0.1107	8.45	18.1	110
		Phenol	2.654	59.98	0.1877	9.37	16.9	
		m-Cresol	3.919	58.70	0.1574	9.90	19.4	
3	A	Acetone	1.941	5.894	0.2464	4.35	4.84	8
3[b]	A	Acetone	2.075	5.410	0.2431	4.37	4.72	19
3	B	Acetone	2.582	8.075	0.0961	4.34	9.36	69
		Phenol	2.252	5.217	0.1422	3.97	6.14	
		m-Cresol	1.774	8.207	0.1375	3.90	7.52	
3	B	Acetone	2.792	9.796	0.0842	4.61	10.74	123
		Phenol	1.697	10.002	0.1475	4.13	8.21	
		m-Cresol	0.571	17.004	0.1753	4.02	9.82	
4[c]	A	Acetone	3.330	1.29	0.0823	3.85	3.98	

Solvents: A = pure methanol, B = methanol–water (40:60, v/v).
[a,b,c] Data shown in Fig. 1.

3. Results and discussion

The efficiency of the three radial compression cartridges packed by Biotage were measured at the plant, using pure methanol as the eluent and acetone as the test sample. The values obtained were 3435, 3413 and 2029 theoretical plates at 150 ml/min (reduced mobile phase velocity, $\nu = 5.68$, reduced plate height, $h = 3.05$; $\nu = 5.74$, $h = 3.07$ and $\nu = 5.60$, $h = 5.16$), respectively.

We repeated the measurements using the same eluent and sample. Then, we performed various experiments with these cartridges over an extended period of time and repeated periodically the efficiency measurements (cf. Table 2). Although longer periods would have been useful for the purpose of our study, the first cartridge was used for a total period of time of nearly 300 h, the second and third cartridges for slightly more than 100 h each. Because of safety regulations, the pump could not be left operating alone, so no overnight or week-end runs could be completed, as normally done in production. It would have been impractical to use the cartridges for longer periods. The efficiency of the analytical column was measured under the same conditions, but no long-term study of the evolution of its efficiency was done.

The experiments performed on the cartridges between successive HETP measurements included repeated concentration gradients as follows. The methanol concentration in water is raised linearly from 40 to 80% in 30 min, followed by an abrupt jump to 0%, and then by a linear gradient from 0 back to 40% methanol. The purpose of these experiments was not to wear down the stationary phase, but the column itself. There are more aggressive experiments to accelerate the aging of the stationary phase. This gradient seemed appropriate to test the stability of the bed itself.

3.1. Results obtained with pure methanol as the eluent

The column efficiencies were measured at different flow velocities, using methanol as the eluent and a 3% acetone solution in methanol as the sample. Acetone is practically not retained in pure methanol, and its retention time can be taken as a good estimate of the column hold up time (t_0). Plate numbers were derived from the bandwidth at half-height. Similar trends are obtained when the plate number is derived from the second moment the determination of which is less accurate. This measurement permits also a qualitative comparison with the factory results. The parameters of the Knox equation obtained are reported in Table 2. As an example, Fig. 1 shows the data obtained (symbols) with columns 1 (Table 2, row 3) and 3 (Table 2, row 11), and with the analytical column (Table 2, last row), as plots of h versus ν (data labelled a, b, c in Table 2). The solid line represents the result of a non-linear fit of the data to the Van Deemter equation [25]. In Fig. 1, minimum values of h equal to 3.6 and 4.4 occur around $\nu = 5.6$ and 4.7 for columns 1 and 3, respectively; the corresponding flow-rates are 120 and 100 ml/min, respectively. These values are in reasonable agreement with the factory values, considering

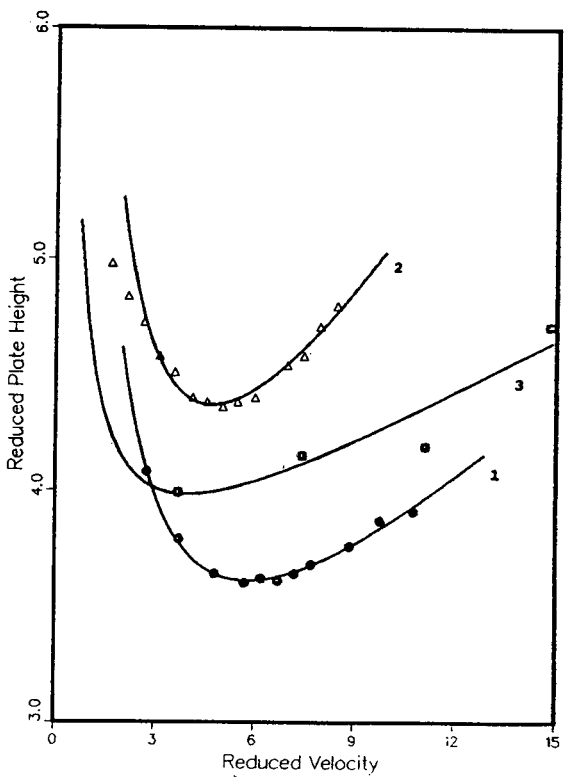

Fig. 1. Plot of the reduced plate height versus the reduced mobile phase velocity representative of the results obtained with the first radial column (1), third radial column (2) and the analytical column (3). Eluent: pure methanol. Sample for analytical column was 20 μl of a 1% acetone solution in the eluent. Sample for the radial columns: 1.5 ml of a 3% acetone solution in methanol. Radial compression for first radial column 6.9 bar and for the third column was 5.2 bar. Experimental data points (symbols) from Table 2 (rows labelled a, b, c) and best fit to the Van Deemter equation (lines).

that two different instrumental settings were used, that the calculation procedures are different, and that efficiency determinations are not highly precise. The values observed for the optimum reduced velocities seem high, considering the efficiencies measured for the columns. Usually, values of the optimum reduced velocity between 2 and 3 are associated with minimum reduced plate heights between 4 and 5. Independent measurements reported elsewhere [19] demonstrate that the extra-column contributions to band broadening due to tubings, valves, connections, injection device and detector cell are negligible.

The agreement was not as good for the second column which, although its characteristics are quite similar to those of column 1 (Table 1), gave only half the efficiency, for no apparent good reasons. This second cartridge, which sat on the shelf for about five months before the beginning of its tests, never gave good performance, with the possible exception of the last test (Table 2). The third cartridge gave performance comparable with that of the first cartridge. The analytical column (column 4) gave an HETP curve in good agreement with the curves obtained for the first and third column, in spite of the large difference in their internal diameters (0.46 vs. 7.5 cm, or a ratio of 266 in cross-section areas). Note, however, that, if the efficiency of the analytical column is intermediate between that of the two cartridges (Fig. 1), the slopes of the asymptotes of the HETP plots and the c terms are larger for the two cartridges than for the analytical column, while the a term is lower. Since the same packing material was used in all columns, a somewhat opposite result was expected, with similar values for the c terms of the different columns, and different values of the a terms for the cartridges and the analytical column, since a characterizes the packing homogeneity [25].

3.2. Results obtained with a methanol–water (40:60) solution as the eluent

The components of the test sample were chosen so that the first one (acetone, $k' = 0.32$) is poorly retained, the second one (phenol, $k' = 2.58$) is moderately retained and the last one (m-cresol, $k' = 5.89$) is rather strongly retained. Excess water was added to the sample solution, and the negative system peak of water was used to measure the breakthrough time. A representative chromatogram is shown in Fig. 2. The peaks tail slightly. The Van Deemter parameters derived from these experiments are included in Table 2. In consistency with the results reported above and obtained with pure methanol, there are no significant changes in the column efficiency during our tests. The most probable explanation for the large changes in the values of the b parameter is their lack of accuracy, due to the insufficient number of data points acquired at low mobile phase velocities. The range of reduced velocities within which measurements

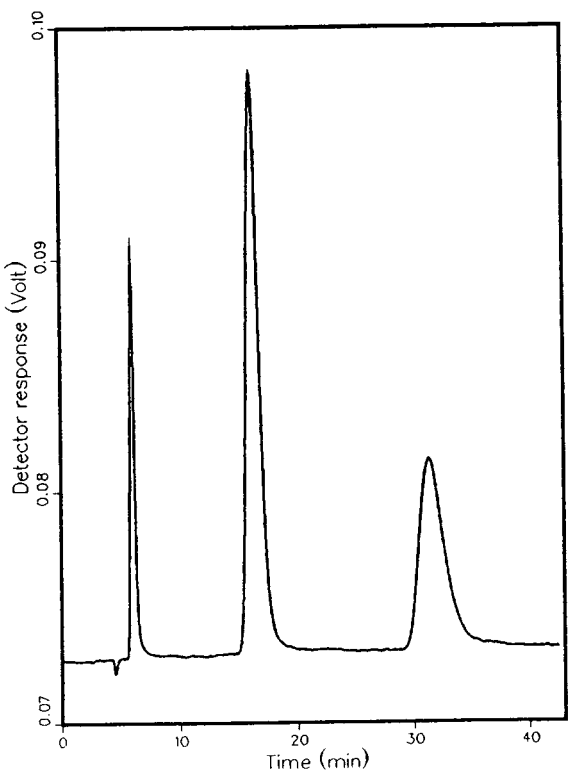

Fig. 2. Typical chromatogram obtained with the second radial compression column (17.5 × 7.5 cm). Components: 1 = acetone; 2 = phenol; 3 = m-cresol. The negative peak is the water system peak. Eluent: methanol–water (40:60, v/v) mixture at 118 ml/min. Radial compression: 6.9 bar.

were done barely exceeds half an order of magnitude. For this reason, it is not justified to attempt to draw conclusions from the fluctuations of the Van Deemter parameters. What is important is the very slow, almost negligible increase in the minimum plate height with passing time, in spite of the punishments inflicted to the column (see above). Repeated steep mobile phase composition gradients are known to trigger rapid degradation of column performance. Radial compression seems to be effective in keeping the packing structure stable.

Some column characteristics are given in Table 1. The dead volumes and the retention factors k' were measured with solvent B for a series of experiments made at ten different values of the flow rate. The standard deviations of the results (a few percents) are low for that kind of data. The results in the Table suggest that the four columns have nearly identical initial packing density, since their total porosity and the retention factors of the three components are the same.

3.3. Correlation between the radial compression pressure, the column inlet pressure and the flow-rate

The inlet pressure, P_i, required to achieve a certain flow-rate cannot be completely independent from the radial compression pressure, P_c, since the column shrinks slightly under the influence of the radial compression, which is the purpose of the design. The inlet pressure is related to the mobile phase flow velocity, u, the mobile phase viscosity, η, the column length, L, and its permeability, k, through the conventional Darcy equation [3,26]

$$u = \frac{k}{\eta} \cdot \frac{P_i}{L} \tag{1}$$

Under the influence of the compression pressure, the external or extra-particle porosity, ϵ_e, decreases slightly. The Blake–Kozeny equation (see Ref. [26]) relates the column permeability, k, its external porosity the specific surface area a_p of the particles (m^2/m^3)

$$k = \frac{\epsilon_e^3}{h_k a_p^2 \epsilon_T (1-\epsilon_e)^2} = \frac{d_p^2 \epsilon_e^3}{h_0(\epsilon_i + \epsilon_e)(1-\epsilon_e)^2} \tag{2}$$

where h_k and h_0 are numerical coefficients. In classical chemical engineering textbooks, the Blake–Kozeny equation does not contain ϵ_T, the total porosity, but then, the flow velocity used is the superficial velocity, $v = F_v/\pi D_c^2$, with F_v = flow rate and D_c = column diameter, i.e., the velocity which would be reached in an empty tube. In chromatography, the velocity is the ratio L/t_0, of the column length to the hold-up time. Obviously $v = \epsilon_T u$, and the two ways to write the equation are equivalent.

For spheres, a_p is equal to $6/d_p$. Packing particles are generally not spheres, so the numerical coefficient h_0 will depend on the shape of the particles, and will vary from one brand to another. The total porosity, ϵ_T, is the sum of the external porosity (ϵ_e) and the internal porosity, ϵ_i, or pore volume. The latter is constant for silica particles which we assume to be incompressible in the pressure range investigated. Thus, ϵ_i should be the same for all columns. The experimental results used to illustrate the following discussion have all been obtained with the second cartridge. Data for the third cartridge are also given in the figures.

When the compression pressure is increased, the particles are compressed together, shift slightly, and the external porosity decreases. This process should take some time, however, and we may expect it to cause a degree of particle abrasion or cracking, hence to result in the formation of fine particles. As a result of the decrease in the external porosity, the flow-rate should decrease if the inlet pressure is kept constant. This point is well supported by the experimental results. As shown in Fig. 3, the hold-up volumes at constant flow-rate of the second and third cartridges (these measurements were not carried out on the first cartridge) decrease with increasing radial compression pressure, showing that the column external porosity decreases. In the range investigated here, the decrease is linear, with a slope equal to −1.03 ml/bar. To keep the flow-rate constant at 200 ml/min, the column inlet pressure must be

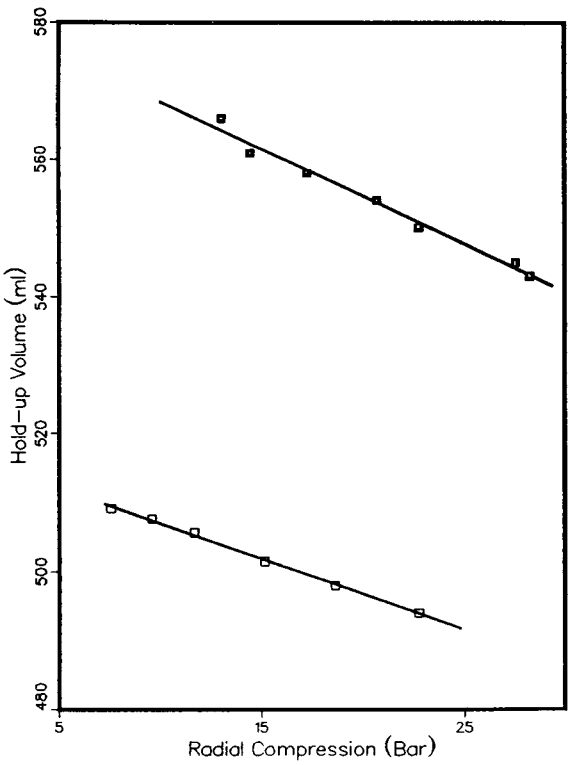

Fig. 3. Variation of the hold-up time of the second (■) and third (□) radial columns with the compression pressure. Constant flow-rates, 200 ml/min (second radial column) and 142 ml/min (third radial column).

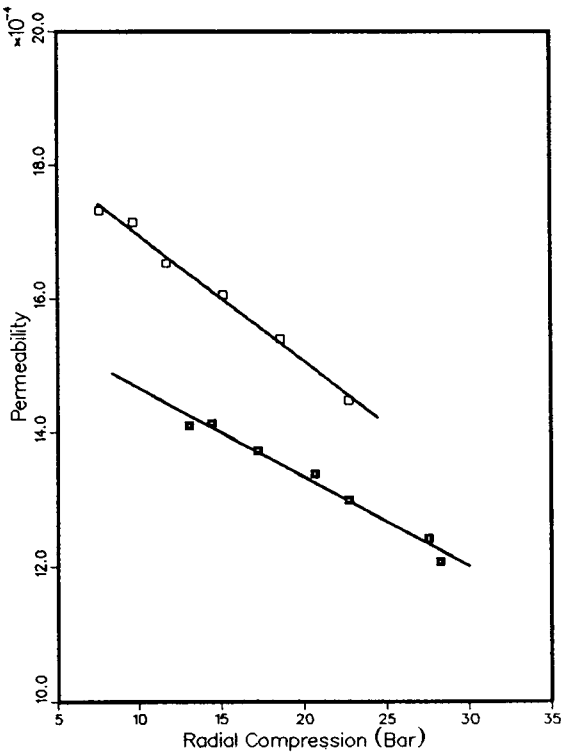

Fig. 4. Plot of the permeability of the second (■) and third (□) radial columns versus the compression pressure. Value of the permeability derived from the data in Figs. 5 and 6, using Eq. 1.

raised. When the compression pressure is increased from 6.9 to 31.0 bar, the inlet pressure required to keep a constant flow-rate of 200 ml/min increases by more than 30%, from 8.0 to 10.6 bar (data not shown). The data fits well to a third-degree polynomial ($P_i = a + b\ P_c + cP_c^2 + dP_c^3$), with coefficients $a = 7.58$, $b = 5.74 \cdot 10^{-2}$, $c = -5.559 \cdot 10^{-4}$ and $d = 6.085 \cdot 10^{-5}$ (all pressures in bar), although a linear fit would be nearly as good. Using the experimental values of the inlet pressure, we can use the Darcy equation (Eq. 1) to calculate the permeability as a function of the compression pressure. The plot of $k_0 = k/d_p^2$ versus the radial compression pressure is given in Fig. 4. Eq. 2 then permits the calculation of an apparent ϵ_e. A plot of ϵ_e versus P_c is shown in Fig. 5. As can be seen, the decrease in ϵ_e is quite significant.

This dependence of the inlet pressure on both the required flow-rate *and* the selected compression pressure is important to understand when operating a radial compression column. The normal mode of operation consists in setting a compression pressure of ca. 6.9 bar when the column is filled with mobile phase, but there is still no inlet pressure applied, and no flow-rate. The valve to the compression chamber is then closed tightly, and the column inlet pressure raised to the required value. Because the compression chamber is closed, the compression pressure rises. The hydrodynamic behavior of the column is complex, and we cannot calculate it at this stage. The actual stress applied to the packing bed at the wall results from the difference between the pressure of the mobile phase at the column wall and the compression pressure

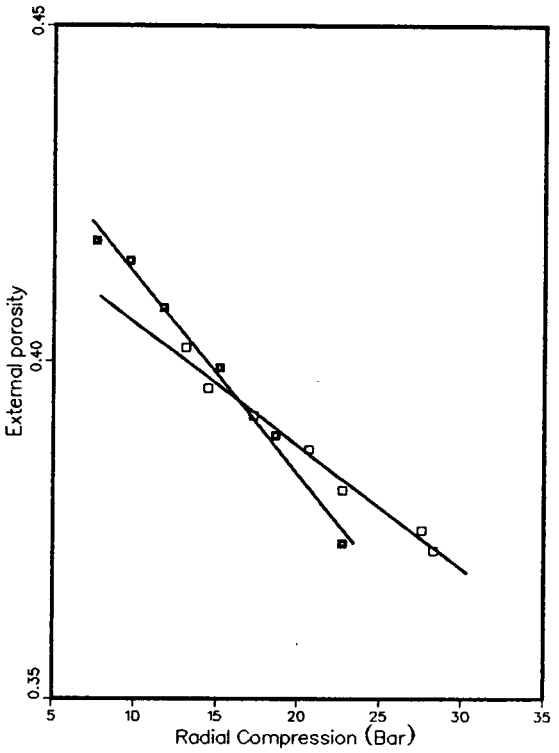

Fig. 5. Plot of the column external porosity versus the compression pressure. Porosity derived from the data in Fig. 7 and Eq. 2. ■ = Third radial column; □ = second radial column.

(neglecting the rigidity of the plastic wall). Under steady-state flow, the latter pressure is constant, while the former decreases linearly from column inlet to outlet. So, the average compression stress applied to the column packing is approximately proportional to $P_c - P_i/2$, and it increases from column inlet to column outlet. Mechanical stress does not transmit in a non-consolidated bed like pressure inside a liquid. The effect of this stress, which is not constant along the column or across it, on the local porosity is yet unknown and it seems impossible to speculate on this issue in the absence of sufficient data. The main references available are in soil mechanics [27] and few of their conclusions can be applied readily to the behavior of chromatographic columns. A detailed investigation of this problem is certainly warranted.

Fig. 6 shows plots of the inlet pressure, and of the radial compression pressure (with the compression chamber closed), as a function of the mobile phase flow-rate required. Above 3.5 bar, the two curves in Fig. 6 are essentially parallel, with an average distance approximately equal to 5.5 bar. Because of the limited data available and of the experimental error, it is not clear whether the radial compression pressure does vary with the flow-rate below 50 ml/min (a possible effect of the rigidity of the cartridge wall), and whether its correlation with the flow-rate is linear (Fig. 6). In Fig. 7, the two lines seem to have a slight angle, but the conclusions are similar.

The flow-rate through the second cartridge increases linearly with the inlet pressure (Fig. 7), with a slope of 0.0315 ± 0.0005 bar/(ml/min) and

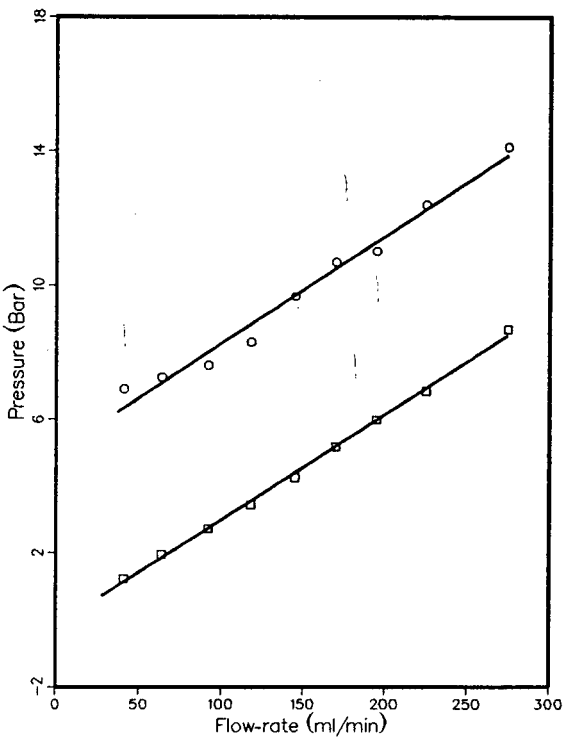

Fig. 6. Plot of the inlet pressure (□) and the radial compression pressure (○) versus the flow-rate for the second radial compression column. The compression chamber is sealed at a compression pressure of 6.9 bar when there is no flow through the column. Lines are the best linear fit to the data.

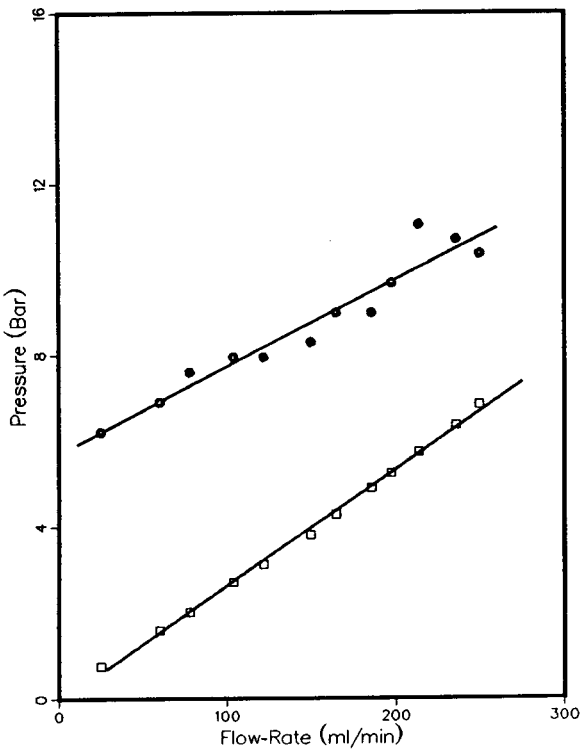

Fig. 7. Plot of the inlet pressure (□) and the radial compression pressure (●) versus the flow-rate for the third radial compression column. The compression chamber is sealed at a compression pressure of 5.2 bar when there is no flow through the column. Lines are the best linear fit to the data.

an intercept of -0.159 ± 0.088 bar, not significantly different from 0. From this slope it is easy to derive the apparent column permeability, hence an average hydrodynamic particle size using Eq. 2. However, the external porosity decreases during these measurements and it is not possible at this stage to account correctly for this effect. For example, the average hydrodynamic particle sizes derived from Darcy's equation (Eq. 1) from the data obtained with the three columns are 24.60 ± 0.60 μm, 21.20 ± 0.60 μm, and 16.90 ± 0.20 μm for values of the compression pressure of 5.2, 6.9 and 20.7 bar, respectively. Obviously, the particle size cannot vary that much with the compression pressure, but this variation reflects the change in the column permeability due the variation of the external porosity.

Thus, the hydrodynamics in a radial compression column is slightly more complicated than in a regular column. This complexity must be taken into account in method development if the dependence of the flow-rate on the column characteristics is calculated from classical correlations, using Darcy's law and the dependence of the permeability on the particle size as derived from measurements made on an analytical column packed with the same stationary phase. The interdependence of the inlet pressure, the compression pressure and the flow-rate may make calibrations and calculations more complex. In production operation, however, there will be no differences with a conventional column. Possible small flow-rate and compression pressure fluctuations (if the compression chamber is kept close) will be proportional to the inlet pressure fluctuations.

After finishing all experiments with the second radial cartridge it was cut open to inspect its inside. There was a 6 mm thick void space at the column entrance (volume 26.5 cm^3, 3.4% of the total volume). This void volume is nearly equal to the decrease in hold-up volume measured during the experiment reported in Fig. 3, and discussed above. The whole stationary phase was found as a semi-compact, cylindrical block of silica, that could be taken out as one piece and inspected, but crumbled easily in the hand. The appearance of the stationary phase was similar in all parts of the column. Six samples of silica were collected from different sites of the cartridge for particle size analysis. The sites were (1) center of the column entrance, (2) a few mm from the wall at the column entrance, (3) center of the middle cross-section, (4) a few mm from the wall at the middle cross-section, (5) center of the column exit and (6) a few mm from the wall at the exit of column.

The results of the particle size analysis carried out with a Coulter Multisizer are reported in Table 3 and Fig. 8. They show that in spite of the punishing treatments administered (see below, Section 3.6), the packing itself has not suffered to any significant extent. The particle size distributions based on particle volumes and numbers are given in Fig. 8a and b, respectively. The

Table 3
Particle size distribution of the packing material after aging

Sample	Dv50 (μm)	Dv10/ Dv90	Dv50/ Dp50
RG1020-C18, virgin	19.98	1.63	1.19
1	20.44	1.56	1.20
2	20.60	1.56	1.14
3	20.55	1.56	1.19
4	20.57	1.56	1.16
5	20.53	1.55	1.18
6	20.49	1.57	1.19
2 (repeat)	20.55	1.56	1.16

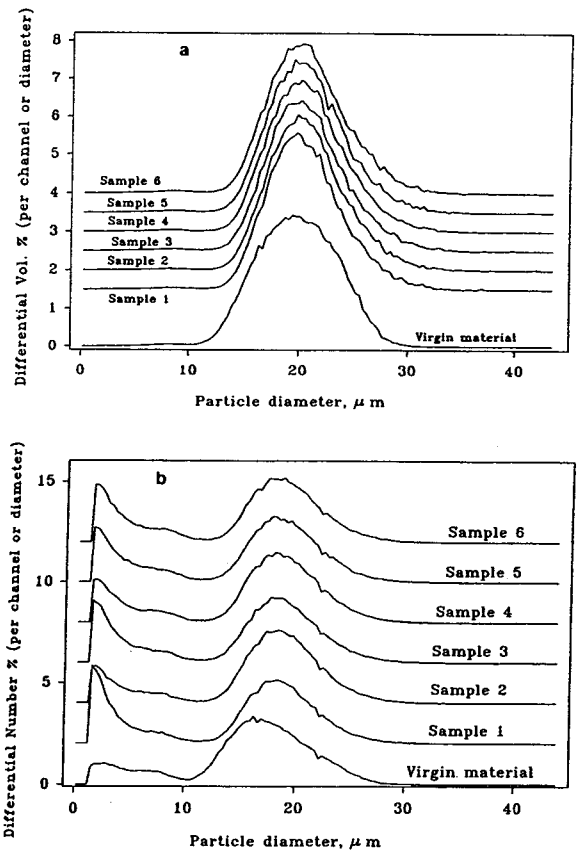

Fig. 8. Particle size distribution of samples of the stationary phase. Results obtained with a Coulter counter. Bottom curve, original material. Samples: 1 = column inlet, center; 2 = column inlet, wall; 3 = column middle, center; 4 = column middle, wall; 5 = column outlet, wall; 6 = column outlet, center. (a) Differential volume distribution, (b) differential number distribution.

volume distributions of all the samples are identical within the limits of errors, and the difference from the distribution in the virgin material is barely significant. The number distributions are slightly different, with a two to three time increase in the number of small particles (below 5 μm) which seems to have very limited consequences. Furthermore, the data reported here are not in agreement with the results previously reported by Marme et al. [13]. Our results suggest on the contrary that there is no migration of the fine particles downstream the column to any significant degree, even after 100 h of aging and a comparable amount of time devoted to various measurements. If anything, there is slightly more fine particles at the entrance of the column (samples 1, 2) than at the exit (samples 5, 6), but the difference is comparable to the error of measurement.

3.4. Effect of radial compression on efficiency

A set of experiments were done at constant flow-rate (200 ml/min) and with various values of the compression pressure to study the possible effect of the compression pressure on the column efficiency. A small sample containing acetone and phenol was injected at each compression pressure. Fig. 9 shows the plot of the reduced plate height versus the compression pressure for the second and the third columns. There is only a moderate effect of the compression pressure on the efficiency of either columns. Although the efficiency of the second column was poor from the beginning (see Table 2), there does not seem to be any significant changes at elevated compression pressures. Paradoxically, the HETP of the third column increases slowly with increasing compression pressure, while we have shown above that the packing becomes denser, more compact, and presumably more homogeneous. Marme et al. [13] claimed that they had identified low-density regions in the packing of their columns. These regions seem to correspond to those still uncompressed during the process of progressively compressing their column. If they exist, their relative importance is expected to

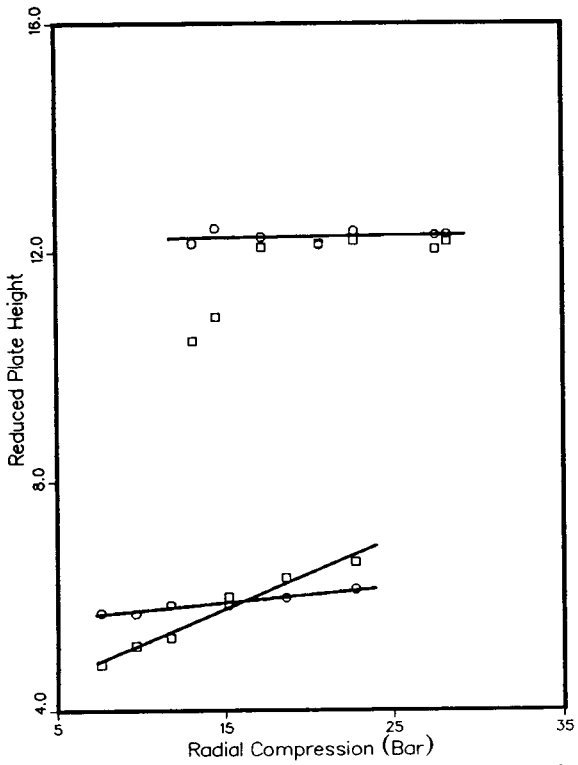

Fig. 9. Effect of the radial compression pressure on the efficiency of the second and third radial columns (17.5 × 7.5 cm). Eluent methanol–water (40:60). Sample: 1.5 ml of acetone (□) and phenol (○) in the eluent. Second radial column (upper data points); flow-rate 200 ml/min. Third radial column (lower data points with fitted line); flow-rate 142 ml/min.

decrease with increasing compression pressure, causing a decrease in the column HETP. This effect does not take place in our experiments. However, as explained above, the packing density of a radially compressed column cannot be entirely homogeneous. This lack of homogeneity, however, does not seem to affect much the efficiency.

3.5. Effect of temperature on the efficiency

Because of the huge thermal mass of the column and the compression chamber, and of the additional influence of the thermal insulation provided by the compression liquid and the plastic wall of the cartridge, the column temperature remains highly constant in a temperature-controlled laboratory. It is nearly impossible to control the temperature of the packing in a radial compression column, nor even the temperature of the column wall itself. Accordingly, no efforts were made to change the column temperature. The only possibility of changing simply the operation temperature is to control the temperature of the mobile phase pumped into the column.

Experiments were carried out to study the possible influence of the eluent temperature if it is different from the initial column temperature, a situation which may occur in practice, either willfully or accidentally. A 2-l bottle of eluent was placed in a temperature-controlled water bath. The bottle content was stirred constantly. The solvent was pumped from the bottle, through the column, and back to the bottle, in closed circuit. At all temperatures different from ambient, there was a slight temperature difference between the solvent in the bottle and the solvent eluting from the column. This difference was minimized by letting the column equilibrate for a long period of time and maintaining a flow-rate of 200 ml/min. When thermal equilibrium was reached (i.e. the solvent temperatures in the bottle and at the column exit were constant), a sample of acetone and phenol was injected, and the column efficiency measured.

The results are reported in Fig. 10, as a plot of the reduced plate height versus the average of the solvent temperatures in the bottle and at the column exit. The effect observed is rather small, may be because the column efficiency is poor ($h = 12$) under the selected experimental conditions (high v) and it is unexpected. The column HETP is minimum at room temperature (ca. 22°C). When the mobile phase and the column wall temperatures are different, a thermal flux takes place, and a radial temperature gradient forms inside the column. The mobile phase viscosity is different along the wall and at the center. The radial thermal flux explains also the temperature difference between the solvent in the bottle and at column exit. As a consequence, the viscosity varies along the column. The vis-

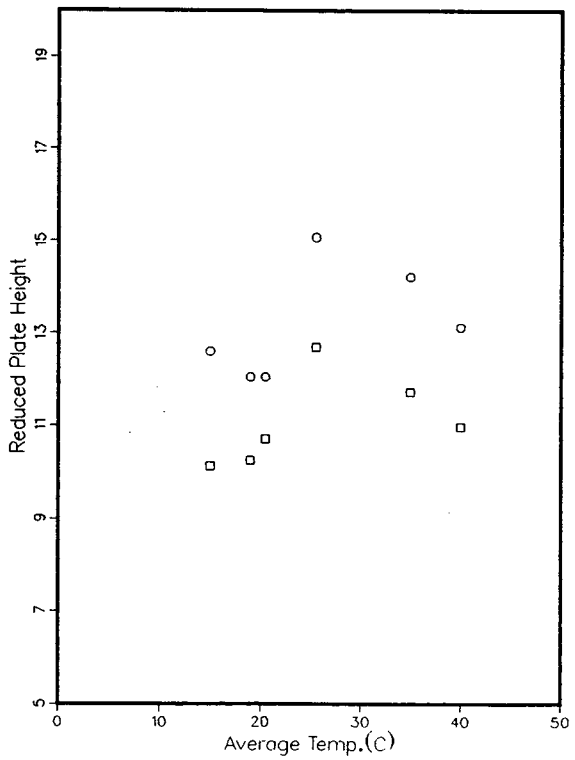

Fig. 10. Effect of the eluent temperature on the efficiency of the second radial column. Eluent: methanol–water (40:60, v/v). Sample: 1.5 ml of a solution of 4% acetone (□) and 4 g/l phenol (○) dissolved in the eluent. Constant flow-rate 200 ml/min. Temperature shown in figure is the average of the temperatures at the inlet and outlet of the column.

cosity gradient causes a mobile phase velocity gradient between the center and the wall, and the isoconcentration surfaces of the sample bands, which should be flat and perpendicular to the column axis, become warped.

This effect increases with increasing temperature difference between column wall and mobile phase. The end result is difficult to predict, however, as we have shown above that the compression stress also is not constant along the column nor along the column radius either. Thus, we superimpose a mobile phase viscosity gradient and a packing density gradient which, both, have probably an approximately cylindrical symmetry. The combination of their effects cannot be predicted at this stage. It could result in an improvement, a degradation, or an insignificant change of the column performance.

It is difficult, however, to explain why the curve is not nearly symmetrical around ambient temperature, and why the HETP goes through a maximum around 30°C, and tends to decrease beyond this temperature. Experiments could not be done at temperatures below 15°C. It does not seem that the decrease in HETP observed at temperatures higher than 30°C could be related to the increase in the diffusion coefficient with increasing temperature, a relatively minor effect [28].

3.6. Channel formation and repair by applying radial compression

Channel formation can take place inside large-diameter columns. A set of experiments were done to test the feasibility of the application of an elevated radial compression pressure to repair these channels. Biotage has demonstrated publicly that if a cartridge was dropped several times from a sufficient height, its efficiency decreased dramatically, but that this efficiency could be restored by applying a higher radial compression pressure. However, no evidence was produced for the presence of channels in the column. We found that it is easy to destroy the column efficiency by running the eluent for several minutes without applying any radial compression pressure. This could be expected since when the mobile phase flows through the column there is an axial pressure gradient. The mobile phase under pressure at the column inlet tends to expand the cartridge wall, fragmenting the packed bed in the process. We performed two sets of similar experiments with the first and the second cartridges.

Fig. 11 shows chromatograms which demonstrate the presence of channels in the degraded column and their repair by applying a high radial compression pressure. This figure was obtained for the second column, at a flow-rate of 206 ml/min. The five chromatograms were obtained for increasing values of the radial compression pressure, from 0 to 27.6 bar. The *y*-axis gives the detector response (UV absorbance). The con-

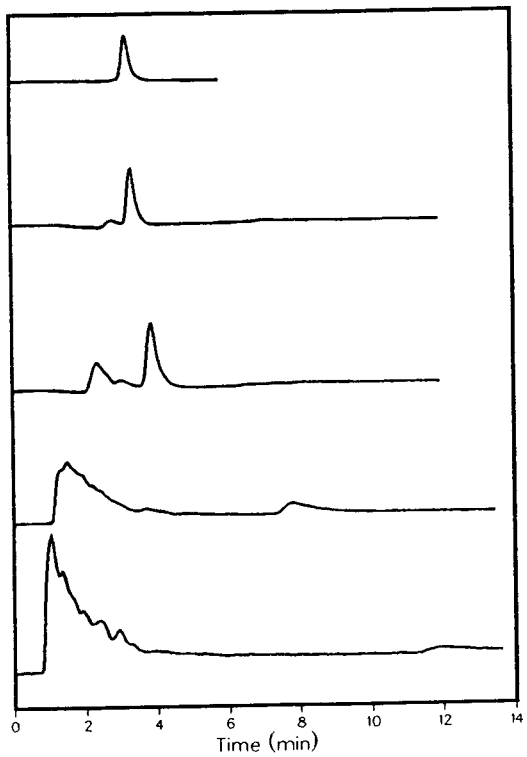

Fig. 11. Typical chromatograms obtained with the second column, and demonstrating the formation (bottom) and progressive healing of channels in the packing upon increase of the radial compression pressure (bottom to top). Solvent: methanol–water (40:60). Sample: 1.5 ml of 4% acetone in the eluent. Flow-rate: 206 ml/min. The *y*-axis is not drawn to the same scale for all the chromatograms. Radial compression pressure (from bottom to top chromatograms): 0, 6.9, 13.8, 20.7 and 27.6 bar.

centration scale decreases from the bottom to the top of the figure, in order to expand the ordinate of the poor chromatograms, for the sake of clarity.

The bottom chromatogram in Fig. 11 exhibits several overlapping, early eluting peaks, beginning around 1 min and a last, small, slowly eluting peak at around 12 min, which is strongly unsymmetrical. The early peaks are due to the sample molecules which are carried with the solvent that passes through the high-permeability channels. The later peak with a long retention is due to the sample molecules which pass through the core of the bed, where the mobile phase velocity is low, due to the channelling. As the radial compression pressure is increased and the bed is progressively compressed, the channels begin to close. The solvent velocity through these channels decreases while the solvent velocity through the bed core increases. As a result, the difference between the retention times of the fastest and slowest peaks decreases, and the various bands begin to coalesce. Eventually, all the peaks have merged when the radial compression pressure reaches 27.6 bar, indicating total repair of the channelling.

Similar results were obtained with the first column, and a more detailed report is given in Table 4. A 1.5-ml sample of a 4% acetone solution was injected while the radial compression pressure was first increased progressively from 0 to 33.1 bar, for a flow-rate of 110 ml/min, and then decreased gradually, until the column showed new signs of channeling. Finally, a few experiments were done with high radial compression pressures to regain the normal column efficiency. Detailed information on the results of these experiments are given in Table 4.

At low compression pressures, and up to 6.9 bar, the channels were such that there was a number of overlapping peaks eluting after around 3 min, while the main peak eluted after more than 10 min. Under normal circumstances, acetone elutes at 4.9 min. As the compression pressure increases, the retention times of the first group of overlapping peaks increase, and these peaks merge. The retention time of the major peak (peak 2) keeps decreasing with increasing compression pressure until, at 27.6 bar, there was a single peak. This suggests that the channels were closed.

In the second part of the experiment, when the compression pressure is decreased again, the column continued to show its restored efficiency until the compression pressure drops to 13.8 bar. At this point, the retention time and the efficiency of the acetone peak were 6.12 min and 1723 plates, respectively, as opposed to the values of 4.908 min and 1877 plates, respectively, under normal conditions, with a compression pressure of only 6.9 bar before the series of experiments. Obviously, the column efficiency is

Table 4
Packing repair by radial compression

Bar	No. of major peaks	t_R (min)		Efficiency Peak 2	Inference
		Peak 1	Peak 2		
6.9	1	–	4.908	1 877	Normal operation
0	2	1.88	–	–	Multiple overlapping peaks in the first peak
4.1	2	2.61	> 12	–	Same as above
5.5	2	2.68	> 10	–	Same as above
6.9	2	3.07	10.35	–	Same as above
8.3	2	3.33	9.28	–	Same as above
10.3	2	2.69	8.06	976	2nd peak larger than the first peak
12.4	2	4.32	7.03	1 695	Intensity of 2nd peak larger than 1st peak
13.8	2	4.96	7.00	1 658	2nd peak 5 times larger than first; column left overnight at 13.8 bar
13.8	2	5.18	6.51	1 871	2nd peak 7 times larger than first
20.7	2	5.19	6.28	17 404	2nd peak 12 times larger than the first; average of two injections
27.6	1	–	6.03	1 573	Average of three injections
33.1	1	–	5.92	1 519	Average of three injections
27.6	1	–	5.97	1 524	Average of three injections
24.1	1	–	6.02	1 605	Average of three injections
20.7	1	–	6.01	1 638	Average of two injections
17.2	1	–	6.06	1 720	Average of three injections
13.8	1	–	6.12	1 723	Average of three injections
10.3	2	5.50	6.24	1 927	Average of three injections
13.8	2	5.36	6.22	1 997	2nd peak 16 times larger than the first
27.6	1	–	5.95	1 591	
22.8	1	–	5.93	1 545	Column left overnight at 27.6 bar but compression decreased to 22.8 bar

completely destroyed by dropping too low the compression pressure. It can be restored to a large extent by applying again a high compression pressure. Note that at 10.3 bar (bottom of Table 4) the column efficiency is high although it still has some channels as indicated by the presence of a second peak.

4. Conclusions

The radial compression technology achieves its goal of offering stable columns with reasonable, reliable efficiency. After several hundred hours of continuous operation, including a number of stressful concentration gradients of the mobile phase composition, the efficiency of the columns did not exhibit any significant changes (Table 2), nor did the stationary phase characteristics. Applying a high radial compression pressure can be used to restore the performance of a badly damaged column, suffering from an acute case of channelling. However, radial compression does not improve significantly the efficiency of good columns. The availability of columns made to order by a specialist is an advantage of the current implementation of this dynamic compression technology. On the other hand, a possible source of loss of efficiency under long term operation arises from the practical impossibility to wash and clean the column inlet and outlet frits without replacing the whole cartridge. These disks are presumably clean on a new cartridge but they are crimped in the cartridge and cannot be replaced by the user.

The study of the influence of the eluent temperature on the column efficiency should be pursued further. It is doubtful, however, that it

will lead to another conclusion than pointing out the need to keep the column temperature constant and pump into the column an eluent which is at the same temperature as the column wall. We are of the opinion, however, that the most important problems to study in the near future are those related to the porosity and the permeability of columns, in connection with dynamic compression technologies, and those involved in the scaling-up of the process, when chromatographic, thermodynamic, kinetic, and hydrodynamic data acquired on analytical size columns are used to predict the behavior of large size preparative columns. Work is in progress along these directions and results will be reported in the near future.

Acknowledgements

This work has been supported in part by Grant CHE-9201662 of the National Science Foundation and by the cooperative agreement between the University of Tennessee and the Oak Ridge National Laboratory. We acknowledge the long-term, free loan by Biotage, Inc. (Charlottesville, VA, USA) of the Model Kiloprep 100 pump, the Model Kiloprep 100 radial compression module and the Linear Scientific UV detector, and the gift of the column cartridges. We thank The PQ Corporation (Conshohocken, PA, USA) for the generous gift of 5 kg of IMPAQ RG1020C18 and the loan of a Linear Scientific UV detector. We appreciate the measurements of the particle size distributions of samples taken from the second cartridge, made by Neil Miller.

We are grateful to Kevin Holland (Biotage), Neil Miller (The PQ Corporation), Klaus Lohse (BTR Separations) and A.M. Katti (Mallinckrodt Specialty Chemicals, St. Louis, MO, USA) for insightful discussions.

References

[1] *J. Chromatogr.*, Vols. 484 (1989), 556 (1991), 557 (1991) and 590 (1992).
[2] J.H. Knox and H.M. Pyper, *J. Chromatogr.*, 363 (1986) 1.
[3] G. Guiochon, S. Golshan-Shirazi and A.M. Katti, *Fundamentals of Preparative and Non-Linear Chromatography*, Academic Press, Boston, MA, 1994.
[4] L.R. Snyder, J.W. Dolan, D.E. Antle and G.B. Cox, *Chromatographia*, 24 (1987) 24.
[5] J.E. Eble, R.L. Grob and L.R. Snyder, *J. Chromatogr.*, 405 (1987) 1.
[6] L.R. Snyder, J.W. Dolan and G.B. Cox, *J. Chromatogr.*, 484 (1989) 437.
[7] S. Golshan-Shirazi and G. Guiochon, *Anal. Chem.*, 61 (1989) 1368.
[8] S. Golshan-Shirazi and G. Guiochon, *J. Chromatogr.*, 517 (1990) 229.
[9] A. Felinger and G. Guiochon, *Biotechnol. Bioeng.*, 41 (1993) 134.
[10] J.C. Giddings, *J. Chromatogr. Sci.*, 1 (1963) 11.
[11] R.M. Nicoud and M. Perrut, in G. Ganetsos and P.E. Barker (Editors), *Preparative and Production Scale Chromatography*, Marcel Dekker, New York, 1992, p. 47.
[12] M. Kaminski, *J. Chromatogr.*, 589 (1992) 61.
[13] S. Marme, M. Hallmann, K.K. Unger, E. Baumeister, K. Albert and E. Bayer, in M. Perrut (Editor), *PREP'92*, Société Française de Chimie, Paris, 1992, p. 135.
[14] J.G. Atwood, G.J. Schmidt and W. Slavin, *J. Chromatogr.*, 171 (1979) 109.
[15] D.R. Absolom and R.A. Barford, *Anal. Chem.*, 60 (1988) 210.
[16] E. Godbille and P. Devaux, *J. Chromatogr.*, 122 (1976) 317.
[17] J.N. Little, R.L. Cotter, J.A. Prendergast and P.D. McDonald, *J. Chromatogr.*, 126 (1976) 439.
[18] H. Colin, P. Hilaireau and J. de Tournemire, *LC·GC*, 8(4) (1990).
[19] M. Sarker and G. Guiochon, *J. Chromatogr. A*, submitted for publication.
[20] P.D. McDonald, R.V. Vivilecchia and D.R. Lorenz, *US Pat.*, 4 211 658 (1980).
[21] C.W. Rausch, Y. Tuvin and U.D. Neue, *US Pat.*, 4 228 007 (1980).
[22] P.D. McDonald and C.W. Rausch, *US Pat.*, 4 250 035 (1981).
[23] M. Verzele, M. de Coninck, J. Vindevogel and C. Dewaele, *J. Chromatogr.*, 450 (1988) 47.
[24] C.R. Wilke and P. Chang, *AIChE J.*, 1 (1955) 264.
[25] J.J. Van Deemter, F.J. Zuiderweg and A. Klinkenberg, *Chem. Eng. Sci.*, 5 (1956) 271.
[26] R.B. Bird, W.E. Stewart and E.N. Lightfoot, *Transport Phenomena*, Wiley, New York, 1960.
[27] D.W. Taylor, *Fundamentals of Soil Mechanics*, Wiley, New York, 1948.
[28] H. Colin, J.C. Diez-Masa, T. Czaychowska, I. Miedziak and G. Guiochon, *J. Chromatogr.*, 167 (1978) 41.

ELSEVIER

Journal of Chromatography A, 683 (1994) 311–320

JOURNAL OF CHROMATOGRAPHY A

Effect of feed concentration on the preparative separation of systems having reversed selectivity

Shenggen Hu[1], Duong D. Do*

Department of Chemical Engineering, University of Queensland, Brisbane, Qld. 4072, Australia

First received 2 June 1993; revised manuscript received 25 May 1994

Abstract

A theoretical study of the effect of feed concentration on the preparative performance of liquid chromatography has been performed for systems having solute-concentration-dependent selectivity. The investigations were based on the numerical simulations of a detailed rate-equation model and the local equilibrium distribution between the fluid and adsorbed phases is assumed to follow a quadratic isotherm. The elimination and the utilisation of the selectivity reversal have been discussed in terms of the optimisation of the preparative performance.

1. Introduction

The establishment of a comprehensive theoretical framework relating the preparative performance of liquid chromatography to the competitive adsorption isotherm, the column parameters and the operating conditions is an important subject which has been actively studied in recent years. Considerable effort has been made to investigate the effects of various factors using numerical or analytical approaches. Felinger and Guiochon [1] have shown that the maximum production rates were obtained for very low values of the retention factor of the first component, of the order of 0.3–0.5. Ghodbane and Guiochon [2] investigated the influence of the relative retention on the column loading capacity and observed that the optimal production rate increases with an increase in the relative retention. By combining an analytical solution of the ideal model of chromatography with the classical expressions of band-broadening effects due to the finite efficiency, Golshan-Shirazi and Guiochon [3] derived expressions for the dependence of the production rate of the second solute of a binary mixture on the relative retention. The effect of mobile phase flow-rate on production rate and recovery in overloaded chromatographic column was also investigated from a theoretical standpoint [4].

Among the issues that have been addressed, one of the simplest, yet of the greatest practical importance, is how the feed concentration affects the preparative performance of liquid chromatography. Knox and Pyper [5] developed an equation for calculating the conditions for the optimum throughput, assuming no competitive adsorption and 100% yield and 100% purity. They concluded that concentration overloading provides the greatest throughput. The numerical

* Corresponding author.

[1] Present address: Queensland Centre for Advanced Technologies, CSIRO, Qld. 4069, Australia.

0021-9673/94/$07.00
SSDI 0021-9673(94)00488-U

simulations carried out by Katti and Guiochon [6] have demonstrated that low-volume, concentrated samples give higher production rates. Using the Craig model, CRAIGSM, to simulate the chromatogram of a binary mixture, Cretier et al. [7] confirmed the existence of the optimum injection concentrations corresponding to the maximum recovered amount of the solute of interest. They also found that the optimum injection concentration is an increasing function of column efficiency. Although the investigations published so far [6–9] have shown that increasing feed concentration is beneficial to the improvement of the preparative performance of liquid chromatography, these studies were basically limited to the cases having Langmuir competitive isotherms, in which the separation factor is a constant.

The Langmuir competitive isotherm is a good first-order approximation of the adsorption behaviour for similar compounds and especially for closely related isomers. In some practical situations, however, compounds would undergo strong sorbate–sorbate interactions in the stationary phase, violating the basic assumption of Langmuir isotherms. Depending on the comparative strengths of the interactions among the molecules of the same species and those between species, deviation from the adsorption behaviour of the Langmuir isotherm may be expected. It has been known that the selectivity in some chromatographic systems depends on the solute concentration, and selectivity reversal may occur in the operational concentration range [10]. The reversal of the elution order of *cis*- and *trans*-androsterone with increasing sample size has been observed [11]. The Langmuir competitive isotherm fails to explain the phenomena of peak reversal, since it assumes a constant separation factor. It has been demonstrated that the LeVan–Vermeulen isotherm can predict the inversion of the elution order of the components of binary mixtures at larger sample sizes [12]. A new isotherm with uneven saturation capacities, induced either by size exclusion or by racemic discrimination of the active sites toward the solutes, was also used to simulate the phenomena of peak reversals [13]. It has been recognised that the inversion of elution order is usually a consequence of selectivity reversal at high concentration. However, the peak reversal in elution occurs only when the sample size is so large that the concentrated sample is not diluted too much during migration inside the column. Otherwise, the sample will be quickly diluted, and the reversal may not occur at all.

Although there have been some studies directed to the phenomena of selectivity reversal at high concentrations, the effect of feed concentration on the preparative performance of liquid chromatography has not yet been well addressed for systems having solute-concentration-dependent selectivity. This work is devoted to deal with this effect by means of the simulations based on a general rate-equation model proposed previously [14].

2. Description of simulated cases

2.1. Equilibrium isotherm

The quadratic isotherm [15,16], suggested by statistical thermodynamics, was selected as the isotherm model for the simulations in this work:

$$q_1 = \frac{A_1 C_1 + A_{12} C_1 C_2}{1 + B_1 C_1 + B_2 C_2 + B_{12} C_1 C_2} \tag{1a}$$

$$q_2 = \frac{A_2 C_2 + A_{21} C_1 C_2}{1 + B_1 C_1 + B_2 C_2 + B_{21} C_1 C_2} \tag{1b}$$

where solute 1 is the early-eluted component at a very small sample size, and solute 2 is the late-eluted component. q_i and C_i are the concentrations of the component i at equilibrium in the stationary and mobile phases, respectively. All concentration units are in mg/ml. A_i, B_i, A_{ij} and B_{ij} are the isotherm parameters, and $B_{12} = B_{21}$. According to the physical meaning of these parameters, A_i, B_i and B_{ij} must be positive, and A_{ij} could be positive or negative. This isotherm defines a solute-concentration-dependent selectivity as follows:

$$S_f = \frac{q_2/C_2}{q_1/C_1} = \frac{A_2 + A_{21} C_1}{A_1 + A_{12} C_2} \tag{2}$$

Depending on the parameter values in Eq. 2, a binary system described by the quadratic isotherm could be with or without selectivity reversal. This work will focus attention to cases having selectivity reversal. By setting S_f (in Eq. 2) equal to 1, the rearrangement of the equation gives

$$C_1 = \frac{A_1 - A_2}{A_{21}} + \frac{A_{12}}{A_{21}} \cdot C_2 \quad (3)$$

This equation defines a boundary which divides the concentration range into two zones. One is for $S_f > 1$, and the other for $S_f < 1$. Although the sign of both A_{12} and A_{21} could be positive or negative, the combination of negative A_{12} and positive A_{21} would produce negative C_1 from Eq. 3 for any positive C_2. This case is physically unrealistic and will be not considered in this work. There are three physically possible cases in terms of the sign combinations of A_{12} and A_{21}. The isotherm parameters for these three cases (i.e. cases 1, 2 and 3) are presented in Table 1. These parameter values were chosen with reference to some experimental data [17]. Lines of C_1 versus C_2 have been plotted as shown in Fig. 1. It is clear by an examination of Fig. 1 that the separation factor is changed from $S_f < 1$ to $S_f > 1$ when the initial high feed concentrations, at which S_f is less than 1, are diluted to a certain extent.

The choice of the quadratic isotherm was based on the considerations that this isotherm model not only defines a solute-concentration-dependent selectivity but also has the theoretical rigour of statistical thermodynamics. In the comparison of various isotherm models for prediction of competitive adsorption data [17], it has been shown that the quadratic isotherm with seven floating parameters gives excellent fit of the experimental data. Because of the seven adjustable parameters, the quadratic isotherm could be fitted to adsorption data of most practical mixtures better than others. The theoretical soundness and empirical adaptability of the selected isotherm would ensure that the choice of the quadratic isotherm is more reasonable than others for the objective in this work.

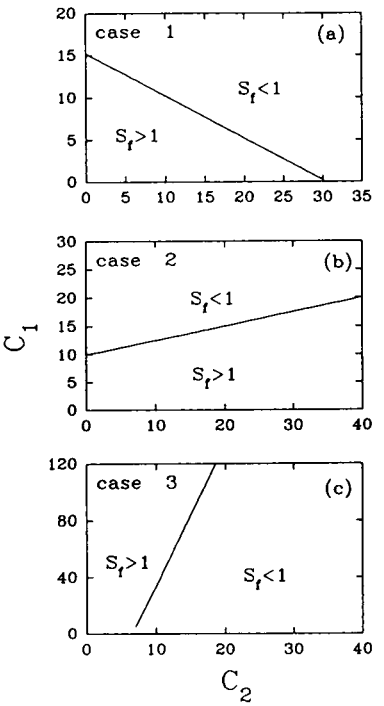

Fig. 1. Concentration zones giving $S_f > 1$ or $S_f < 1$.

2.2. Simulation model and conditions

The aim of this work is to study the effect of feed concentration on the preparative separation for systems with selectivity reversal by means of

Table 1
Parameters of quadratic isotherm

Case	A_1	A_2	B_1	B_2	A_{12}	A_{21}	B_{12}
1	2.0	2.76	0.04	0.065	0.025	−0.05	0.01
2	2.0	2.80	0.04	0.065	−0.02	−0.08	0.01
3	2.2	2.86	0.03	0.06	0.1	0.01	0.01

numerical simulations of a model. The feed concentration studied may be relatively high. Despite the numerous applications of lumped parameter models, the lumped kinetic coefficients in these models have to be solute-concentration dependent in order to accurately predict elution profiles for cases with high feed concentration and large sample size [18]. Because of this limitation, a simple lumped kinetic model with constant (i.e. solute-concentration independent) lumped parameters may be not sufficient for studies on selectivity reversal at high feed concentration. Therefore, a detailed rate-equation model, in which parameters, such as pore diffusivity, film mass transfer coefficient and axial diffusion coefficient, are basically independent of solute concentration, was used in the simulations of this work. The details of the model formulation and the numerical solution procedure based on the method of orthogonal collocation on finite elements were reported elsewhere [14].

The column for the simulations in this chapter was chosen as follows: column length $L = 25$ cm; average particle diameter $d_p = 10$ μm; void fraction of the packed bed $\epsilon_b = 0.5$; particle porosity $\epsilon_p = 0.4$. The superficial velocity, v_f, is $1.2 \cdot 10^{-4}$ m/s, which is equivalent to a reduced velocity ($v_f d_p / \epsilon_b D_{AB}$) of 40. The corresponding pressure drop of the column at this velocity is about 20 atm (1 atm = 101 325 Pa). The physical properties of the system are assumed to be as follows: the viscosity of the mobile phase was $\mu = 1.3$ cP; the solvent density was 1 g/ml. The molecular diffusivity of solute in bulk phase was $D_{AB} = 6 \cdot 10^{-11}$ m^2/s [19] and the pore diffusivity of solutes was $D_p = 8 \cdot 10^{-12}$ m^2/s. The Peclet number (Pe), accounting axial dispersion, and the film mass transfer coefficient (k_f), estimated by the correlations in literature [20,21], were 10 000 and $2 \cdot 10^{-5}$ m/s, respectively.

3. Results and discussion

The simulations of elution profiles were carried out for various feed compositions and concentrations by the numerical solutions of the dynamic model, using the model parameters in the previous section. The production rate and recovery yield were then determined from the simulated elution profiles. The definitions of production rate, recovery yield and load factor are the same as those in a previous report [14]. The product purity was set to be 99% for all the simulations.

The production rates (P) and recovery yields (Y) of case 1 under different feed concentrations were plotted against load factor (L_f) in Figs. 2 and 3 for feed composition 1:1. It was shown in these figures that the use of a properly diluted feed solution would permit an improvement in both production rate and the corresponding recovery yield. The maximum production rates of both solutes were increased more than 25%, when the feed concentrations were reduced from 40/40 to 5/5. However, the over-diluted feed solution (i.e. the feed concentrations are 1/1) does not enjoy this improvement. This is because the production rate depends not only on the separation factor but also on the column ad-

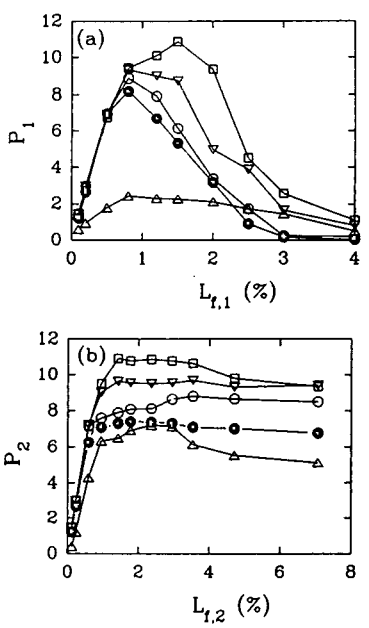

Fig. 2. Production rate versus load factor for case 1. Feed concentrations (C_1/C_2): ● = 40/40; ○ = 20/20; ▽ = 10/10; □ = 5/5; △ = 1/1.

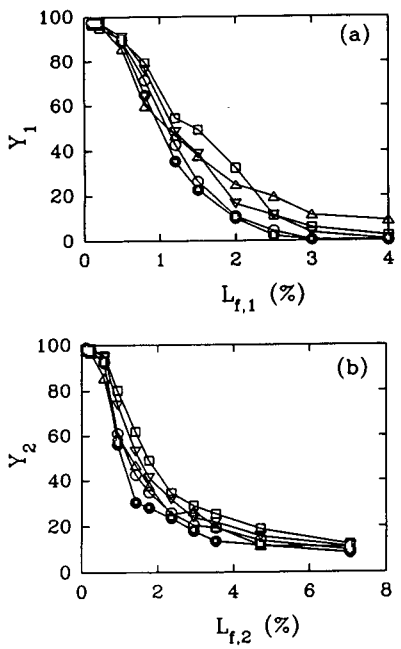

Fig. 3. Recovery yield versus load factor for case 1. Feed concentrations (C_1/C_2): ● = 40/40; ○ = 20/20; ▽ = 10/10; □ = 5/5; △ = 1/1.

sorption capacity which is in equilibrium with the feed concentration. It is suggested from these results that the production rates under very high recovery yield (i.e. corresponding low load factor) are not sensitive to the feed concentrations. The recovery yields corresponding to the maximum production rates are not very high. If this moderate recovery yield is acceptable for a given separation, the dilution of concentrated feed solution would be a worthwhile practice at least for a system such as case 1. The improvement on the preparative performance by the dilution of concentrated feed solution can be explained by the elimination of selectivity reversal. The separation factor for case 1 at the feed concentrations of 40/40 is less than 1, which means a selectivity reversal. As a consequence of the selectivity reversal, the solutes would undergo a certain degree of elution inversion, depending on the sample size. When the feed concentrations of both solutes are reduced to 5, the separation factor is always larger than 1 in the injection as well as in the whole process of elution, and the separation of the solute bands, therefore, consistently proceeds.

The elution profiles at load factors of 0.5 and 1.5% for the two different feed concentrations were shown in Fig. 4. It can be seen by comparing the elution profiles in Fig. 4a that the feed concentration has no significant influence on the touching-band separation. The difference in the retention times of different feed concentrations is due to the longer injection duration for the lower feed concentration at a fixed injection amount. The results in Figs. 4a and b imply that the selectivity reversal arising from high feed concentrations does not affect the separation with the requirement of very high recovery yield. The reason for this is that a small volume of sample solution can be quickly diluted due to the smoothing effect of axial dispersion and mass transfer resistance. On the contrary, the feed concentration does affect the separation at the load factor of 1.5% as shown in Fig. 4b. The elution profiles in the figure indicated that the separation under a lower feed concentration is

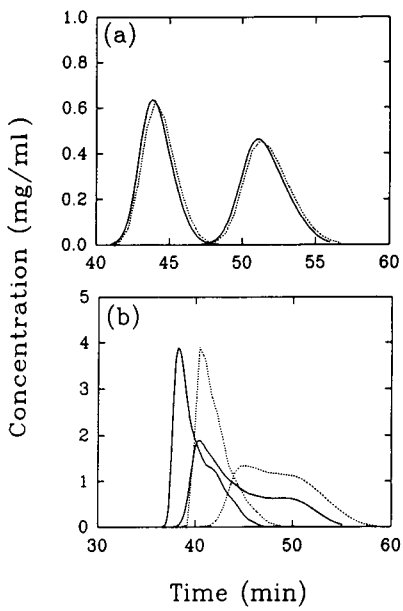

Fig. 4. Elution profiles for different feed concentrations for case 1. Feed concentration (C_1/C_2): solid lines, 40/40; dotted lines, 5/5. Sample size: (a) $L_{f,i} = 0.5\%$; (b) $L_{f,i} = 1.5\%$.

better than that for a high feed concentration. Although the elution profiles in Fig. 4b show no peak reversal, the elution order of the fronts of solute bands was indeed reversed to some extent during the injection and the early stage of elution, and then back to normal due to the dilution of band concentrations. It is the transient selectivity reversal that negatively influence the band separation. Fig. 4b also illustrates that there is no much difference on the peak heights for a given load factor, even though the feed concentrations were significantly different. This feature is particularly useful in practice, since the product concentrations are not significantly decreased by the proper dilution of feed solution.

The production rates and recovery yields of case 1 were presented in Figs. 5 and 6 for feed composition 5:1, and in Figs. 7 and 8 for feed composition 1:5. The production rates for diluted feed solutions at favourable sample sizes are always higher than those for higher feed concentrations, no matter what feed composition is involved. The corresponding recovery yields

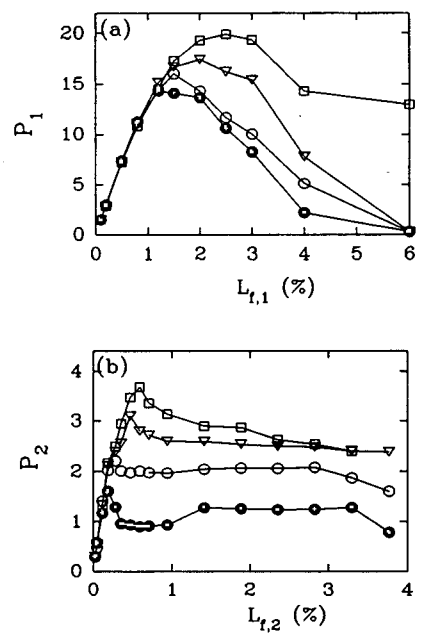

Fig. 5. Production rate versus load factor for case 1. Feed concentrations (C_1/C_2): ● = 40/8; ○ = 20/4; ▽ = 10/2; □ = 5/1.

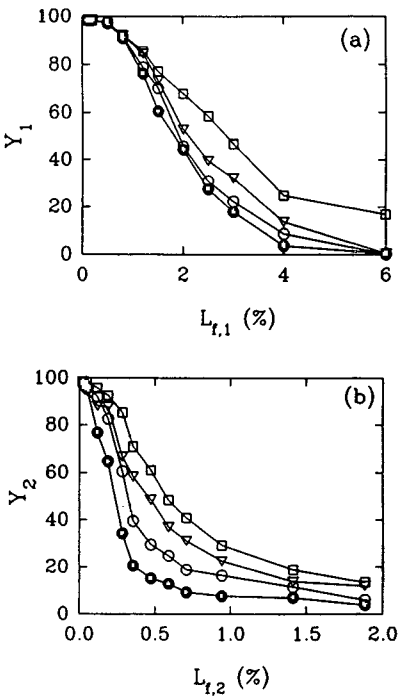

Fig. 6. Recovery yield versus load factor for case 1. Feed concentrations (C_1/C_2): ● = 40/8; ○ = 20/4; ▽ = 10/2; □ = 5/1.

are also increased with a decrease in feed concentration. The separation factor corresponding the initial feed concentrations (i.e. 40/8 or 8/40) is changed from $S_f < 1$ to $S_f > 1$ after dilution to certain extent. Obviously, the elimination of selectivity reversal is also responsible for the improvement on the preparative performance for feed mixtures with compositions other than 1:1.

To investigate the influence of the isotherm parameters, simulations were performed for cases 2 and 3. Figs. 9–12 show the production rates and recovery yields as functions of load factor for these two cases. The feed compositions and concentrations corresponding to the filled symbols in these figures were selected such that the separation factors are less than 1. By the stepwise dilution of the feed solution, the maximum production rates and the corresponding recovery yield can be improved. Similar to the results of case 1, the feed concentration has no effect on the separation having a high recovery

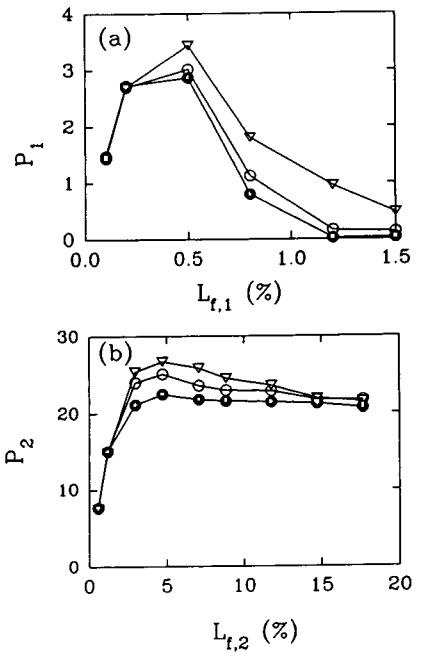

Fig. 7. Production rate versus load factor for case 1. Feed concentrations (C_1/C_2): ● = 8/40; ○ = 4/20; ▽ = 2/10.

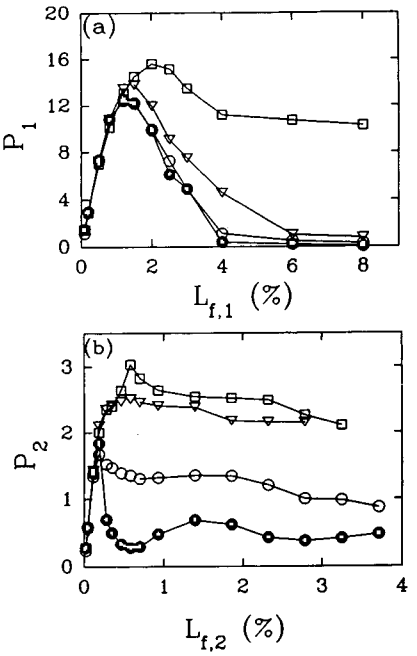

Fig. 9. Production rate versus load factor for case 2. Feed concentrations (C_1/C_2): ● = 40/8; ○ = 20/4; ▽ = 10/2; □ = 5/1.

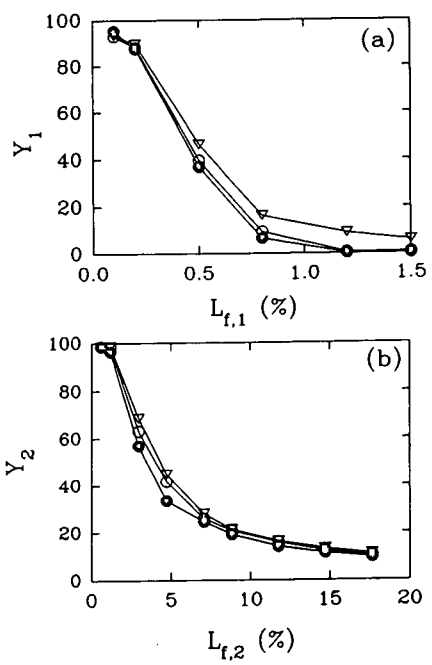

Fig. 8. Recovery yield versus load factor for case 1. Feed concentrations (C_1/C_2): ● = 8/40; ○ = 4/20; ▽ = 2/10.

yield. Simulations were also carried out to study the effect of the dilution of high feed concentrations which are located in the zones of $S_f > 1$, and the results show that the dilution for these situations have negative effects. Undoubtedly, the dilution of feed solution with high concentration would be an advantage only if the selectivity determined by the feed concentrations is reversed.

So far, we have demonstrated that the elimination of selectivity reversal by the dilution can improve the production rate and recovery yield at appropriate sample sizes. On the other hand, the selectivity reversal can be utilised to increase the production rate of solute 2, but the corresponding recovery yield is low. Fig. 13 shows the inversion of elution order observed at large sample sizes. When the inversion of elution order occurs, the band front of solute 1 emerges later than solute 2, while the rear boundary of the band for solute 1 is eluted out earlier than solute 2. As shown in the figure, the concentration

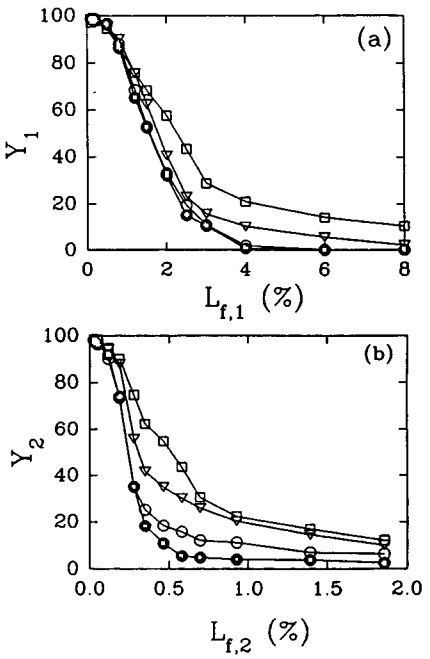

Fig. 10. Recovery yield versus load factor for case 2. Feed concentrations (C_1/C_2): ● = 40/8; ○ = 20/4; ▽ = 10/2; □ = 5/1.

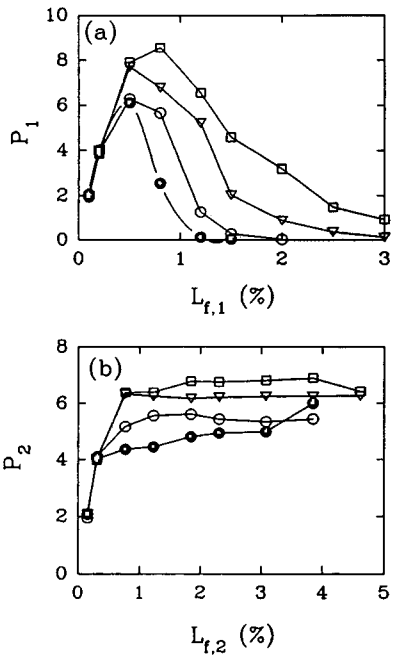

Fig. 11. Production rate versus load factor for case 3. Feed concentrations (C_1/C_2): ● = 40/40; ○ = 20/20; ▽ = 10/10; □ = 5/5.

band of solute 1 is completely embraced by the band of solute 2, and the recovery of pure solute 1 from the elution fractions is, therefore, impossible. However, the elution fractions containing solute 2 with high purity can be collected from the band front and the tailing part. If the selective reversal is maintained sufficiently long by injecting a large sample, the reversal displacement, i.e, solute 2 displaced by solute 1, would occur. As a result, a peak containing nearly pure solute 2 is formed before the band front of solute 1. Intuitively, the smaller the separation factor calculated at the feed concentrations, the stronger the reversed displacement effect. As shown in Fig. 13, the concentration of solute 2 in the first peak is even higher than that in feed solution due to the effect of reversed displacement.

Figs. 14 and 15 show the production rate and recovery yield of solute 2 obtained under the conditions of peak reversal. It is seen that a tremendous increase in the production rate is achieved by the reversal displacement, although the recovery yield remains low. If most of the injected sample can be recycled without causing significant problems, the utilisation of the effect of reversed displacement would provide a means to considerably increase the production rate of solute 2.

The simulations reported in this work are based on the quadratic isotherm which is derived from the statistical thermodynamics. A practical system may obey an isotherm other than the quadratic isotherm. However, the qualitative rules developed in this work could be reasonably extended to systems with other isotherms, as long as the phenomena of selectivity reversal takes place at certain high feed concentrations. Finally, it should be pointed out that the validity of the simulation results and the qualitative rules need no experimental confirmation, since the simulations were based on first principles.

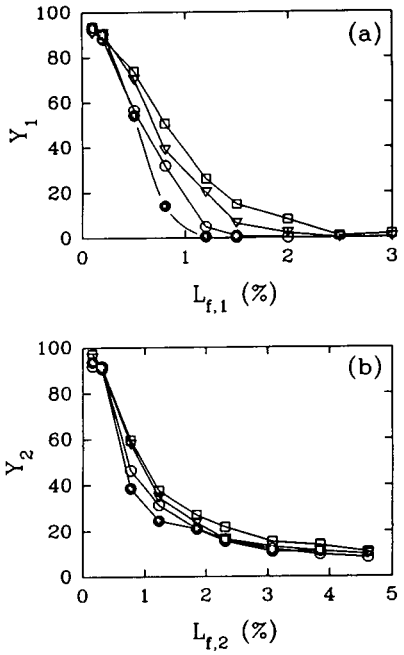

Fig. 12. Recovery yield versus load factor for case 3. Feed concentrations (C_1/C_2): ● = 40/40; ○ = 20/20; ▽ = 10/10; □ = 5/5.

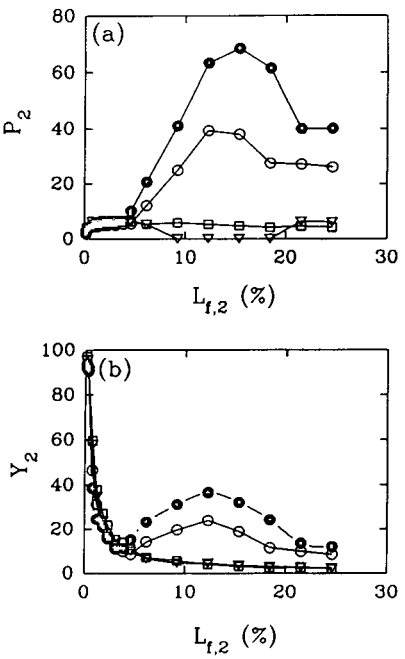

Fig. 14. Production rate and recovery yield of solute 2 for case 3. Feed concentrations (C_1/C_2): ● = 40/40; ○ = 20/20; ▽ = 10/10; □ = 5/5.

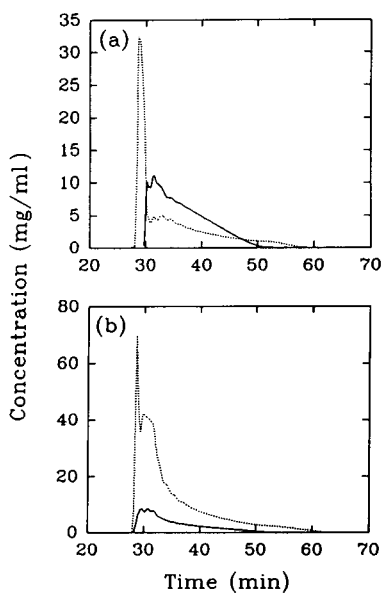

Fig. 13. Elution profiles with peak reversal. (a) Case 3; feed concentrations (C_1/C_2): 40/40; $L_{f,2}$ = 12%. (b) Case 1; feed concentrations (C_1/C_2): 8/40; $L_{f,2}$ = 40%. Solid lines = solute 1; dotted lines = solute 2.

4. Conclusions

It has been demonstrated that the elimination of selectivity reversal, arising from high feed concentrations, by the dilution of feed solution would improve the preparative performance, especially for separations with a medium recovery yield. Cautions are also needed to avoid over-dilution, which gives low production rate. For separations with the requirement of very high recovery yield, the feed solution can be directly injected without the need of dilution, because the feed concentration has no effect on the touching-band separations. In the situation where the recycle of the major fraction of an injected sample is technically and economically feasible, the reversed displacement effect, taking place at large sample sizes, should be implemented in order to maximise the production rate of solute 2, i.e. the late-eluted component at a very small sample size.

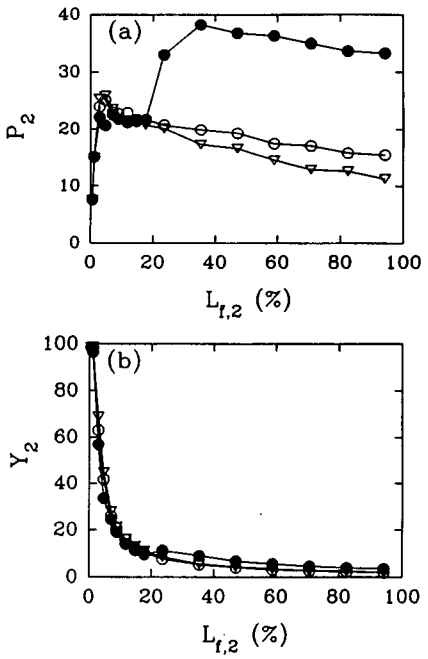

Fig. 15. Production rate and recovery yield of solute 2 for case 1. Feed concentrations (C_1/C_2): ● = 8/40; ○ = 4/20; ▽ = 2/10.

References

[1] A. Felinger and G. Guiochon, *J. Chromatogr.*, 591 (1992) 31.
[2] S. Ghodbane and G. Guiochon, *J. Chromatogr.*, 450 (1988) 27.
[3] S. Golshan-Shirazi and G. Guiochon, *J. Chromatogr.*, 523 (1990) 1.
[4] S. Ghodbane and G. Guiochon, *J. Chromatogr.*, 452 (1988) 209.
[5] J.H. Knox and H.M. Pyper, *J. Chromatogr.*, 363 (1986) 1.
[6] A. Katti and G. Guiochon, *Anal. Chem.*, 61 (1989) 982.
[7] G. Cretier, L. Macherel and J.L. Rocca, *J. Chromatogr.*, 590 (1992) 175.
[8] V. Svoboda, *J. Chromatogr.*, 464 (1989) 1.
[9] J. Newburger and G. Guiochon, *J. Chromatogr.*, 484 (1989) 153.
[10] F.D. Antia and Cs. Horváth, *Ber. Bunsenges. Phys. Chem.*, 93 (1989) 961.
[11] M.J. Gonzales, A. Jaulmes, P. Valentin and C. Vidal-Madjar, *J. Chromatogr.*, 386 (1986) 333.
[12] S. Golshan-Shirazi and G. Guiochon, *J. Chromatogr.*, 545 (1990) 1.
[13] T. Gu, G.-J. Tasi and G.T. Tsao, *AIChE J.*, 37 (1991) 1333.
[14] S.-G. Hu, D.D. Do and Md.M. Hossain, *J. Chromatogr.*, 605 (1992) 175.
[15] D.M. Ruthven, *Principles of Adsorption and Adsorption Processes*, Wiley, New York, 1984.
[16] A.M. Katti, Z. Ma and G. Guiochon, *AIChE J.*, 36 (1990) 1722.
[17] J. Zhu, A.M. Katti and G. Guiochon, *J. Chromatogr.*, 552 (1991) 71.
[18] S. Golshan-Shirazi and G. Guiochon, *J. Chromatogr.*, 603 (1992) 1.
[19] M.T. Tyn and T.M. Gusek, *Biotechnol. Bioeng.*, 35 (1990) 327.
[20] S.F. Chung and C.Y. Wen, *AIChE J.*, 14 (1968) 857.
[21] S.G. Foo and R.G. Rice, *AIChE J.*, 54 (1975) 1149.

ELSEVIER

Journal of Chromatography A, 683 (1994) 321–334

JOURNAL OF CHROMATOGRAPHY A

Gradient elution in micellar liquid chromatography I. Micelle concentration gradient

Lillian S. Madamba-Tan[1], Joost K. Strasters[2], Morteza G. Khaledi*

Department of Chemistry, North Carolina State University, Raleigh, NC 27695-8204, USA

First received 22 June 1993; revised manuscript received 9 May 1994

Abstract

Gradient elution in micellar liquid chromatography (MLC) is discussed. On the basis of the gradient elution theory, first developed by Snyder, equations were derived for the prediction of gradient retention times in micelle concentration gradient from isocratic data. Likewise, partition coefficients into micelles and stationary phase, and subsequently isocratic retention at different micelle concentrations can be estimated from two gradient runs. However, more studies need to be done to achieve better agreement between isocratic and gradient data. The equations will be useful for efficient development of practical separations by MLC.

1. Introduction

Gradient elution in reversed-phase high-performance liquid chromatography has been widely studied over the past years. Snyder and his coworkers [1–5] have derived equations describing gradient elution in hydro–organic reversed-phase liquid chromatography (RPLC) and have extensively studied the theoretical and experimental basis of these equations. This technique has been mainly used to solve the general elution problem that exists in the separation of mixtures containing compounds with a wide range of polarities. Likewise, gradient elution has the advantage of increasing the column peak capacity with adequate resolution as well as increasing detection sensitivity and decreasing band tailing and separation time [4,5]. The major disadvantage is solvent demixing, i.e., the preferential uptake of one mobile phase component by the stationary phase. This would result in a change in the composition of the stationary phase during the gradient run and thus leads to variations in the column dead time. In addition, the column will have to be re-equilibrated with the initial mobile phase composition for repetitive analysis.

In micellar liquid chromatography (MLC), gradient elution can be performed by increasing the micelle concentration (and/or an organic modifier concentration) during the course of the separation. Micelles provide hydrophobic and electrostatic sites of interaction with hydrophobic and ionic compounds in the aqueous media. Hence, the retention of hydrophobic and charged solutes is inversely proportional to micelle concentration. In addition to solvent

* Corresponding author.

[1] Present address: Warner-Lambert Company, 170 Tabor Road, Morris Plains, NJ 07950, USA.

[2] Present address: Sterling Winthrop, 1250 Collegeville Road, P.O. Box 5000, Collegeville, PA 19246, USA.

0021-9673/94/$07.00
SSDI 0021-9673(94)00450-N

strength, selectivity is also greatly influenced by micelle concentration [6].

At moderate concentrations of ionic surfactants, the amount of free surfactant in a micellar solution is approximately constant such that any change in the total surfactant concentration would result only in a change in the micelle concentration [7]. Consequently, the composition of the stationary phase (which is only modified with the monomer surfactant) remains constant during the micelle concentration gradient [8–11]. Therefore, the problem of solvent demixing is solved and column regeneration is not necessary after each gradient run [10,11]. The only re-equilibration process necessary before the next gradient run is to flush the mixer and other pre-column as well as column dead volumes with the initial mobile phase. Hence, this technique can be used for repetitive, routine analysis with considerable savings in time and solvent.

Another alternative to perform gradient elution in MLC is to increase the concentration of an organic solvent (e.g. propanol) within a limited range. In this case, however, the composition of the stationary phase might change since the addition of an organic solvent in the micellar mobile phases results in desorption of ionic surfactants from the stationary phase depending on the concentration of the additive [12]. However, we have observed that limited organic concentration gradient (e.g. 3–15% propanol) can be performed in the presence of micelles without disturbing the column equilibration as will be discussed in the following paper [13]. Cole and Dorsey [14] have recently reported that the presence of a small concentration of propanol can greatly reduce the column re-equilibration time after gradient elution in conventional RPLC. Bear in mind that in the case of adding propanol to the micellar mobile phases, the stationary phase will also be partly modified with the organic modifier as well as with surfactants. In addition, the results from this laboratory have shown that the combination of micelles and organic solvents can provide simultaneous enhancement of separation selectivity and solvent strength [6,15–18].

In this paper, the theory of micelle concentration gradient elution in MLC is discussed and the experimental verification of the theory is presented. In the following paper, the use of organic solvent gradient in MLC will be discussed.

2. Theory

2.1. Gradient retention time

Derivation of the equations to describe micellar gradient elution is analogous to the ones described by Snyder et al. [1,2] for linear solvent strength (LSS) gradients in RPLC. The LSS gradients are linear concentration gradients wherein the concentration of the modifier in the mobile phase is changed with time in a linear manner [19]. This type of gradient was used because it is less complicated to work with and it provides easy calculation of retention as a function of experimental conditions.

The relationship between retention factor and micelle concentration in MLC has been reported [20–23]. The following form of the equation was used as the initial equation in this study:

$$1/k' = 1/P_{sw}\phi + S[\mathrm{M}] \quad (1)$$

where k' is the solute retention factor, P_{sw} is the partition coefficient of a compound between the mobile phase and the stationary phase, ϕ is the phase ratio, S is equal to $K_{mw}/P_{sw}\phi$ (K_{mw} is the binding constant of the solute to the micelle) and [M] is the micelle concentration and is equal to [surfactant] − CMC (CMC is the critical micelle concentration). In order to create a gradient in solvent strength, a linear change in the micelle concentration is created [19] as:

$$[\mathrm{M}] = A + BV \quad (2)$$

This equation shows the change in micelle concentration at the outlet of the gradient forming device as a function of V which is volume of the mobile phase delivered by this device at any time, t, from the start of the gradient, i.e., at the beginning of the gradient, $V = 0$. A and B are the y-intercept and the slope, respectively. Since

$V = 0$ at the beginning of the gradient, A is then equal to the initial micelle concentration and B is the measure of the slope of the total concentration change during the course of the gradient [24].

Combining Eqs. 1 and 2 yields:

$$1/k' = 1/P_{sw}\phi + SA + SBV \tag{3}$$

Let

$$1/k'_0 = 1/P_{sw}\phi + SA \tag{3a}$$

and

$$b = SBV_m \tag{3b}$$

where k'_0 is the retention factor at the initial mobile phase, b is the gradient steepness parameter and V_m is the column dead volume. Then,

$$1/k' = 1/k'_0 + b(V/V_m) \tag{4}$$

If k'_a is the instantaneous or "actual" value of k' for the band of interest, then

$$1/k'_a = 1/k'_0 + b(V/V_m) \tag{5}$$

Therefore, solving for k'_a, the following equation is obtained

$$k'_a = (V_m k'_0)/(V_m + (bVk'_0)) \tag{6}$$

At any given time, the instantaneous or "actual" value of the corrected retention volume, V'_a, can be expressed as

$$V'_a = V_m k'_a = V_a - V_m \tag{7}$$

where V_a is the total retention volume for the solute. Substituting Eq. 7 for k'_a

$$(V'_a/V_m) = (V_m k'_0)/(V_m + (bVk'_0)) \tag{8}$$

For gradient elution, Snyder and co-workers [1–4] expressed retention as

$$\int_0^{V_g} (dV/V'_a) = 1 \tag{9}$$

where V_g is the corrected gradient retention volume ($V_g = V_R - V_m$) of the band of interest, dV is the differential volume of the mobile phase that has passed through the band center during the migration of the band along the column. Using Eq. 8, the expression given below is obtained:

$$\int_0^{V_g} [(V_m + k'_0 bV)/(k'_0 V_m^2)]\, dV = 1 \tag{10}$$

Performing the integration and rearranging the terms the final equation is obtained:

$$V_g = [V_m/b]\{(-1/k'_0) + [(1/k'_0)^2 + 2b]^{1/2}\} \tag{11}$$

To change retention volume to retention time, the following relationship can be written, using the volume flow rate, F:

$$t_g = (V_g/F) + t_0 \tag{12}$$

Substituting Eq. 11 for V_g, the equation for the gradient retention time (t_g) in MLC is derived:

$$t_g = ((t_0/b) \cdot \{(-1/k'_0) + [(1/k'_0)^2 + 2b]^{1/2}\}) + t_0 \tag{13}$$

However, this equation does not take into account the delay time, i.e. the time before the gradient actually reaches the top of the column. This delay time, t_D, includes the delay time from the instrument (tubings and other connections) as well as the intentional delay time added by the chromatographer. Thus the observed gradient retention time is actually the calculated t_g plus t_D, i.e.,

$$t_{R,g} = t_g + t_D \tag{14}$$

During this time, t_D, elution of compounds is essentially isocratic. Thus, when the gradient reaches the top of the column, the solute band has already traveled a fraction of the column. This is known as solute pre-elution. Consequently, correction for this should also be made.

The gradient reaches the solute band when

$$X_s = X_g \tag{15}$$

where X_s and X_g are the distances the solute and the gradient have traveled through the column. This equation can also be written as

$$u_s(t_D + t) = u_0 t \tag{16}$$

where u_s is the velocity of the solute, u_0 is the velocity of the gradient and t is the time elapsed

since the start of the gradient. Rearranging terms and solving for t,

$$t = t_D/[(u_0/u_s) - 1] \quad (17)$$

The term $[(u_0/u_s) - 1]$ is equal to the retention factor in the initial mobile phase, k'_0, as shown below:

$$k'_0 = (t_R - t_0)/t_0 = (t_R/t_0) - 1$$
$$= [(L/u_s)/(L/u_0)] - 1 = (u_0/u_s) - 1 \quad (18)$$

Therefore, Eq. 17 becomes

$$t = (1/k'_0)t_D \quad (19)$$

Consequently, the corrected delay time will be

$$t'_D = t_D + t \quad (20)$$

Using Eq. 20 and rearranging terms,

$$t'_D = t_D(1 + 1/k'_0) \quad (21)$$

Another parameter which should be corrected for solute pre-elution is the column dead time, t_0 [3].

The length of the column used in the calculation of t_g is actually shorter than the original length due to the solute pre-elution. The fraction of the column that the solute band has traveled, f, can be expressed as

$$f = t'_D/t_R \quad (22)$$

where t_R is the retention time of the solute.

Using Eq. 21 and the relationship

$$t_R = t_0(1 + k'_0) \quad (23)$$

then simplifying, f can be calculated using the equation

$$f = t_D/(t_0 k'_0) \quad (24)$$

The corrected dead time is then

$$t'_0 = (1 - f)t_0 \quad (25)$$

and the corrected gradient steepness parameter is

$$b' = (1 - f)b \quad (26)$$

Using the corrected values of t_D and t_0 in Eq. 13 yields:

$$t_{R,g} = ((t'_0/b')\{(-1/k'_0) + [(1/k'_0)^2 + 2b(1 - f)]^{1/2}\}) + t'_0 + t'_D \quad (27)$$

Simplifying, the final equation for the gradient retention time for MLC is

$$t_{R,g} = ((t_0/b)\{(-1/k'_0) + [(1/k'_0)^2 + 2b(1 - f)]^{1/2}\}) + t_0 + t_D \quad (28)$$

2.2. Estimates of values of $P_{sw}\phi$ and K_{mw}

The $P_{sw}\phi$ and K_{mw} values for individual solutes can be determined using isocratic data from the slopes and intercepts of the linear plots of $1/k'$ vs. [M] as illustrated by Eq. 1. This approach, however, is time consuming and is experimentally inconvenient because most of the samples requiring separation by gradient elution cannot be easily studied using isocratic techniques. An alternative approach would be to obtain the values of these physicochemical parameters based on two gradient runs as described below.

Rearranging Eq. 28 yields:

$$(t_{R,g} - t_D - t_0)(b/t_0) = (-1/k'_0) + [(1/k'_0)^2 + 2b(1 - f)]^{1/2} \quad (29)$$

Let $T = (t_{R,g} - t_D - t_0)/t_0$, thus

$$Tb = (-1/k'_0) + [(1/k'_0)^2 + 2b(1 - f)]^{1/2} \quad (30)$$

Rearranging terms, squaring both sides of the equation and simplifying:

$$T^2b^2 + (2Tb/k'_0) = 2b(1 - f) \quad (31)$$

Recalling, $b = SBV_m$, $1/k'_0 = 1/P_{sw}\phi + SA$ and $S = K_{mw}/P_{sw}\phi$. Substituting these in Eq. 31, Eq. 32 is obtained:

$$K_{mw}(T^2BV_m + 2TA) = [2P_{sw}\phi(1 - f)] - 2T \quad (32)$$

Values of $P_{sw}\phi$ and K_{mw} can therefore be obtained by the numerical solution of two simultaneous equations obtained from two gradient runs.

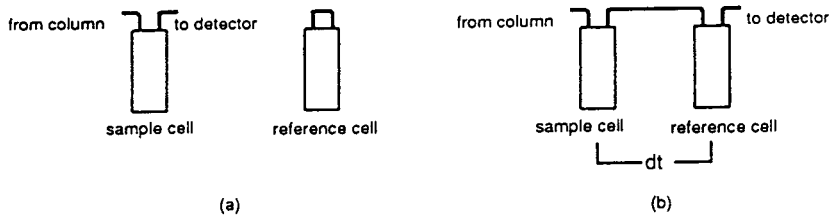

Fig. 1. Configuration of the detector cells: (a) normal detection; (b) differential detection.

$$K_{mw} = 2(T_2 - T_1)/[(T_1^2 B_1 V_m) + (2T_1 A_1) - (T_2^2 B_2 V_m) - (2T_2 A_2)] \quad (33)$$

where 1 and 2 refers to two different gradient runs with different steepness as defined by B_1 and B_2.

In this case, T_2 should be greater than T_1 meaning gradient retention time in gradient 2 should be greater than that in gradient 1 so that a positive value of the K_{mw} is obtained. By substituting the value of K_{mw} in Eq. 32, the value of $P_{sw}\phi$ can be calculated. Once the values of K_{mw} and $P_{sw}\phi$ are known, Eq. 1 can be used to predict the isocratic retention time at different micelle concentrations.

3. Experimental

3.1. Equipment

All experiments were performed using an ISCO gradient liquid chromatograph incorporating two ISCO Model 2350 pumps and an IDS PC-88 computer as the controller. Two kinds of detectors were used, i.e., a Spectra-Physics UV detector and a Kratos fluorescence detector used to confirm the data obtained from the UV detector. Chromatographic data were collected using the ISCO Chemresearch chromatographic data management/system controller version 2.4 and an IDS PC-88 computer.

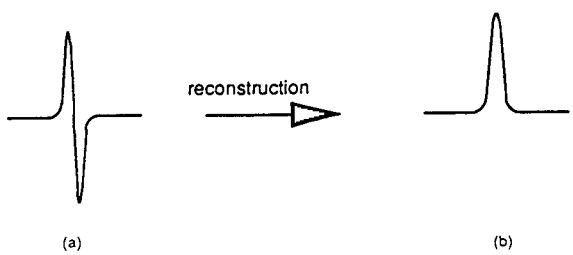

Fig. 2. Appearance of the peaks obtained: (a) from differential detection; (b) from normal detection or after reconstruction of the differential peak.

The flow-rate was 1 ml/min for all measurements. The critical micelle concentration of 8 m*M* was used in all calculations of gradient retention times.

The analytical and the guard columns were water jacketed and thermostated at 40°C with a Lauda refrigerating circulator Model RMS-6 (Brinkmann Instruments).

3.2. Reagents

Sodium dodecyl sulfate (SDS) was obtained from Sigma (St. Louis, MO, USA) and was used as received. Surfactant solutions were prepared using deionized, distilled water (Milli-Q reagent water system) and were filtered using a 0.45-μm nylon-66 membrane filter (Schleicher & Schuell, Keene, NH, USA). All the mobile phases contained 3% (v/v) 2-propanol (HPLC grade) and 0.02 *M* phosphate buffer obtained from Fischer Scientific (Raleigh, NC, USA). The pH was adjusted to 2.5. Solutes were obtained from various manufacturers and were used as received. Solutions were prepared either by dissolving solutes in 2-propanol or in aqueous micellar solution. All other solvents were HPLC grade and obtained from Fisher Scientific.

3.3. Column

The column was laboratory-packed, 15 × 0.46 cm I.D., packed with 5 μm particle size and 300 Å pore size C_{18} Nucleosil packing from Phenomenex (Torrance, CA, USA) using a column

packer was obtained from Alltech (Deerfield, IL, USA). The slurry and the packing solvents were acetone and methanol respectively and the packing pressure was 6000 p.s.i. (1 p.s.i. = 6894.76 Pa).

The void volume of the system was determined by injecting pure water. A value of 1.78 ± 0.01 ml was obtained for the laboratory-packed column which was used for all k' and $t_{R,g}$ calculations.

UV Detector baseline shift

The experiments were done using a UV detector. However, under normal detection (Fig. 1a),

Table 1
Calculated and experimental gradient retention times using a reconstructed chromatogram from the UV detector and the fluorescence detector

Compound	Gradient retention time (min)			
	Gradient 1		Gradient 2	
	Calculated	Experimental	Calculated	Experimental
UV detector				
Nap	15.39	16.67	19.67	18.80
Ant	19.18	20.61	26.74	26.17
Ph	17.34	20.06	23.28	25.28
P	20.46	21.79	29.17	28.66
D-G	6.64	7.01	6.64	6.99
D-F	11.38	11.74	12.35	12.02
D-K	15.37	15.85	18.68	17.75
DD-K	14.23	14.99	16.78	16.19
D-W	9.06	9.15	9.33	9.27
D-Y	26.47	26.89	38.76	34.41
DD-Y	23.58	24.56	33.30	32.36
D-M	11.70	11.97	12.79	12.08
D-L	16.53	16.92	20.31	18.91
D-R	16.21	16.73	20.24	18.93
D-Nor-L	15.74	16.08	19.00	17.64
Fluorescence detector				
Nap	15.39	16.68	19.67	18.77
Ant	19.18	20.77	26.74	26.13
Ph	17.34	20.22	23.28	25.16
P	20.46	21.68	29.17	28.57
D-G	6.64	7.03	6.64	6.97
D-F	11.38	11.72	12.35	11.99
D-K	15.37	15.93	18.68	17.67
DD-K	14.23	14.86	16.78	16.09
D-W	9.06	9.17	9.33	9.25
D-Y	26.47	26.55	38.76	35.53
DD-Y	23.58	23.88	33.30	31.12
D-M	11.70	11.99	12.79	12.02
D-L	16.53	16.92	20.31	18.85
D-R	16.21	16.71	20.24	18.92
D-Nor-L	15.74	16.00	19.00	17.60

Mobile phase: 0.10–0.50 *M* SDS, 0.02 *M* phosphate buffer, 3% PrOH, pH 2.5.

steeply sloping baselines were obtained when performing micelle concentration gradient due to large changes in the refractive index of the mobile phase. In order to alleviate this problem, the detector set-up was modified to differential detection (Fig. 1b).

Fig. 2a shows the appearance of the peaks obtained from differential detection. Therefore, some sort of an integration or reconstruction step is needed in order to achieve a normal peak (Fig. 2b).

The reconstruction step was done using the equation given below.

$$A_{\text{sample}}[t] = A_{\text{observed}}[t] + A_{\text{sample}}[t - \mathrm{d}t] \qquad (34)$$

Retention data were then collected after reconstruction.

This reconstruction step, however, might introduce additional error in the determination of retention. To verify that the results of the integration is acceptable, a fluorescence detector was connected in series with the UV detector. It was determined that the difference in retention times measured from the two detectors due to additional tubing is negligible.

The results of the verification are shown in Table 1 and Fig. 3. As shown from the figure, no significant difference is evident when comparing the plots for the reconstructed chromatograms (UV detector) and that for the unreconstructed ones (fluorescence detector). Therefore, the retention data from the UV detector are acceptable.

4. Results and discussion

4.1. Verification of equation

In MLC, gradient retention times, $t_{R,g}$, can be predicted using Eq. 28 provided that K_{mw} and $P_{sw}\phi$ are known. The values of K_{mw} and $P_{sw}\phi$ for the test solutes were determined from the slopes and intercepts of the linear $1/k'$ vs. [M] plots measured under isocratic elution. Results are given in Table 2 and as shown, excellent linearity ($r^2 > 0.997$) was obtained for all compounds under study with the exception of DF. For very hydrophobic solutes, the numerical analysis sometimes produces negative values to

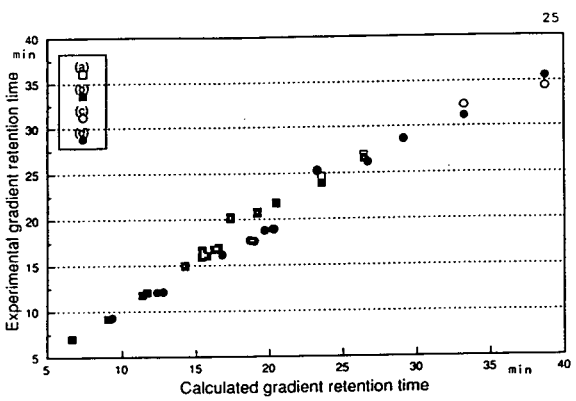

Fig. 3. Comparison of calculated and experimental gradient retention data using a reconstructed chromatogram from the UV detector and an unreconstructed chromatogram from the fluorescence detector; $t_0 = 1.78$ min, $t_D = 5$ min. Mobile phase: 0.10–0.50 *M* SDS, 0.02 *M* phosphate buffer, 3% PrOH, pH 2.5: $t_G = 15$ min, $A = 0.092$, $B = 0.267$; $t_G = 60$ min, $A = 0.092$, $B = 0.00667$. (a) UV detector, $t_G = 15$ min; (b) fluorescence detector, $t_G = 15$ min; (c) UV detector, $t_G = 60$ min; (d) fluorescence detector, $t_G = 60$ min.

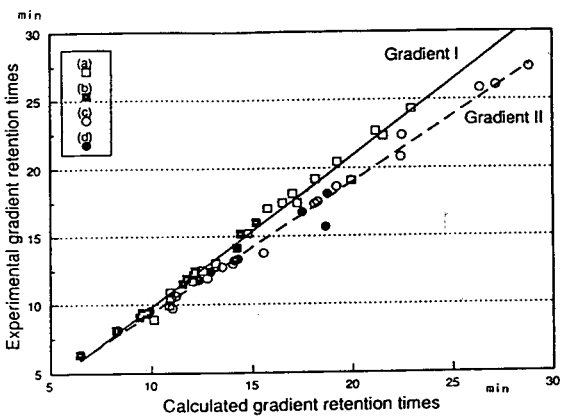

Fig. 4. Comparison of calculated and experimental gradient retention data; $t_0 = 1.78$ min, $t_D = 5$ min or 8.5 min. Mobile phase: 0.02 *M* phosphate buffer, 3% PrOH, pH 2.5: (a) 0.10–0.50 *M* SDS gradient, $t_G = 15$ min, $A = 0.092$, $B = 0.02667$; (b) 0.04–0.20 *M* SDS gradient, $t_G = 15$ min, $A = 0.032$, $B = 0.01067$; (c) 0.10–0.50 *M* SDS gradient, $t_G = 60$ min, $A = 0.092$, $B = 0.00667$; (d) 0.04–0.20 *M* SDS gradient, $t_G = 60$ min, $A = 0.032$, $B = 0.00267$.

Table 2
Regression data from $1/k'$ vs. [M] plots for 40 different kinds of compounds

Compound	r^2	$P_{sw}\phi$	K_{mw}
F	0.998	26.5 ± 16.1	37.4 ± 23.1
FF	0.998	145.0 ± 263.1	113.9 ± 207.1
FFF	0.998	173.5 ± 251.2	83.1 ± 120.8
FFFF	0.999	920.0 ± 2169.9	178.7 ± 421.7
DF	0.915	−51.9 ± 729.1	−131.3 ± 1845.8
RF	1.000	−77.3 ± 2.6	−63.0 ± 2.1
KF	1.000	−57.1 ± 13.4	−64.3 ± 15.2
Y	1.000	16.2 ± 0.7	64.7 ± 2.8
AY	1.000	14.6 ± 0.8	108.7 ± 6.0
LY	1.000	45.0 ± 3.1	137.5 ± 9.3
GLY	1.000	58.7 ± 8.7	189.4 ± 26.2
W	1.000	96.0 ± 4.5	153.5 ± 7.1
LW	1.000	161.9 ± 17.7	193.0 ± 21.1
D-G	0.997	11.2 ± 2.0	38.5 ± 6.9
D-F	0.998	24.2 ± 3.6	45.7 ± 7.0
D-W	0.998	19.8 ± 3.4	52.7 ± 9.3
D-K	0.999	76.9 ± 0.2	102.7 ± 0.4
DD-K	0.999	55.4 ± 11.5	82.3 ± 17.1
D-M	0.998	24.8 ± 4.2	44.8 ± 7.8
D-L	0.998	51.7 ± 11.3	56.1 ± 12.4
D-R	0.999	136.2 ± 68.0	172.7 ± 86.3
D-Nor-L	0.999	46.6 ± 10.4	54.8 ± 12.4
D-Y	0.999	377.1 ± 217.3	187.7 ± 108.3
DD-Y	0.999	252.7 ± 106.1	156.6 ± 65.8
BZA	0.999	5.8 ± 0.2	11.1 ± 0.5
B	1.000	15.7 ± 0.4	17.0 ± 0.4
BZO	0.999	5.9 ± 0.2	11.8 ± 0.6
NB	0.999	10.0 ± 0.5	15.4 ± 0.8
T	1.000	45.1 ± 1.1	40.7 ± 1.0
Nap	1.000	138.5 ± 5.3	103.8 ± 4.0
Ant	1.000	581.6 ± 140.3	278.9 ± 67.3
Ph	1.000	306.4 ± 29.8	187.6 ± 18.3
Py	1.000	864.5 ± 335.7	361.0 ± 140.2
2-CP	0.998	8.1 ± 0.6	17.9 ± 1.4
3-CP	0.999	13.5 ± 1.0	27.3 ± 2.0
2,3-DCP	0.999	28.9 ± 5.2	51.4 ± 9.3
2,5-DCP	0.999	30.9 ± 3.6	48.9 ± 5.7
2,4,5-TCP	1.000	78.0 ± 14.3	95.4 ± 17.6
2,4,6-TCP	0.999	62.1 ± 13.0	80.2 ± 16.9
PCP	1.000	161.5 ± 40.3	133.8 ± 33.4

$P_{sw}\phi$ due to small values of the intercepts relative to the experimental errors and because of the high correlation between K_{mw} and $P_{sw}\phi$. However, highly accurate retention data can still be predicted using these two parameters combined, despite the fact that $P_{sw}\phi$ no longer has a physical meaning. A compilation of characteristic constants for micelle interaction is available in the literature [25]. In so far as the data set presented here overlaps with the ones discussed in Ref. [25], there is good agreement with respect to the order of magnitude of the solute–micelles interaction after correction for the aggregation number. However, a more thorough comparison of the values is not appropriate due to differences in the applied experimental conditions, most notable, the temperature.

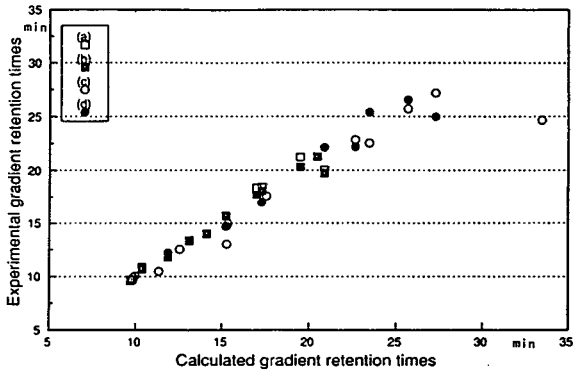

Fig. 5. Comparison of calculated and experimental gradient retention data with pump going from 0 to 100% solvent B vs. 10–90% solvent B; $t_0 = 1.78$ min, $t_D = 5$ min. Mobile phase: 0.02–0.10 *M* SDS, 0.02 *M* phosphate buffer, 3% PrOH, pH 2.5: $t_G = 15$ min, $A = 0.012$, $B = 0.00533$; $t_G = 60$ min, $A = 0.012$, $B = 0.00133$. (a) 0–100% solvent B, $t_G = 15$ min; (b) 10–90% solvent B, $t_G = 15$ min; (c) 0–100% solvent B, $t_G = 60$ min; (d) 10–90% solvent B, $t_G = 60$ min.

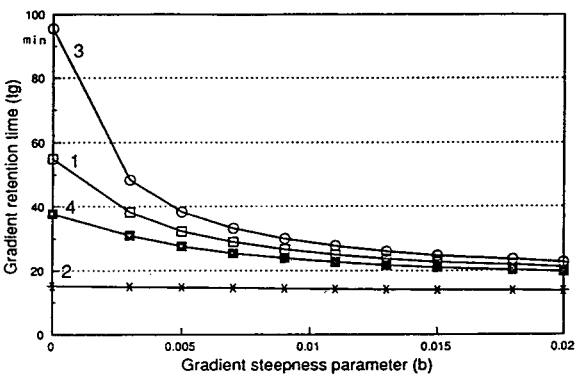

Fig. 6. Effect of gradient steepness parameter (b) on the gradient retention time: (1) $P_{sw}\phi = 291$ and $K_{mw} = 70$; (2) $P_{sw}\phi = 291$ and $K_{mw} = 560$; (3) $P_{sw}\phi = 1164$ and $K_{mw} = 70$; (4) $P_{sw}\phi = 1164$ and $K_{mw} = 560$.

Table 3
Calculated and experimental gradient retention times

Compound	Gradient retention time (min)			
	Gradient 1		Gradient 2	
	Calculated	Experimental	Calculated	Experimental
0.10–0.50 M SDS gradient				
F	10.92	10.87	10.95	10.37
FF	17.01	18.12	19.93	19.09
FFF	21.15	22.70	27.16	26.05
KF	15.76	17.03	18.24	17.54
RF	18.14	19.19	22.46	22.37
2,4,5-TCP	13.16	13.00	13.49	12.72
2,4,6-TCP	12.51	12.47	12.76	11.89
PCP	16.51	17.45	18.10	17.38
T	14.78	15.18	15.56	13.73
Ph	19.22	20.45	22.41	20.79
P	22.92	24.30	28.84	27.39
B	10.88	9.94	11.21	10.59
Nap	17.24	17.43	19.19	18.63
Ant	21.53	22.33	26.37	25.82
W	10.12	8.90	11.03	9.72
LW	12.04	11.71	14.03	12.95
0.04–0.20 M SDS gradient				
DF	14.22	14.13	18.64	15.65
2-CP	9.53	9.40	9.84	9.31
3-CP	11.73	11.91	12.91	12.37
2,3-DCP	14.40	15.16	17.47	16.74
2,5-DCP	15.18	15.97	18.73	18.12
BZA	8.26	8.12	8.33	8.16
NB	11.54	11.48	12.36	11.76
BZO	8.25	8.07	8.33	8.12
Y	9.41	9.07	9.91	9.51
AY	6.47	6.33	6.48	6.37
LY	12.07	12.15	14.07	13.20
GLY	12.16	12.44	14.28	13.29

Mobile phase: x *M* SDS, 0.02 *M* phosphate buffer, 3% PrOH, pH 2.5.

Subsequently, the values for the gradient steepness parameter, b, and k'_0 were calculated from Eqs. 3a and 3b which allowed the calculation of $t_{R,g}$ from Eq. 28.

Calculated gradient retention times were obtained by first calculating the values of A and B using Eq. 3 for gradient 1 (gradient time, $t_G = 15$ min) and for gradient 2 ($t_G = 60$ min). These values and the $P_{sw}\phi$ and K_{mw} values obtained from isocratic elution were substituted into Eq. 28 resulting in the calculated gradient retention times.

Eq. 28 was then verified by comparing calculated and experimental gradient retention time values for 39 different solutes (polar, non-polar and ionic compounds consisting of amino acids, peptides, polyaromatic hydrocarbons, substituted benzenes and chlorophenols).

The gradient retention times for these solutes were experimentally determined using two SDS gradients (0.10–0.50 *M* and 0.04–0.20 *M* SDS) depending on the hydrophobicity of the compounds. Likewise, two gradient times (gradient 1 and gradient 2) were used.

Good agreement was observed between the experimental and calculated retention times with a slope of 1.00 and $r = 0.99$ (Table 3 and Fig. 4). The largest error observed was less than ± 15%.

It has been reported that for reciprocating pumps, better results can be obtained by performing a 10 to 90% solvent B gradient (the stronger solvent in the gradient) rather than going from 0 to 100%. This was examined for the instrument used. As shown in Table 4 and Fig. 5, there is no significant difference between the plots for the gradients performed at 10 to 90% solvent B and at 0 to 100%. Thus, for the instrument used, retention in gradient elution is not greatly influenced by this factor. The slopes of predicted vs. observed gradient retention times for the two gradients (0–100% and 10–90%) were 1.00 and 0.97, respectively.

The effect of b on the gradient retention times for different $P_{sw}\phi$ and K_{mw} values was examined using Eq. 28 and the results are shown in Fig. 6. As expected, for a steeper gradient, smaller gradient retention times were obtained. This change is more pronounced for compounds having larger $P_{sw}\phi$ and smaller K_{mw} values i.e. compounds having more interaction with the stationary phase.

The majority of observations related to gradient 2 showed experimental retention times that were less than the predicted values (Tables 3 and 4). This might indicate the presence of systematic errors. In order to figure out the source of the systematic errors, the gradient shape delivered by the instrument and the flow-rate error of the instrument were measured.

The actual gradient shapes at two gradient times were obtained by using pure methanol as the initial mobile phase and methanol with a few drops of acetone as the final mobile phase. The increase in the absorbance as the concentration of acetone is increased was determined. This was compared with the ideal gradient shape. The difference between the %B of the actual and the ideal gradient, ΔB, at 12 min was measured and the results are given in Table 5. The ΔB obtained for the pump operating from 0–100% B and from 10–100% B are almost equal for both gradients. The same is true for the two gradients which have different gradient times.

Likewise, the %B for the actual gradient is slightly higher than that for the ideal gradient. This would correspond to a slight decrease in the gradient retention time as compared to the theoretical value.

Flow-rate studies also illustrate this effect as shown in Fig. 7. The pumps were set such that the total flow-rate is equal to 1 ml/min. The figure shows the deviation of the actual flow-rate from this value. The errors observed were all positive which means that the flow-rates observed were greater than 1 ml/min. At 0% B, only pump A is pumping the solvent and a 0% error was observed. When pump B was used together with pump A, the observed error was increased. When using pump B only, an error of about 2.5% was observed. Therefore, the error in the flow-rate is due mostly to pump B. An excellent discussion on the various factors contributing to errors in flow-rate has been published by Foley et al. [26] where potential sources include the differences in pressure coefficients of viscosity of the solvents used for a gradient. Although the relevant coefficients were not available for the system under discussion, a significant difference in viscosity exists between the A and B solvents.

Therefore, the systematic error observed was due primarily to the errors in the operation of the instrument for the gradient runs. Thus, the use of a better instrument should produce better correlation, i.e., less error, between the experimental and the calculated values.

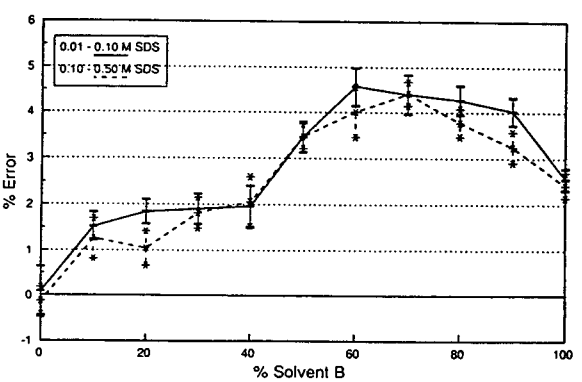

Fig. 7. Flow-rate errors generated by the instrument using different concentrations of A and B solvents.

Table 4
Calculated and experimental gradient retention times with pump going from 0 to 100% solvent B vs. 10–90% solvent B

Compound	Gradient retention time (min)			
	Gradient 1		Gradient 2	
	Calculated	Experimental, $A = 0.012$, $B = 0.00533$	Calculated	Experimental, $A = 0.012$, $B = 0.00133$
0–100% Solvent B gradient				
DF	20.88	20.01	33.47	24.67
2-CP	11.87	11.87	12.56	12.54
3-CP	15.23	15.62	17.56	17.55
2,3-DCP	19.50	20.29	25.66	25.71
2,5-DCP	20.48	21.24	27.27	27.18
BZA	9.70	9.69	9.86	9.93
NB	14.12	13.99	15.35	14.92
BZO	9.80	9.71	9.98	10.03
Y	13.12	13.34	15.27	13.02
AY	10.38	10.89	11.36	10.46
LY	16.99	18.33	22.66	22.83
GLY	17.29	18.41	23.46	22.53
10–90% Solvent B gradient				
DF	20.88	19.73	33.47	24.99
2-CP	11.87	11.79	12.56	12.21
3-CP	15.23	15.67	17.56	16.92
2,3-DCP	19.50	20.29	25.66	25.40
2,5-DCP	20.48	21.30	27.27	26.55
BZA	9.70	9.54	9.86	9.72
NB	14.12	13.95	15.35	14.68
BZO	9.80	9.68	9.98	9.60
Y	13.12	13.30	15.27	14.66
AY	10.38	10.65	11.36	10.85
LY	16.99	17.68	22.66	22.10
GLY	17.29	18.03	23.46	22.16

Mobile phase: 0.02–0.10 *M* SDS, 0.02 *M* phosphate buffer, 3% PrOH, pH 2.5.

Table 5
Measured difference of %B between the actual and the ideal gradient at 12 min

Gradient time (min)	Pump setting (%B)	ΔB (%)
15	0–100	2
	10–90	3
60	0–100	2
	10–90	2

4.2. Estimation of K_{mw} and $P_{sw}\phi$ values

The validity of Eq. 32 was verified by calculating the values of K_{mw} and $P_{sw}\phi$ using the calculated gradient retention times. The observed errors from this verification were within the expected experimental errors. The next step would then be to use the experimental gradient retention times. However, this gave K_{mw} and $P_{sw}\phi$ values which do not agree with the data in

Table 6
Comparison of isocratic k' values calculated from two gradient runs and measured experimentally from isocratic runs

Compound	k' at two micelle concentrations			
	Gradient		Isocratic	
	0.092 *M*	0.192 *M*	0.092 *M*	0.192 *M*
FF	9.19	7.83	11.01	5.17
FFF	13.91	10.93	17.59	8.41
RF	12.77	8.20	13.69	5.85
KF	8.09	7.23	9.92	4.16
Y	3.06	1.74	4.41	0.90
AY	3.26	2.26	1.01	0.90
LY	4.29	2.30	2.70	1.27
GLY	4.65	2.57	2.62	1.21
W	4.84	1.33	4.93	2.57
LW	6.65	4.08	6.83	3.52
D-F	5.57	4.43	3.27	1.63
D-W	4.33	3.30	2.33	1.11
D-K	7.74	5.21	5.43	2.56
DD-K	7.12	4.95	4.66	2.25
D-M	5.80	5.64	3.42	1.71
D-L	8.36	5.78	6.17	3.08
D-R	8.21	5.37	6.00	2.77
D-Nor-L	7.72	5.35	5.68	2.82
D-Y	17.87	10.70	15.81	7.44
DD-Y	15.79	8.64	12.42	5.90
BZA	2.44	1.51	2.26	1.45
BZO	2.04	1.15	2.22	1.41
NB	4.67	3.17	3.35	2.04
Nap	9.45	7.55	11.10	5.55
Ant	15.64	11.22	18.65	9.01
Ph	14.77	10.66	14.30	6.97
Py	18.76	12.50	21.74	10.40
2-CP	3.09	1.85	2.42	1.44
3-CP	4.48	2.67	3.10	1.72
2,3-DCP	5.95	3.31	4.08	2.17
2,5-DCP	6.52	3.65	4.61	2.43

Table 2. Better correlation is observed for neutral compounds and for gradient runs using low surfactant concentrations.

An inherent error in gradient elution is the fact that the actual [M] at a certain time, t, is not exactly equal to the predicted [M]. This difference would affect the retention behavior of compounds. This effect is larger for ionic compounds because these types of compounds are more sensitive to variations in the [M].

Another possible source of error arises from the use of high surfactant concentrations so as to elute hydrophobic compounds from the reversed-phase column in a reasonable amount of time. One assumption for Eq. 1 is that CMC, aggregation number and the structure of the micelle do not change as a result of a change in the surfactant concentration. The use of high surfactant concentration in the gradient (from 0.10 to 0.50 *M* SDS) would lead to variation in the CMC and consequently, altering the amount of adsorbed surfactant on the stationary phase. This would drastically increase errors made in the calculation of K_{mw} and $P_{sw}\phi$.

Another important source of error would be the uncertainties in the measurement of the column dead volume. During the gradient the mobile phase composition is constantly changing which subsequently influences the void volume.

One way of reducing this error would be to use a less hydrophobic stationary phase as well as the use of shorter columns. This would allow the use of lower surfactant concentration yet eluting the hydrophobic compounds in a reasonable amount of time.

Despite large errors obtained for the K_{mw} and $P_{sw}\phi$ values, the isocratic k' values were still calculated for different [M] using Eq. 1. This is then compared with the experimental isocratic k'. As shown in Table 6, two gradient runs can be used to estimate isocratic k' value. However, the average % difference between the isocratic k' values calculated from the two gradient runs and from isocratic elution is quite large. Likewise, this method may not give accurate values for K_{mw} and $P_{sw}\phi$ values but can still be used as a scouting technique for the estimation of isocratic k' as well as predict band positions in isocratic elution for a mixture of compounds. However, the results from gradient elution could still be improved by using more accurate gradient formers, shorter columns and less hydrophobic stationary phases.

Acknowledgement

The authors gratefully acknowledge the support of this research by the US National Institutes of Health (GM 38738).

Appendix A

List of compounds used

Compound	Abbreviation
Amino acids and peptides	
Phenylalanine	F
Aspartic acid–phenylalanine	DF
Arginine–phenylalanine	RF
Lysine–phenylalanine	KF
Tyrosine	Y
Alanine–tyrosine	AL
Leucine–tyrosine	LY
Glycine–leucine–tyrosine	GLY
Trytophan	W
Leucine–tryptophan	LW
Dansylated amino acids	
Dansyl-glycine	D-G
Dansyl-phenylalanine	D-F
Dansyl-trytophan	D-W
Dansyl-lysine	D-K
Didansyl-lysine	DD-K
Dansyl-methionine	D-M
Dansyl-leucine	D-L
Dansyl-norleucine	D-Nor-L
Dansyl-arginine	D-R
Dansyl-tyrosine	D-Y
Didansyl-tyrosine	DD-Y
Aromatic compounds	
Benzaldehyde	BZA
Benzene	B
Benzonitrile	BZO
Nitrobenzene	NB
Toluene	T
Napthalene	Nap
Anthracene	Ant
Phenanthrene	Ph
Pyrene	P
Chlorophenols	
2-Chlorophenol	2-CP
3-Chlorophenol	3-CP
2,3-Dichlorophenol	2,3-DCP
2,5-Dichlorophenol	2,5-DCP
2,4,5-Trichlorophenol	2,4,5-TCP
2,4,6-Trichlorophenol	2,4,6-TCP
Pentachlorophenol	PCP

References

[1] L.R. Snyder, J.W. Dolan and J.R. Grant, *J Chromatogr.*, 165 (1979) 3.
[2] L.R. Snyder, in Cs. Horváth (Editor), *High-Performance Liquid Chromatography —Advances and Perspectives*, Vol. 1, Academic Press, New York, 1980, Ch. 4.
[3] M.A. Quarry, R.L. Grob and L.R. Snyder, *J. Chromatogr.*, 285 (1984) 1.
[4] M.A. Quarry, R.L. Grob and L.R. Snyder, *J. Chromatogr.*, 285 (1984) 19.

[5] J.W. Dolan, L.R. Snyder and M.A. Quarry, *Chromatographia*, 24 (1987) 261.
[6] M.G. Khaledi, E. Peuler and J. Ngeh-Ngwainbi, *Anal. Chem.*, 59 (1987) 2738.
[7] C. Tanford, *The Hydrophobic Effect: Formation of Micelles and Biological Membranes*, Wiley-Interscience, New York, 1973, p. 49.
[8] J.S. Landy and J.G. Dorsey, *J. Chromatogr. Sci.*, 22 (1984) 68.
[9] J.G. Dorsey, M.G. Khaledi, J.S. Landy and J.L. Lin, *J. Chromatogr.*, 316 (1984) 183.
[10] M.G. Khaledi, *Biochromatography*, 3 (1988) 20.
[11] J.S. Landy and J.G. Dorsey, *Anal. Chim. Acta*, 178 (1985) 179.
[12] M.F. Borgerding, W.L. Hinze, L.D. Stafford, G.W. Fulp and W.C. Hamlin, *Anal. Chem*, 61 (1989) 1353.
[13] L.S. Madamba-Tan, J.K. Strasters and M.G. Khaledi, *J. Chromatogr. A*, 683 (1994) 335.
[14] L.A. Cole and J.G. Dorsey, *Anal. Chem.*, 62 (1990) 16.
[15] M.G. Khaledi, J.K. Strasters, A.H. Rodgers and E.D. Breyer, *Anal. Chem.*, 62 (1990) 130.
[16] J.K. Strasters, E.D. Breyer, A.H. Rodgers and M.G. Khaledi, *J. Chromatogr.*, 511 (1990) 17.
[17] A.S. Kord and M.G. Khaledi, *Anal. Chem.*, 64 (1992) 1894.
[18] A.S. Kord and M.G. Khaledi, *Anal. Chem.*, 64 (1992) 1900.
[19] P. Jandera and J. Churáček, *Gradient Elution in Column Liquid Chromatography —Theory and Practice*, Elsevier, Amsterdam, 1985.
[20] D.W. Armstrong and F. Nome, *Anal. Chem.*, 53 (1981) 1662.
[21] D.W. Armstrong, *Sep. Purif. Methods*, 14 (1985) 213.
[22] M. Arunyanart and L.J. Cline Love, *Anal. Chem.*, 56 (1984) 1557.
[23] A.S. Kord, J.K. Strasters and M.G. Khaledi, *Anal. Chim. Acta*, 246 (1991) 131.
[24] P. Jandera and J. Churáček, *J. Chromatogr.*, 91 (1974) 223.
[25] J.P. Foley, *Anal. Chim. Acta*, 231 (1990) 237.
[26] J.P. Foley, J.A. Crow, B.A. Thomas and M. Zamora, *J. Chromatogr.*, 478 (1989) 287.

ELSEVIER

Journal of Chromatography A, 683 (1994) 335–345

JOURNAL OF CHROMATOGRAPHY A

Gradient elution in micellar liquid chromatography II. Organic modifier gradients

Lillian S. Madamba-Tan[1], Joost K. Strasters[2], Morteza G. Khaledi*

Department of Chemistry, North Carolina State University, Raleigh, NC 27695-8204, USA

First received 22 June 1993; revised manuscript received 9 May 1994

Abstract

The application of organic modifier gradients in micellar liquid chromatography (MLC) is discussed. The equation derived by Snyder and co-workers describing gradient elution in hydro–organic reversed-phase LC was verified for organic solvent gradients in the presence of micelles. It is also demonstrated that the use of these gradients require little re-equilibration time due to the limited range of organic modifier concentration used in the gradient. This would result in shorter analysis time. Lastly, a practical application of the use of propanol and acetonitrile gradients in MLC is described.

1. Introduction

In gradient elution the mobile phase composition is varied during the course of the separation process in order to provide a continuous increase in the strength of the mobile phase entering the column. Hydro–organic gradients involve an increase in the percentage of the organic modifier in the mobile phase during the run. The result will be faster separation of later-eluting peaks while separating the early-eluting solutes as well as enhanced detectability. Hence, gradient elution provides a solution to the general elution problem.

The theoretical and experimental aspects of gradient elution in reversed-phase liquid chromatography (RPLC) have been studied extensively over the past years [1–7]. Snyder et al. [1] have derived an equation to describe gradient elution in hydro–organic RPLC:

$$t_g = [(t_0/b) \log 2.3k_0'b(1-f) + 1] + t_D + t_0 \qquad (1)$$

where t_g is the gradient retention time, t_0 is the column dead time, b is the gradient steepness parameter, k_0' is the isocratic retention factor at initial mobile phase condition, f is the fraction of the column the solute has already traveled before the gradient reaches it, and t_D is the system delay time. The validity of this equation has been verified experimentally [2]. This equation can be used to predict gradient retention time from gradient data but more importantly, it can also be used to predict isocratic retention data from gradient runs (scouting technique) [8].

* Corresponding author.

[1] Present address: Warner-Lambert Company, Morris Plains, NJ 07950, USA.

[2] Sterling Winthrop, 1250 Collegeville Road, P.O. Box 5000, Collegeville, PA 19246, USA.

0021-9673/94/$07.00
SSDI 0021-9673(94)00451-E

The major disadvantage commonly associated with gradient elution is the additional time required to re-equilibrate the column with the initial gradient conditions after each run [2,5]. Studies show that significant quantities of the organic modifier in the mobile phase are extracted by the stationary phase [9,10]. As the concentration of the organic solvent changes during the gradient run, the alkyl bonded phase is solvated to a varying extent [11]. The changing solvation of the stationary phase makes it necessary to re-equilibrate the column to its starting conditions. Complete column re-equilibration usually requires flushing the column with about 15 column volumes of the initial mobile phase [7] before the next sample injection. This re-equilibration time results in longer analysis times.

Different methods to reduce the column re-equilibration time have been studied extensively [2,7,11,12]. The use of a reverse gradient following the completion of the initial gradient has been suggested [2]. However, this does not show any significant advantage as compared to returning directly to the starting conditions [7]. Another study done by Frenz and Horváth [12] suggested the use of a series of different solvents in the order of decreasing affinity for the stationary phase as column regenerants. A recent study on column regeneration was done by Cole and Dorsey [11]. The addition of a constant volume of 3% 1-propanol in the mobile phase throughout the solvent gradient provides consistent solvation of the stationary phase. This provides a dramatic reduction in the column re-equilibration time of up to 78%.

In micellar liquid chromatography (MLC), gradient elution can be performed by increasing the micelle concentration and/or by increasing the concentration of an organic modifier. No column re-equilibration is needed after a micellar gradient due to the constant composition of the stationary phase during the course of the gradient. Solvent strength in MLC can also be controlled by changing the concentration of an organic modifier.

Reduced chromatographic efficiency has been the major drawback of MLC due to poor resistance to mass transfer. It has been shown that the addition of 3% 1-propanol to the micellar mobile phase provides better "wetting" of the stationary phase which improves the mass transfer of the solutes between the mobile phase and the stationary phase and consequently the chromatographic efficiency [13].

In addition, the results from this laboratory have proven that not only does the presence of an organic modifier compensate for the otherwise weak solvent strengths of micellar eluents, but also the combination of micelles and organic solvent provides pronounced selectivity for the separation [14–19]. As a result, a study of both micellar gradients (i.e. increasing the micelle gradient) and organic modifier gradients (i.e. increasing the concentration of the organic modifier) is worth pursuing. In the first part of this study, we reported the theory and experimental verification for a micelle concentration gradient [20].

In this paper, the use of organic solvent gradient in MLC is discussed. It is demonstrated that Eq. 1 can be used to describe organic solvent gradients in the presence of micelles. The use of gradient elution to predict the retention under isocratic conditions is also presented. In addition, it will be shown that the column re-equilibration time after each organic solvent gradient run is very short. Lastly, the gradient capability of this technique is illustrated.

2. Experimental

2.1. Equipment

All experiments were done using an ISCO gradient liquid chromatograph incorporating two ISCO Model 2350 pumps and an IDS PC-88 computer as the controller. The detector used was an Applied Biosystems Model 783A programmable absorbance detector (wavelength set at 254 nm). Chromatographic data were collected using a Yokogawa Model 3021 pen recorder and the ISCO Chemresearch chromatographic data management/system controller version 2.4 with an IDS PC-88 computer.

The flow-rate used for all measurements was 1 ml/min. The analytical column and the guard column were water jacketed and thermostated at 40°C with a Lauda refrigerating circulator Model RMS-6 (Brinkmann Instruments).

2.2. Reagents and solutions

The surfactant used was sodium dodecyl sulfate (SDS) obtained from Sigma (St. Louis, MO, USA) and used as received. Surfactant solutions were prepared using deionized, distilled water (Milli-Q reagent water system) and were filtered using a 0.45-μm nylon-66 membrane filter (Schleicher & Schuell, Keene, NH, USA).All the mobile phases contained 0.02 *M* phosphate buffer and varying concentrations of organic modifier (2-propanol or acetonitrile which are HPLC grade) and SDS depending on the gradient used. The pH was adjusted to 2.5. In addition, all the mobile phases were degassed by sonicating for 15 min prior to use.

Solutes were obtained from various manufacturers and were used as received. Solutions were prepared by either dissolving the solutes in 2-propanol, in acetonitrile or in aqueous micellar solution. Concentrations of the solute solutions were adjusted such that reasonable peak heights are obtained.

All solvents were HPLC grade and obtained from Fisher Scientific.

2.3. Column

The column used was a laboratory-packed column, 15×0.46 cm I.D. Blank column (Supelco, Bellefonte, PA, USA) packed with 5 μm particle size and 300 Å pore size Nucleosil C_{18} packing from Phenomenex (Torrance, CA, USA) using a column packer from Alltech (Deerfield, IL, USA). The slurry and the packing solvents were acetone and methanol, respectively and the packing pressure used was 6000 p.s.i. (1 p.s.i. = 6894.76 Pa).

The void volume of the system was evaluated by injecting pure water. The first disturbance of the baseline was assumed to be V_m. A value of 2.11 min was obtained for the laboratory-packed column which was used for all k' and t_g calculations.

3. Results and discussion

3.1. Verification of the gradient equation

The equation for gradient elution developed by Snyder et al. has already been found to be applicable to gradient elution in conventional RPLC with hydro–organic mobile phases. However, the validity of this equation for organic solvent gradients in the presence of micelles should be examined. This was done using 9 dansylated amino acids.

In order to calculate gradient retention times using Eq. 1, the values for b and k'_0 were determined under isocratic conditions from the linear relationship between log k' and volume fraction of organic modifier in the mobile phase, φ as:

$$\log k' = \log k'_m - S\phi \quad (2)$$

where k' is the isocratic retention factor, k'_m is the retention factor in a purely aqueous micellar mobile phase at a fixed micelle concentration and S is the slope of the log k' vs. φ in the micellar eluent. The values of S and k'_m were calculated from the slope and intercept, respectively.

The validity of this equation in MLC has been demonstrated for different types of organic modifiers and for a broad range of ionic and non-ionic compounds [14–19].

The gradient steepness parameter, b, was calculated using the expression

$$b = \frac{S\,\Delta\varphi\,t_0}{t_G} \quad (3)$$

where $\Delta\varphi$ is the change in the volume fraction of the organic modifier during the gradient. By substituting the values of k'_0 and b into Eq. 1, calculated values of the gradient retention time were obtained.

The experimental gradient retention times were then obtained for two gradients with differ-

ent gradient times, t_G (15 and 60 min). A total delay time of 5 min was incorporated in all the gradients used. The mobile phase contained 2-propanol, 0.06 *M* SDS and 0.02 *M* phosphate buffer with the pH adjusted to 2.5. The propanol concentration was varied from 3 to 15% (v/v) for the two gradients used. Note that in addition to the organic solvent content, the elution strength of micellar mobile phases is also influenced by concentration of micelles.

The experimental retention time ($t_{R,expt}$) obtained were compared with the calculated retention time ($t_{R,calc}$). The results of this verification is given in Table 1 and Fig. 1. As shown, the calculated gradient retention times agree closely with the experimental gradient retention time. Errors obtained were less than 5% which were mainly negative errors, i.e., the experimental values lie below ideal curve. This can be attributed to systematic errors contributed by the instrument used [20]. The close agreement between the experimental and calculated data indicates that the integrity of the micelles is maintained during the gradient runs. Since there is no discernible difference in the prediction errors of the early- and late-eluting compounds, a breakdown of the micelles at higher organic modifier concentration is not apparent.

Table 1
Verification of Eq. 1 used to predict retention times from characteristic values derived from isocratic runs for organic modifier gradients in the presence of micelles

Compound	t_G = 15 min		t_G = 60 min	
	$t_{R,calc}$ (min)	$t_{R,expt}$ (min)	$t_{R,calc}$ (min)	$t_{R,expt}$ (min)
D-G	7.15	7.22	7.15	7.24
D-F	11.94	11.98	12.31	12.26
DD-K	16.13	15.71	17.10	16.76
D-W	9.46	9.32	9.53	9.41
D-K	18.85	18.34	20.45	19.76
D-M	12.16	12.38	12.68	12.74
D-L	18.37	18.73	20.65	20.61
D-R	20.14	19.65	22.48	21.72
D-Nor-L	17.42	17.49	19.16	19.07

Shown are the calculated and experimental gradient times, $t_{R,calc}$ and $t_{R,expt}$, respectively, as determined for a number of dansylated amino acids in two gradients, both 3 to 15% propanol but with different gradient times t_G. Other mobile phase conditions: 0.06 *M* SDS, 0.02 *M* phosphate buffer, 3–15% PrOH, pH 2.5. Standard abbreviations for amino acids were used.
D = dansylated amino acids; DD = didansylated amino acids.

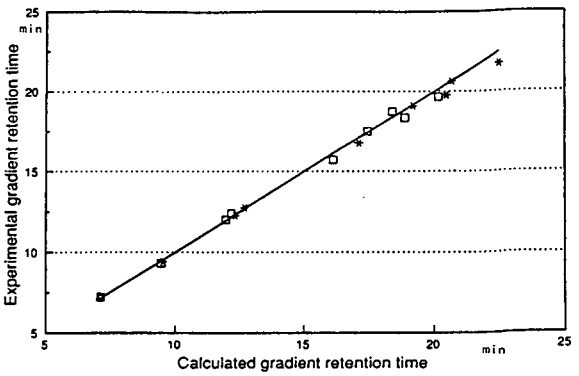

Fig. 1. Verification of Eq. 1 for organic solvent gradient in MLC: comparison of the calculated and experimental gradient retention times (□: t_G = 15 min; *: t_G = 60 min; line: ideal). Mobile phase: 0.06 *M* SDS, 0.02 *M* phosphate buffer, pH 2.5; gradients: 3 to 15% 2-propanol.

Eq. 1 can also be used to predict isocratic retention from gradient retention data. This capability has been effectively used in HPLC and is known as the scouting method. Further verification of Eq. 1 and the scouting method in MLC was performed by predicting the isocratic parameters using the retention data from two gradient runs with different t_G values [8]. This gives two equations for t_g, i.e.,

$$t_{g,1} = [(t_0/b_1)\ \log\ 2.3k'_0b_1(1-f) + 1] + t_D + t_0 \quad (4)$$

and

$$t_{g,2} = [(t_0/b_2)\ \log\ 2.3k'_0b_2(1-f) + 1] + t_D + t_o \quad (5)$$

From Eq. 3:

$$\beta = b_1/b_2 = t_{G,2}/t_{G,1} \quad (6)$$

The values for k'_0, b_1 and b_2 can be obtained by solving the three simultaneous Eqs. 4–6. Consequently, the values for the solvent strength parameter, S, can be estimated from Eq. 3. The results of this procedure are given in Table 2 and

Table 2
Comparison of gradient steepness b for the 15- (b_1) and 60-min (b_2) gradients, retention factor in 3% propanol (k'_0) and slope (S) of log k' vs. organic modifier concentration as determined from isocratic runs and the two gradient runs

Compound	Isocratic				Gradient			
	b_1	b_2	k'_0	S	b_1	b_2	k'_0	S
D-G	0.049	0.012	2.39	2.92	0.045	0.011	2.43	2.67
D-F	0.037	0.009	4.90	2.21	0.032	0.008	4.88	1.90
D-K	0.027	0.007	9.02	1.59	0.025	0.006	8.60	1.48
DD-K	0.028	0.007	7.29	1.65	0.029	0.007	7.05	1.72
D-W	0.032	0.008	3.53	1.91	0.029	0.007	3.46	1.72
D-M	0.048	0.012	5.11	2.85	0.044	0.011	5.21	2.61
D-L	0.041	0.010	9.30	2.41	0.037	0.009	9.40	2.19
D-R	0.031	0.008	10.17	1.86	0.029	0.007	9.67	1.72
D-Nor-L	0.037	0.009	8.45	2.22	0.033	0.008	8.34	1.96

Fig. 2. As shown, there is good agreement between values obtained from gradient and those from isocratic runs. Knowing the values for k'_0 *and* S from the gradient data, one can predict the isocratic retention from:

$$\log k' = \log k'_0 - S\varphi_0$$

where φ_0 represents the initial organic modifier concentration. As shown in Fig. 3 and Table 3, there is an excellent agreement between the retention factors determined from isocratic experiments and those predicted from two gradient runs.

3.2. Re-equilibration studies

One problem observed for gradient elution in RPLC with hydro–organic eluents is the need for column re-equilibration between gradient runs [2,5]. It has been observed that many column volumes of initial mobile phase composition are needed to re-equilibrate the column before the next gradient analysis. This is due to the fact that the composition of the stationary phase is altered by solvation of the bonded alkyl chains as the concentration of the organic modifier is increased during a gradient run. Generally, column re-equilibration can be achieved by flushing the column with 15 column volumes of the starting mobile phase [7].

When using micelles in the mobile phase, the surfactant monomers are adsorbed onto the stationary phase. It has been reported that the presence of 3% propanol in the mobile phase would provide over 90% monolayer coverage of the alcohol on the stationary phase [21]. An increase in the concentration of the organic modifier in the micellar mobile phase during the course of an organic solvent gradient might alter the composition of the stationary phase through the displacement of the adsorbed surfactant monomers from the stationary phase by the organic modifier. In addition, the critical micelle concentration (CMC) of a surfactant depends on the concentration of the organic co-solvent and a change in the CMC would lead to a change in the surface concentration of the adsorbed monomer surfactant. This would disturb the equilibration of the column that might require long re-equilibration times. Fortunately, however, this was not the case here as shown below.

Re-equilibration studies were performed by determining the effect of a 15-min re-equilibration time (or 15-ml re-equilibration volume) after each gradient run on the reproducibility of the retention time of 10 dansylated amino acids. If the stationary phase equilibrium is disturbed, one would observe poor reproducibility of the retention behavior especially for early-eluting compounds. Each solute was injected 15 times to determine the reproducibility of their retention

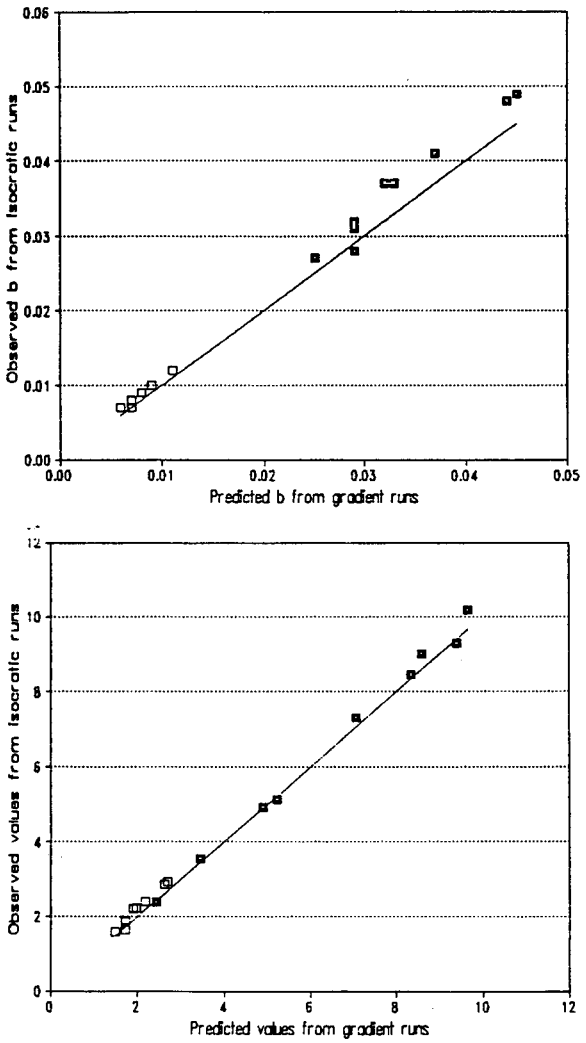

Fig. 2. Comparison of values of b_1 (top, ■), b_2 (top, □), k'_0 (*bottom*, ■) *and* S (bottom, □) obtained from isocratic and gradient runs. Lines = ideal.

times which is an indication of the column re-equilibration. Two gradients with different gradient times (as given above) were used. The mobile phase contained 0.15 *M* SDS, 0.02 *M* phosphate buffer (pH 2.5) and 2-propanol concentration varying from 3 to 15% (v/v). The average values and relative standard deviations of the first three and last three injections were calculated. Results of this series of experiments are given in Table 4. As shown, standard deviation values are less than 0.10 min after a 15-min re-equilibration time. Even smaller S.D. values are observed for the shorter retained compounds. These are the compounds which are most affected by the existence of column non-equilibration. Since the retention times of these early peaks do not vary significantly, additional washing of the column with the initial mobile phase is no longer necessary. This means that the column is already completely re-equilibrated after 15 min or 15 ml of initial mobile phase. Since the process of column re-equilibration actually starts when the initial mobile phase reaches the top of the column, the delay time of the chromatographic system (the time it takes for the starting mobile phase to travel from the pump to the top of the column) was measured and found to be 3.5 min. Therefore the column re-equilibration time is actually only 11.5 min or 11.5 ml of the starting mobile phase (since the flow-rate used in the experiment was 1 ml/min).

A more precise value of the re-equilibration time was then determined using the procedure reported by Cole and Dorsey [11] using phenylalanine as the test solute. Under the mobile phases conditions, phenylalanine is a short retained compound ($k' < 2$) and therefore it will be greatly affected by lack of column equilibrium. The gradient was held at the final mobile phase composition for at least 20 min (equivalent to 20 ml of final mobile phase) to ensure complete equilibration of the stationary phase with the final mobile phase. Following this 20-min equilibration period, the mobile phase was immediately returned to the initial composition. Phenylalanine was injected at a rate of 1 injection per minute for 28–30 min. The retention time was then plotted against the time elapsed after the gradient run. The column was considered to be completely equilibrated when the retention time of phenylalanine reached a constant value. Experiments were repeated at two different SDS concentrations, i.e., 0.30 and 0.15 *M*, in order to determine the effect of surfactant concentration on the column re-equilibration. The propanol concentration was varied from 3 to 15% (v/v). In addition, experiments were performed at 0.30 *M* SDS where the acetonitrile

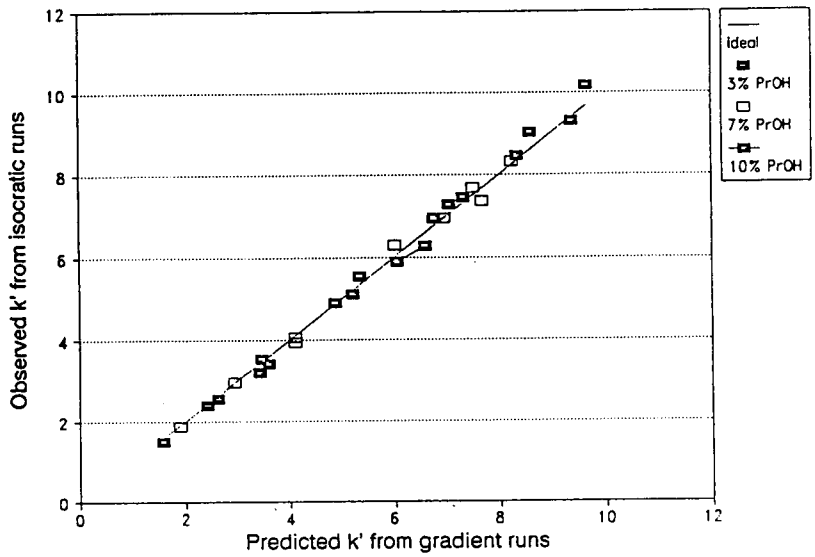

Fig. 3. Comparison of k' values obtained from isocratic and gradient runs.

concentration was varied from 3 to 20%. Conductivity experiments showed that the micelles remained intact within this range of acetonitrile concentration.

Fig. 4 shows the re-equilibration time for the three different mobile phases. A constant value of the retention was initially observed due to the delay time of the system. For the three different mobile phases, a re-equilibration time of about 11 min or 11 ml of initial mobile phase is required after each gradient run. Considering the delay time of the chromatographic system, it actually requires 7.5 min or 7.5 ml of the initial mobile phase to re-equilibrate the column. Note that some of the test solutes are charged and therefore their retention is very sensitive towards changes in the stationary phase composition, especially the concentration of the adsorbed surfactant.

The main reason behind the short re-equilibra-

Table 3
Comparison of isocratic k' values obtained from isocratic runs and calculated from two gradient runs for various propanol concentrations, φ

Compound	k'					
	Isocratic			Gradient		
	$\varphi = 0.03$	$\varphi = 0.07$	$\varphi = 0.10$	$\varphi = 0.03$	$\varphi = 0.07$	$\varphi = 0.10$
D-G	2.39	1.87	1.48	2.43	1.90	1.58
D-F	4.90	4.05	3.40	4.88	4.10	3.59
D-K	9.02	7.69	6.93	8.60	7.50	6.77
DD-K	7.29	6.30	5.54	7.05	6.02	5.34
D-W	3.53	2.95	2.56	3.46	2.95	2.62
D-M	5.11	3.93	3.21	5.21	4.10	3.42
D-L	9.30	7.37	6.28	9.40	7.68	6.60
D-R	10.17	8.32	7.45	9.67	8.25	7.33
D-Nor-L	8.45	6.93	5.89	8.34	6.96	6.08

Table 4
Reproducibility studies of retention after a 15-min column re-equilibration

Compound	t_G = 15 min		t_G = 60 min	
	t_R (min)	R.S.D. (%)	t_R (min)	R.S.D. (%)
D-G	3.74	0.02	3.79	0.02
D-F	5.75	0.03	5.86	0.03
DD-K	7.15	0.05	7.32	0.05
D-R	8.81	0.02	9.01	0.04
D-W	4.51	0.01	4.60	0.02
D-K	8.28	0.03	8.47	0.03
DD-Y	14.79	0.07	15.88	0.05
D-M	5.86	0.01	5.99	0.04
D-L	9.08	0.02	9.36	0.04
D-Y	17.63	0.04	19.07	0.09

Mobile phase: 0.15 *M* SDS, 0.02 *M* phosphate buffer, 3–15% PrOH, pH 2.5. Retention time values reported are the averages of the first three and last three injections. R.S.D. = Relative standard deviation.

tion time is the limited range of gradient. The amount of change in the concentration of organic modifier (i.e. 3–15%) is too small to cause any significant (or noticeable) effect on the composition of the stationary phase. One can then anticipate similar results to be observed in ion-pair LC and conventional RPLC with hydro–organic mobile phases. In order to verify this theory, additional experiments were performed using the same range of 2-propanol and acetonitrile concentrations (i.e., 3–15% for 2-propanol and 3–20% for acetonitrile), in hydro–organic RPLC (no surfactant present) and in ion-pair LC. Acetone was used as the test solute because with these mobile phases, phenylalanine is no longer shortly retained. The type of solute should not have an effect of column re-equilibration.

Results of this experiment are shown in Fig. 5. A re-equilibration time of about 11 min was also obtained for both pure hydro–organic (no surfactant) and hydro–organic with surfactant concen-

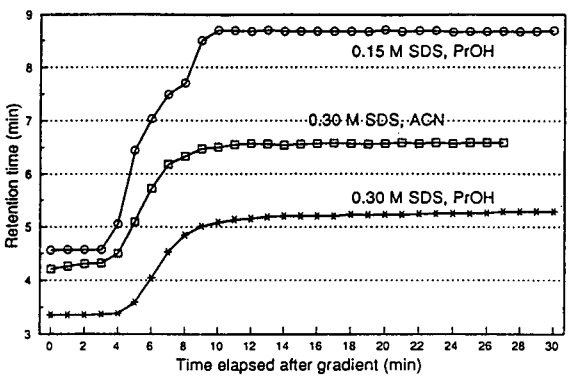

Fig. 4. Determination of column re-equilibration time with micelles in the mobile phase using phenylalanine as the test solute. Mobile phase: 0.30 or 0.15 *M* SDS, 0.02 *M* phosphate buffer, pH 2.5; gradients: 3–15% 2-propanol or 3–20% acetonitrile (ACN).

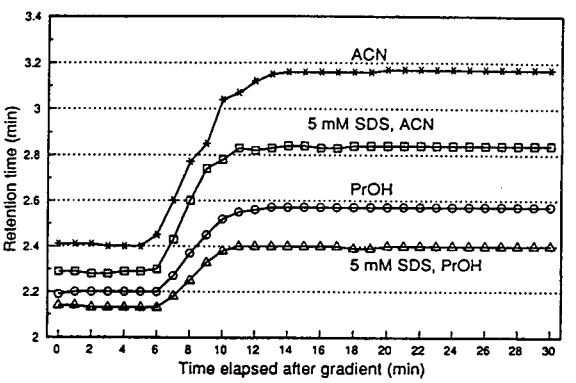

Fig. 5. Determination of column re-equilibration time without the presence of micelles in the mobile phase using acetone as the test solute. Mobile phases: either 0 or 5 m*M* SDS, 0.02 *M* phosphate buffer, pH 2.5; gradients: 3–15% 2-propanol or 3–20% acetonitrile.

tration at 5 m*M* (which is about or less than the CMC, i.e. no micelles) which is the same as that observed in MLC. Therefore, the short re-equilibration time is mainly due to the limited range of organic modifier concentration used in the gradient. The change in the concentration of the organic modifier is apparently not large enough to change the concentration of the adsorbed surfactant monomer on stationary phase and/or the amount of the extracted organic solvent. It is important to note that a limited range of organic modifier is of limited use for solving general elution problem in conventional RPLC and in ion-pair chromatography. In MLC, however, organic modifier gradients are useful since one can use a limited range of organic modifier concentration and compensate the solvent strength with a concurrent micelle concentration gradient. (Note that no column re-equilibration is needed after a micelle concentration gradient.) As can be seen in the following examples, the presence of micelles makes it possible to elute very hydrophobic compounds with a relatively low concentration of organic modifier. In addition, this will provide an opportunity to incorporate unique selectivities in MLC with the enhancement of solvent strength [15–19].

3.3. Test of gradient capability

The capability of an organic modifier gradient in MLC was studied using a seven-component mixture composed of phenylalanine (F), aspartic acid–phenylalanine (DF), lysine–phenylalanine (KF), phenylalanine–phenylalanine (FF), triphenylalanine (FFF), tetraphenylalanine (FFFF) and pentaphenylalanine (FFFFF), under isocratic and gradient conditions. Four isocratic runs and two gradient runs were performed using mobile phases containing 2-propanol and acetonitrile as the organic modifiers. The mobile phases also contained 0.30 *M* SDS, 0.02 *M* phosphate buffer and the pH was adjusted to 2.5.

Fig. 6 shows the separation of the mixture using propanol as the organic modifier. When using 3% (v/v) 2-propanol in the mobile phase

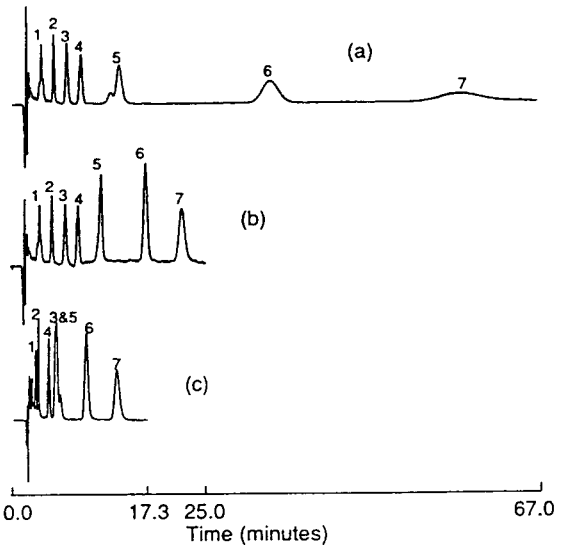

Fig. 6. Separation of a seven-component test mixture. Mobile phase: 0.30 *M* SDS, 0.02 *M* phosphate buffer, pH 2.5 with propanol added. (a) Isocratic separation with 3% 2-propanol, (b) gradient separation with 3 to 15% 2-propanol and (c) isocratic separation with 15% 2-propanol. Peaks: 1 = DF; 2 = F; 3 = KF; 4 = FF; 5 = FFF; 6 = FFFF; 7 = FFFFF.

(Fig. 6a), all peaks as well as the early-eluting peaks (peaks 1–4) are very well resolved. The later peaks, however, have very large retention time values which means long separation time such as peak 7 which elutes at about 58 min. In addition, peaks 6 and 7 are very broad which severely limits the detection sensitivity.

An increase in the percentage of the organic modifier does not give a better separation as shown in Fig. 6c. The use of 15% 2-propanol shortened the retention time dramatically resulting in a decrease in the resolution of peaks 1 and 2 which elute very near t_0. Peak reversal between peaks 3 and 4 is observed as well as coelution of peaks 3 and 5.

Gradient elution was then used for the separation. The 2-propanol concentration was varied from 3 to 15% for 5 min and was held at 15% 2-propanol for 20 min. The chromatogram is shown in Fig. 6b. The separation is complete after 25 min. Including the re-equilibration time, this would result in an overall run time of about 32.5 min. Peaks 1–4 are very well resolved and

Table 5
Comparison of theoretical plates obtained from isocratic and gradient runs using propanol and acetonitrile

Compound	Theoretical plates					
	Propanol[a]			Acetonitrile[a]		
	a	b	c	a	b	c
FF	2007	3233	1995	1839	3184	2315
FFFF	1047	4793	2015	930	3987	2099
FFFFF	467	3597	1880	Not eluted	4278	2102

[a] a = isocratic separation with 3% propanol or 3% acetonitrile; b = gradient separation with 3–15% 2-propanol or 3–20% acetonitrile; c = isocratic separation with 15% propanol or 20% acetonitrile.

peaks 5–7 elute within a reasonable amount of time. Detection sensitivity of the last peaks was also increased.

Acetonitrile was also used as shown in Fig. 7. Isocratic separation was done with 3% acetonitrile in the mobile phase (Fig. 7a). Peak 7 does not elute after 2 h or could be too broad to be detected. Good resolution, however, is observed for peaks 1–4.

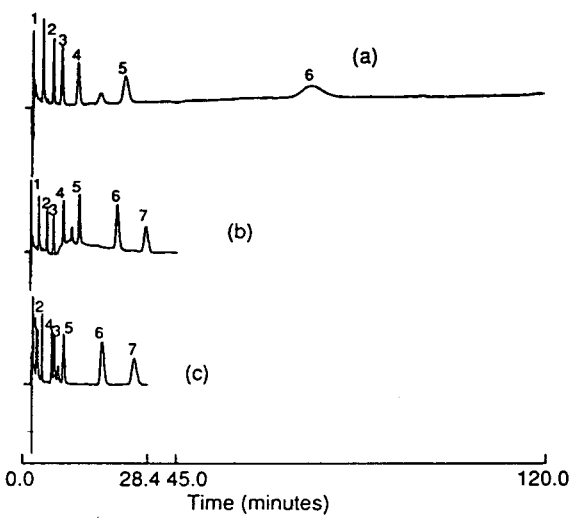

Fig. 7. Separation of a seven-component test mixture. Mobile phase: 0.30 *M* SDS, 0.02 *M* phosphate buffer, pH 2.5 with acetonitrile added. (a) Isocratic separation with 3% acetonitrile, (b) gradient separation with 3 to 20% acetonitrile and (c) isocratic separation with 20% acetonitrile. Peaks: 1 = DF; 2 = F; 3 = KF; 4 = FF; 5 = FFF; 6 = FFFF; 7 = FFFFF.

Another isocratic run was done using 20% acetonitrile (Fig. 7c). A reduction of the separation time to about 25 min and a dramatic increase in the detection sensitivity are observed. However, poor resolution is observed for the early-eluting peaks especially for peaks 3 and 4; peak reversal between these two peaks was observed as well. Likewise, peaks 1 and 2 elute very near t_0.

A better separation is again obtained when using gradient elution as shown in Fig. 7b. The acetonitrile concentration was varied from 3 to 20% for 5 min and was held at 20% acetonitrile for 40 min. The advantages of gradient elution are again observed.

Finally, it is worth noting that the peak efficiencies under gradient elution conditions were better than those under isocratic condition for both propanol and acetonitrile systems (Table 5.)

Acknowledgement

The authors gratefully acknowledge the support of this work by a research grant from the US National Institutes of Health (GM 38738).

References

[1] L.R. Snyder, J.W. Dolan and J.R. Grant, *J. Chromatogr.*, 165 (1979) 3.

[2] L.R. Snyder, in Cs. Horváth (Editor), *High-Performance Liquid Chromatography —Advances and Perspectives*, Vol. 1, Academic Press, New York, 1980, Ch. 4.

[3] M.A. Quarry, R.L. Grob and L.R. Snyder, *J. Chromatogr.*, 285 (1984) 1.

[4] M.A. Quarry, R.L. Grob and L.R. Snyder, *J. Chromatogr.*, 285 (1984) 19.

[5] J.W. Dolan, L.R. Snyder and M.A. Quarry, *Chromatographia*, 24 (1987) 261.

[6] J.W. Dolan, *LC·GC*, 5 (1987) 384.

[7] J.W. Dolan, *LC·GC*, 5 (1987) 466.

[8] M.A. Quarry, R.L. Grob and L.R. Snyder, *Anal. Chem.*, 58 (1986) 907.

[9] R.M. McCormick and B.L. Karger, *J. Chromatogr.*, 199 (1980) 259.

[10] R.M. McCormick and B.L. Karger, *Anal. Chem.*, 52 (1980) 2249.

[11] L.A. Cole and J.G. Dorsey, *Anal. Chem.*, 62 (1990) 16.

[12] J. Frenz and Cs. Horváth, *J. Chromatogr.*, 282 (1983) 249.

[13] J.G. Dorsey, M.T. DeEchegaray and J.S. Landy, *Anal. Chem.*, 55 (1983) 924.

[14] M.G. Khaledi, E. Peuler and J. Ngeh-Ngwainbi, *Anal. Chem.*, 59 (1987) 2738.

[15] M.G. Khaledi, J.K. Strasters, A.H. Rodgers and E.D. Breyer, *Anal. Chem.*, 62 (1990) 130.

[16] J.K. Strasters, E.D. Breyer, A.H. Rodgers and M.G. Khaledi, *J. Chromatogr.*, 511 (1990) 17.

[17] A.S. Kord and M.G. Khaledi, *Anal. Chem.*, 64 (1992) 1894.

[18] A.S. Kord and M.G. Khaledi, *Anal. Chem.*, 64 (1992) 1900.

[19] A.S. Kord and M.G. Khaledi, *J. Chromatogr.*, 631 (1993) 125.

[20] L.S. Madamba-Tan, J.K. Strasters and M.G. Khaledi, *J. Chromatogr. A*, 683 (1994) 321.

[21] R.P.W. Scott and C.F. Simpson, *Faraday Symp. Chem. Soc.*, 15 (1980) 69.

ELSEVIER

Journal of Chromatography A, 683 (1994) 347–353

JOURNAL OF CHROMATOGRAPHY A

Chromatographic and ^{1}H NMR support for a proposed chiral recognition model

William H. Pirkle*, Christopher J. Welch☆

School of Chemical Sciences, University of Illinois, Urbana, IL 61801, USA

Received 12 April 1994

Abstract

Liquid chromatography and ^{1}H NMR spectroscopy were used in an investigation of a chiral recognition rationale which was previously advanced to account for the resolution of naproxen (NAP-COOH) enantiomers on brush-type chiral stationary phases, **CSP-1** and **CSP-2**, identical except for tether length. **CSP-1** has recently been commercialized as the Whelk-O 1. This chiral stationary phase (CSP), basically an immobilized enantiomer of N-(3,5-dinitrobenzoyl)-4-amino-1,2,3,4-tetrahydrophenanthrene, was designed to have a cleft in which one enantiomer is preferentially bound. The cleft consists of π-acidic and π-basic aromatic systems held more or less perpendicular to each other. Aromatic substituents in the analyte were expected to be held in this cleft by simultaneous face-to-face and face-to-edge $\pi-\pi$ interactions. To ascertain whether analytes are truely bound in this cleft, NMR studies of mixtures of several naproxen-like analytes and chiral solvating agent **3**, a soluble version of the selector used in **CSP-1**, were undertaken. Additional motivation for the study came from the observation that the enantiomers of NAP-COOH and NAP-COOMe elute in a different order than do the enantiomers of NAP-CONHMe, and NAP-CON(Me)$_2$. This difference in the elution order of the amide derivatives with respect to the esters and free acid was not totally unexpected, for the chiral recognition hypothesis used in the design of the chiral selector allowed for such an eventuality. It was known from reciprocal chromatographic studies that the enantiomers of soluble analogs of the Whelk-O 1 CSP show different elution orders on naproxen-derived amide CSPs than they do on naproxen-derived ester CSPs. These data aided in formulation of the initial chiral recognition rationale. Evidence for the occurance of the specific molecular interactions suggested by this rational is provided by the presently described ^{1}H NMR study of the enantioselective complexation of the enantiomers of NAP-COOH, NAP-COOMe, NAP-CONHMe, and NAP-CON(Me)$_2$ by a single enantiomer of a soluble analog of the Whelk-O 1 CSP.

1. Introduction

Chiral stationary phases (CSPs) **1** and **2**, designed for the chromatographic separation of the underivatized enantiomers of the commercially important 2-arylpropionic acid, naproxen [1,2], afford excellent separations not only for the underivatized enantiomers of naproxen but also for a number of related non-steroidal anti-inflammatory drugs (NSAIDs) such as ibuprofen, fenoprofen and flurbiprofen. Moreover, CSP **2** is useful for separating the enantiomers of

* Corresponding author.

☆ Present address: Regis Technologies, Inc., 8210 Austin Avenue, Morton Grove, IL 60053, USA.

0021-9673/94/$07.00
SSDI 0021-9673(94)00477-Q

a large number of compounds of diverse types [3]. The mechanistic concepts underlying the design of CSPs **1** and **2** were developed largely through the use of chromatographic data. The final design was reached with the aid of CPK[1] space-filling models. The essential aspect of the design is to incorporate a cleft in which face-to-face and face-to-edge $\pi-\pi$ interactions occur simultaneously with an aromatic substituent present near the stereogenic center of the analyte. A proximate hydrogen bond acceptor site is also required by the chiral recognition rationale. This paper reports the results of an ^{1}H NMR solution study of the structure of the complexes derived from naproxen (NAP-COOH) and naproxen derivatives (NAP-COOMe, NAP-CONHMe, NAP-CON(Me)$_2$) and the chiral solvating agent (CSA) **3**, a soluble analogue of the selector used in CSPs **1** and **2** (Fig. 1).

An illustration of the rationale advanced to account for the observed separation of naproxen enantiomers on CSPs **1** and **2** is presented in Fig. 2 [1,2]. Four possible diastereomeric adsorbates derived from an (*S*,*S*)-CSP and the two enantiomers of naproxen are represented using computer-generated space-filling molecular model representations. The alkyl tether of the CSP is represented as an *n*-propyl substituent, and distances between the two components of the diastereomeric complexes have been exaggerated for the sake of clarity. Each of the component molecules is represented in a conformation which is presumed to be of relatively low energy and hence extensively populated. The dihedral angle between the methine hydrogen and the carbonyl oxygen of naproxen and its derivatives is taken to be *ca.* 180°. The dinitrobenzoyl ring system of the (*S*,*S*)-CSP is viewed edge on, with the amide hydrogen projecting toward the viewer.

Each of the four adsorbate pairs pictured in Fig. 2 are held together by a combination of hydrogen bonding and $\pi-\pi$ interaction forces. The hydrogen bond formed between the amide hydrogen of the CSP and the carboxylate oxygen of the analyte molecule can occur at either of the two oxygens of the carboxylate system. These adsorbates are designated as **C** and **H**, depending on whether the hydrogen bond occurs at the carbonyl oxygen or the hydroxyl oxygen. Furthermore, the face to face $\pi-\pi$ interaction can involve interaction of the naphthyl ring of naproxen (or, in the general case, the aryl substituent of the NSAID) with either face of the dinitrobenzamide system of the CSP, resulting in

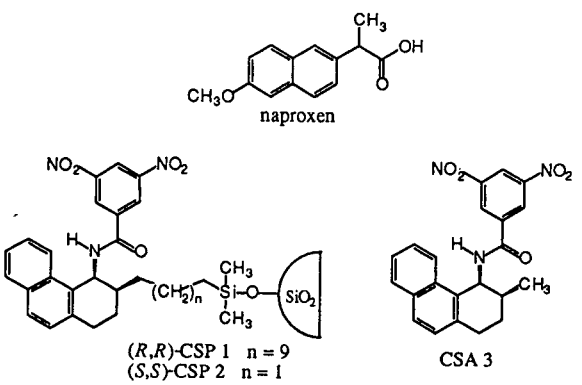

Fig. 1. Structures of CSPs **1** and **2** and CSA **3** used in the study.

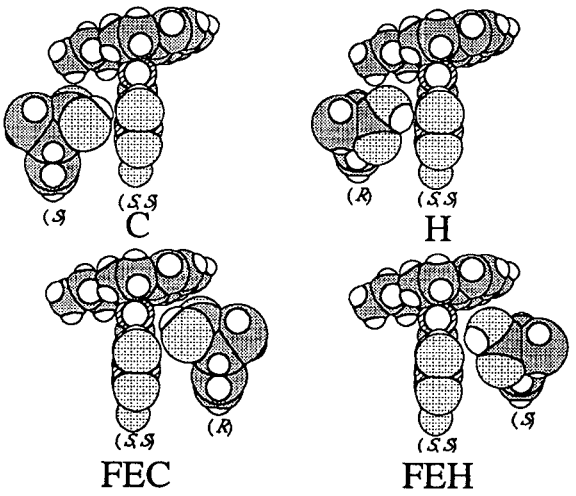

Fig. 2. Computer-generated space-filling molecular model representations of the four diastereomeric adsorbates proposed to account for separation of naproxen enantiomers on CSPs **1** and **2**.

[1] Corey–Pauling–Koltun, CPK® Models are available from Harvard Apparatus, Inc., 22 Pleasant Street, South Natick, MA 01760, USA.

the four possible adsorbates pictured in Fig. 2. CSPs **1** and **2** have been designed so as to encourage binding within the "cleft" formed by the two aromatic systems. Binding within this cleft is believed to allow the formation of a face-to-edge $\pi-\pi$ interaction (**FE**) involving the dihydrophenanthrene ring of the CSP and the aryl ring of the NSAID. The shortened tether of CSP **2** may provide further preference for the binding of analytes within this cleft, since the formation of adsorbates **C** and **H** may be sterically impeded by the underlying silica support [2].

Adsorbate **FEH** is believed to illustrate the predominant mode of interaction between the CSP and the more retained enantiomer of naproxen. By utilizing the hydroxyl oxygen as a hydrogen bonding site, the methine hydrogen is directed toward the dihydrophenanthrene portion of the CSP. The small size of this hydrogen permits the two components to approach closely where the slightly acidic methine hydrogen may undergo weak bonding to the π-cloud of the dihydrophenanthrene system. Additionally, the hydroxyl group may simultaneously hydrogen bond to the proximate nitro group. From the models, it would appear that the hydroxyl proton in adsorbate **FEH** is positioned so as to allow a trifurcated hydrogen bond between the two carboxyl and one of the nitro group oxygens. No experimental evidence is offered for this however. Adsorbate **FEC** is believed to illustrate the predominant adsorbate formed by the less retained enantiomer.

The naproxen derivatives illustrated in Fig. 3 were prepared in order to test the chiral recognition rationale presented in Fig. 2. Unlike NAP-COOH and NAP-COOMe, the amide derivatives NAP-CONHMe and NAP-CON(Me)$_2$ contain but one oxygen which can serve as a hydrogen bond accepting site, thus only adsorbates **C** and **FEC** need be considered. Considerations of both steric encumbrance to adsorbate formation and the potential contribution of energetically favorable face to edge $\pi-\pi$ interaction suggest that the heterochiral [(*S*,*S*)-CSA · (*R*)-analyte] adsorbate **FEC** should be more stable. Thus, for amide derivatives of naproxen, CSPs **1** and **2** are expected to selectively retain the enantiomer which affords the heterochiral adsorbate, whereas the enantiomer which affords the homochiral [(*S*,*S*)-CSA · (*S*)-analyte] adsorbate is known to be retained in the case of the free acid [1,2]. Ester derivatives, like the free acid, contain two oxygens, thus all four adsorbates pictured in Fig. 2 must be considered. However, since the oxygen involved in hydrogen bonding in adsorbate **FEH** is sterically less accessible in the ester than in the acid and the ester cannot utilize the postulated trifurcated hydrogen bond, one might anticipate somewhat attenuated enantioselectivity for the ester relative to the acid.

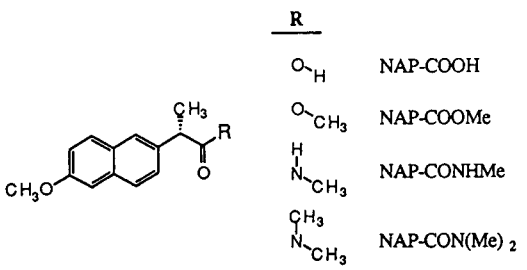

Fig. 3. Derivatives of (*S*)-naproxen used in the study. Small amounts of the corresponding compounds derived from racemic naproxen were also prepared for the HPLC study.

2. Experimental

2.1. General methods

All reagents were of pharmaceutical or reagent grade and were used without further purification. Solvents used were HPLC grade or distilled prior to use. (*S*)-Naproxen, (+)-6-methoxy-α-methyl-2-naphthyleneacetic acid, was obtained from Aldrich (Milwaukee, WI, USA). Racemic naproxen was kindly donated by Sepracor (Marlborough, MA, USA). The preparation of CSPs **1** [1] and **2** [2] has been described previously. NAP-COOMe was prepared via Fischer esterification with methanol. Amide derivatives NAP-CONHMe and NAP-CON(Me)$_2$ were prepared from the corresponding acid chloride, which was generated using oxalyl chloride. Chromatographic analysis was performed using an Altex Model 100A pump, a Rheodyne Model

7125 injector with a 20-μl sample loop, a Linear UVIS 200 variable wavelength absorbance monitor set at 254 nm, and a Hewlett-Packard HP 3394 integrating recorder. All chromatographic experiments were carried out at a nominal flow-rate of 2.00 ml/min. Column void time was measured by injection of 1,3,5-tri-*tert.*-butylbenzene. All ^{1}H NMR chemical shifts are reported in ppm (δ) relative to tetramethylsilane.

3. Results and discussion

3.1. HPLC studies

Data pertinent to the separation of the enantiomers of the naproxen derivatives on CSPs **1** and **2** are shown in Table 1. The ester derivative, NAP-COOMe, shows retention of the enantiomer forming the homochiral adsorbate [i.e. the (*R*) enantiomer is selectively retained on an (*R*,*R*)-CSP, and the (*S*) enantiomer is selectively retained on an (*S*,*S*)-CSP]. The enantioselectivity observed for the ester is somewhat smaller than that observed for the free acid. The naproxen amide derivatives show retention of the enantiomer forming the heterochiral adsorbate, with the dimethylamide, NAP-CON(Me)$_2$, showing greater enantioselectivity than the methylamide, NAP-CONHMe. These results lend support to the suggestion that adsorbate **FEH** may be the preferred mode of interaction of free acid and methyl ester with the CSP, whereas adsorbate **FEC** may be the preferred mode of interaction of the amide derivatives.

Further support the for this chiral recognition rationale is provided by studies of the reciprocal chromatographic situation, in which a variety of amide, ester and ionic-linked naproxen-derived CSPs were used to resolve the enantiomers of soluble analogues of the CSPs **1** and **2** [4].

3.2. ^{1}H NMR studies

Examination of molecular models of proposed adsorbates **FEC** and **FEH**, believed to account for the predominant adsorption of naproxen and its derivatives on CSPs **1** and **2**, suggests that ^{1}H NMR solution studies should afford some insight into the chiral recognition process. In adsorbate **FEC**, the methine hydrogen of naproxen is oriented away from the tetrahydrophenanthrene ring of the CSP whereas in adsorbate **FEH**, this hydrogen is forced into the π-cloud of the tetrahydrophenanthryl ring. One would expect that an upfield chemical shift would be observed for this methine signal in cases where adsorbate **FEH** is formed to a great extent. In cases where formation of adsorbate **FEC** is favored, the methyl group of naproxen is similarly expected to be shifted upfield.

Solutions of a 1:1 mixture of either enantiomer of CSA **3** with each of the four (*S*)-naproxen analytes shown in Fig. 3 were prepared as 12.5 m*M* solutions in deuterochloroform and examined by ^{1}H NMR spectroscopy at ambient temperature. Table 2 shows the major chemical

Table 1
Separation of the enantiomers of naproxen derivatives on (*R*,*R*)-CSP **1** and (*S*,*S*)-CSP **2**

Compound	(*R*,*R*)-CSP **1**			(*S*,*S*)-CSP **2**		
	k_1'	α	Retained[a]	k_1'	α	Retained[a]
NAP-COOH	4.73	2.15	Homochiral	2.88	2.98	Homochiral
NAP-COOMe	2.31	1.35	Homochiral	3.42	1.42	Homochiral
NAP-CONHMe	13.48	1.45	Heterochiral	18.73	1.41	Heterochiral
NAP-CON(Me)$_2$	4.24	2.61	Heterochiral	5.24	3.24	Heterochiral

Mobile phase, 20% 2-propanol in hexane with 1 g/l ammonium acetate; flow-rate, 2.00 ml/min; ambient temperature. k_1' = Retention factor for initially eluted enantiomer; α = separation factor.
[a] Absolute configuration of retained enantiomer relative to absolute configuration of the CSP.

Table 2
Changes in ^{1}H NMR chemical shifts upon interaction of the four (*S*)-naproxen derivatives with either enantiomer of CSA **3**

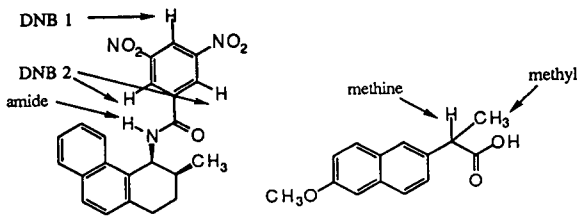

Complex	CSA **3**			Naproxen		
	DNB 1	DNB 2	Amide	Methine	Methyl	Stability[a]
(*S*)-NAP-COOH + (*R*,*R*)-CSA	−0.05	−0.02	+0.05	−0.02	−0.03	Less
(*S*)-NAP-COOH + (*S*,*S*)-CSA	−0.08	−0.05	+0.11	−0.17	−0.05	More
(*S*)-NAP-COOMe + (*R*,*R*)-CSA	−0.07	−0.04	+0.14	−0.03	−0.10	Less
(*S*)-NAP-COOMe + (*S*,*S*)-CSA	−0.10	−0.05	+0.22	−0.24	−0.10	More
(*S*)-NAP-CONHMe + (*R*,*R*)-CSA	−0.14	−0.04	+0.53	−0.10	−0.17	More
(*S*)-NAP-CONHMe + (*S*,*S*)-CSA	−0.16	−0.04	+0.62	−0.40	−0.14	Less
(*S*)-NAP-CON(Me)$_2$ + (*R*,*R*)-CSA	−0.20	−0.07	+0.64	−0.09	−0.19	More
(*S*)-NAP-CON(Me)$_2$ + (*S*,*S*)-CSA	−0.06	−0.02	+0.24	−0.02	−0.03	Less

Conditions: analyte concentrations, 12.5 m*M* in C^2HCl_3; spectrometer frequency, 200 MHz; temperature, ambient.
[a]Relative stability of the diastereomeric complexes as inferred from chromatographic studies.

shift differences induced in CSA **3** and the naproxen derivatives through their interactions. The induced chemical shifts of the proton in the 4-position and of the two protons in the 2- and 6-positions of the dinitrobenzoyl ring of CSA **3**, reported as DNB 1 and DNB 2 in Table 2, are indicative of $\pi-\pi$ interaction, for mutual upfield chemical shifts are often noted upon formation of face to face $\pi-\pi$ complexes. The downfield shift of the amide hydrogen of CSA **3** reflects its participation in hydrogen bonding. Changes in the chemical shift of the methine and α-methyl protons of the various naproxen derivatives are expected to be sensitive to shielding effects from the tetrahydrophenanthrene ring of CSA **3** as described above.

The enantiomer of NAP-COOH which gives rise to the homochiral adsorbate is known to be preferentially retained on both CSPs **1** and **2**. Similarly, it is the homochiral complex of (*S*)-NAP-COOH and (*S*,*S*)-CSA **3** which shows a larger downfield shift in the amide hydrogen resonance and larger upfield shifts in the DNB proton resonances, both indicative of more extensive complexation. The homochiral complex also shows a larger upfield shift in the naproxen methine resonance, presumably owing to the previously discussed shielding to be expected in adsorbate **FEH**. NAP-COOMe also shows larger shifts in the amide, DNB and methine resonances for the more stable homochiral diastereomeric pair, again supporting the original chiral recognition rationale.

As in the chromatographic studies, it is the heterochiral adsorbate pair of NAP-CON(Me)$_2$ which is the most stable, as evidenced by the large shifts in the amide and DNB resonances observed for the heterochiral complex. In the previously discussed chiral recognition rationale, adsorbate **FEC** is presumed to be the predominant retention mode for amide derivatives of naproxen. This model predicts that shielding of the methine proton, which was important in the acid and ester derivatives, should be relatively unimportant for the amides, whereas some shielding of the naproxen methyl group at the stereogenic center may be expected. The results show that the methine hydrogen is indeed rela-

tively unaffected by complexation and that the methyl group is shifted upfield by nearly 0.2 ppm in the heterochiral complex.

All of the chemical shift perturbations observed in the ^{1}H NMR spectra of the diastereomeric complexes of NAP-COOH, NAP-COOMe, and NAP-CON(Me)$_2$ with CSA **3** support the chiral recognition rationale originally based upon chromatographic data and examination of molecular models. However, the behavior of NAP-CONHMe is somewhat surprising. Large shifts in DNB and amide hydrogen resonances are observed in both diastereomeric complexes. Furthermore, the less stable homochiral adsorbate pair (based upon chromatographic analysis) shows an extremely large upfield shift for the methine resonance, a result which cannot easily be reconciled with the proposed model. These results suggest that both of the diastereomeric complexes are quite stable. While the predominant heterochiral adsorbate is believed to be as pictured in adsorbate **FEC**, the nature of the homochiral adsorbate is unknown. Examination of molecular models suggests that an adsorbate structure similar to adsorbate **FEH** in which the amide hydrogen of NAP-CONHMe is directed into the π-cloud of the tetrahydrophenanthrene ring of CSA **3** may account for the enhanced stability of the homochiral complex. Such hydrogen bonding to the π-clouds of aromatic systems has been proposed to be important in other chiral recognition systems [5] and has received a good deal of recent attention [6,7].

Chromatographic analysis of naproxen derivatives was carried out on CSPs **1** and **2** using chloroform as eluent. The results, summarized in Table 3, shed some light upon the interesting behavior of NAP-CONHMe in the NMR study.

The results presented in Table 3, when contrasted with the results presented in Table 2, demonstrate the influence of mobile phase composition on the chromatographic separation of the enantiomers of naproxen derivatives. Interestingly, the enantiomers of NAP-CONHMe, although relatively strongly retained, are not resolved on either CSP **1** or CSP **2** when chloroform is used as a mobile phase. This result is consistent with the ^{1}H NMR data which indicates that the diastereomeric adsorbates derived from either enantiomer of CSA **3** and (*S*)-NAP-CONHMe are both quite stable, differing negligibly in this regard in chloroform.

4. Conclusions

A variety of chromatographic evidence, as well as ^{1}H NMR studies using a chiral solvating agent, has been used to investigate the mechanism of enantioselective retention of naproxen and its derivatives by the recently developed CSPs **1** and **2**. These investigations support the original chiral recognition rationale advanced to account for these separations. The current study provides insight which may prove useful both for understanding the resolution of non-NSAID analytes on CSP **2** (CSP **2** is commercially available as the Whelk-O 1 CSP from Regis Technologies) and for the design of improved CSPs.

Table 3
Chromatographic separation of the enantiomers of naproxen derivatives using chloroform as a mobile phase

Compound	CSP β1			CSP **2**		
	k_1'	α	Retained[a]	k_1'	α	Retained[a]
NAP-COOMe	0.19	1.37	Homochiral	0.28	1.43	Homochiral
NAP-COONHMe	1.80	1.00	–	1.75	1.00	–
NAP-CON(Me)$_2$	0.64	1.66	Heterochiral	0.51	2.24	Heterochiral

Conditions: mobile phase, 100% chloroform; flow-rate, 2.00 ml/min; temperature, ambient. k_1' = Retention factor for initially eluted enantiomer; α = separation factor.

[a] Absolute configuration of retained enantiomer relative to absolute configuration of CSP.

Acknowledgements

This work was supported by a grant from the National Science Foundation and by a Department of Education Advanced Opportunities in Chemistry Graduate Fellowship. HPLC solvents have been generously donated by EM Scientific.

References

[1] W.H. Pirkle, C.J. Welch and B. Lamm, *J. Org. Chem.*, 57 (1992) 3854.

[2] W.H. Pirkle and C.J. Welch, *J. Liq. Chromatogr.*, 15 (1992) 1947.

[3] W.H. Pirkle and C.J. Welch, *Tetrahedron Asymm.*, 5(5) (1994) 777.

[4] C.J. Welch, *Ph.D. Thesis*, University of Illinois–Urbana, Urbana, IL, 1992.

[5] W.H. Pirkle, T.C. Pochapsky, G.S. Mahler, D.E. Corey, D.S. Reno and D.M. Alessi, *J. Org. Chem.*, 51 (1986) 4991.

[6] S. Suzuki, P.G. Green, R.E. Bumgarner, S. Dasgupta, W.A. Goddard and G.A. Blake, *Science*, 257 (1992) 942.

[7] M.A. Viswamitra, R. Radhakrishnan, J. Bandekar and G.R. Desiraju, *J. Am. Chem. Soc.*, 115 (1993) 4868.

ELSEVIER

Journal of Chromatography A, 683 (1994) 355–365

JOURNAL OF CHROMATOGRAPHY A

Prediction of inorganic and organic ion behaviour with polyvalent eluents in ion chromatography

Carlos Mongay, Carmen Olmos, Agustín Pastor*

Department of Analytical Chemistry, Faculty of Chemistry, University of Valencia, Dr. Moliner 50, 46100 Burjasot (Valencia), Spain

First received 2 March 1994; revised manuscript received 25 May 1994

Abstract

A model is presented that relates the capacity factor, k', to experimental stationary and mobile phase elution variables (resin capacity, dry resin mass, dead volume, concentration and pH) and to the protonation constants of the specimens involved. Application of the model to elution with different concentrations of phthalic acid using a low-capacity quaternary ammonium column permits the determination of the selectivity coefficients of each ion-exchange equilibrium and the establishment of the theoretical k' (pH) curves at a constant eluent concentration, which are seen to coincide with the experimental curves. The model is able to predict solute behaviour and optimize separation by establishing the corresponding acidity conditions. Likewise, this model is a possible tool for studying ion-exchange and non-polar interactions of ions with ion-exchange columns.

1. Introduction

Selectivity coefficients and distribution coefficients are based on ion-exchange equilibria [1]. In liquid chromatography the capacity factor, k', is used as a measure of the elution power of the mobile phase with respect to a solute ion in a given resin. Thus, by relating the capacity factor with the solute and mobile and stationary phase characteristics, expressions may be derived that allow us to predict the corresponding retention times in a particular column on modifying experimental elution variables such as eluent concentration or pH.

Many workers have applied this method to both gravity ion chromatography (gravity-IC) [2] and high-performance ion chromatography (HPIC) [3–5], using monoanionic eluents in all instances, i.e., those giving rise to a single anion-exchange species (ions from strong acids, monovalent ions of weak acids or polyvalent ions operating in a pH range where a single species predominates).

If the sample also contains monoanionic species, the expression $\log k' = \text{constant} - (j/i) \log C$, were C is the eluent concentration and i and j are the eluent and sample ionic charges, respectively, has been systematically applied [6]. This expression is also employed in cation exchanges [7]. Maki and Danielson [8] applied this proportionality to the retention of inorganic ions (F^-, Cl^-, NO_2^-, Br^-, NO_3^-, I^-, SCN^- and SO_4^{2-}) with different naphthalenesulfonic acids as eluents. On comparing the slopes of the

* Corresponding author.

0021-9673/94/$07.00
SSDI 0021-9673(94)00485-R

experimental straight lines, log k' versus log C, applying the theoretical i and j values, they found that with the exception of the monovalent ions using 2-naphthalenemonosulfonic acid ($j/i = 1$), the remaining slopes are all greater than expected. They argued that apparently for both 1,5-naphthalenedisulfonate and 1,3, 6 or 7-naphthalenetrisulfonate, the effective charge of the bulky eluent with two widely spaced sulfonate groups is less than the true charge during the ion-exchange process involving small anions. Likewise, slope discrepancies exist when phthalic acid (pH 6.25) is used as the eluent, in spite of its lesser bulk. In this case, the anion is presumed to exhibit entirely a charge of 2 [9]. A case in point was reported by Haddad and Cowie [10], who employed phthalic acid as the mobile phase at pH 5.3, where the mono- and divalent forms coexist in the same proportion (50%); consequently, they considered the eluent to behave as a single species of charge −1.52. Analogously, Haddad and Cowie regarded the samples as single species possessing a fractional charge of a magnitude dependent upon the protonation constants.

When the sample consists of polyanionic species and the eluent used remains monoanionic, the proportionality between k' and concentration is not direct, as the participation of all the ion species present must be considered in the ion exchange. Beukenkamp et al. [11] deduced an expression corresponding to gravity-IC, although the resulting equation has rarely been applied.

The purpose of this study was to obtain an expression to relate k' to eluent concentration and pH, with the aim of applying it to the general case of polyanionic eluents and samples. To this effect we considered all the ion-exchange reactions that may occur between the ion species present in both the eluent and sample, each being regulated by a factor capable of determining degree of contribution.

At constant pH, pairs of values (k', eluent concentration) are obtained experimentally; on substitution in the mathematical expression they enable us to calculate the corresponding selectivity coefficients, along with the respective contributions of each equilibrium.

Subsequently, and in this case keeping the eluent concentration constant, the corresponding relationship between k' and pH may be established. This in turn facilitates the establishment of acidity conditions for optimum separation.

2. Theory

2.1. Polyprotic eluent

Monoanionic sample anion

Consider a polyprotic eluent, H_nP, with accumulated protonation constants β_i, and a type HA sample with a constant, β_{1A}, operating in a pH range where the different protonated forms of both the eluent and sample may coexist. As initially the resin, R, is associated with the different eluent forms ($R_iH_{n-i}P$, with $1 \leq i \leq n$), the following ion-exchange reactions occur within it:

$$\begin{aligned}
&A^- + RH_{n-1}P \rightleftharpoons RA + H_{n-1}P^- && x_1\\
&A^- + \tfrac{1}{2}R_2H_{n-2}P \rightleftharpoons RA + \tfrac{1}{2}H_{n-2}P^{2-} && x_2\\
&A^- + \frac{1}{i}R_iH_{n-i}P \rightleftharpoons RA + \frac{1}{i}H_{n-i}P^{i-} && x_i\\
&A^- + \frac{1}{n}R_nP \rightleftharpoons RA + \frac{1}{n}P^{n-} && x_n
\end{aligned} \qquad (1)$$

In this process each equilibrium participates with a contribution x_i. The global balance is given by the following:

$$\left(\sum x_i\right)A^- + \sum\left(\frac{x_i}{i}R_iH_{n-i}P\right) \rightleftharpoons \left(\sum x_i\right)RA + \sum\left(\frac{x_i}{i}H_{n-i}P^{i-}\right) \qquad (2)$$

Taking into account that the condition $\Sigma_{i=1}^{n} x_i = 1$ is always satisfied, the global selectivity coefficient, E, like the equilibrium constant for ion exchange for the global reaction 2, is given by

$$E_0 = \frac{[RA]\cdot[H_{n-1}P^-]^{x_1}\cdot[H_{n-2}P^{2-}]^{\frac{x_2}{2}}\cdot\ldots\cdot[H_{n-i}P^{i-}]^{\frac{x_i}{i}}\cdot\ldots\cdot[P^{n-}]^{\frac{x_n}{n}}}{[A^-]\cdot[RH_{n-1}P]^{x_1}\cdot[R_2H_{n-2}P]^{\frac{x_2}{2}}\cdot\ldots\cdot[R_iH_{n-i}P]^{\frac{x_i}{i}}\cdot\ldots\cdot[R_nP]^{\frac{x_n}{n}}} = \frac{[RA]\cdot\prod[H_{n-i}P^{i-}]^{\frac{x_i}{i}}}{[A^-]\cdot\prod[R_iH_{n-i}P]^{\frac{x_i}{i}}} \qquad (3)$$

This selectivity coefficient remain constant with pH.

On the other hand, we define the mass distribution coefficient, D_g, for the exchange of an ion A^- as

$$D_g = \frac{[RA]}{[A^-] + [HA]} = \frac{[RA]}{[A^-] + (1 + \beta_{1A}h)} \quad (4)$$

where $h = [H^+]$. If the ratio [RA]/[A] obtained from Eq. 3 is substituted in Eq. 4, we find that

$$D_g = \frac{E_0}{(1 + \beta_{1A}h)} \cdot \frac{\prod [R_iH_{n-i}P]^{\frac{x_i}{i}}}{\prod [H_{n-i}P^{i-}]^{\frac{x_i}{i}}} \quad (5)$$

In turn, the capacity factor, k', is related to the mass distribution coefficient by the following expression [1]:

$$k' = \frac{t_r - t_0}{t_0} = D_g \cdot \frac{W}{V_0} \quad (6)$$

where W is the dry resin mass and V_0 the dead volume. By substituting the value of D_g obtained in Eq. 5 in Eq. 6, we observe

$$k' = \frac{WE_0}{V_0(1 + \beta_{1A}h)} \cdot \frac{\prod [R_iH_{n-i}P]^{\frac{x_i}{i}}}{\prod [H_{n-i}P^{i-}]^{\frac{x_i}{i}}} \quad (7)$$

In order to resolve this expression, we must establish the concentrations of each of the n eluent–resin forms. An equation may be developed to show that in the resin phase the total concentration of species occupying active points is reflected by the corresponding exchange capacity, Q. If, moreover, we take into account that the amount of resin-bound sample is negligible (<1%) compared with the amount of associated eluent, then

$$Q = \sum (i[R_iH_{n-i}P]) \quad (8)$$

The remaining $(n-1)$ equations may be defined if as a first approximation we accept that the bond between the eluent species $H_{n-i}P^{i-}$ and the resin is i times more intense than when bonding occurs between two monovalent charges. As the concentration of each resin-bound eluent species is proportional to its concentration in solution, these $(n-1)$ equations are given by

$$\frac{[R_iH_{n-i}P]}{[RH_{n-1}P]} = \frac{ik[H_{n-i}P^{i-}]}{k[H_{n-1}P^-]} \quad (9)$$

On resolving the system represented by Eqs. 8 and 9, we find that

$$[R_iH_{n-i}P] = \frac{Qi\beta_{n-i}h^{n-i}}{n^2 + \sum [(n-i)^2\beta_ih^i]} \quad (10)$$

The substitution of Eq. 10 in the numerator of the Eq. 7 and of the different eluent species concentrations as a function of their molar fractions in the denominator of Eq. 7 yields the following equation:

$$k' = \frac{WE_0}{V_0(1 + \beta_{1A}h)} \cdot \frac{\prod \left(\frac{Qi\beta_{n-i}h^{n-i}}{n^2 + \sum [(n-i)^2\beta_ih^i]} \right)^{\frac{x_i}{i}}}{\prod \left[\frac{C\beta_{n-i}h^{n-i}}{1 + \sum (\beta_ih^i)} \right]^{\frac{x_i}{i}}}$$

$$= \frac{WE_0}{V_0(1 + \beta_{1A}h)} \cdot \prod \left[\frac{Qi\left(1 + \sum \beta_ih^i\right)}{C\left(n^2 + \sum [(n-i)^2\beta_ih^i]\right)} \right]^{\frac{x_i}{i}} \quad (11)$$

where C is the total eluent concentration. This expression contains n unknowns, i.e., the $(n-1)$ contributions x_i of each equilibrium to the total ion exchange and the value of the global selectivity coefficient, E_0.

Resolution of this expression requires the determination of the capacity factors of the eluate at different eluent concentrations, operating at a known and constant pH. Under these conditions, the above expression is reduced to

$$k' = P \prod \left[\frac{1}{C} \right]^{\frac{x_i}{i}} = \frac{P}{C^{\left[\sum \left(\frac{x_i}{i}\right)\right]}} \quad (12)$$

where P is a constant encompassing the selectivity coefficient, the sample and eluent protonation constants, operating pH, dead volume, resin capacity and resin dry mass. Knowing the contributions x_i and the selectivity coefficient, E_0, Eq. 11 allows us to determine the curves k'(pH) corresponding to a monovalent sample with a polyvalent eluent.

As a particular case, a multiply charged species, behaving within the operating pH range as a monoanionic species, would exhibit the following generic exchange equilibrium:

$$A^{j-} + \frac{j}{i} R_i H_{n-i} P \rightleftharpoons R_j A + \frac{j}{i} H_{n-i} P^{i-} \quad (13)$$

The reasoning is the same as above, but in this case the distribution coefficient is given by

$$D_g = \frac{[R_j A]}{[A^{j-}]} \quad (14)$$

This yields the following expression:

$$k' = \frac{W}{V_0} \cdot E_0 \cdot \prod \left[\frac{Qi\left(1 + \sum \beta_i h^i\right)}{C\left(n^2 + \sum [(n-i)^2 \beta_i h^i]\right)} \right]^{\frac{jx_i}{i}} \quad (15)$$

When operating at a constant pH, the derived capacity factor is

$$k' = \frac{P}{C\left[j \Sigma \left(\frac{x_i}{i}\right)\right]} \quad (16)$$

This is the expression usually employed for the elution of inorganic ions using likewise totally dissociated inorganic eluents [12], and whose logarithmic representation establishes whether the process is predominantly an ion exchange [13]. On the other hand, the different value of the contributions explains the slope variations observed in some reports [9].

Dianionic sample anion

In this case two exchangeable ionic species exist (A^{2-} and HA^-), whose generic exchange equilibria are expressed by

$$\begin{aligned} A^{2-} + \frac{2}{i} R_i H_{n-i} P &\rightleftharpoons R_2 A + \frac{2}{i} H_{n-i} P^{i-} \; x_{i0} \\ HA^- + \frac{1}{i} R_i H_{n-i} P &\rightleftharpoons RHA + \frac{1}{i} H_{n-i} P^{i-} \; x_{i1} \end{aligned} \quad (17)$$

Each of the n equilibria considered for species A^{2-} contributes with a value x_{i0} to the total process, versus x_{i1} in the case of species HA^-. The global exchange equations are

$$\begin{aligned} &\left(\sum x_{i0}\right) A^{2-} + \sum \left(\frac{2x_{i0}}{i} \cdot R_i H_{n-i} P\right) \\ &\quad \rightleftharpoons \left(\sum x_{i0}\right) RA + \sum \left(\frac{2x_{i0}}{i} \cdot H_{n-i} P^{i-}\right) \\ &\left(\sum x_{i1}\right) HA^- + \sum \left(\frac{x_{i1}}{i} \cdot R_i H_{n-i} P\right) \\ &\quad \rightleftharpoons \left(\sum x_{i1}\right) RHA + \sum \left(\frac{x_{i1}}{i} \cdot H_{n-i} P^{i-}\right) \end{aligned} \quad (18)$$

with respective selectivity coefficients expressed by

$$\begin{aligned} E_0 &= \frac{[R_2 A] \cdot \prod [H_{n-i} P^{i-}]^{\frac{2x_{i0}}{i}}}{[A^{2-}] \cdot \prod [R_i H_{n-i} P]^{\frac{2x_{i0}}{i}}} \\ E_1 &= \frac{[RHA] \cdot \prod [H_{n-i} P^{i-}]^{\frac{x_{i1}}{i}}}{[HA^-] \cdot \prod [R_i H_{n-i} P]^{\frac{x_{i1}}{i}}} \end{aligned} \quad (19)$$

where $\Sigma x_{i0} = 1$ and $\Sigma x_{i1} = 1$.

In this case the mass distribution coefficient is defined by

$$\begin{aligned} D_g &= \frac{[R_2 A] + [RHA]}{[A^{2-}] + [HA^-] + [H_2 A]} \\ &= \frac{1}{(1 + \beta_{1A} h + \beta_{2A} h^2)} \\ &\quad \cdot \left(\frac{[R_2 A]}{[A^{2-}]} + \frac{[RHA] \beta_{1A} h}{[HA^-]}\right) \end{aligned} \quad (20)$$

Substituting Eqs. 19 and 20 in Eq. 6 yields

$$\begin{aligned} k' = &\frac{W}{V_0 (1 + \beta_{1A} h + \beta_{2A} h^2)} \\ &\cdot \left(\frac{E_0 \prod [R_i H_{n-i} P]^{\frac{2x_{i0}}{i}}}{\prod [H_{n-i} P^{i-}]^{\frac{2x_{i0}}{i}}} \right. \\ &\left. + \frac{E_1 \beta_{1A} h \prod [R_i H_{n-i} P]^{\frac{x_{i1}}{i}}}{\prod [H_{n-i} P^{i-}]^{\frac{x_{i1}}{i}}} \right) \end{aligned} \quad (21)$$

Accepting the same considerations that led to Eq. 10, the latter is substituted in Eq. 21 to give

$$k' = \frac{W}{V_0(1+\beta_{1A}h+\beta_{2A}h^2)} \cdot \left\{ E_0 \prod \left[\frac{Qi\left(1+\sum \beta_i h^i\right)}{C\left\{n^2+\sum[(n-i)^2\beta_i h^i]\right\}} \right]^{\frac{2x_{i0}}{i}} + E_1\beta_{1A}h \prod \left[\frac{Qi\left(1+\sum \beta_i h^i\right)}{C\left\{n^2+\sum[(n-i)^2\beta_i h^i]\right\}} \right]^{\frac{x_{i1}}{i}} \right\} \quad (22)$$

This general expression contains $2n$ unknowns, i.e., the values of x_{i0} and x_{i1} and the selectivity coefficients E_0 and E_1. Again, in order to determine these values, we operate at a known and constant pH, using several eluent concentrations. In this case the expression may be represented as follows:

$$k' = \frac{P_1}{C^{\sum\left(\frac{2x_{i0}}{i}\right)}} + \frac{P_2}{C^{\sum\left(\frac{x_{i1}}{i}\right)}} \quad (23)$$

where P_1 and P_2 are constants. Resolution of the expression is possible by applying an algorithm allowing minimum square fitting (provided that $1 \leq i \leq n$ is always satisfied).

Polyanionic sample anion

In the case of an H_mA sample (weak acid with m ionic species), a total of m generic exchange equilibria may be determined; the resulting equation would have m terms symmetric with those of Eq. 22, with $n \cdot m$ unknowns:

$$k' = \frac{W}{V_0\left(1+\sum_{j=1}^{m}\beta_j h^j\right)} \cdot \sum_{j=0}^{m-1} \left\{ E_j\beta_j h^j \cdot \prod_{i=1}^{n} \left[\frac{Qi\left(1+\sum_{i=1}^{n}\beta_i h^i\right)}{C\left\{n^2+\sum_{i=1}^{n}[(n-i)^2\beta_i h^i]\right\}} \right]^{\frac{m-j}{i}x} \right\} \quad (24)$$

In theory, this would allow us to determine elution times as a function of pH, and corresponding to any ion-exchange process. However, although the mathematical resolution of this expression is feasible through the application of certain fitting methods, error propagation in the calculation of parameters is greatly amplified; as

Table 1
Protonation constants at 40°C

Acid	Log β_1	Log β_2
Phthalic	5.442	8.420
Acetic	4.769	
Lactic	3.873	
Succinic	5.654	9.842
Malic	5.117	8.561
Tartaric	4.372	7.390
Oxalic	4.338	5.628
Sulfuric	2.01	

Table 2
Contributions and global selectivity coefficients of monoanionic sample anions

Anion	x_1	x_2	E_0
Acetate	0.637	0.363	0.198
Lactate	0.549	0.451	0.148
Fluoride	0.381	0.619	0.132
Chloride	0.423	0.577	0.220
Nitrite	0.304	0.696	0.381
Bromide	0.265	0.735	0.498
Nitrate	0.252	0.748	0.663
Sulfate	0.165	0.835	0.136

Table 3
Contributions and global selectivity coefficients of dianionic sample anions

Anion	x_{10}	x_{20}	x_{11}	x_{21}	E_0	E_1
Succinate	0.349	0.651	0.358	0.642	0.0607	0.183
Malate	0.322	0.678	0.456	0.544	0.0385	0.188
Tartrate	0.426	0.574	0.275	0.725	0.0430	0.231
Oxalate	0.490	0.510	0.570	0.430	0.0649	0.300
Sulfate	0.168	0.832	0.844	0.156	0.1228	7.355

a result, a great volume of precise experimental data would be required.

3. Experimental

We verified the validity of the above equations using phthalic acid as mobile phase as it is very commonly used in ion chromatography.

As solutes we prepared solution mixtures of the different forms studied: completely dissociated inorganic ions (F^-, Cl^-, NO_2^-, Br^- and NO_3^-) that contribute a single ionic species to the ion-exchange equilibria, partially dissociated inorganic ions (SO_4^{2-}) and partially dissociated mono- and divalent organic ions (acetic, lactic, succinic, malic, tartaric and oxalic acids).

3.1. Apparatus

We employed a Shimadzu ion chromatograph consisting of a basic module (HIC-6A) equipped with a manual valve injector (20-μl sample loop) and monopiston pump (LP-6A), temperature control oven for column and detector (CTO-6AS), ion conductivity detector (CDD-6A) and recorder–integrator (C-R6A Chromatopac) for signal processing. pH measurements were performed using a Crison Digilab 517 pH meter.

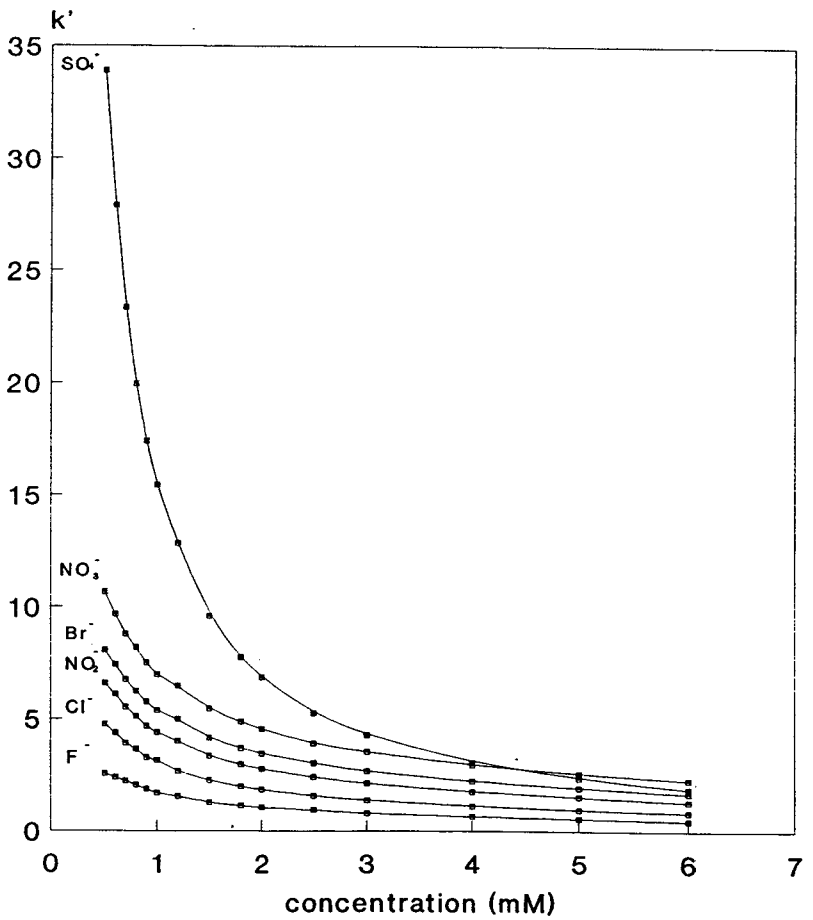

Fig. 1. Variation of k' with phthalic acid concentration with inorganic anions as sample.

3.2. Stationary phase

A Shimpack IC-AI column (100 × 4.6 mm I.D.) filled with quaternary ammonium polymethacrylate (particle size 12.5 μm; mass W = 0.92 g dry resin) was used. This was a low-capacity organic polymer column (Q = 0.050 mequiv./g), capable of supporting maximum pressures of 25 kg/cm^2, with an operating temperature of up to 50°C and a wide pH range (2–12).

3.3. Reagents and materials

Phthalic acid was prepared in ultrapure water (Nanopure II, Barnstead), adjusting the pH with tris(hydroxymethyl)aminomethane to limit the increase in background conductivity. Filtering was performed through 0.45-μm membranes with vacuum–ultrasound degasification. The mobile phase flow-rate was 1.5 ml/min; at 40°C, the dead time was 0.82 min, corresponding to the time to the peak injection exit.

Stock standard solutions (1000 mg/l) of the anions were prepared in ultrapure water, using appropriate amounts of the sodium or potassium salts of the inorganic ions or the organic free acids. Dilutions of this stock solution were prepared for both individual and mixed injection. The anion concentrations were 200 mg/l for the

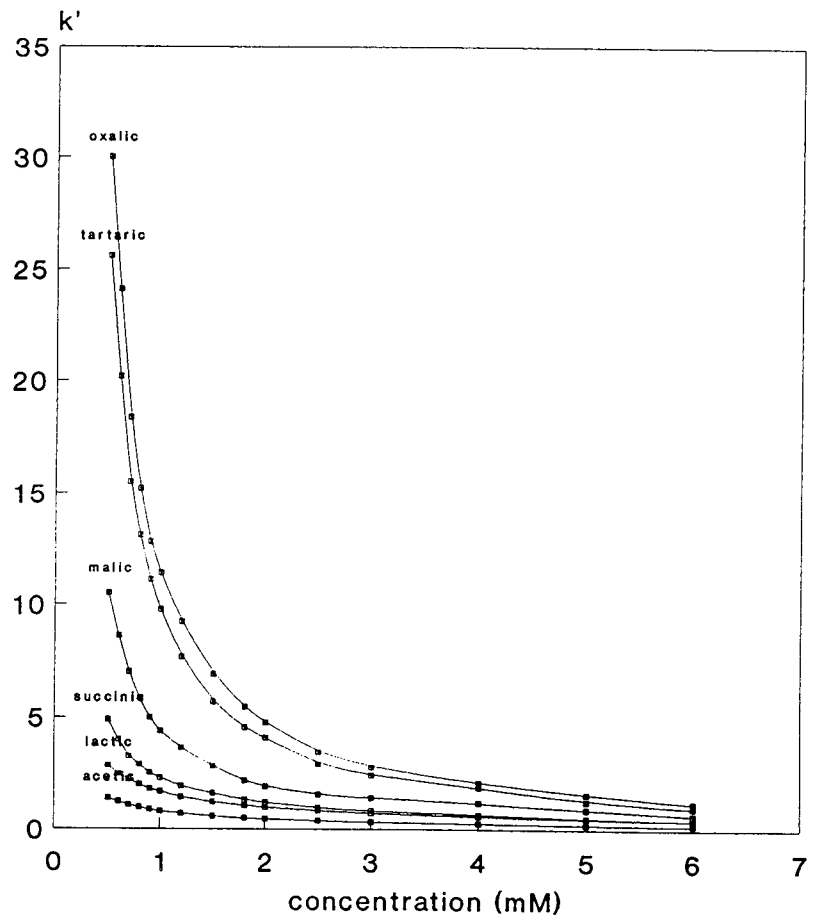

Fig. 2. Variation of k' with phthalic acid concentration with organic anions as sample.

organic ions and 20, 40, 60, 40, 120 and 160 mg/l for F^-, Cl^-, NO_2^-, Br^-, NO_3^- and SO_4^{2-}, respectively.

Table 1 shows the accumulated (40°C) protonation constants of the sample and eluent acids [14].

4. Results and discussion

We have developed a general equation for polyanionic samples and eluents that relates the capacity factor, k', to a number of different variables pertaining to the eluent (pH, C), resin phase (V_0, W, Q) and the eluent (β_i) and sample (β_j) protonation constants. The equation is thus able to determine the retention times of any ion-exchange process as a function of any of these variables.

4.1. k'(C) curves

At constant pH, pairs of values (k', C) are obtained that, when applied to the general equation, provide the selectivity coefficients, E_i, and contributions made by each ion-exchange reaction in the total process.

This method was applied to elutions with phthalic acid ($n = 2$) at pH 4.2 over the concentrations range 6–0.5 mM. The capacity factors of each of the anions tested were determined. The corresponding values are shown in Figs. 1 and 2 for inorganic and organic species, respectively.

Monoanionic sample anion

The inorganic anions were evaluated (including SO_4^{2-}, presuming the contribution of HSO_4^- to be negligible), together with acetic and lactic acid. In this case, involving only two unknowns ($n = 2$ and $x_1 + x_2 = 1$), Eq. 16 becomes

$$k' = \frac{P}{C^{\left[j\left(\frac{x_1}{1}+\frac{x_2}{2}\right)\right]}} = \frac{P}{C^{\left(j-\frac{x_2}{2}j\right)}} \qquad (16a)$$

which may be linearized, yielding

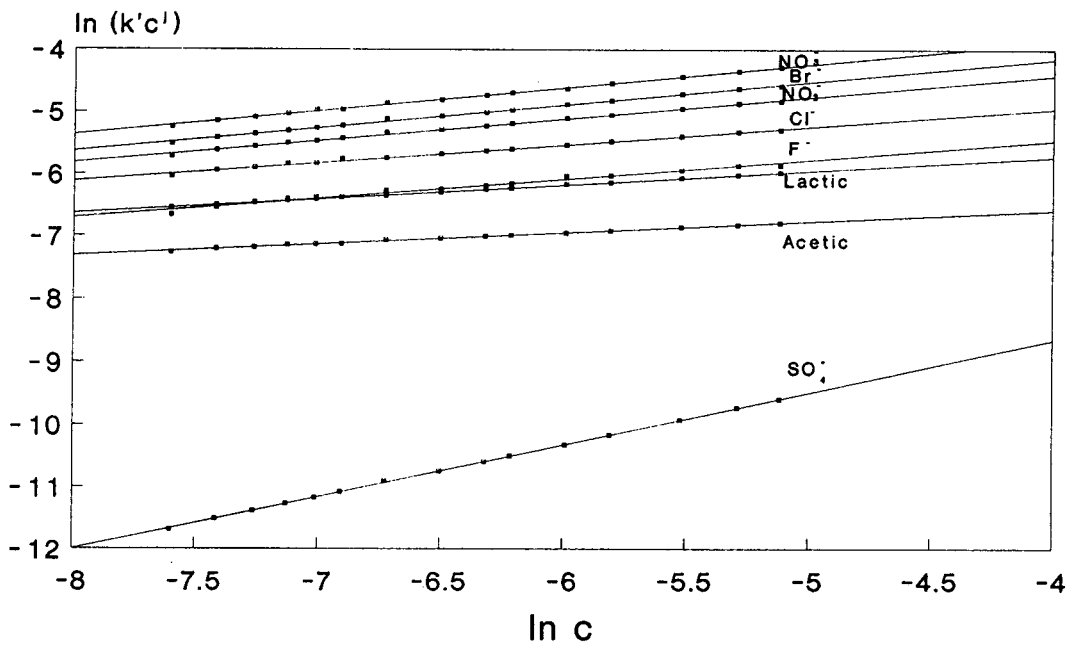

Fig. 3. Plot $\ln(k'c^j)$ vs. $\ln c$; $j = 2$ for sulfate and $j = 1$ for the other anions.

$$\ln(k'C^j) = \ln P + \left(\frac{jx_2}{2}\right) \ln C \quad (25)$$

where $j = 2$ for sulfate and $j = 1$ for the remaining monoanions (Fig. 3). The linearity resulting in all cases shows the process to be an ion exchange.

This expression is then used to calculate the contribution, x_i, of each exchange reaction, along with the corresponding global selectivity coefficient, E_0, of each component. Table 2 shows the results obtained, which were used to plot the k'(pH) curves for comparison with the respective experimental curves.

The linearity obtained corroborates the validity of the model when applied to dianionic eluents; in the case of the monoanionic ions, it moreover leads to the expression commonly described in the literature.

Dianionic sample anion

When working with succinic, malic, tartaric and oxalic acids, we apply Eq. 23, which requires the application of a fitting method to calculate the parameters implied, since linearization is not possible. By applying the Marquard algorithm [15] we obtain the contributions of the different specimens to the ion-exchange equilibrium, and also the corresponding selectivity coefficients

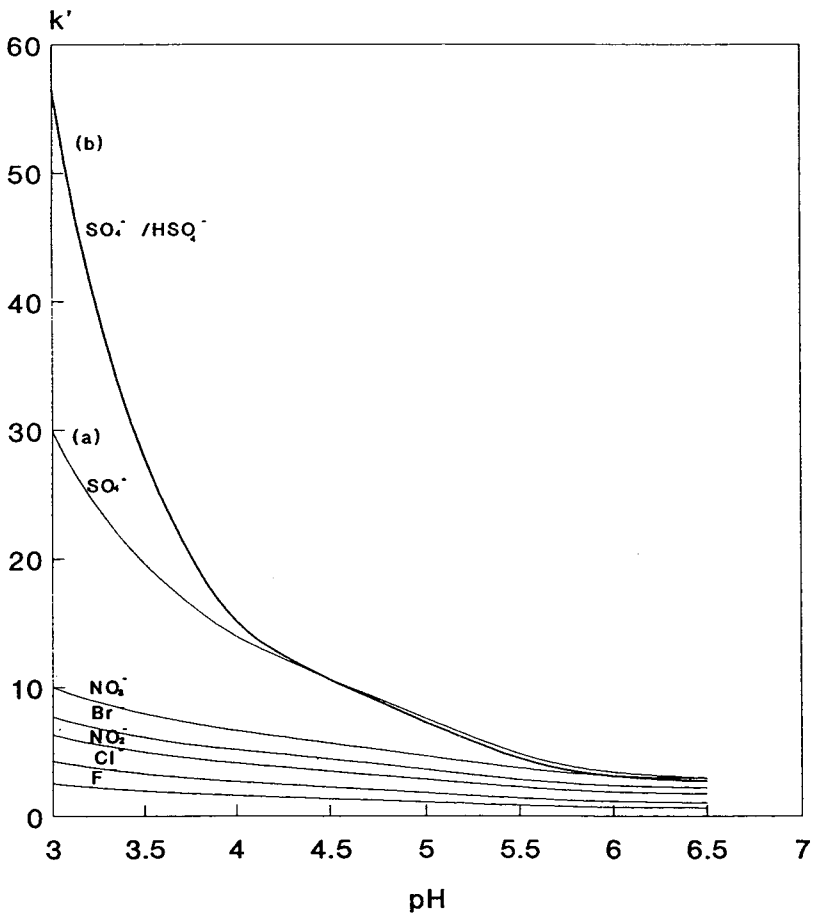

Fig. 4. Theoretical k'(pH) curves for inorganic anions as sample.

(Table 3). Analogously, these values may be used to derive the theoretical curves as a function of pH.

4.2. k'(pH) curves

In these cases we plot k' versus pH for a constant eluent concentration (1.2 mM) (Fig. 4).

Inorganic anions

The corresponding curves are in good agreement with the experimental curves (Fig. 5), with the exception of sulfate (Fig. 4, curve a), which exhibits the greatest deviation. As this cannot be due to having neglected the presence of HSO_4^-, we treat SO_4^{2-} as a dianionic species, obtaining Fig. 4, curve b as a result. This curve is much more similar to the corresponding experimental curve.

Organic anions

The theoretical curves of these acids are shown in Fig. 6. In general, the theoretical curves agree with the corresponding experimental curves (Fig. 7), except for those obtained with the oxalic anion at low pH, where some differences are observed. Likewise, at pH higher than 6 where all anions elute very close together, some changes were detected in the elution order. In these cases other mechanisms besides ionic

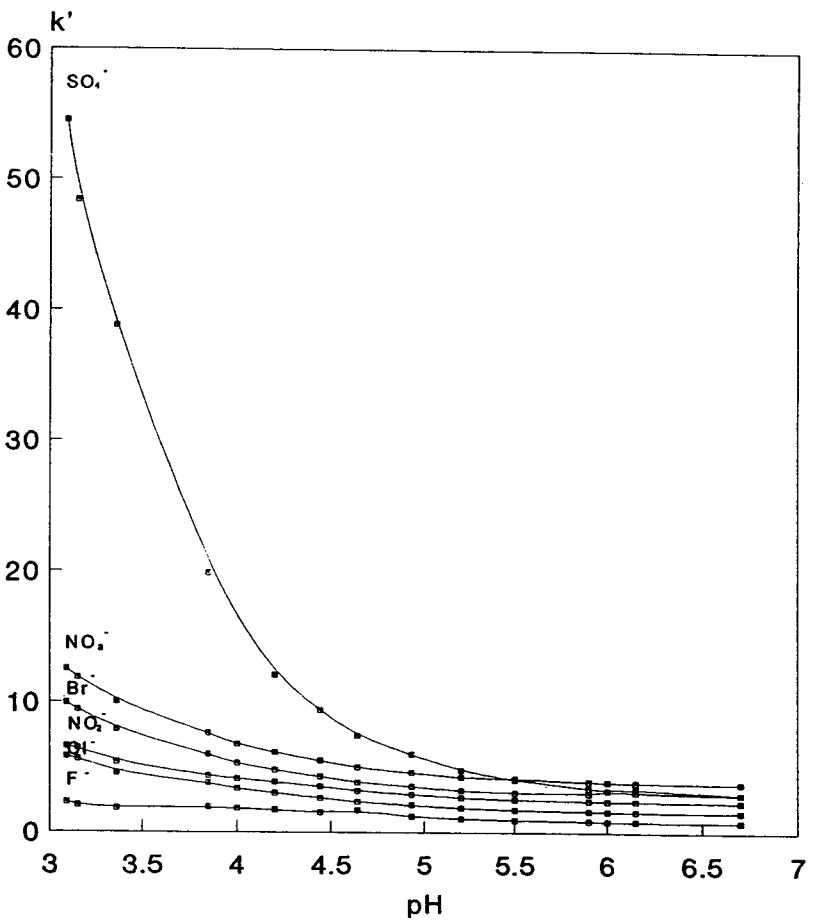

Fig. 5. Experimental k'(pH) curves for inorganic anions as sample.

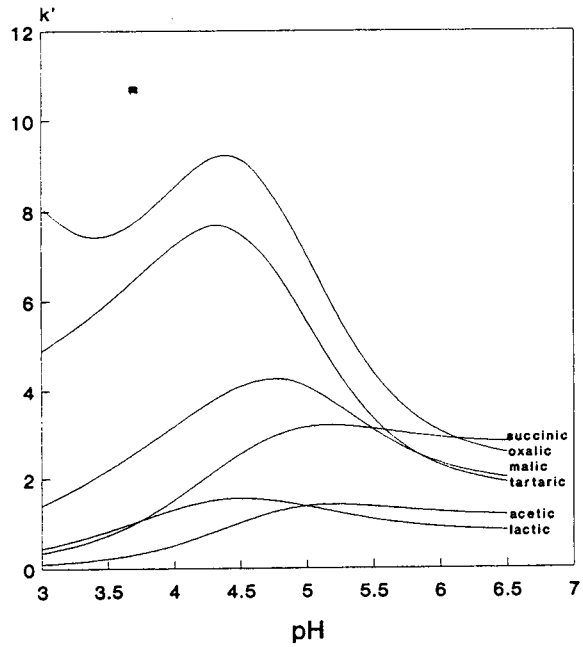

Fig. 6. Theoretical k'(pH) curves for organic anions as sample.

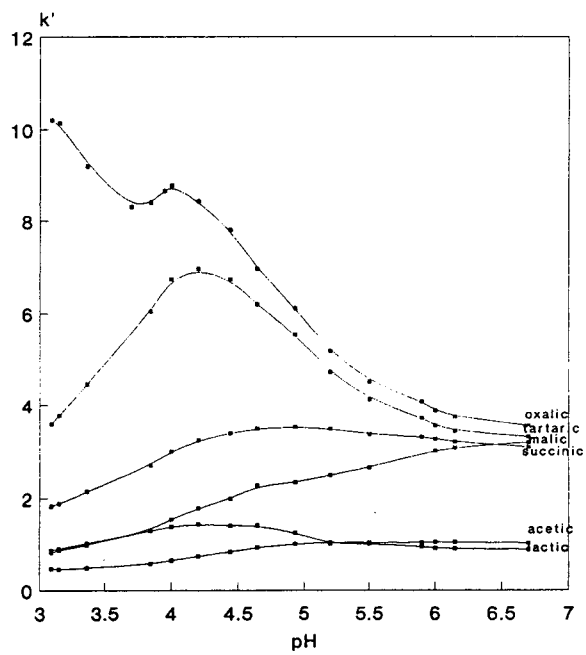

Fig. 7. Experimental k'(pH) curves for organic anions as sample.

exchange are implicated. The non-polar interactions, such as exclusion, are dependent on the size of the substrate cavity and the volume of the sample molecules. It is possible that the selection process by size takes place fundamentally at low pH values, where the concentrations of both the eluent and the sample ions are decreased.

This acceptable agreement between the theoretical and experimental curves for both mono- and dianionic samples allows us to predict the behaviour of the different species through ion chromatography when eluted with polyvalent mobile phases.

For a determinate system, the non-fitting of the model can indicate the existence of non-polar interactions between the substrate, eluent and sample.

References

[1] D.T. Gjerde and J.S. Fritz, *Ion Chromatography*, Hüthig, Heidelberg, 2nd ed., 1987.
[2] W. Rieman, III, and H.F. Walton, *Ion Exchange in Analytical Chemistry*, Pergamon Press, New York, 1970.
[3] R.E. Smith, *Ion Chromatography Applications*, CRC Press, Boca Raton, FL, 1988.
[4] H. Small and T.E. Miller, Jr., *Anal. Chem.*, 54 (1982) 462–469.
[5] P.R. Haddad and G.H. Brownie, *Educ. Chem.*, 25 (1988) 12–14.
[6] J.G. Dorsey, J.P. Foley, W.T. Cooper, R.A. Barford and H.G. Barth, *Anal. Chem.*, 62 (1990) 324–356R.
[7] P.R. Haddad and R.C. Foley, *Anal. Chem.*, 61 (1989) 1435–41.
[8] S.A. Maki and N.D. Danielson, *Anal. Chem.*, 63 (1991) 699–703.
[9] D.T. Gjerde, G. Schmuckler and J.S. Fritz, *J. Chromatogr.*, 187 (1980) 35–45.
[10] P.R. Haddad and C.E. Cowie, *J. Chromatogr.*, 303 (1984) 321–330.
[11] J. Beukenkamp, W. Rieman, III, and S. Lindenbaum, *Anal. Chem.*, 26 (1954) 505–512.
[12] R.D. Rocklin, C.A. Pohl and J.A. Schibler, *J. Chromatogr.*, 411 (1987) 107.
[13] J.H. Knox and J. Jurand, *J. Chromatogr.*, 87 (1973) 95–108.
[14] L.G. Sillien and A.E. Martell, *Stability Constants of Metal–Ion Complexes*, 2nd ed., 1964, and *Supplement No. 1*, 1971, Chemical Society, London.
[15] D.M. Marquard, *J. Soc. Ind. Appl. Math.*, 11 (1963) 431–441.

ELSEVIER

Journal of Chromatography A, 683 (1994) 367–376

JOURNAL OF CHROMATOGRAPHY A

Calculation of programmed temperature gas chromatography characteristics from isothermal data IV. Prediction of peak widths

T.I. Al-Bajjari[1], S. Le Vent*, D.R. Taylor

Department of Chemistry, University of Manchester Institute of Science and Technology, Manchester M60 1QD, UK

First received 10 January 1994; revised manuscript received 29 April 1994

Abstract

Two alternative theoretical procedures are described for the calculation of peak widths in programmed temperature gas chromatograms from corresponding isothermal widths. The essential distinction between the procedures for the case of essentially temperature-independent column efficiency is noted. Application to a limited set of isothermal width and retention time data and comparison with experimental programmed temperature results reveals the unsatisfactory nature of one of the procedures. The other method is then applied to a more extensive set of compounds and programmed temperature conditions.

1. Introduction

Previous papers in this series [1–3] have been concerned with the prediction of retention times, elution temperatures, retention indices and equivalent temperatures in programmed temperature gas chromatography (PTGC) from experimental retention times obtained under isothermal conditions. In testing theory by experiment, the temperature programme considered was restricted to the single linear temperature–time ramp, although the theory presented covered more general situations (multiple plateaus and ramps). The present paper extends predictions to those of PTGC peak (time-)width from isothermal widths, again with application to experiments involving a single linear ramp programme. [Since the experiments involve the use of (a) column temperatures above the boiling point of the sample diluent (dichloromethane), and (b) split injection mode, the effects of solvent condensation on the stationary phase have not been considered here.] Two distinct theoretical procedures are described for this purpose and tested on selected experimental data, with a view to choosing the best predictor and then applying this to a more extensive set of compounds and conditions. A further paper [4] will describe an extension of the chosen method to peak asymmetry. The composite calculation of retention times, peak widths and peak asymmetries then permits the prediction of overall shapes of chromatograms from injected mixtures, particularly those with components of similar retention time. Associated with this prediction will be the calculation of various numerical parame-

* Corresponding author.

[1] Present address believed to be: Chemistry Department, University of Mosul, Mosul, Iraq.

0021-9673/94/$07.00
SSDI 0021-9673(94)00647-4

ters, each (in its own way) a measure of either peak-pair or overall chromatographic resolution. Variation of PTGC conditions (in this work, only initial column temperature and rate of temperature increase) will then allow prediction of optimum resolution conditions ("optimization"). The calculations in this and subsequent papers have been performed without estimation of error.

2. First general procedure for PTGC width prediction

The following considerations are independent of (a) peak shape (Gaussian, triangular, etc; symmetrical or otherwise), (b) where peak width is measured (half-height, triangular base, etc).

It will be supposed that there are two additive contributions to peak width, w: (i) peak dispersion due to the characteristics of the column, w_c, and (ii) peak dispersion due to extracolumn factors (finite rates of injection, evaporation into the column, passage to the detector), w_e.

$$w = w_c + w_e \tag{1}$$

For a particular chromatograph, carrier gas flow-rate, injected compound and injection technique, one might expect w_e to be independent of column temperature (or temperature programme). If, however, carrier gas pressure differential, rather than flow-rate, is kept constant (as is the practice of the authors), carrier gas flow-rate (and therefore column dead time) will depend in a small way upon column temperature/programme and this may have a corresponding small effect upon w_e. For the present purposes, it will be assumed that the effect on the overall w is negligible, i.e. w_e will be taken as independent of column temperature/programme.

For a particular injected compound, the column term w_c will certainly depend upon column temperature for isothermal runs and upon the temperature programme for non-isothermal runs. For isothermal runs, represent w_c as w_{ci}. The contribution to this for passage through an infinitesimal fraction dF of the column is then $dw_{ci} = w_{ci}\,dF$. Now $dF = dt/t_{Ri}$, where dt is the corresponding infinitesimal time and t_{Ri} is the isothermal time (or strictly the column contribution to this) given by [1][2]

$$t_{Ri} = t_0[1 + k_1 \exp(k_2/T)] \tag{2}$$

(t_0 = isothermal column dead time, a weak function of temperature [1]; k_1, k_2 = column characteristics for a particular compound and assumed as before [1] to be independent of thermodynamic temperature T). On the basis of these equations,

$$dw_{ci} = w_{ci}\,dt/t_{Ri} = w_{ci}\,dt/\{t_0[1 + k_1 \exp(k_2/T)]\} \tag{3}$$

For a programmed temperature run, the value of w_c, w_{cp}, is obtained by integration of Eq. 3 between zero time and the programmed temperature retention time [1,2] t_R (again strictly the column contribution),

$$w_{cp} = \int_0^{t_R} w_{ci}\,dt/t_{Ri} \tag{4}$$

w_{ci} and t_0 depend upon T, and T depends upon t according to the temperature programme used.

Using Eq. 1, Eq. 4 may be rewritten as

$$w_{cp} = \int_0^{t_R} (w_i - w_e)\,dt/t_{Ri} = \int_0^{t_R} w_i\,dt/t_{Ri} - w_e$$

since [1] $\int_0^{t_R} dt/t_{Ri} = 1$; w_i is the total isothermal width (another function of T). Since w_p, the total programmed temperature width = $w_i + w_e$,

$$w_p = \int_0^{t_R} w_i\,dt/t_{Ri} \tag{5}$$

If w_i and t_{Ri} are known as functions of T, these integrals may be evaluated, usually nu-

[2] This is equivalent to stating that the logarithm of the capacity factor ($k' = t_{Ri}/t_0 - 1$) is a linear function of T^{-1}. Higher order functions will be considered at a later stage in this paper.

merically. The determination of t_R, required for the integration, has been described previously [1]. Several general possibilities for integral evaluation will be considered below.

For a temperature programme comprising a single linear ramp, $T = T_i + k_3 t$, $T_e = T_i + k_3 t_R$ and Eq. 5 becomes

$$w_p = k_3^{-1} \int_{T_i}^{T_e} w_c \, dT/t_{Ri}$$

$$= k_3^{-1} \int_{T_i}^{T_e} w_c \, dT/\{ t_0[1 + k_1 \exp(k_2/T)]\} \quad (6)$$

(T_i is the initial column temperature, T_e is the temperature at elution and k_3 the heating rate, cf. Ref. 1).

As an example of a more complicated temperature programme consider an initial isothermal at T_i lasting for a time t_1 after injection, followed by a linear ramp (heating rate = k_3 as before). This merely exemplifies the procedure to be used for more elaborate programmes, but in fact the single ramp was used in the present experimental tests of the theory. Elution could occur either during the isothermal period (corresponding to a calculated isothermal retention time = $t_0[1 + k_1 \exp(k_2/t_i)]$ less than t_1) when the width will obviously be w_i (at T_i) —designated $w_i(T_i)$— or during the ramp period. For the latter situation, the integral of Eq. 5 is written as a sum of two integrals, i.e.

$$w_p = \int_0^{t_1} w_i \, dt/t_{Ri} + \int_{t_1}^{t_R} w_i \, dt/t_{Ri}$$

$$= w_i(T_i) t_1 / t_{Ri}(T_i) + \int_{t_1}^{t_R} w_i \, dt/t_{Ri}$$

$$= w_i(T_i) t_1 / t_{Ri}(T_i) + \int_{t_1}^{t_R} w_i \, dt/\{t_0[1 + k_1 \exp(k_2/T)]\}$$

with $T = T_i + k_3(t - t_1)$. The integral in the final expression could be written

$$\int_0^{t_R^*} w_i \, dt^* / \{ t_0[1 + k_1 \exp(k_2/T)]\}$$

(with $t^* = t - t_1$ and $t_R^* = t_R - t_1$) or

$$k_3^{-1} \int_{T_i}^{T_e} w_i \, dT/\{ t_0[1 + k_1 \exp(k_2/T)]\}$$

in which $T_e = T_i + k_3(t_R - t_1) = T_i + k_3 t_R^*$.

In order to evaluate the integral of Eq. 5, it is desirable to express isothermal width in terms of isothermal retention time. Empirical polynomial functions, with best-fit parameters determined from experimental isothermal data, are considered here. Such functions have reasonable experimental support in the present applications. Fig. 1a shows the dependence of w_i upon t_R for *n*-octane on a capillary column coated with silicone elastomer for six temperatures ranging from 353 to 423 K. Fig. 1b shows the composite dependence for five homologous *n*-alkanes (C_8–C_{12}) at the same six temperatures. Both plots shows close approximation to linearity, and indeed to direct proportionality, the latter corresponding to column efficiency being temperature-independent (and by Fig. 1b solute independent also). For the present purpose, the simple linearity/proportionality will be extended to a low order polynomial, which could be applicable to a single compound, a homologous series or even a wider range of compounds, i.e.

$$w_i = \sum_{j=0}^{n} q_j t_{Ri}^j \text{ (with low } n) \quad (7)$$

Combination of Eqs. 5 and 7 then gives

$$w_p = \int_0^{t_R} \sum_{j=0}^{n} q_j t_{Ri}^{j\,-1} \, dt$$

$$= q_0 + q_1 t_R + \int_0^{t_R} \sum_{j=2}^{n} q_j t_{Ri}^{j\,-1} \, dt \quad (8)$$

by virtue of the fact that $\int_0^{t_R} dt/t_{Ri} = 1$. If q_j ($j \geq 2$) = 0, $w_p = q_0 + q_1 t_R$, exactly as for the isothermal case. Despite the near linearity shown in Fig. 1, this simple prediction is in fact *not*

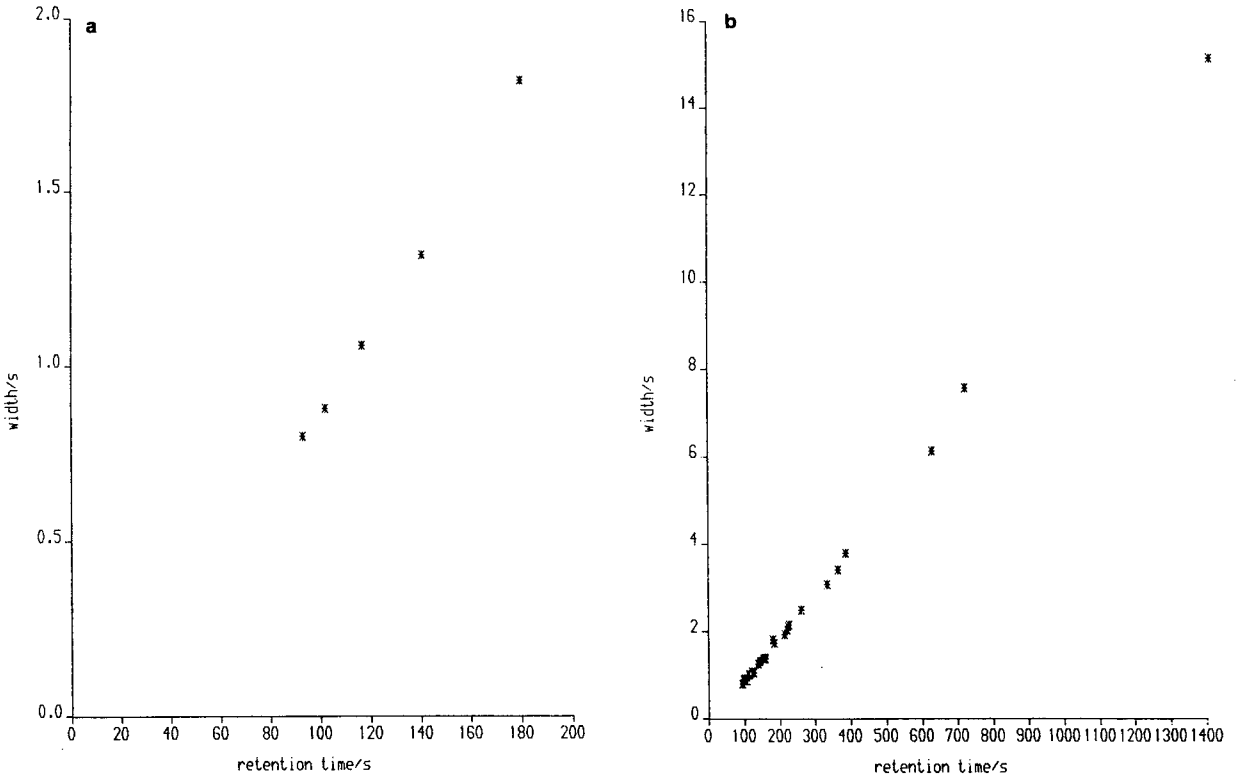

Fig. 1. Dependence of isothermal peak width upon retention time for (a) *n*-octane and (b) five *n*-alkanes (C_8–C_{12}) each at six temperatures (353, 373, 393, 403, 413, 423 K) (SE-54 column).

realised and this point will be considered further below.

The integrals of Eq. 8 may be evaluated numerically; the Romberg method (see Ref. [5]) has been used in this work. Before integration is possible, the following information is required:

(a) The q coefficients of the equation. These are obtained by fitting least squares relationships between w_i and t_{Ri}; orders up to four have been considered. Relationships have been considered both for single compounds and for a homologous series of compounds (in each case at several temperatures).

(b) The relationship of t_{Ri} and thus of k' to T. In previous papers [1–3], this has been Eq. 2 and this is equivalent to

$$\ln k' = \ln k_1 + k_2/T$$

i.e. the logarithm of capacity factor taken as a linear function of reciprocal temperature —the thermodynamic significance of k_1 and k_2 has been given previously [1]. In the present work this has been extended to powers of reciprocal temperature up to four.

(c) The dependence of t_0 upon T. As previously [2], relationships of the type $t_0 = A + BT$ and $t_0 = A + B\sqrt{T}$ have been considered, with the parameters determined by least squares methodology. The differences between predictions from the two types of formulae are in fact small. For the predictions tested experimentally and presented in the present paper, only the second of the two formulae has been used.

(d) The temperature programme. For multiramp/multiplateau programmes, the integrals have to be written as sums of other integrals, one for each step; plateau integrals are then easily written —see above for an example involving a

single plateau followed by a single linear ramp. In the present work, experimental testing has been restricted to a programme comprising only a single linear ramp, whence the time integrals are easily converted into temperature ones by replacing dt by $k_3^{-1}\,dT$, and the integration limits 0 and t_R by T_i and T_e.

(e) t_R or equivalently T_e, the upper integration limit. This has been considered previously [1,2], where Eq. 2 was used for t_{Ri}. As in (b), this has been extended here to higher powers of T^{-1} in the expression for ln k'.

Two computer programmes in Turbo Pascal have been written, for use on an IBM-type microcomputer, to calculate programmed temperature widths; one of the programmes is for a single temperature ramp and the other for an initial isothermal followed by such a ramp. A combination of keyboard and filed input provides (a) selection facilities for (i) the type of dead time vs. temperature relationship, (ii) the orders of polynomials for both ln k' and w_i (limited to a maximum of one less than the number of points), (b) isothermal data for (i) the dead time vs. temperature relationship (or coefficients A and B directly), (ii) width vs. retention time for a set of compounds (as appropriate), (iii) retention time, dead time and width for a specific named compound, and (c) information about the temperature programme, i.e. initial temperature T_i, heating rate k_3 and (where appropriate) the duration of the initial isothermal t_1.

3. Second general procedure for PTGC width prediction

Another way of approaching the prediction of programmed temperature widths, completely different from the procedure described above, is based upon the use of two effective retention times for each isothermal peak; these times are $t_{Ri} \pm w_i/2$. Using procedures described previously [1], but now allowing the possibility in the polynomial relationship of ln k' to T^{-1} of an order higher than 1, each of the two sets of isothermal retention times (one compound, various temperatures) has been used to predict a programmed temperature retention time. The difference between these has then been equated to the programmed temperature width. As before, width may be variously defined, e.g. at half height.

Two further microcomputer Pascal programmes (for a single temperature ramp and for an initial isothermal followed by a ramp) have been written to calculate programmed temperature widths by this alternative procedure. A combination of keyboard and filed input provides (a) selection facilities for the type of dead time vs temperature relationship, (b) isothermal data for (i) the dead time vs temperature relationship (or coefficients A and B directly), (ii) retention time, dead time and width for a specific named compound, and (c) information about the temperature programme. Programmed temperature widths are calculated for all ln k' vs T^{-1} polynomials up to order 4 (or for one less than the number of points for the compound when the latter is less than 5).

The single ramp programme was also adapted for use on an Amdahl 5890-300E mainframe computer. This adaptation allowed calculation in a single run for several compounds and for all combinations of initial temperatures of 333.2, 353.2, 373.2, 393.2, 413.2 K and heating rates of 5.0, 7.0, 10.0, 15.0 K min^{-1}.

4. Comparison of general procedures for special case of columns with essentially temperature-independent efficiencies

For the case of columns which show a near linear dependence of width upon retention time under isothermal conditions (and this includes direct proportionality), it has already been shown that the first procedure gives the same linear relationship between width and retention time under programmed temperature conditions. A different situation will now be demonstrated for the second general method when there is direct proportionality, i.e. temperature-independent efficiency.

If the two subtracted retention times, leading

edge and trailing edge, are represented by t_{RL} and t_{RH}, with corresponding isothermal retention times of $t_{Ri} - w_i/2$ and $t_{Ri} + w_i/2$, then

$$1 = \int_0^{t_{RL}} dt/(t_{Ri} - w_i/2) = \int_0^{t_{RH}} dt/(t_{Ri} + w_i/2)$$

If now $w_i = q_1 t_{Ri}$

$$1 - q_i/2 = \int_0^{t_{RL}} dt/t_{Ri} = \int_0^{t_R} dt/t_{Ri} - \int_{t_{RL}}^{t_R} t_R\, dt/t_{Ri}$$

$$= 1 - \int_{t_{RL}}^{t_R} t_R\, dt/t_{Ri}$$

and

$$1 + q_i/2 = \int_0^{t_{RH}} dt/t_{Ri} = \int_0^{t_R} dt/t_{Ri} + \int_{t_R}^{t_{RH}} dt/t_{Ri}$$

$$= 1 + \int_{t_R}^{t_{RH}} dt/t_{Ri}$$

whence $q_1 = \int_{t_{RL}}^{t_{RH}} dt/t_{Ri}$. Because the integration range is now very narrow and of magnitude equal to the programmed temperature width w_p, the integrand may be assumed constant and equal to the reciprocal of t_e, the isothermal retention time *corresponding to the elution temperature*. As a consequence of this, $w_p = q_1 t_e$ equal to the peak width for an isothermal run at the programmed temperature elution temperature T_e. This is a quite different prediction to that of the first procedure, where t_e in the proportionality relationship would be replaced

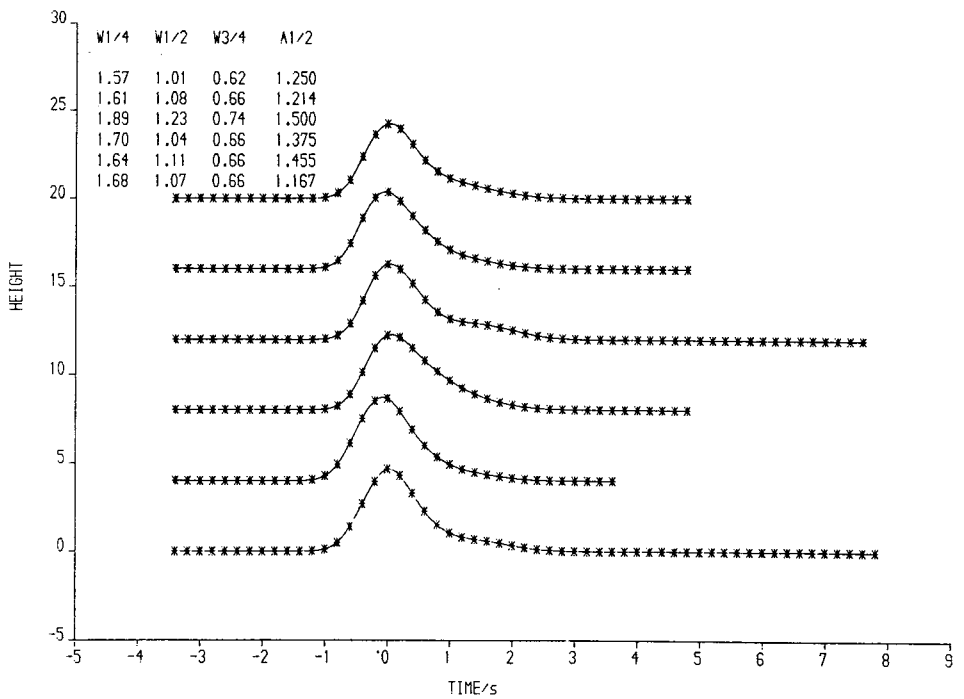

Fig. 2. Typical replicate record of peaks (393 K isothermal for *n*-nonane, SE-54 column) with cubic spline curves and statements of peak widths (at quarter, half and three quarter heights) and asymmetry [4]. Originals have replicate curves (and points) and results of analysis in corresponding colours —here lowest curve corresponds to highest analysis line. In this example, there is a vertical offset of replicates but no horizontal one.

by t_R, the programmed temperature retention time.

The computer programmes for the second procedure also calculate the programmed temperature width as the width for an isothermal run at T_e. This has been done by interpolation in a least squares linear plot of isothermal width vs. retention time, both with and without origin forcing. Proximity of these calculated programmed temperature widths and $t_{RH} - t_{RL}$ reflects proximity to proportionality of isothermal width and retention time over the temperature range of interest. As Fig. 1 shows, this is close in the present experimental studies.

5. Experimental testing of predictive procedures

The general experimental procedure has been described previously [2]; two Hewlett-Packard coated capillary columns (25 m × 0.2 mm I.D., 33 μm film thickness), types SE-54 (5% phenyl-

Table 1
Comparison of experiment and half height width predictions: initial testing, all methods, *n*-decane and *n*-dodecane (SE-54 column)

(a) Isothermal data (specific compounds only)

	Temperature/K	Retention time/s	Dead time/s	Width/s
Decane	353.2	387.0	67.9	3.80
Dodecane		1411.2		15.14
Decane	373.2	225.8	71.2	2.16
Dodecane		629.5		6.14
Decane	393.2	156.9	74.1	1.40
Dodecane		335.1		3.08
Decane	403.2	138.5	75.6	1.26
Dodecane		261.5		2.50
Decane	413.2	125.8	77.1	1.06
Dodecane		212.9		1.94
Decane	423.2	116.8	78.9	1.06
Dodecane		179.8		1.82

(b) Predicted programmed temperature widths/s

Methods: (1a) Eq. 5 + isothermal width = polynomial function of retention time, single compound (*n*-decane or *n*-dodecane); (1b) Eq. 5 + isothermal width = polynomial function of retention time, set of compounds (*n*-alkanes C_8–C_{12}); (2a) two-retention-time method: $t_{RH} - t_{RL}$; (2b) isothermal width at T_e, linear regression through origin; (2c) isothermal width at T_e, linear regression not through origin. The polynomial order is shown in [ ] for ln (capacity factor) vs. reciprocal temperature, and in { } for width vs. retention time.

Method	Decane	Dodecane	Method	Decane	Dodecane
(1a)[1]{1}	1.71	3.26	(2a)[2]	1.39	2.04
(1a)[1]{2}	1.72	3.19	(2a)[3]	1.42	2.02
(1a)[2]{1}	1.70	3.24	(2b)[1]	1.48	2.25
(1a)[2]{2}	1.70	3.17	(2b)[2]	1.47	2.27
(1b)[1]{1}	1.72	3.35	(2b)[3]	1.47	2.27
(1b)[1]{2}	1.71	3.25	(2c)[1]	1.41	1.94
(1b)[2]{1}	1.70	3.33	(2c)[2]	1.41	1.96
(1b)[2]{2}	1.69	3.23	(2c)[3]	1.40	1.96
(2a)[1]	1.60	2.21	Experiment	1.41	2.03

Temperature programme: single ramp, initial temperature 373.2 K, heating rate 7.0 K min^{-1}.

Table 2
Comparison of experiment and half-height width predictions

Compound	Width/s					
	Heating rate = 5 K min^{-1}		Heating rate = 10 K min^{-1}		Heating rate = 15 K min^{-1}	
	Predicted[a]	Observed[b]	Predicted[a]	Observed[b]	Predicted[a]	Observed[b]
Initial temperature = 353.2 K						
n-Octane	1.08	1.07 (0.01)	1.04	0.92 (0.02)	1.02	0.87 (0.03)
	1.13		1.03		0.96	
n-Nonane	1.48	1.42 (0.01)	1.32	1.10 (0.03)	1.20	1.00 (0.07)
	1.49		1.24		1.10	
n-Decane	2.06	1.92 (0.05)	1.62	1.38 (0.04)	1.38	1.13 (0.05)
	1.96		1.47		1.25	
n-Undecane	2.66	2.45 (0.04)	1.84	1.54 (0.06)	1.46	1.24 (0.03)
	2.42		1.69		1.39	
n-Dodecane	3.08	2.57 (0.16)	1.94	1.66 (0.05)	1.48	1.26 (0.05)
	2.76		1.86		1.52	
Initial temperature = 393.2 K						
n-Octane	0.94	0.90 (0.03)	0.90	0.89 (0.04)	0.86	0.87 (0.03)
	0.88		0.86		0.84	
n-Nonane	1.08	0.97 (0.02)	1.00	0.92 (0.02)	0.92	0.87 (0.02)
	1.00		0.94		0.90	
n-Decane	1.34	1.15 (0.07)	1.16	1.02 (0.06)	1.02	0.92 (0.03)
	1.23		1.11		1.03	
n-Undecane	1.66	1.40 (0.06)	1.32	1.16 (0.03)	1.12	1.02 (0.04)
	1.55		1.32		1.18	
n-Dodecane	2.06	1.87 (0.10)	1.50	1.37 (0.09)	1.20	1.13 (0.04)
	1.98		1.58		1.36	

Two-retention-time method, *n*-alkanes (SE-54 column), single ramp temperature programme
[a] First line of each pair: first order in ln k' vs. T^{-1}. Second line of each pair: second order in ln k' vs. T^{-1}.
[b] Estimated standard error of mean based upon six replicates.

methylsilicone coating) and SE-30 (100% methylsilicone) were used (arranged in parallel configuration). Two solutions of mixed solutes in dichloromethane —50 mm^3 of each solute in 25 cm^3 of solvent— were subjected to chromatographic separation: (i) a mixture of normal hydrocarbons (C_8–C_{13}), together with three ketones (nonan-5-one, *n*-propanoylbenzene and *n*-butanoylbenzene), (ii) a mixture of methyl carboxylic esters (C_8–C_{12}). The chromatograph was connected via an analogue-to-digital converter to a computer integrator (Trilab 2500). This instrument maintained, for each chromatographic run, a record of bunch-averaged intensity against incremental time. It also had a programmed facility for analysing these data to obtain, for each peak, retention time, effective start and finish times (determined by successive significant gradient methodology) and area. A BBC Basic computer programme (written by Mr. G.O. Hughes) then processed the composite of primary and derived data and also activated transmission to a BBC Model B computer, via an RS232 serial link, of peak data between start and finish times but with the addition of a few pre-start and post-finish points. Data were accumulated for sets of six chromatograms, obtained under identical isothermal or programmed temperature conditions. The accumulated data were then transferred via a KERMIT communication package to a file on an Amdahl 5890 mainframe computer. A Pascal programme on

Table 3
Comparison of experiment and half-height width predictions

Compound	Width/s					
	Heating rate = 5 K min^{-1}		Heating rate = 10 K min^{-1}		Heating rate = 15 K min^{-1}	
	Predicted[a]	Observed[b]	Predicted[a]	Observed[b]	Predicted[a]	Observed[b]
Initial temperature = 373.2 K						
Methyl octanoate	1.66	1.90 (0.04)	1.34	1.40 (0.08)	1.14	1.10 (0.05)
	2.00		1.42		1.20	
Methyl nonanoate	2.24	2.26 (0.10)	1.54	1.54 (0.05)	1.22	1.20 (0.01)
	2.44		1.60		1.28	
Methyl decanoate	2.52	2.62 (0.13)	1.58	1.67 (0.01)	1.18	1.26 (0.04)
	2.56		1.64		1.32	
Methyl undecanoate	2.72	2.94 (0.09)	1.62	1.73 (0.13)	1.18	1.35 (0.04)
	2.76		1.74		1.38	
Methyl dodecanoate	2.78	2.88 (0.18)	1.58	1.78 (0.17)	1.12	1.51 (0.09)
	2.84		1.70		1.28	
Initial temperature = 413.2 K						
Methyl octanoate	1.20	1.08 (0.11)	1.02	1.14 (0.13)	0.90	0.92 (0.10)
	1.16		1.04		0.96	
Methyl nonanoate	1.40	1.32 (0.07)	1.12	1.21 (0.11)	0.94	0.96 (0.08)
	1.38		1.18		1.06	
Methyl decanoate	1.64	1.64 (0.07)	1.20	1.28 (0.06)	0.96	1.06 (0.04)
	1.66		1.32		1.14	
Methyl undecanoate	1.96	1.98 (0.07)	1.30	1.42 (0.06)	1.00	1.18 (0.05)
	2.04		1.48		1.24	
Methyl dodecanoate	2.18	2.34 (0.10)	1.36	1.57 (0.08)	1.00	1.44 (0.09)
	2.26		1.50		1.18	

Two-retention-time method, methyl carboxylic esters (SE-30 column), single ramp temperature programme.
[a] First line of each pair: first order in ln k' vs. T^{-1}. Second line of each pair: second order in ln k' vs. T^{-1}.
[b] Estimated standard error of mean based upon six replicates.

this computer sorted the data into a new file so that data for successive runs were contiguous *for each compound*. This new file then became the input of a FORTRAN programme which, for each compound, (a) plotted the peak data points for successive runs (with vertical and horizontal offset as desired and using a different colour for each run), (b) joined the points with cubic spline curves, and (c) computed peak widths at quarter, half and three-quarter-heights (and peak asymmetries —to be considered in a subsequent publication [4]). Features (a) and (b) required GINOF plotting and NAG subroutines, available on the Amdahl computer. A typical plot (rendered here in monochrome) is shown in Fig. 2. Averages and standard deviations of sets of six corresponding heights could then be obtained. Only the widths at half-height were used in comparisons of observation and prediction.

For the purpose of the predictions, column dead times were required at various temperatures. These were determined by the method of Al-Thamir et al. [6], using retention times for successive members of homologous series [*n*-alkanes for the components of solution (i) and methyl carboxylic esters for the components of solution (ii)].

As an initial test, the predictions from the two procedures were compared with one another and with experiment for two hydrocarbons, *n*-decane and *n*-dodecane for a single ramp temperature programme with an initial temperature of 373.2

K, a heating rate of 7.0 K min^{-1} and the SE-54 column. This is shown in Table 1. The general conclusions here are as follows.

(a) The second procedure, including the use of isothermal width at T_e, gives significantly better predictions than the first procedure, particularly when second and third order polynomials are used in ln k' vs. T^{-1} relationships.

(b) The first procedure, however, significantly overestimates the width (at least for these test compounds and certainly more so for dodecane than for decane). The reason for this is not apparent to the authors. Furthermore, progressing from first to second or third order polynomials for ln k' vs. T^{-1} has little effect on predicted widths.

As a consequence of this initial testing, all further comparisons between theory and experiment were performed on the basis of the two-retention-time method, *i.e.* $t_{RH} - t_{RL}$. Typical results are shown in Tables 2 and 3. Other results are available [7]. Agreement is generally satisfactory; certainly some cases are better than others and there are a few cases where agreement is poor.

Copies of computer programmes referred to above are available from the authors. The Pascal data sorting programme will probably not be of general utility.

References

[1] E.E. Akhporhonor, S. Le Vent and D.R. Taylor, *J. Chromatogr.*, 405 (1987) 67.
[2] E.E. Akhporhonor, S. Le Vent and D.R. Taylor, *J. Chromatogr.*, 463 (1989) 271.
[3] E.E. Akhporhonor, S. Le Vent and D.R. Taylor, *J. Chromatogr.*, 504 (1990) 269.
[4] T.I. Al-Bajjari, S. Le Vent and D.R. Taylor, *J. Chromatogr. A*, 683 (1994) 377.
[5] P.W. Williams, *Numerical Computation*, Nelson, London, 1972, p. 154.
[6] W.K. Al-Thamir, J.H. Purnell, C.A. Wellington and R.J. Laub, *J. Chromatogr.*, 173 (1979) 388.
[7] T.A. Al Bajjari, *Ph.D. Thesis*, Manchester, 1990.

ELSEVIER

Journal of Chromatography A, 683 (1994) 377–384

JOURNAL OF CHROMATOGRAPHY A

Calculation of programmed temperature gas chromatography characteristics from isothermal data V. Prediction of peak asymmetries and resolution characteristics

T.I. Al-Bajjari[1], S. Le Vent, D.R. Taylor*

Department of Chemistry, University of Manchester Institute of Science and Technology, Manchester M60 1QD, UK

Received 10 January 1994[2]

Abstract

A previously described procedure for the calculation of peak widths in programmed temperature gas chromatograms from corresponding isothermal widths has been adapted to the analogous calculation of peak asymmetries. Comparison with experimental data is satisfactory. Composite predictions of retention times, widths and asymmetries are then used to predict (a) the forms of complete chromatograms comprising close peaks, (b) resolution characteristics of such chromatograms and (c) optimum programmed temperature conditions.

1. Introduction

Previous papers in this series [1–4] have been concerned with (a) prediction of retention times, elution temperatures, retention indices, equivalent temperatures and peak widths in programmed-temperature gas chromatography (PTGC) from experimental retention times obtained under isothermal conditions and (b) comparison of theory and experiment, the latter restricted to the single linear temperature–time ramp (although the theory presented covered more general situations). The present paper extends predictions and experimental comparisons to PTGC peak asymmetry. The predictive procedure used is quite similar to one successfully used previously [4] for peak width. This procedure was based upon the subtraction of two calculated "retention times", one for a point on the ascending section of a peak, e.g. at half height, and the other for the point at the same height on the descending section. The extension to asymmetry was simply to include the predicted peak maximum, i.e. the true retention time, as a third time. If now one assumes a two-parameter function for peak shape, the composite calculation of retention times, peak widths and peak asymmetries then allows the prediction of overall forms of mixture chromatograms, in particular those where components have similar retention times. Associated with this prediction is the

* Corresponding author.

[1] Present address: believed to be Chemistry Department, University of Mosul, Mosul, Iraq.

[2] Publication delayed at the authors' request.

0021-9673/94/$07.00
SSDI 0021-9673(94)00332-4

calculation of various measures of peak-pair and overall resolution. Variation of PTGC conditions (here only initial column temperature and rate of temperature increase) then allows prediction of optimum resolution conditions, subject to a not excessive time for the chromatographic experiment. Similar optimizations have been described by other authors previously [5].

2. Peak asymmetry and shape

Chromatographic peaks have commonly been treated as either gaussian (for which there is reasonable theoretical support) or isosceles-triangular in shape. Such shapes are symmetrical and each is fully described by two parameters, such as (maximum) height and width at half-height (or, in place of the latter, standard deviation). In practice however, there always exists some degree of asymmetry —either fronting or tailing— in a peak and further parameters are then necessary to describe the shape. Asymmetry is known to arise from several causes, e.g. proportionality failure of mobile and stationary phase concentrations, column overloading, or slow injection. In the present work, it has been assumed that instrumental/operator effects on width and asymmetry are minimized and essentially constant, i.e. that band shape is solely an analyte/column/temperature characteristic. A commonly used function for an asymmetric peak is the exponentially modified gaussian [6]. This is a convolution integral, characterized by three parameters: height, standard deviation and exponential decay constant. This means that a single asymmetry parameter is sufficient to define deviations from symmetry and this has been assumed in the present work. However, a simpler three-parameter function has been used in simulated chromatograms, viz. a bi-gaussian. This uses one gaussian for the ascent and a second one for the descent. Its disadvantage is a discontinuity of curvature at the peak maximum, but generally this has not been observable in our simulations. For the purpose of the resolution characteristics considered here, the choice of shape function is in fact of no relevance.

Peak asymmetry A, at a particular fractional height, is conventionally defined as the ratio b/a, where b is the time difference between the fractional height point on the trailing edge and the peak maximum (t_R) and a is the time difference between the peak maximum (t_R) and the corresponding point on the leading edge. (For a bi-gaussian, A should be independent of fractional height.) Width w is, of course, equal to $a + b$ so that (w,A) and (a,b) statements are readily interconvertible. A Pascal programme was written for use on an Amdahl 5890 mainframe to calculate PTGC retention times, peak widths and asymmetries from corresponding isothermal data together with information on the dependence of column dead time upon temperature. The latter was either (a) in the form of data pairs to be fitted to a least squares linear relationship of dead time to thermodynamic temperature or its square root or (b) as previously determined coefficients for one of these relationships; for the predictions reported in the present paper, only the square root option was used. As previously indicated, the calculation was essentially that of three "retention times" for each compound, the true retention time and the two fractional height times, one on each edge. As in the previous programme for the calculation of width [4], there was a choice of polynomial order for the logarithm of capacity factor ($\ln k'$) against the reciprocal of thermodynamic temperature (T^{-1}). In the previous programme, the value was calculated for all orders up to 4 *within the single run* but, for the present programme, a single order (up to three) was selected in the data file. This programme handled up to twenty compounds and all single temperature–time ramp combinations of initial temperatures (333.2 to 393.2 K in 10.0 K steps) and heating rates (1.0 to 15.0 K min^{-1} in 1.0 K min^{-1} steps) within one run and also calculated resolution characteristics (see below) for a chromatogram of a mixture of the compounds. The chosen characteristics are independent of relative abundance and detector response factors.

3. Comparison of calculated and observed asymmetries

The experimental procedure for obtaining chromatograms using capillary columns under both isothermal and programmed temperature conditions has been previously described [2,4], as has a description of the computational procedure for displaying replicate details of individual peaks (isothermal or programmed temperature) and associated width information at various fractional heights [4]. The FORTRAN programme used for this purpose also computes and displays half-height asymmetry for the replicate runs (see Fig. 2 of ref. [4] for an example). Average values may then be compared with predictions. Table 1 presents a typical comparison for methyl carboxylate esters with an SE-30 column, a single temperature–time ramp starting at 373.2 K, and employing both first- and second-order polynomials for ln k' against T^{-1}. Isothermal data for 393.2 to 433.2 K (in 10.0 K steps) were used in the predictions. Quality of agreement varies but is generally satisfactory, bearing in mind the given standard errors of the observations and assumed —but not calculated in the present work— errors of similar magnitude for the predictions.

4. Resolution characteristics

The ideal chromatogram is one for which individual peaks of analytical interest are cleanly separated from one another, i.e. are well resolved. The optimization of experimental conditions to further this objective in the various kinds of chromatographic experiment has been extensively covered previously. A summary (to 1986) has been provided by Schoenmakers [7]. Quantitative resolution characteristics are of two kinds: (a) for adjacent pairs of peaks —"elementary criteria", and (b) for a complete chromatogram. Some of these criteria (i) depend upon relative peak area [i.e. on the product of relative quantity (mass or amount of substance) and

Table 1
Comparison of experiment and half-height asymmetry predictions

Compound	Asymmetry					
	Heating rate = 5 K min^{-1}		Heating rate = 10 K min^{-1}		Heating rate = 15 K min^{-1}	
	Predicted[a]	Observed[b]	Predicted[a]	Observed[b]	Predicted[a]	Observed[b]
Methyl octanoate	0.73 0.88	0.85 (0.10)	0.83 0.90	0.93 (0.07)	0.89 0.93	0.91 (0.07)
Methyl nonanoate	0.86 0.94	0.74 (0.06)	0.89 0.92	0.83 (0.09)	0.91 0.95	0.86 (0.12)
Methyl decanoate	0.85 0.86	0.73 (0.11)	0.88 0.90	0.84 (0.11)	0.91 0.95	0.92 (0.09)
Methyl undecanoate	0.84 0.84	0.67 (0.10)	0.85 0.83	0.71 (0.06)	0.85 0.83	0.92 (0.16)
Methyl dodecanoate	0.80 0.84	0.76 (0.14)	0.87 0.99	0.83 (0.14)	0.91 1.14	0.83 (0.14)

Methyl carboxylic esters (SE-30 column), single-ramp temperature programme, initial temperature 373.2 K.
[a] First line of each pair: first order in ln k' vs. T^{-1}. Second line of each pair: second order in ln k' vs. T^{-1}.
[b] Values in parentheses: estimated standard errors of mean based upon six replicates.

Table 2
Typical section of output from width/asymmetry predictive computer programme

Name	Retention time/s	Width/s	Asymmetry	R_s	*APR*	*POF*/s	*APOF*/s
Diethyl malonate	356.40	2.194	0.800				
				0.660	0.645	−1.273	−1.359
Octan-1-ol	358.88	2.217	0.731				
				1.781	1.731	2.945	2.837
Acetophenone	365.59	2.222	0.649				

Single-ramp temperature programme, SE-54 column. First-order polynomial for log k' vs. T^{-1}. Heating rate = 5.0 K min^{-1}, initial temperature = 353.2 K. Resolution product = 1.176, asymmetric peak resolution product = 1.118, normalized resolution product = 0.789, normalized asymmetric peak resolution product = 0.791, sum of peak overlap functions = 1.672 s, sum of asymmetric peak overlap functions = 1.477 s, highest retention time (analysis time) = 365.6 s. The following "modified" values include only resolutions < 1.50 or peak overlap functions < 0.00 s: modified resolution product = 0.990, modified asymmetric peak resolution product = 0.968, modified sum of peak overlap functions = −1.273 s, modified sum of asymmetric peak overlap functions = −1.359.

Table 3
Elementary optimization criteria for mixture/column of Table 2 for selected single-ramp programmed-temperature conditions

Initial temperature/K	Parameter	Heating rate/K min^{-1}						
		2.0	4.0	6.0	8.0	10.0	12.0	14.0
343.2	$R_{s,12}$	0.17	0.15	0.48	0.72	0.92	1.08	1.22
	$R_{s,23}$	0.32	0.76	1.42	1.91	2.31	2.64	2.92
	APR_{12}	0.17	0.15	0.47	0.71	0.89	1.05	1.17
	APR_{23}	0.32	0.75	1.38	1.85	2.23	2.54	2.80
	POF_{12}/s	−5.55	−3.98	−1.92	−0.85	−0.21	0.19	0.47
	POF_{23}/s	−4.52	−1.11	1.55	2.83	3.52	3.90	4.12
	$APOF_{12}$/s	−5.53	−4.03	−1.99	−0.92	−0.29	0.11	0.39
	$APOF_{23}$/s	−4.55	−1.18	1.46	2.74	3.42	3.81	4.03
363.2	$R_{s,12}$	0.65	0.90	1.10	1.27	1.40	1.52	1.62
	$R_{s,23}$	1.75	2.27	2.67	3.00	3.28	3.52	3.73
	APR_{12}	0.63	0.88	1.07	1.22	1.35	1.45	1.55
	APR_{23}	1.70	2.19	2.57	2.88	3.14	3.36	3.55
	POF_{12}/s	−1.63	−0.35	0.31	0.70	0.93	1.08	1.18
	POF_{23}/s	3.49	4.63	5.10	5.28	5.32	5.30	5.24
	$APOF_{12}$/s	−1.74	−0.45	0.21	0.60	0.83	0.99	1.09
	$APOF_{23}$/s	3.36	4.51	4.98	5.16	5.21	5.20	5.14
383.2	$R_{s,12}$	1.51	1.65	1.76	1.86	1.95	2.03	2.11
	$R_{s,23}$	3.46	3.74	3.99	4.20	4.39	4.55	4.70
	APR_{12}	1.44	1.57	1.68	1.77	1.85	1.92	1.99
	APR_{23}	3.29	3.55	3.78	3.97	4.14	4.29	4.42
	POF_{12}/s	1.49	1.62	1.69	1.71	1.72	1.71	1.70
	POF_{23}/s	7.33	7.02	6.73	6.46	6.22	6.00	5.80
	$APOF_{12}$/s	1.36	1.50	1.57	1.61	1.62	1.62	1.61
	$APOF_{23}$/s	7.18	6.88	6.60	6.34	6.11	5.90	5.70

First-order polynomial for log k' vs. T^{-1}. The first/second line of each pair is for the (first and second)/(second and third) eluted peaks. N.B. Order of elution varies with conditions.

detector response (in terms of the same quantity)], and/or (ii) involve peak asymmetry [8]. Those used in the present work are independent of relative peak area; some of them ignore asymmetry while others include it. Extension of characteristics of type b are so-called "composite criteria" and include other factors, principally total analysis time. These criteria are based upon the paradigm that good resolution at the expense of excessive analysis time is unacceptable on ergonomic grounds. Such criteria were not used in the present study, however.

Four elementary criteria have been considered here:

(a) *Resolution* [8] (R_s): defined as $2(t_2 - t_1)/(w_1 + w_2)$, where t_1, t_2 are retention (peak maximum) times for adjacent bands ($t_2 > t_1$) and w_1, w_2 are base peak widths, defined for (bi-) gaussians as four times the (mean) standard deviation or equivalently as $\sqrt{(2/\ln 2)}$ times the width at half height; this shape has been assumed here.

(b) *Asymmetric peak resolution* [9] (*APR*): defined as $(t_2 - t_1)/(b_1 + a_2)$, where a, b are asymmetric peak parameters defined above but appropriate to the peak "base".

(c) *Peak overlap function* (*POF*): a new function, with dimension of time, defined as $t_2 - t_1 - (w_1 + w_2)/2$. This may be positive or negative; zero corresponds approximately to a peak pair just resolved, and increasingly positive values to a larger gap between the peaks.

(d) *Asymmetric peak overlap function* (*APOF*): the analogue of c when asymmetry is properly considered, and defined as $t_2 - t_1 - b_1 - a_2$ with a, b as in b above.

Table 4
Complete chromatogram resolution criteria for mixture/column of Table 2 for selected single-ramp programmed-temperature conditions

Initial temperature/K	Parameter[a]	Heating rate/K min^{-1}						
		2.0	4.0	6.0	8.0	10.0	12.0	14.0
343.2	1	0.06	0.12	0.68	1.39	2.13	2.86	3.56
		0.06	0.11	0.65	1.31	1.99	2.66	3.29
	2	0.90	0.55	0.75	0.80	0.82	0.83	0.83
		0.90	0.55	0.76	0.80	0.82	0.83	0.83
	3	−10.1	−5.09	−0.37	1.99	3.31	4.10	4.59
		−10.1	−5.21	0.53	1.82	3.14	3.93	4.42
363.2	1	1.13	2.05	2.95	3.80	4.61	5.36	6.06
		1.08	1.92	2.74	3.51	4.22	4.88	5.50
	2	0.79	0.82	0.83	0.83	0.84	0.84	0.84
		0.79	0.82	0.83	0.84	0.84	0.84	0.85
	3	1.85	4.29	5.41	5.98	6.25	6.38	6.42
		1.62	4.05	5.19	5.76	6.05	6.18	6.23
383.2	1	5.22	6.16	7.03	7.83	8.57	9.26	9.91
		4.75	5.58	6.33	7.01	7.65	8.24	8.79
	2	0.85	0.85	0.85	0.85	0.85	0.85	0.85
		0.85	0.85	0.85	0.85	0.85	0.85	0.86
	3	8.82	8.64	8.42	8.18	7.94	7.71	7.50
		8.54	8.38	8.17	7.95	7.73	7.51	7.31

First-order polynomial for log k' vs. T^{-1}.

[a] 1 = Resolution product (first line), asymmetric peak resolution product (second line); 2 = normalized resolution product (first line), normalized asymmetric peak resolution product (second line); 3 = peak overlap function sum/s (first line), asymmetric peak overlap function sum/s (second line).

These elementary criteria have then been compounded to form ten complete chromatogram parameters as follows:

(e) *Resolution product*: the product of all R_s in the chromatogram —the number of factors in the product is one less than the number of peaks.

(f) *Asymmetric peak resolution product*: as e but using *APR* instead of R_s.

(g) *Normalized resolution product*: as e but using the ratio of $R_s/\langle R_s \rangle$ [$\langle R_s \rangle$ being the (arithmetic) mean of the R_s].

(h) *Normalized asymmetric peak resolution product*: as g but using *APR* instead of R_s.

(i) *Peak overlap function sum*: the sum of *POF* in the chromatogram.

(j) *Asymmetric peak overlap function sum*: as i but using *APOF* instead of *POF*.

(k) *Modified resolution product*: as a but including in the product only those R_s less than a given "critical value". Essentially this is based upon the idea that two peaks are adequately separated when the critical value is reached; beyond this value, the peaks become increasingly separated but this does not improve the analytical value of separating overlapping peaks. A critical value of 1.5 has been used here, but this can be changed in the computer data file.

(l) *Modified asymmetric peak resolution product*: as j but with *APR* instead of R_s; the same critical value has been used.

(m) *Modified peak overlap function sum*: as c but including in the sum only those *POF* less than a given "critical value", specified in the computer programme data file, and chosen here as zero.

(n) *Modified asymmetric peak overlap function sum*: as m but with *APOF* instead of *POF*.

The four elementary (for each adjacent peak pair) and the ten chromatogram parameters are evaluated and printed for each temperature programme in the mainframe Pascal programme evaluating peak width and asymmetry, described above. The further parameter, analysis time equated to the longest retention time was also printed. The programme was tested on a solute mixture [4] of diethyl malonate, octan-1-one and acetophenone on an SE-54 capillary column; elution order varied with temperature programme conditions. Typical predictions are shown in Tables 2 to 4; further information is available elsewhere [10]. The small variation with conditions for the two normalized resolution products (g and h) is interesting and would suggest limiting value of these parameters.

The resolution parameters and the analysis time were also written by the Pascal programme to a file used as input data to a very simple mainframe FORTRAN programme, utilising two GINOSURF routines available in a package on

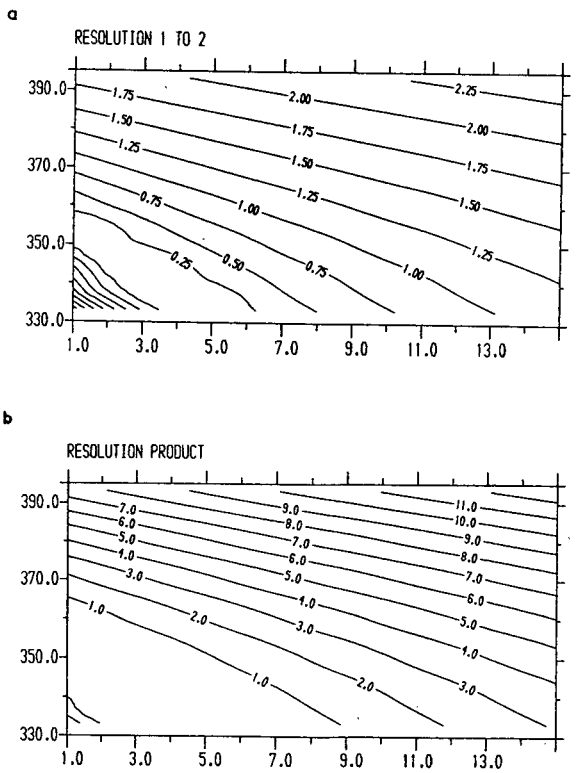

Fig. 1. Contour diagrams showing (a) resolution between peaks for the first two eluted compounds [of (i) diethyl malonate, (ii) octan-1-ol and (iii) acetophenone on an SE-54 column] and (b) resolution product. The abscissae are heating rates/K min^{-1} and the ordinates initial temperatures/K. The contours in the lower left corner ascend in value towards the corner [0.25, 0.50, 0.75, 1.00, 1.25, 1.50, 1.75, 2.00 for (a); 1.0, 2.0 for (b)]. The valley crossing from ca. 350 K min^{-1} to 5 K represent a changeover in order of elution [(ii) then (iii) then (i) in the lower left corner; (i) then (ii) then (iii) elsewhere]. The upper right corner represents good pair and overall resolution/selectivity but at the expense of long analysis time.

the Amdahl 5890 computer. This latter programme produced two kinds of "three-dimensional" plot —(i) isometric projection (with selectable viewing angle), and (ii) contour— of chosen parameters against initial temperature and heating rate. The programme was modified as required to select the chosen parameters and plot types. Fig. 1 shows two examples of contour plots: resolution between the first two eluted compounds and resolution product. These plots

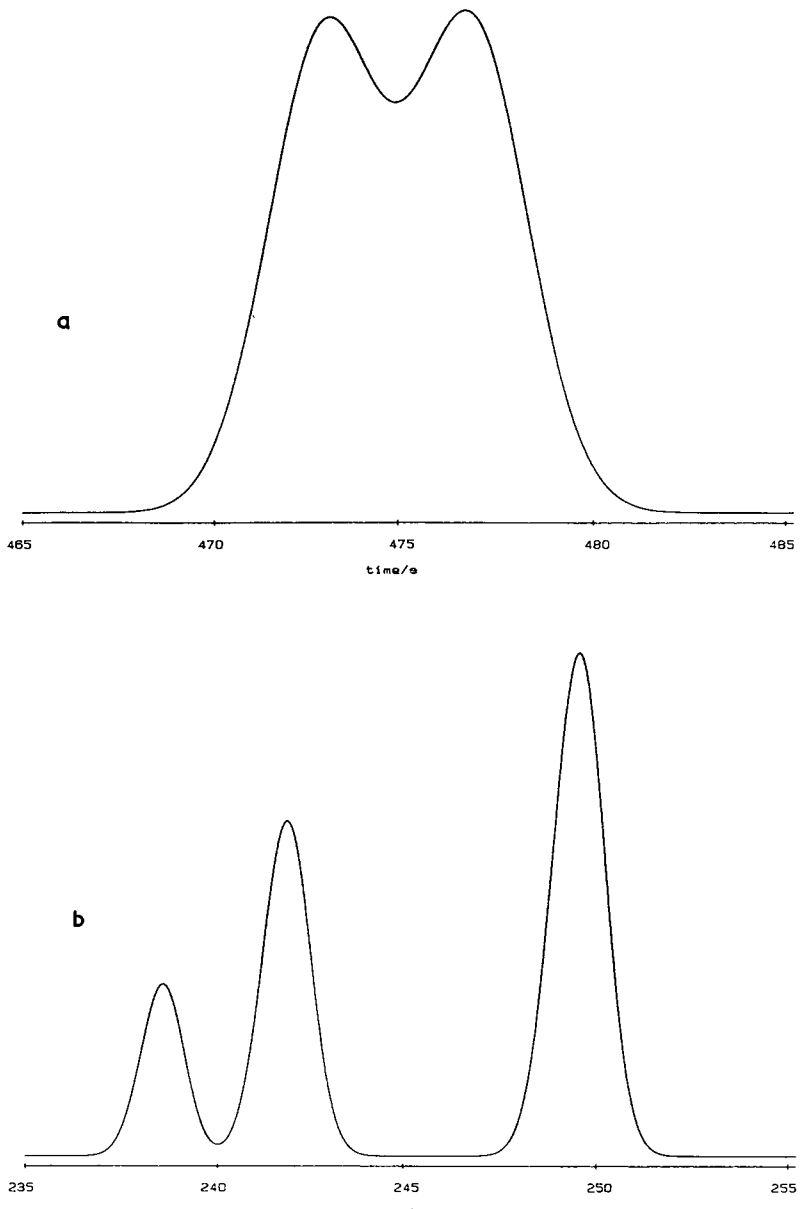

Fig. 2. Two examples of predicted chromatograms [bi-gaussian peaks with areas in ratio 1:2:3 for (i) diethyl malonate, (ii) octan-1-one and (iii) acetophenone on SE-54 column: (a) initial temperature = 343.2 K, heating rate = 4.0 K min^{-1} [peaks for (i) and (ii) on the left are not separated]; (b) initial temperature = 363.2 K, heating rate = 10.0 K min^{-1}.

allow visual selection of optimum/satisfactory programmed temperature conditions.

A third computer programme was written in Turbo Pascal for use on an IBM 8086 microcomputer (with 8087 coprocessor) with Hewlett-Packard 7470A graph plotter connected to the computer through an IEEE 488 card. This programme plots a simulated chromatogram from given relative amounts, response factors, retention times, half-height widths and half-height asymmetries (isothermal or programmed temperature, observed or predicted), and includes a choice of peak shape between (scalene) triangular and bi-gaussian. A procedure for transferring a screen-displayed chromatogram to printer paper (as an alternative or addition to plotting) was incorporated into the programme; this was provided by Dr. M.J. Parrott and was more efficient than the usual "print screen" facility. Fig. 2 shows simulated, temperature programmed, bi-gaussian chromatograms for the test mixture used in the mainframe Pascal programme; the composition is such that peak areas are in the ratio 1:2:3 for diethyl malonate, octan-1-ol and acetophenone, respectively. This provides an alternative procedure for assessing resolution/selectivity quality for programmed conditions without actually performing the experiment.

Copies of the various computer programmes referred to above are available from the authors.

References

[1] E.E. Akhporhonor, S. Le Vent and D.R. Taylor, *J. Chromatogr.*, 405 (1987) 67.
[2] E.E. Akhporhonor, S. Le Vent and D.R. Taylor, *J. Chromatogr.*, 463 (1989) 271.
[3] E.E. Akhporhonor, S. Le Vent and D.R. Taylor, *J. Chromatogr.*, 504 (1990) 269.
[4] T.I. Al-Bajjari, S. Le Vent and D.R. Taylor, *J. Chromatogr. A*, 683 (1994) 367.
[5] D. Repka, J. Krupčík, A. Brunowská, P.A. Leclerq and J.A. Rijks, *J. Chromatogr.*, 463 (1989) 235; and references cited therein.
[6] R.E. Pauls and L.B. Rogers, *Anal. Chem.*, 49 (1977) 625; and references cited therein.
[7] P.J. Schoenmakers, *Optimization of Chromatographic Selectivity* (*Journal of Chromatography Library*, Vol. 35), Elsevier, Amsterdam, 1986.
[8] P.J. Schoenmakers, *Optimization of Chromatographic Selectivity* (*Journal of Chromatography Library*, Vol. 35), Elsevier, Amsterdam, 1986, p. 116.
[9] P.J. Schoenmakers, J.K. Strasters and Á. Bartha, *J. Chromatogr.*, 458 (1988) 355.
[10] T.A. Al-Bajjari, *Ph.D. Thesis*, University of Manchester, Manchester, 1990.

ELSEVIER

Journal of Chromatography A, 683 (1994) 385–396

JOURNAL OF CHROMATOGRAPHY A

Gas chromatographic retention behaviour of polychlorinated naphthalenes on non-polar, polarizable, polar and smectic capillary columns

U. Järnberg[a]*, L. Asplund[a], E. Jakobsson[b]

[a]*Laboratory for Environmental Analytical Chemistry, Institute of Applied Environmental Research, Stockholm University, S-171 85 Solna, Sweden*

[b]*Department of Environmental Chemistry, Wallenberg Laboratory, Stockholm University, S-106 91 Stockholm, Sweden*

First received 16 March 1994; revised manuscript received 31 May 1994

Abstract

Six commercially available gas chromatography columns were investigated for performance in separating polychlorinated naphthalenes (PCNs). Retention behaviour on the investigated phases is compared and retention data for 40 congeners on a 5% phenyl–methylpolysiloxane column is reported. For all columns, except the octylmethylpolysiloxane and the smectic, a relation between substitution pattern and retention was found, where substitution in adjacent positions as well as α-substitution increase the retention time. A mathematical model based on these findings was developed and used to predict the relative retention of all congeners from di- up to octachloronaphthalene, on a 5% phenyl–methylpolysiloxane column.

1. Introduction

Polychlorinated naphthalenes (PCNs) are two-ringed aromatic compounds substituted with chlorine atoms in one to eight positions, numbered as in Fig. 1. Positions 1, 4, 5, 8 and 2, 3, 6, 7 are sometimes referred to as α and β, respectively. Altogether 75 different structures are possible and it has not yet been established how many of these are present in technical formulations and in environmental samples. Table 1 lists all possible structures and some properties together with a number system. This numbering convention is consistent with that originally proposed for PCNs by Wiedmann and Ballschmiter [1].

PCNs exhibit similar physical properties as polychlorinated biphenyls (PCBs), i.e. excellent weathering resistance and electrical insulation properties and chemical and thermal stability.

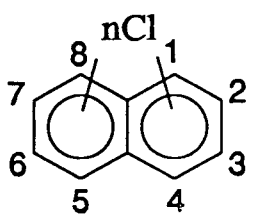

Fig. 1. Generalized structure of polychlorinated naphthalenes.

* Corresponding author.

0021-9673/94/$07.00
SSDI 0021-9673(94)00515-B

Table 1
Numbering, properties and retention data of polychlorinated naphthalenes.

PCN number [a]		α-Cl	Substitution	B.p.[b]	M.p.[b]	Obs. t_R	Pred. t_R
Monochloronaphthalenes							
1		1	1-	259.3[760]	−4 to 2.3		
2		0	2-	256	58–60		
Dichloronaphthalenes							
3	B	1	1,2-	295–298	34–37	1.089	1.089
4	B	1	1,3-	291[775]	61.5–62	1.035	1.058
5	B	2	1,4-	286–287[740]	68–72	1.055	1.055
6	B	2	1,5-	Subl.	106.5–107	1.062	1.055
7		1	1,6-	Subl.	48.5–49		1.055
8		1	1,7-	285–286	61.5–64		1.055
9	B	2	1,8-	Decomp.	88–89.5	1.181	1.181
10		0	2,3-		119.5–120.5		1.067
11	B	0	2,6-	285	135–141	1.060	1.060
12	B	0	2,7-		114–116	1.060	1.060
Trichloronaphthalenes							
13	B	1	1,2,3-		81–84	1.414	1.398
14		2	1,2,4-		92		1.371
15	B	2	1,2,5-		74–79	1.363	1.371
16	B	1	1,2,6-		90–92.5	1.370	1.366
17	B	1	1,2,7-		88	1.388	1.366
18	B	2	1,2,8-		83	1.388	1.436
19		2	1,3,5-		102–103		1.315
20	B	1	1,3,6-		80.5–81	1.291	1.310
21	B	1	1,3,7-		112.5–113	1.309	1.310
22	B	2	1,3,8-		89.5	1.444	1.379
23		3	1,4,5-		130–131		1.384
24	B	2	1,4,6-		65–68	1.317	1.315
25		1	1,6,7-		109–109.5		1.342
26	B	0	2,3,6-		90–91	1.393	1.393
Tetrachloronaphthalenes							
27	B	2	1,2,3,4-		196–198	1.787	1.820
28	B	2	1,2,3,5-		141	1.745	1.745
29		1	1,2,3,6-				1.754
30	B	1	1,2,3,7-		115	1.775	1.754
31	N	2	1,2,3,8-		128		1.941
32		3	1,2,4,5-				1.824
33	B	2	1,2,4,6-		111	1.641	1.637
34		2	1,2,4,7-		140–144		1.637
35		3	1,2,4,8-				1.824
36		2	1,2,5,6-		164		1.711
37		2	1,2,5,7-		114		1.637
38		3	1,2,5,8-				1.824
39		1	1,2,6,7-				1.754
40		2	1,2,6,8-		125–127		1.832
41		2	1,2,7,8-				1.907
42	B	2	1,3,5,7-		178–181	1.562	1.562
43	B	3	1,3,5,8-		131	1.746	1.749
44	B	1	1,3,6,7-		119–120	1.679	1.679

Table 1 (*continued*)

PCN number [a]		α-Cl	Substitution	B.p.[b]	M.p.[b]	Obs. t_R	Pred. t_R
Tetrachloronaphthalenes cont.							
45		2	1,3,6,8-				1.758
46	*B*	4	1,4,5,8-		183	1.936	1.936
47	*B*	2	1,4,6,7-		139	1.692	1.670
48		2	2,3,6,7-		135		1.796
Pentachloronaphthalenes							
49		3	1,2,3,4,5-		168.5		2.352
50		2	1,2,3,4,6-		147		2.151
51		2	1,2,3,5,6-				2.151
52	B	2	1,2,3,5,7-		171	2.050	2.033
53	N	3	1,2,3,5,8-		174–176		2.234
54		1	1,2,3,6,7-				2.199
55	N	2	1,2,3,6,8-		112–114		2.267
56	N	2	1,2,3,7,8-		115–117		2.385
57	N	3	1,2,4,5,6-		136–139		2.219
58		3	1,2,4,5,7-				2.101
59	N	4	1,2,4,5,8-		150–151		2.302
60		2	1,2,4,6,7-				2.033
61		3	1,2,4,6,8-		135		2.101
62		3	1,2,4,7,8-				2.219
Hexachloronaphthalenes							
63	N	3	1,2,3,4,5,6-		132–134	2.809	2.809
64	N	3	1,2,3,4,5,7-		164–166	2.655	2.647
65	N	4	1,2,3,4,5,8-		163.5–164.5	2.861	2.861
66		2	1,2,3,4,6,7-		205–206	2.589	2.589
67		2	1,2,3,5,6,7-		234–235	2.589	2.589
68	N	3	1,2,3,5,6,8-		153–154	2.655	2.647
69	N	3	1,2,3,5,7,8-		148–149	2.679	2.647
70	N	2	1,2,3,6,7,8-		158–160	2.886	2.886
71		4	1,2,4,5,6,8-		175–177	2.705	2.705
72		4	1,2,4,5,7,8-		136–137	2.705	2.705
Heptachloronaphthalenes							
73		3	1,2,3,4,5,6,7-			3.250	3.310
74		4	1,2,3,4,5,6,8-		194	3.265	3.368
Octachloronaphthalene							
75		4	1,2,3,4,5,6,7,8-		197.5–203	3.981	4.030

Relative retention times were determined on a 5% phenyl–methylpolysiloxane column (HP Ultra 2, 50 m) and calculated relative to pentachlorobenzene (1.000).

[a] B denotes standards obtained from Prof. Udo A. Th. Brinkman. N, identity/property is according to Nikiforov [2].

[b] ????????

Therefore technical formulations under trade names such as Halowax (Koppers Company Inc., Pittsburgh, PA, USA), Nibren Wax (Bayer, Leverkusen, Germany), Seekay Wax (Imperial Chemical Industries, Manchester, UK) and Clonacire Wax (Prodelec, Paris, France) have found numerous applications such as dielectrics in capacitors, sealant for electrical equipment, oil additive, wood preservative and impregnating agent for paper and textile [3]. Apart from

deliberate production and leakage to the environment as a result of careless use, PCNs are also released to the environment through the use of PCBs, due to its presence as a micro-contaminant in technical PCB formulations [4]. Several high-temperature processes such as waste incineration and metal reclamation have also been found to produce PCNs [5–7].

PCNs were recognized as early as 1939 as toxic compounds when cases of occupational exposure resulted in the death of several workers in capacitor factories [8]. General toxicological effects exhibited by PCNs are skin defects (chloracne among exposed humans, hyperkeratosis among exposed animals) and liver damage. Chloracne and liver damage have been found to be more pronounced with the higher chlorinated PCNs, i.e. penta- and hexachlorinated naphthalenes [3]. Some of the hexa- and heptachlorinated naphthalenes have been studied in enzyme induction tests; EROD (7-ethoxyresorufin-*o*-deethylase) and AHH (aryl hydrocarbon hydroxylase) enzyme induction. These results indicated a TCDD-like toxicity of two to three orders of magnitude less than 2,3,7,8-tetrachlorodibenzo-*p*-dioxin [9].

Long-term release to the environment in combination with persistency of this substance group, has lead to PCNs being a ubiquitous pollutant. Levels of total PCNs in background biota have been reported ranging from 0.03 to 2 ppb measured on a lipid weight basis [10–13].

PCN levels are commonly reported as total PCNs rather than on an individual congener basis, due to lack of pure reference substances as well as difficulties in achieving a complete congener separation. Only a few investigations have reported levels of individual peaks according to their elution order on a specific column. The results of these investigations show that some congeners appear to be preferentially retained in biota. These constitute the first eluting peak of each homologue group on a 5% phenylmethylsilylated GC column and have the same retention times as the following congeners; 1,3,5,7-tetrachloronaphthalene; 1,2,3,5,7-pentachloronaphthalene; 1,2,3,4,6,7- and 1,2,3,5,6,7-hexachloronaphthalene (coeluting) and 1,2,3,4,5,6,7-heptachloronaphthalene [13–16].

Brinkman and co-workers [17–19] have previously reported extensive chromatographic data on different liquid chromatographic systems for most of the lower chlorinated congeners included in this investigation. Beland and Geer [20] studied the gas chromatographic separation on two packed columns; 10% Carbowax on 60–80 mesh Chromosorb W and 5% Bentone34–10% OV-101 on 100–120 mesh Supelcoport and reported data for 20, mainly lower chlorinated congeners.

Chromatographic separation of polychlorinated naphthalenes as a group has been successfully accomplished on a high resolution gel permeation column [4]. To a certain extent, PCNs may be separated from the bulk of PCBs together with non-planar PCBs on a 2-(1-pyrenyl)-ethyl(dimethyl)silylated (PYE) silica HPLC column [21]. On this type of column the successful separation of two hexachloronaphthalenes (1,2,3,4,5,6- and 1,2,3,5,6,7-hexachloronaphthalene) has been reported [16].

The primary aims of the present investigation were to find a set of GC columns that separate as many congeners as possible in order to be able to determine specifically the environmentally more persistent ones and especially the two previously mentioned hexachloronaphthalenes, and secondly, to investigate the general versatility of different stationary phases in use for analysis of halogenated polycyclic aromatic compounds (XPAC).

2. Experimental

2.1. Chemicals

Halowax 1014 (a technical mixture with approximately 62% chlorine content) was a gift from Koppers Company Inc., Pittsburgh, PA, USA. Of the individual polychlorinated naphthalene standards, all di- to pentachloronaphthalenes used in this investigation (labelled

B in Table 1) were a generous gift from Prof. Udo A. Th. Brinkman, Free University, Amsterdam. The synthesis of these substances and their data were published previously [17]. 1,2,3,4,6,7-, 1,2,3,5,6,7-, 1,2,4,5,6,8-, 1,2,4,5,7,8-hexa, 1,2,3,4,5,6,7-hepta-, and octachloronaphthalene were synthesized as described previously [16,22]. Pentachlorobenzene was a kind gift from Prof. Carl-Axel Wachtmeister at the Wallenberg Laboratory, Stockholm University.

2.2. Columns

Columns were selected to represent stationary phases having different polarities, or exhibiting interactions related to solute geometry, i.e. length-to-breadth ratio and planarity. A column with 5% phenyl–methylpolysiloxane on carborane was also included as this phase, according to Rotzsche [23], has a quasi-aromatic structure that we expected could exhibit specific electron donor–acceptor interactions.

Table 2 lists the investigated columns together with their characteristics.

2.3. Instrumentation

Gas chromatography was performed on a Hewlett Packard 5890 gas chromatograph equipped with a split/splitless injector and a Hewlett Packard 5970B mass selective detector operated in the selected-ion monitoring mode (SIM). Ions from di- up to heptachloronaphthalene were monitored throughout the chromatogram (196, 230, 264, 300, 334 and 368 amu).

Carrier gas was helium 99.995% with all columns, and standard settings for column head pressure were used according to column dimensions.

Temperature programs were established through the injection of approximately 120 ng of

Table 2
Column characteristics

Column name	Manufacturer	Stationary phase	Dimensions (length × I.D.)	Film thickness (μm)	Character
Ultra 1	Hewlett Packard	Dimethylpolysiloxane	50 m × 0.32 mm	0.32	non-polar
Ultra 2	Hewlett Packard	5% Phenyl–dimethyl polysiloxane	50 m × 0.20 mm	0.33	low-polar/ polarizable
HT 5	Scientific Glass Engineering	5% Phenyl–dimethyl polysiloxane on carborane	25 m × 0.22 mm	0.10	low-polar/ quasi-aromatic
CP-Sil 88	Chrompack	100% Cyanopropyl–polysiloxane	50 m × 0.32 mm	0.32	polar
SB-Octyl 50	Lee Scientific	50% *n*-Octyl–dimethyl polysiloxane	50 m × 0.20 mm	0.25	non-polar/ structural interactions
SB-Smectic	Lee Scientific	Biphenylcarboxylate ester methylpolysiloxane	25 m × 0.32 mm	0.15	medium-polar/ structural interactions

Table 3
Instrument parameters

Column	Injector/detector temp (°C)	Injector pressure (hPa)	Temperature program temp(time)/rate
HP Ultra 1	280/290	180	90(2)–200/25–290(36.6)/2
HP Ultra 2	280/290	180	90(2)–200/25–290(36.6)/2
HT5	290/290	90	90(2)–200(2)/15–290(9.3)/2
CP-Sil 88	240/240	180	90(2)–150(2)/15–230(6)/2
SB-Octyl	280/290	180	90(2)–200(2)/20–270(7.5)/1.5
SB Smectic	250/250	90	90(2)–150(2)/10–180(8)/2–230(25)/1.5

Halowax 1014. When and if a satisfactory separation was achieved for Halowax 1014, individual PCN standards were injected together with pentachlorobenzene as retention time reference, and relative retention times were established. Thus, individual standards were analysed only on the most promising columns. GC settings and temperature programs are listed in Table 3.

3. Results and discussion

3.1. General performance

None of the investigated columns was able to resolve all PCN congeners as single peaks. Neither did any of them separate the two hexachloronaphthalenes (1,2,3,4,6,7- and 1,2,3,5,6,7-hexaCN). According to Williams et al. [24] this separation was unsuccessful on several other columns as well. Table 4 lists the number of resolved peaks in Halowax 1014 in each homologue group for the columns in the present investigation (in this text resolved refers to a valley at half the peak height of the smaller peak, which is normally handled by chromatographic data systems). For comparison, the total number of congeners in each homologue group is also given in the table. It should be noted that a strict comparison between some of the columns is not appropriate, due to differing column lengths. Our view is that four columns were more versatile for PCN analysis than the others, namely 5% phenyl–methylpolysiloxane (HP Ultra 2), 50% octyl–methylpolysiloxane (SB-Octyl), 100% cyanopropylpolysiloxane (CP-Sil 88) and the smectic phase (SB Smectic).

On the non-polar dimethylpolysiloxane column (HP Ultra 1), PCNs of different homologue groups eluted as distinctly separated clusters. Increasing the polarity of the column phase yielded an increased resolution within each

Table 4
Comparison of column versatility

Column name	Number of resolved peaks					
	di-CN	tri-CN	tetra-CN	penta-CN	hexa-CN	hepta-CN
Total no.	10	14	22	14	10	2
Ultra-1	5	8	13	11	6	1
Ultra-2	5	8	12	11	6	2
HT5	5	7	13	10	6	1
Cp-Sil 88	3	7	12	10	6	2
SB-Octyl	4	6	12	9	7	2
SB-Smectic	3	7	11	8	6	2

homologue group as illustrated in Fig. 2a and b. A further increase in polarity led to the different homologue groups sliding into each other (Fig. 2c).

The 5% phenyl–methylpolysiloxane column (HP Ultra 2) clearly separated PCNs of different homologue groups showing no difficulties with overlap.

The 5% phenyl–methylpolysiloxane on carborane (HT 5) did not seem to exhibit any separation characteristics different from the other 5% phenyl–methylpolysiloxane column.

On the 50% octyl–methylpolysiloxane column (SB Octyl) PCNs eluted in rather distinct groups according to their chlorine content in much the same way as on the dimethylpolysiloxane column. Several peaks appeared reversed on this column and among the hexachloronaphthalenes one more peak was resolved, presumably one of 1,2,3,4,5,7- or 1,2,3,5,6,8-hexaCN. This may indicate the presence of an additional interaction as compared to the other non-polar column. However, this column did not show any specific retention of the 1,3,5,7-tetraCN, 1,2,3,5,7-pentaCN and the 1,2,3,5,6,7-hexaCN which may be expected to be more planar than the other congeners. This leads to the conclusion that the interaction related to planarity, as suggested by Fischer et al. [25] on this type of column, is not strong enough to exhibit the same difference between PCN congeners as that found between non-ortho- and ortho substituted PCBs.

The 100% cyanopropylpolysiloxane column (CP Sil 88) exhibited more resolution within each homologue group as illustrated previously. Total number of resolved peaks was similar to the other columns but the first pentachloronaphthalene peak was resolved into two, of which the first one is expected to be the 1,2,4,6,7-pentaCN and the second is tentatively identified as the 1,2,3,5,7-pentaCN. In a sample of Guillemot egg from the Baltic, analysed on this column, two pentaCN peaks were present at the same retention times as the two previously mentioned pentaCN showing that these are present in the environment. As previously illustrated in Fig. 2c, considerable overlap of homologue groups on this column, and especially with the tetrachloronaphthalenes into the pentachloronaphthalenes, may cause difficulties in peak assignment, and when quantifying as fragment ions may interfere with molecular ions from lower chlorinated species.

The smectic column (SB Smectic) exhibited some overlap between homologue groups. This column was found to change its selectivity to PCNs drastically when modifying the temperature program and it seemed important to optimize the temperature program according to the separation needs. It was possible to obtain separation between two additional hexachloronaphthalenes 1,2,4,5,6,8-, and 1,2,4,5,7,8-hexaCN, though some resolution was then lost among the lower chlorinated congeners. With this phase the retention order was completely different from the other phases indicating the presence of a different type of interaction. This column specimen showed some problem with peak distortion, especially with the relatively high sample load required to analyse the minor PCN peaks in Halowax 1014.

3.2. Retention mechanisms

All columns investigated, except the SB-octyl and the SB-smectic, exhibited essentially the same retention order within each homologue group indicating that the retention behaviour on these columns relates to the same property of the PCN congeners. Apart from a general increase in the retention with increasing number of chlorine substituents, the position of the substituent is of great importance. The following observations were all connected with an increased retention; 1) increasing number of α-chlorines 2) increasing number of chlorines substituted in adjacent positions, the effect increasing in the order; $\alpha\beta$; $\beta\beta$; $\alpha\alpha$, 3) an uneven distribution of chlorine substituents between the rings and 4) the occurrence of 2,6-substitution. This behaviour is illustrated by the elution order of the dichloronaphthalenes:

1,3 < 1,4 < 1,5 & 2,6 & 2,7 < 1,2 < 1,8

The elution order of all the investigated standards, on a 5%phenyl–methylpolysiloxane column, is given in Table 5.

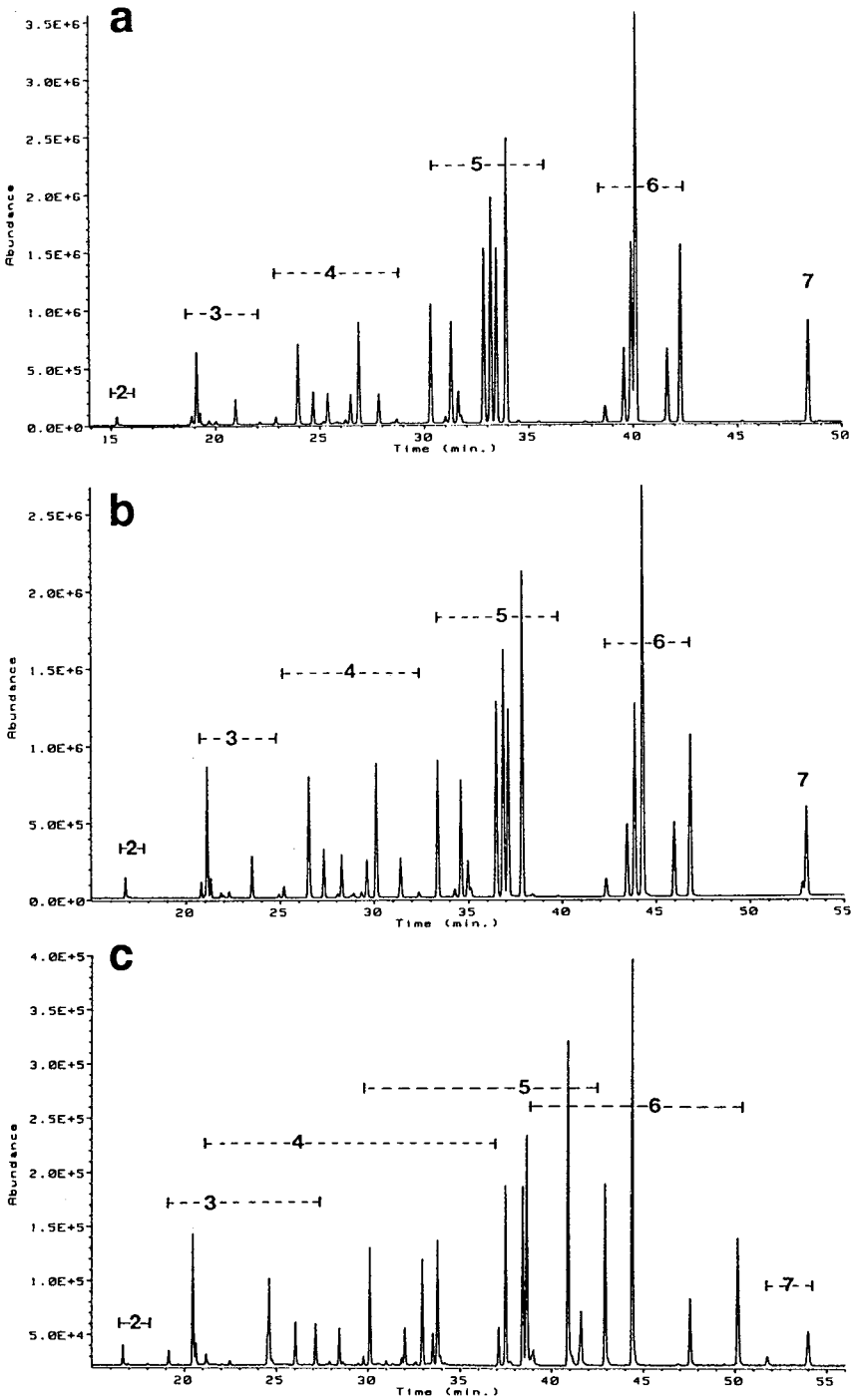

Fig. 2. Total ion chromatograms of technical PCN mixture Halowax 1014 on (a) dimethylpolysiloxane (HP Ultra 1, 50 m), (b) 5% phenyl–methylpolysiloxane (HP Ultra 2, 50 m) and (c) 100% cyanopropylpolysiloxane (CP-Sil 88, 50 m). Details on these columns are given in Table 2, and temperature programs in Table 3.

Table 5
Comparison of retention order on two different phases.

5% Phenyl–methylpolysiloxane	Smectic
Dichloronaphthalenes	
	1,4-
1,3-	1,3-
1,4-	1,5-
1,5-; 2,6-; 2,7-	2,7-
1,2-	1,2-
1,8-	1,8-
	2,6-
Trichloronaphthalenes	
1,3,6-	1,4,6-
1,3,7-	1,3,6-
1,4,6-	1,2,5-
1,2,5-	1,2,7-
1,2,6-	1,2,3-
1,2,7-; 1,2,8-	1,2,8-
2,3,6-	1,3,8-
1,2,3-	1,2,6-
1,3,8-	2,3,6-
Tetrachloronaphthalenes	
1,3,5,7-	1,3,5,7-
1,2,4,6-	1,2,4,6-
1,3,6,7-	1,4,6,7-
1,4,6,7-	1,3,5,8-
1,2,3,5-; 1,3,5,8-	1,3,6,7-
1,2,3,7-	1,2,3,5-
1,2,3,4-	1,2,3,4-
1,4,5,8	1,2,3,7-
	1,4,5,8-
Hexachloronaphthalenes	
1,2,3,4,6,7-, 1,2,3,5,6,7-	1,2,3,4,6,7-; 1,2,3,5,6,7-
1,2,3,4,5,7-, 1,2,3,5,6,8-	1,2,3,5,7,8-
1,2,3,5,7,8-	1,2,3,4,5,7-; 1,2,3,5,6,8-
1,2,4,5,6,8-, 1,2,4,5,7,8-	1,2,4,5,6,8-; 1,2,4,5,7,8-, Resolved in two peaks
1,2,3,4,5,6-	1,2,3,6,7,8-
1,2,3,6,7,8-	1,2,3,4,5,6-
Heptachloronaphthalenes	
1,2,3,4,5,6,7	1,2,3,4,5,6,8-
1,2,3,4,5,6,8-	1,2,3,4,5,6,7-

Brinkman et al. [18] previously reported a strong relation between adjacent substitution and increased retention for di- and tetraCN in liquid chromatography using the system silica–*n*-hexane for the lower chlorinated PCN congeners. They reported that especially the 1,8-, 2,3-, di- and 1,4,5,8-tetraCN congeners were strongly retained compared with 1,4-, 1,5-, di- and 1,3,5,7-tetraCN congeners.

The observations on adjacent substitution seem to hold for several other substituted aromatics as well such as polychlorobenzenes [26], ethyl- and trimethylbenzenes [27] and polychlorinated dibenzofurans [28]. This may be the case for polychlorobiphenyls as well though the relation is complicated by the fact that these molecules are not rotationally fixed. The last eluting PCB congeners in each homologue group, on a 5% phenyl–methylpolysiloxane column, are in fact the 3,3′4,4′-tetra-, 3,3′4,4′5-penta- and 3,3′4,4′5,5′-hexachlorobiphenyls all substituted in adjacent positions [29].

The observation of the relative importance of $\alpha\alpha$-substitution agrees with investigations on other substance groups and corresponding positions. In the data of Hale et al. [28], 1,9-substituted dibenzofurans are the last eluting congeners within each homologue group. For PCBs, however, which are free to rotate around the biphenyl bridge bond, substitution in the 2,2′-positions results in a deviation from planarity causing a decreased retention on 5% phenyl–methylpolysiloxane column [29].

Considering the non-polar dimethylpolysiloxane column as separating according to the boiling point or more strictly to vapour pressure, the observed retention behaviour indicates that solute–phase and solute–solute interactions are based on the same property of the PCNs. Increasing polarity is generally associated with increasing boiling point. However, both 1,3,5,7-tetrachloronaphthalene on the one hand and 1,4,5,8-tetrachloronaphthalene on the other hand are expected to lack an overall dipole

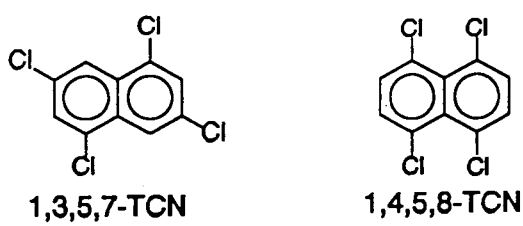

Fig. 3. Tetrachloronaphthalenes with an "even" and "uneven" chlorine substitution, respectively.

moment (Fig. 3). Nevertheless, the latter one is strongly retained compared to the former one. However, the unevenly substituted 1,4,5,8-tetrachloronaphthalene may be considered to have regions where the delocalized electron density is decreased as well as regions where electron density is enhanced. These regions may result in orientation forces between solute–solute and solute–phase molecules.

Lee et al. [30] introduced the terminology of centres of positive or negative charge concerning polarizable stationary phases such as phenyl–methylpolysiloxane and this terminology may be adequate for the discussed polychlorinated naphthalenes as well. Thus, it seems likely that separation of PCNs on non-polar, polarizable and polar phases rests mainly on interactions related to some polar property of the individual congener.

As mentioned previously, the retention behaviour was more complicated on the smectic column. In addition to the previously discussed interactions that may relate to π-electrons of the biphenyls of the smectic phase, a retention based on molecular geometry of the solute may be present as suggested by several authors [31–33]. Markides et al. [32] described the separation mechanism on this type of phase as a combination of retention related to length-to-breadth ratio and planarity as well as Van der Waals interactions. Nishioka et al. [33] found a relation between retention and length-to-breadth ratio L/B for polycyclic aromatic compounds. Compounds with a high L/B were more retained than those with a low ratio. This seems to hold also for PCNs. Table 5 is a comparison of retention order between a 5% phenyl–methylpolysiloxane (HP Ultra 2) column and the smectic column. It can be seen, for instance, that the 1,4- substituted di- tri- and tetrachloronaphthalenes tend to elute earlier on the smectic column than on the 5% phenyl–methylpolysiloxane column while the "longer" 2,6- substituted di- and trichloronaphthalenes are correspondingly more retained.

It is possible to assess a quantitative relationship between substitution pattern and retention so that the retention order can be predicted. Hale et al. [28] proposed a model for predicting retention indices for polychlorinated dibenzofurans. The model is derived truly empirically and accounts for the number and position of chlorine substituents as well as intra- and interring effects of different substituents. Naphthalene is, however, a fused polycyclic aromatic molecule and may be expected to behave somewhat differently from dibenzofuran derivatives. We therefore developed a new model based on the above findings. Using the retention data from the 5% phenyl–methylpolysiloxane (HP Ultra 2) column in the present investigation, a model was set up describing the relation between substitution pattern and relative retention (*rrt*) on this column. The model assumes full additivity and has the following general appearance:

$$rrt = Ax + By + Cz + Du + Ev$$

where x, y, z, u, v are the number of chlorines or pairs with the respective $\alpha(A)$, $\beta(B)$, adjacent $\alpha\beta(C)$, adjacent $\alpha\alpha(D)$, adjacent $\beta\beta(E)$ substitution. The coefficients A, B, C, D and E were obtained by solving equations describing the relation between substitution pattern and relative retention for the standard substances of four homologue groups. Thus four sets of coefficients were calculated (di-, tri-, tetra- and hexachlorinated). These coefficients were further optimized to minimize the residual sum of squares between observed and predicted relative retention times using the Newtonian search algorithm in the personal computer package Solver (a module in Microsoft Excel).

In Table 1 the observed and predicted relative retention times for di- up to hexachlorinated naphthalenes are given. Predicted relative retention times for hepta- and octachloronaphthalenes were calculated using coefficients for hexachloronaphthalenes.

The model is based on a selection of congeners available and may not be fully representative since some critical congeners are missing, i.e. 2,3,6,7-tetraCN. With few exceptions however, the predicted and observed values follow closely and the predicted order is mostly correct.

One major objective for the development of the retention time model was to provide a hint

on the identities of several of the unknown peaks present in Halowax and in environmental samples. Special attention was drawn to the pentachloronaphthalenes since very few of these are available as pure standards. Therefore, coefficients for the pentaCN were interpolated from those of tetra- and hexachloronaphthalenes and relative retention times were calculated. It appears that, even though predicted values are somewhat off scale from the relative retention of the observed pentaCN peaks, the predicted elution order seems reasonable. In order to test and develop the model for the pentaCN, several congeners with different substitution are needed.

4. Conclusions

This investigation indicates that a full congener separation requires the involvement of several different molecular properties. At present, a combination of liquid chromatography and the most versatile gas chromatographic columns can resolve approximately 60 congeners. From the experience of previous results and the present investigation it can be expected that the number of PCN congeners actually present in the technical mixture Halowax 1014 and in the environment exceeds 60. The retention time model developed in this investigation may be a useful tool in search for the presently unknown identities of several PCN peaks found in the technical mixture Halowax 1014 and in environmental samples. The predicted relative retention times for pentachloronaphthalenes suggest that the identity of one of the persistent pentaCN found in Baltic Guillemot egg may be the 1,2,4,6,7-pentaCN.

Acknowledgements

Jill Järnberg at the Swedish National Institute of Occupational Health, is gratefully acknowledged for invaluable contributions to the refinement of the PCN retention model by the introduction of computer optimization.

References

[1] T. Wiedmann and K. Ballschmiter, *Fresenius' J. Anal. Chem.*, 346 (1993) 800–804.
[2] V.A. Nikoforov, R.H. Wightman, A. Auger, M. Malaiyandi and D.T Williams, Poster presented at *Dioxin '92, 12th International Symposium on Dioxins and Related Compounds, Tampere, Finland, August 24–28, 1992*; also published in *Varian Instrument Application*, Vol. 22 No. 1, 1993, p. 10.
[3] F. Kover, *Environmental hazard assessment report: Chlorinated naphthalenes*, EPA Report 560/8-75-001, NTIS publication PB-248834, National Technical Information Service, Springfield, VA, 1975.
[4] P. Haglund, E. Jakobsson, L. Asplund, M. Athanasiadou and Å. Bergman, *J. Chromatogr.*, 634 (1993) 79–86.
[5] E. Benfenati, G. Mariani, R. Fanelli and S. Zuccotti, *Chemosphere*, 22 (1991) 1045–1052.
[6] T. Wiedmann and K. Ballschmiter, *Organohalogen Compounds*, 9 (1992) 331–334.
[7] T. Takasuga, 1993, personal communication.
[8] L. Greenburg, M.R. Mayers and E.R. Smith, *J. Ind. Hyg. Toxicol.*, 21 (1939) 29–38
[9] A. Hanberg, F. Waern, L. Asplund, E. Haglund and S. Safe, *Chemosphere*, 20 (1990) 1161–1164.
[10] B. Jansson, L. Asplund and M. Olsson, *Chemosphere*, 13 (1984) 33–41.
[11] L. Asplund, B. Jansson, C. de Wit, S. Bergek, M. Hjelt, C. Rappe, T. Odsjö and M. Olsson, *Organohalogen Compounds*, 1 (1990) 405–408.
[12] J. Koistinen, *Chemosphere*, 20 (1990) 1043–1048.
[13] U. Järnberg, L. Asplund, C. de Wit, A-K. Grafström, P. Haglund, B. Jansson, K. Lexén, M. Strandell, M. Olsson and B. Jonsson, *Environm. Sci. and Techn.*, 27 (1993) 1364–1374.
[14] L. Asplund, B. Jansson, G. Sundström, I. Brandt and U.A.Th. Brinkman, *Chemosphere*, 15 (1986) 619–628
[15] L. Asplund, E. Jakobsson, Haglund, P. and Å. Bergman, *Chemosphere*, 28 (1994) 2075–2086.
[16] E. Jakobsson, L. Eriksson and Å. Bergman, *Acta Chem. Scand.*, 46 (1992) 527–532.
[17] U.A.Th. Brinkman and H.G.M. Reymer, *J. Chromatogr.*, 127 (1976) 203–243.
[18] U.A.Th. Brinkman, A. De Kok, H.G.M. Reymer and G. de Vries, *J. Chromatogr.*, 129 (1976) 193–209.
[19] U.A.Th. Brinkman and G. de Vries, *J. Chromatogr.*, 169 (1979) 167–182.
[20] F.A. Beland and R.D. Geer, *J. Chromatogr.*, 84 (1973) 59–65.
[21] P. Haglund, L. Asplund, U. Järnberg and B. Jansson, *Chemosphere*, 20 (1990) 7–9; 887–894.
[22] E. Haglund and Å. Bergman, *Chemosphere*, 19 (1989) 195–200.
[23] H. Rotzsche, *Stationary Phases for Gas Chromatography (Journal of Chromatography Library*, Vol. 48), Elsevier, Amsterdam, 1991, p. 224–226.

[24] D.T. Williams, B. Kennedy and G.L. LeBel, *Chemosphere*, 27 (1993) 795–806.
[25] R. Fischer and K. Ballschmiter, *Fresenius' Z. Anal. Chem.*, 332 (1988) 441.
[26] J.K. Haken and I.O.O. Korhonen, *J. Chromatogr.*, 265 (1983) 323–327.
[27] M. Ichiba, H. Hama, S. Yukitake, M. Kubota, S. Kawasaki and K. Tomokuni, *Int. Arch. Occup. Environ. Health*, 64 (1992) 325–327.
[28] M.D. Hale, F.D. Hileman, T. Mazer, T.L. Shell, R.W. Noble and J.J. Brooks, *Anal. Chem.*, 57 (1985) 640–648.
[29] M.D. Mullin, C.M. Pochini, S. McCrindle, M. Romkes, S.H. Safe and L.M. Safe, *Environ. Sci. Technol.*, 18 (1984) 468–476.
[30] M.L. Lee, J.C. Kuei, N.W. Adams, B.J. Tarbet, M. Nishioka, B.A. Jones and J.S. Bradshaw, *J. Chromatogr.*, 302 (1984) 303–318.
[31] Z. Witkiewicz, *J. Chromatogr.*, 251 (1982) 311–337.
[32] K.E. Markides, M. Nishioka, B.J. Tarbet, J.S. Bradshaw and M.L. Lee, *Anal. Chem.*, 57 (1985) 1296–1299.
[33] M. Nishioka, B.A. Jones, B.J. Tarbet, J.S. Bradshaw and M.L. Lee, *J. Chromatogr.*, 357 (1986) 79–91.

ELSEVIER

Journal of Chromatography A, 683 (1994) 397–401

JOURNAL OF CHROMATOGRAPHY A

Short communication

Gas chromatographic analysis of diastereomers and enantiomers of β,γ-unsaturated esters and various analogues of butenolides including mint and isomint lactone and comparison with the high-performance liquid chromatographic analysis of their diastereomers☆

Amruta S. Tambe*, Sujata S. Biswas, P.K. Zubaidha

Organic Chemistry: Technology Division, National Chemical Laboratory, Pune 411 008, India

First received 16 March 1994; revised manuscript received 21 June 1994

Abstract

Butenolide is an α,β-unsaturated lactone. The butenolide moiety is present in numerous biologically active natural products, especially insect sex hormones. A method was developed for the synthesis of butenolides from β,γ-unsaturated esters. Separation of diastereomers and enantiomers of these esters and butenolides including mint and isomint lactone and heritionin by GC is reported. The order of elution of isomers of mint and isomint lactone was identified as *RR*, *SS*, *SR* and *RS* on a Chirasil-Val-D column. This was also confirmed by injecting these samples on to a column with an L-configuration. The separation of diastereomers by HPLC was also tried and the results were compared with those obtained by GC.

1. Introduction

Recently a shorter route for the synthesis of heritol was reported [1]. The separation of the diastereomers and enantiomers of analogous β,γ-esters and lactones was tried by GC on packed and capillary columns and by reversed-phase HPLC and the results were compared. There have been a few reports of enantiomer separations of butyrolactones [2–5] and derivatives of γ-lactones [6–8] and also direct separation using cyclodextrin derivatives as stationary phases [9–14]. However, enantiomer resolution of α,β-unsaturated γ-lactones to our knowledge has not been reported.

2. Experimental

2.1. GC

A Hewlett-Packard Model 5880A gas chromatograph modified for capillary columns with a level 4 integrator and a flame ionization detector was used. Fused-silica capillary columns (25 m × 0.25 mm I.D., 0.12-μm layer) coated with D- and L-Chirasil-Val were purchased from

* Corresponding author.

☆ NCL Communication No. 5972.

0021-9673/94/$07.00
SSDI 0021-9673(94)00587-Y

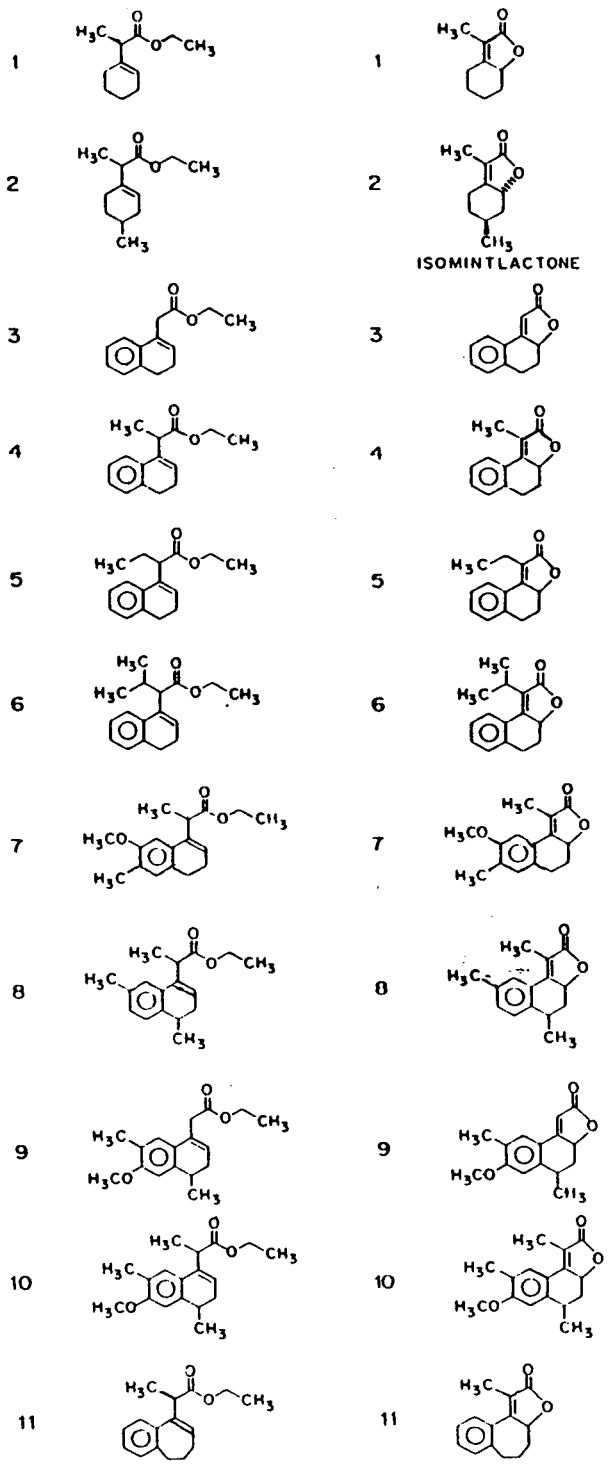

Fig. 1. Structures of the β,γ-esters and lactones.

Chrompak (Middelburg, Netherlands). Stainless-steel packed columns of (1) 3% SE-30 and (2) 2% Apiezon L on Chromosorb W AW DMCS (6 ft. $\times \frac{1}{8}$ in. I.D.; 1 ft. = 30.48 cm, 1 in. = 2.54 cm) were prepared. The experimental conditions used are given in the tables and figures. The structures of the β,γ-esters and lactones analysed are shown in Fig. 1.

2.2. HPLC

HPLC analyses were carried out on a system from Millipore–Waters Chromatography Division (Milford, MA, USA) equipped with Model 510 solvent-delivery pumps, a Model 680 automated gradient controller, a Rheyodyne Model 7225 fixed-volume (20-μl) injector, a Model 440 UV absorbance detector (254 nm) or a Waters Lamda-max 481 LC spectrophotometer (214 nm) and a Hewlett-Packard Model 3390A integrator. A Waters radial compression cartridge (μBondapak C_{18}, 10 μm, 10 cm) fitted in a Z-module system was used as a reversed-phase column. Methanol was purified to chromatographic quality in our laboratory. A Milli-Q system (Millipore, Bedford, MA, USA) was used to purify water. The mobile phase was filtered through a Millipore filter (0.45 μm) using a Millipore all-glass filter apparatus.

3. Results and discussion

3.1. Diastereomers

α,β-Unsaturated lactones

Table 1 gives the retention data for diastereomers of lactones and β,γ-esters for both GC and HPLC analysis.

GC. Whereas an SE-30 column is unable to separate diastereomers, an Apiezon L column gives a very good separation of the diastereomers of lactones **2** and **8**. As there was no separation between the diastereomers of lactone,

Table 1
Retention data for the diastereomers of lactones and β,γ-esters obtained by GC and HPLC

Compound No. and percentage composition (*cis*:*trans*) from NMR	GC with 2% Apiezon L column							HPLC with μBondapak C_{18} column (10 μm)[a]						
	Lactones				Esters			Mobile phase: MeOH: buffer[b]	Lactones			Esters		
	Temperature (°C)	Retention time (min)		α	Retention time (min)		α		Retention time (min)		α	Retention time		α
2 (80:20)	160	8.66	9.77	1.13	3.28	4.48	1.37	50:50	7.60	8.43	1.1	–	–	–
8 (60:40)	200	32.67	33.94	1.04	9.55	16.97	1.78	75:25	6.08	9.48	1.56	19.98	21.92	1.10
9 (60:40)[c]	220	35:25[d]	–	–	8.36	14.95	–	75:25	6.58	9.38	1.43	15.40	13.00	–
						18.03							17.48	
10 (60:40)	220	34.32	–	–	8.22	14.63	1.78	75:25	6.64	10.68	1.61	29.88	–	–

GC: injector temperature = oven temperature + 40°C; detector temperature = 300°C; carrier gas, nitrogen at a flow-rate of 30 ml/min.
HPLC: UV detection at 254 nm for **8**, **9** and **10** lactones and esters and 218 nm for **2** lactone and ester.
[a] For lactone **2** a reversed-phase column was used: Novapak C_{18}, 5 μm.
[b] Buffer = 0.7 *M* triethylammoniumphosphate (pH 3).
[c] (*E*)-**9** shows anamolous behaviour; it may form an α,β-ester that can separate into positional isomers.
[d] Lactone **9** shows a broad peak with a hump.

9 and **10** by GC, the analysis was successfully achieved by HPLC.

HPLC. The elution sequence is the *trans* isomer before the *cis* isomer, in contrast to GC, where the *cis* isomer elutes first. This was confirmed by injecting pure mint and isomint lactone (**2**) and pure *cis*- and *epi*-heritol (**10**). Diastereomer separation of L-**2** and L-**10** by HPLC can be seen in Fig. 2, which also shows the peak of an impurity developed after keeping the samples in methanol for a few days. The lactone ring may be opening to form a hydroxy ester on keeping in methanol.

β,γ-Esters

GC. The esters with two asymmetric carbon atoms separate well into their diastereomers when injected on to both SE-30 and Apiezon L columns. The ester **9** shows three peaks, a major peak (60%) followed by two peaks each with 20% composition on the Apiezon L column. The same pattern is observed on capillary chiral and achiral columns. This is possible only if some kind of reaction is taking place at high temperature. If an α,β-ester is formed then it may show two positional isomers due to restricted rotation (the ester group and hydrogen can be on either side of the double bond). The first major peak may be a β,γ-ester and the other two equal peaks are positional isomers of the α,β-ester that is formed. We thought HPLC analysis might resolve the problem.

HPLC. Ester **8** is well separated into the diastereomers but ester **10** shows only one peak. Ester **9** shows three peaks even by HPLC, only the sequence of elution is altered (Fig. 3). The middle peak is major (60%) with two peaks (20% each) on either side. ^{1}H NMR spectrometry also shows the presence of isomers.

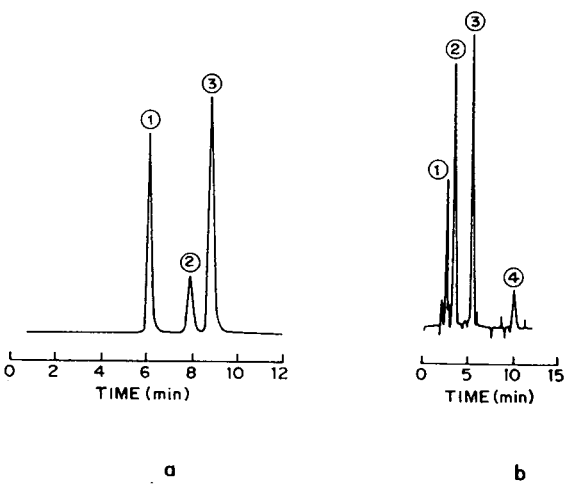

Fig. 2. (a) Diastereomer separation of lactone **2** by HPLC. Column, Novapak C_{18}, 5 μm (10 cm × 5 mm I.D.); mobile phase; methanol–buffer (50:50) (pH 3); flow-rate, 1 ml/min; UV detection at 218 nm. Peaks: 1 = impurity developed on keeping; 2 = isomint lactone; 3 = mint lactone. (b) Diastereomer separation of lactone **10** (heritionin) by HPLC. Column, μBondapak C_{18}, 10 μm (10 cm × 8 mm I.D.); mobile phase, methanol–buffer (75:25) (pH 3); flow-rate, 2 ml/min; UV detection at 254 nm. Peaks: 1 = impurity developed on keeping (lactone ring may be opened); 2 = *trans*-heritionin; 3 = *cis*-heritionin; 4 = impurity.

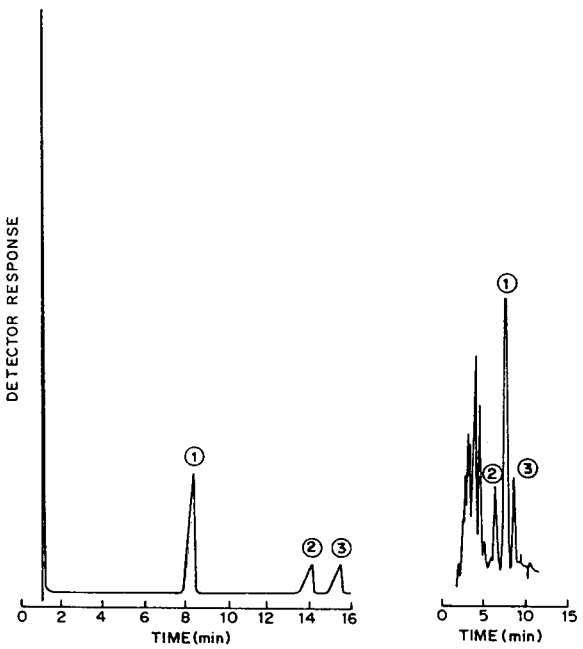

Fig. 3. (a) GC of ester **9** on Chirasil-Val-D. Oven temperature, 170°C; injector temperature, 210°C; detector temperature, 250°C; carrier gas, nitrogen at a flow-rate of 2 ml/min; splitting ratio, 1:100. Peaks: 1 = β,γ-ester; 2 and 3 = positional isomers of α,β-ester. (b) HPLC of ester **9**. Conditions as in Fig. 2b. Peaks: 2 = β,γ-ester; 1 and 3 = positional isomers of α,β-ester.

Therefore, we conclude that the positional isomers of α,β-esters are being separated.

3.2. Enantiomers

α,β-Unsaturated lactones

All the lactones show enantiomeric separation at least to some extent. Fig. 4 shows the separation of mint and isomint lactone into their enantiomers. The sequence of elution of the isomers is identified as *RR*, *SS*, *SR* and *RS* on the Chirasil-Val D column on injecting pure (*RR*)-(−) and (*RS*)-(+)-enantiomers [15]. The order of elution is reversed on a column with opposite configuration. Lactones **9** and **10** can be separated only into their diastereomers even on the chiral column.

β,γ-Esters

Only esters **2**, **8** and **10** show the presence of enantiomers but the α values are small. For all the three esters the *cis* isomer shows splitting whereas the *trans* isomer does not separate into enantiomers.

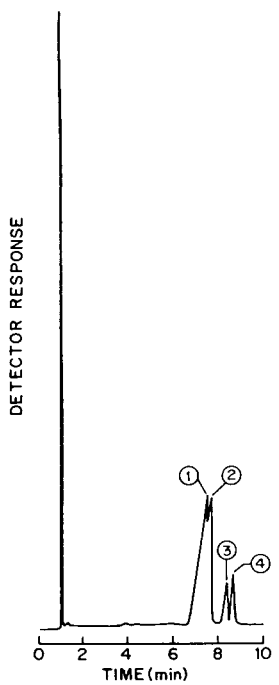

Fig. 4. Enantiomer separation of mint lactone and isomint lactone on Chirasil-Val-D. Oven temperature, 120°C; other conditions as in Fig. 3a. Peaks: 1 = (*RR*)-mint lactone; 2 = (*SS*)-mint lactone; 3 = (*SR*)-isomint lactone; 4 = (*RS*)-isomint lactone.

4. Conclusions

The diastereomer separation of β,γ-esters and butenolides including mint and isomint lactone and heritionin was achieved by GC and HPLC and the results were compared. Separation of the enantiomers of mint lactone and isomint lactone could be achieved on Chirasil-Val-D at 120°. The order of elution of isomers on this column was identified as *RR*, *SS*, *SR* and *RS*.

References

[1] P.K. Zubaidha, S.P. Chavan, U.S. Racherla and N.R. Ayyangar, *Tetrahedron*, 47 (1991) 5759.
[2] S. Hunig, N. Klaunzer and K. Gunther, *J. Chromatogr.*, 481 (1989) 387.
[3] A. Tambute, M. Linne, M. Caude and R. Rosset, *J. Chromatogr.*, 448 (1988) 55.
[4] E. Francotte and D. Lohmann, *Helv. Chim. Acta*, 70 (1987) 1969.
[5] D.W. Armstrong, A.M. Stalcup, M.L. Hilton, J.D. Duncan, J.R. Faulkner and S.C. Chang, *Anal. Chem.*, 62 (1990) 1610.
[6] K.H. Engel, R.A. Flath, W. Albrecht and R. Tressel, *J. Chromatogr.*, 479 (1989) 176.
[7] K.H. Engel, W. Albrecht and J. Heidlas, *J. Agric. Food Chem.*, 38 (1990) 244.
[8] A. Mosandl, M. Gessner, C. Guenther, W. Deger and G. Singer, *J. High Resolut. Chromatogr. Chromatogr. Commun.*, 10 (1987) 67.
[9] W.A. Konig, S. Lutz, C. Colberg, N. Schmidt, G. Wenz, E. Bey, A. Mosandl, C. Guenther and A. Kustermann, *J. High Resolut. Chromatogr. Chromatogr. Commun.*, 11 (1988) 621.
[10] D.W. Armstrong, W.Y. Li, C.D. Chang and J. Pitha, *Anal. Chem.*, 62 (1990) 914.
[11] W.Y. Li, H.L. Jin and D.W. Armstrong, *J. Chromatogr.*, 509 (1990) 303.
[12] V. Schurig, M. Jung, D. Schmalzing, M. Schleimer, J. Duvekot, J.C. Buyten, J.A. Peene and P. Mussche, *J. High Resolut. Chromatogr.*, 13 (1990) 470.
[13] V. Schurig, D. Schmalzing, U. Muhleck, M. Jung, M. Schleimer, P. Mussche, J. Duvekot and J.C. Buyten, *J. High Resolut. Chromatogr.*, 13 (1990) 713.
[14] K. Grob, H.P. Neukom, H.G. Schmarr and A. Mosandl, *J. High Resolut. Chromatogr.*, 13 (1990) 433.
[15] A.S. Tambe, P.K. Zubaidha, S.S. Biswas and N.R. Ayyangar, presented at the *3rd International Symposium on Chiral Discrimination, Tübingen, 5–8 October 1992.*

ELSEVIER

Journal of Chromatography A, 683 (1994) 402–406

JOURNAL OF CHROMATOGRAPHY A

Short communication

Improved method for the separation of ranitidine and its metabolites based on supercritical fluid chromatography

M.S. Smith[a,*], J. Oxford[a], M.B. Evans[b]

[a]*Glaxo Research and Development Ltd., Park Road, Ware, Herts. SG12 ODP, UK*
[b]*University of Hertfordshire, College Lane, Hatfield, Herts. AL10 9AB UK*

First received 16 May 1994; revised manuscript received 27 June 1994

Abstract

The analysis by supercritical fluid chromatography (SFC) of ranitidine and its metabolites isolated from biological fluids is demonstrated. Chromatography was performed using a cyanopropyl column (100 × 4.6 mm I.D.) with supercritical carbon dioxide modified by a mixture of methanol–methylamine–water as the mobile phase. Separation of ranitidine from its acidic and basic metabolites is achieved in under 10 min. The investigation demonstrates the suitability of SFC for the analysis of polar drug compounds from biological matrices.

1. Introduction

Ranitidine hydrochloride is a H_2 receptor antagonist used as an inhibitor of gastric secretion in the treatment of patients who have peptic ulceration. Metabolism studies in rat, dog, rabbit and marmoset have shown that ranitidine (I) forms four metabolites, namely: ranitidine N-oxide (II), ranitidine S-oxide (III), desmethyl ranitidine (IV) and the 5-substituted-2-furan carboxylic acid (V) [1,2] as shown in Fig. 1. A number of methods have been described for the determination of ranitidine in drug substances and biological fluids [3–15]. However, none of the previously reported LC methods enable the simultaneous separation of ranitidine and all of its known metabolites.

Supercritical fluid chromatography (SFC) is a technique with superior kinetics to those of liquid chromatography and is capable of separation efficiencies approaching those of gas chromatography. Furthermore when used with polar mobile phases there are indications that SFC may be used for the assay of polar analytes with no on-column decomposition [16,17].

Accordingly it was decided to investigate the possibility of using packed-column SFC for the simultaneous analysis of ranitidine and its acidic and basic metabolites.

2. Experimental

SFC was performed on 100 × 4.6 mm I.D. stainless-steel columns packed with either 3- or 5-μm cyanopropyl or aminopropyl silica (Phase Separations, Queensferry, UK). Columns were heated in a Model TC1900 oven (ICI Scientific Instruments, Dingley, Australia) at temperatures between 50 and 80°C. The mobile phase con-

* Corresponding author.

0021-9673/94/$07.00
SSDI 0021-9673(94)00600-8

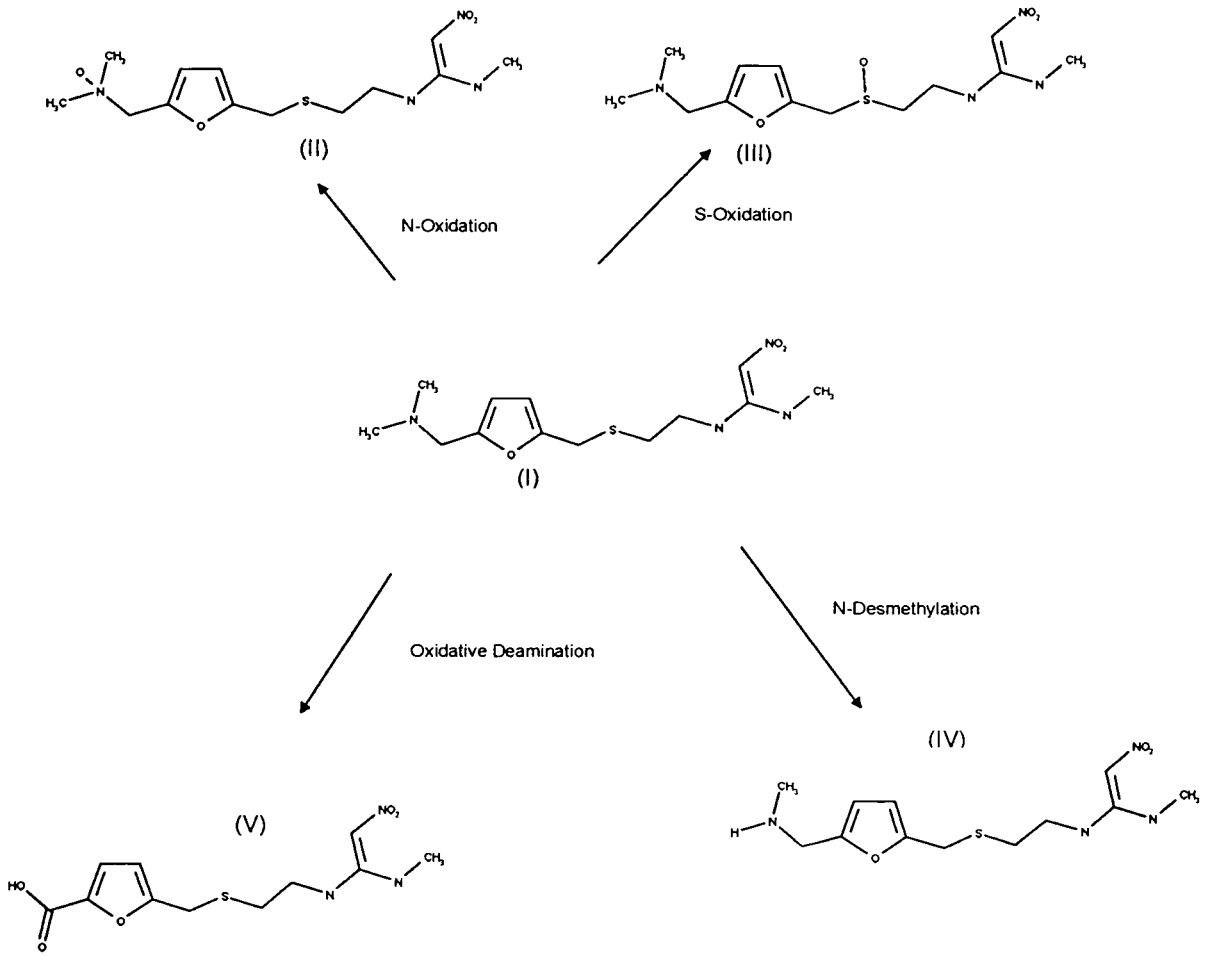

Fig. 1. The metabolism of ranitidine.

sisted of mixtures of carbon dioxide (British Oxygen Gases, London, UK), methanol, methylamine and water pumped through the system by Model 302 and 303 piston pumps (Gilson, Middleton, WI, USA) controlled by means of an Apple II GS microcomputer. The pumphead was cooled to −15°C by means of a RTE-4 refrigerated bath cooler (Jencons, Leighton Buzzard, UK) to facilitate the filling of the pump with liquid mobile phase. Samples were introduced by means of a Rheodyne Model 7125 injector fitted with a 10-μl loop. The column effluent was monitored by a Model 757 variable-wavelength UV detector (Kratos Analytical, Ramsey, NJ, USA). A Tescom back pressure regulator (Tescom Instruments, Elk River, MI, USA) was used to maintain supercritical conditions.

2.1. Reagents and materials

HPLC-grade methanol was obtained from BDH (Poole, UK) whilst 40% (v/v) aqueous methylamine was obtained from Aldrich.

Ranitidine hydrochloride, ranitidine N-oxide, ranitidine S-oxide, desmethyl ranitidine and the furoic acid analogue were synthesised in the Chemistry Division of Glaxo Research and Development, Ware, UK.

3. Results and discussion

The initial attempt to separate the metabolites of ranitidine was performed using an aminopropyl bonded phase with supercritical carbon dioxide modified with methanol as the mobile phase. Ranitidine, ranitidine S-oxide, ranitidine N-oxide and desmethyl ranitidine as can be seen in Fig. 2 were found to be separated within 9 min; however, there were signs of peak tailing in the case of desmethyl ranitidine. The furoic acid analogue was not eluted even with high pressures and modifier concentrations indicating irreversible adsorption onto the basic stationary phase.

Clearly a different strategy was required to facilitate a simultaneous separation of the acidic and basic metabolites. In the first instance, the stationary phase was changed to cyanopropyl silica which is a non-basic sorbent that is less likely to retain acidic or basic analytes irreversibly. The cyanopropyl silica proved to be an ideal stationary phase for the furoic acid metabolite which was eluted in less than 2 min at 53°C. The basic components, however, were strongly retained by the stationary phase, especially ranitidine and ranitidine N-oxide, which were retained for over 30 min even using high pressures and a 20% methanol concentration.

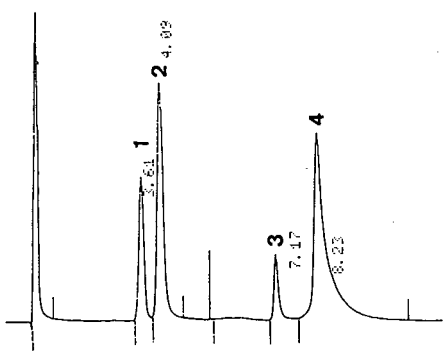

Fig. 2. The separation of ranitidine (1), ranitidine S-oxide (2), ranitidine N-oxide (3) and desmethyl ranitidine (4) on an aminopropyl column by SFC. Column, 10 × 0.46 cm, 5-μm aminopropyl bonded silica; inlet pressure, 3600 p.s.i.; mobile phase, carbon dioxide–methanol, a linear gradient of 15 to 20% methanol and a flow-rate of 3 to 4 ml/min over 10 min; temperature, 53°C. Values at peaks are retention times in min.

Janicot et al. [18] have successfully separated the alkaloids narcotine, papaverine, thebaine, ethylmorphine, codeine, morphine and cryptopine from a poppy straw extract by SFC using a mixture of methanol, aliphatic amine and water as eluent along with an aminopropyl bonded silica column. They suggested that the amine effectively precluded analyte retention by residual silanols whilst the water enhanced the alkaloid–amine–aminopropyl chain interactions. Thus if an amine, which competes well with an eluite for residual silanols, is included in the mobile phase at a sufficiently high concentration; retention of the eluite will occur only by a solvophobic mechanism [19]. Since the basicities of the alkaloids examined by Janicot et al. were not too dissimilar to the basic ranitidine metabolites it was decided to test the applicability of methanol, methylamine and water as modifiers for carbon dioxide for the analysis of ranitidine. The concentration of methylamine in the modifier was found to be critical, the greater the concentration of methylamine the longer the retention of the analytes, also above a 3% amine level difficulties were encountered due to column blockage. Below 1% the amine gave rise to negligible selectivity between ranitidine and ranitidine S-oxide as can be seen from the data in Table 1.

Accordingly a 1% methylamine level was chosen as the standard modifier concentration for all subsequent investigations. Methylamine was introduced as a 40% aqueous solution, the water was obviously important because little selectivity was observed when the same concentration of amine was added by means of a 33% solution in methylated spirits. Janicot et al. used an aminopropyl bonded silica to separate the basic alkaloids. However, with ranitidine and its basic metabolites ample retention could already be achieved using a cyanopropyl bonded phase. Thus by reducing the silanol interactions for ranitidine and ranitidine N-oxide with the amine modifier all five compounds might be expected to be separated and in fact this was found to be the case as shown in Fig. 3.

The experiments with model compounds indicate the potential of SFC in drug metabolism

Table 1

Effect of the methylamine concentration (in the modifier) on the capacity ratios of ranitidine and its metabolites

Component	Capacity ratio			
	Methylamine concentration in the modifier (%)			
	0.5	1	3	4
I	2.83	2.90	3.09	3.08
III	2.83	3.15	3.57	3.64
IV	3.91	4.38	4.69	4.85
V	4.79	4.97	6.41	6.85
II	7.98	9.94	10.79	10.84

Column, 10 × 0.46 cm 3 μm cyanopropyl bonded silica; pressure inlet, 4000 p.s.i. (1 p.s.i. = 6894.76 Pa); mobile phase composition, carbon dioxide–(methanol + 0.5–4% methylamine + 1% water) (80:20, v/v); flow-rate, 2.5 ml/min; temperature, 71°C.

studies. Not only was the resolution achieved superior to that obtained by LC but also the speed of analysis was improved. Accordingly it was decided to test the method using biological extracts containing drug and metabolites.

The metabolism of drugs in the body occurs largely in the liver. A convenient method of monitoring drug metabolism in vitro involves using isolated hepatocytes. In this procedure a liver is removed from an animal, the hepatocytes, which contain all the detoxifying liver enzymes necessary for metabolism to occur, are isolated and incubated with the target drug, in this instance ranitidine [20]. The drug and its metabolites were recovered by solid-phase extraction (SPE), as described previously [16], and submitted for SFC. Typical results are shown in Fig. 4, which indicate that the metabolism of the ranitidine has occurred in the presence of both guinea pig and rat hepatocytes. As can be seen both species produce little or no furoic acid metabolite and the guinea pig produces a higher proportion of ranitidine N-oxide relative to the rat.

In a further experiment ranitidine metabolites present in rat urine, isolated by SPE, were analysed by SFC. The results obtained as shown

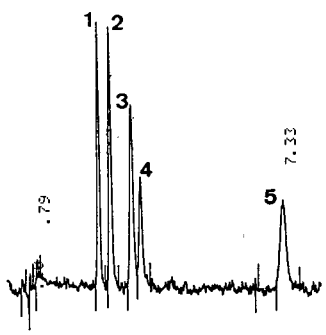

Fig. 3. Isocratic elution of ranitidine and its metabolites by SFC. Column, 10 × 0.46 cm, 3-μm cyanopropyl bonded silica; inlet pressure, 3200 p.s.i.; mobile phase, carbon dioxide–methanol–40% aqueous methylamine–water (80:19.6:0.2:0.2); flow-rate, 3 ml/min; temperature, 71°C. Peaks: 1 = I; 2 = III; 3 = IV; 4 = V; 5 = II.

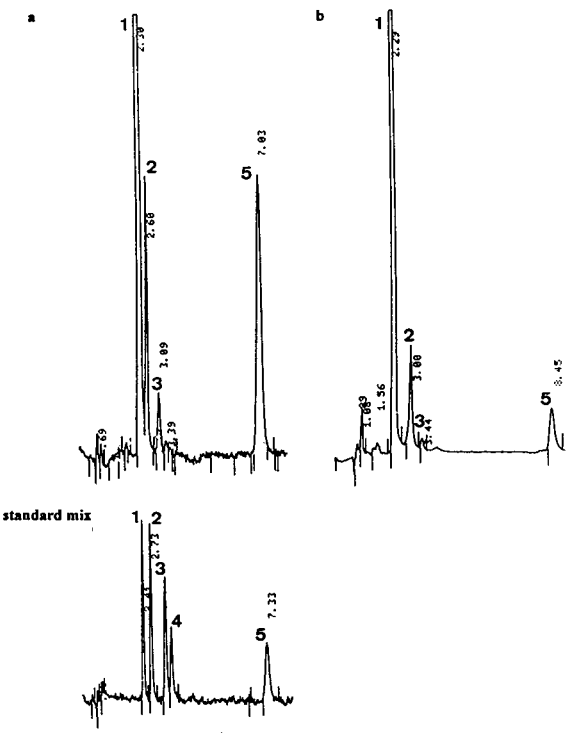

Fig. 4. SFC analysis of ranitidine from (a) rat and (b) guinea pig hepatocytes. Conditions and peak numbering as in Fig. 3.

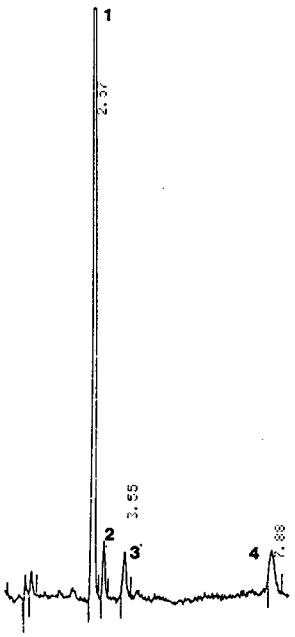

Fig. 5. SFC separation of ranitidine and its metabolites from rat urine. Conditions as in Fig. 3. Peaks: 1 = I; 2 = III; 3 = IV; 4 = II.

in Fig. 5 again emphasise the potential of SFC in this context.

4. Conclusions

Studies involving model compounds and biological samples reveal the potential of SFC for the analysis of drugs and their phase 1 metabolites.

Acknowledgement

David Cross is gratefully acknowledged for the supply of the samples derived from isolated hepatocytes.

References

[1] J.A. Bell, F.A.A. Dallas, W.J.N. Jenner and L.E. Martin, *Biochem. Soc. Trans.*, 8 (1980) 93.
[2] L.E. Martin, J.A. Bell, P.F. Carey, F.A.A. Dallas, G.T. Dixon and W.N. Jenner, in J.J. Misiewicz and K.G. Wormsley (Editors), *The Clinical Use of Ranitidine, Proceedings from the Second International Symposium on Ratinidine, London, 8–9 Oct. 1981*, The Medicine Publishing Foundation, Oxford, 1981.
[3] P.F. Carey and L.E. Martin, *J. Liq. Chromatogr.*, 2 (1979) 1291.
[4] G. Mullersman and H. Derendorf, *J. Chromatogr.*, 381 (1986) 385.
[5] H.M. Vandenberghe, S.M. MacLeod, W.A. Mahon, P.A. Lebert and S.J. Soldin, *Therapeutic Drug Mon.*, 2 (1980) 379.
[6] W.Th. Kok, J.J. Halvax, W.H. Voogt, U.A.Th. Brinkman amd R.W. Frei, *Anal. Chem.*, 57 (1985) 2580.
[7] P.F. Carey, L.E. Martin and M.B. Evans, *Chromatographia*, 19 (1984) 200.
[8] P. Ficarra, R. Ficarra and A. Tommasini, *J. Pharm. Biomed. Anal.*, 2 (1984) 119.
[9] P.F. Carey, L.E. Martin and P.E. Owen, *J. Chromatogr.*, 225 (1981) 161.
[10] G.W. Milay, O.H. Drummer, A. Marshall, R.A. Smallwood and W.J. Louis, *J. Pharm. Sci.*, 69 (1980) 1155.
[11] H.T. Karnes, K. Opong-Mensah, D. Farthing and L.A. Beightol, *J. Chromatogr.*, 422 (1987) 165.
[12] G. Guiso, C. Fracasso, S. Caccia and A. Abbiati, *J. Chromatogr.*, 413 (1987) 363.
[13] A.M. Rustum, A. Rahman and N.E. Hoffman, *J. Chromatogr.*, 421 (1987) 418.
[14] J. Boutagy, D.G. More, I.A. Munro amd G.M. Shenfield, *J. Liq. Chromatogr.*, 7 (1984) 1651.
[15] H. Kubo, Y. Kobayashi and K. Tokunaga, *Anal. Lett.*, 18 (1985) 245.
[16] M.S. Smith, *Ph.D. Thesis*, Hatfield Polytechnic, Hatfield, 1990.
[17] M.B. Evans, M.S. Smith and J. Oxford, *J. Chromatogr.*, 479 (1989) 170.
[18] J.L. Janicot, M. Caude and R. Rosset, *J. Chromatogr.*, 437 (1988) 351.
[19] K.E. Bij, Cs. Horváth, W.R. Melander and A. Nahum, *J. Chromatogr.*, 203 (1981) 65.
[20] D. Cross, *Ph.D. Thesis*, Hatfield Polytechnic, Hatfield, 1991.

ELSEVIER

Journal of Chromatography A, 683 (1994) 407–410

JOURNAL OF CHROMATOGRAPHY A

Short communication

Solute trapping in off-line supercritical fluid extraction using controlled modifier condensation

Jiří Vejrosta[a,*], Alena Ansorgová[a], Josef Planeta[a], David G. Breen[b], Keith D. Bartle[b], Anthony A. Clifford[b]

[a]*Institute of Analytical Chemistry, Academy of Sciences of the Czech Republic, Veveří 97, 611 42 Brno, Czech Republic*
[b]*School of Chemistry, University of Leeds, Leeds LS2 9JT, UK*

First received 29 April 1994; revised manuscript received 5 July 1994

Abstract

A new approach to solvent trapping, based on controlled modifier condensation, is presented. The trapping system consists of a fused-silica capillary (30 cm × 500 μm I.D.) equipped with a cryofocusing device. As a trapping mechanism, nebulization of expanding supercritical mixture with condensing modifier, followed by analyte trapping into moving liquid layer is assumed. In spiking experiments a urea-based herbicide, flufenoxuron, was extracted with 10% methanol-modified CO_2 and recoveries of over 90% were found. The resulting solvent volumes needed for quantitative trapping are much lower (ca. 0.3 ml) than in the case of direct bubbling through bulk liquid.

1. Introduction

In previous work [1] a new off-line trapping method for analytical supercritical fluid extraction (SFE) was proposed. A solute precipitating from an expanding supercritical phase was trapped on the surface of the inner wall of a piece of fused-silica tubing. It was found that a relatively small volume of liquid solvent (50–100 μl) was required to rinse the precipitated solute efficiently from the trapping capillary. The resulting solutions were of higher solute concentration when compared to solutions obtained by direct trapping into liquid solvents. An added advantage was that the solution obtained by this method could be analysed directly without further concentration.

The described method was successfully tested with model fluoranthene solutions spiked onto inert glass beads. Recoveries around 96% were found up to linear flow velocities of 2 m s^{-1} (measured at ambient conditions) of expanding CO_2 in the trapping capillary. As proposed, the method can be used with pure extracting fluid. When pure CO_2 or N_2O are used, however, their solubilizing power is often insufficient for efficient extraction of polar analytes. Then the extracting power can be enhanced by adding of polar modifiers such as methanol or other organic solvents. The object of the present work was to investigate whether the described method could be used when the extracting fluid is modified and whether the modifier could be exploited in the trapping process.

When a relatively volatile modifier is present at low concentration, the modifier evaporates

* Corresponding author.

0021-9673/94/$07.00
SSDI 0021-9673(94)00637-7

almost completely following decompression of the extracting fluid and the proposed trapping procedure described previously can be applied as in the case of a pure fluid. At higher modifier concentrations a proportion of the total modifier remains in the gaseous state following depressurization of the fluid at a given capillary temperature. The remaining modifier liquifies and forms a film on the inner wall of the capillary. The precipitated analytes are trapped in the liquid film rather than on the capillary wall. The analytes are thereafter swept out the capillary as the liquid modifier moves down the trapping capillary and are collected as a solution in liquid modifier in a vial. The aim of this paper is to verify the assumed trapping mechanism quantitatively when modifier condensation is controlled by a cryofocusing device. A urea-based herbicide, flufenoxuron, is used as a model solute for the investigation.

2. Experimental

All extractions were performed on a laboratory-built system consisting of a Varian 8500 syringe pump with a cooled head and a heated extraction cell linked to a specially designed and constructed trapping device. The pressure in the cell was maintained using 15 cm length of fused-silica capillary tubing with an internal diameter of either 20 or 25 μm as a linear flow restrictor. The end of the restrictor was located in a ceramic heating device which was programmed to a desired temperature to prevent restrictor plugging. The tip of the restrictor was located inside a 30 cm × 500 μm I.D. fused-silica capillary. The extraction system and trapping device is shown schematically in Fig. 1. The extracting fluid employed was CO_2 modified with 10% of methanol by volume (ECM Speciality Gases, Stoke on Trent, UK). The trapping system was equipped with a cryogenic cooling device which operated on an 8 cm length of the 500 μm I.D. capillary. The cooling device was located immediately after the ceramic restrictor heater. The cooling was provided by expanding carbon dioxide supplied from another source and controlled

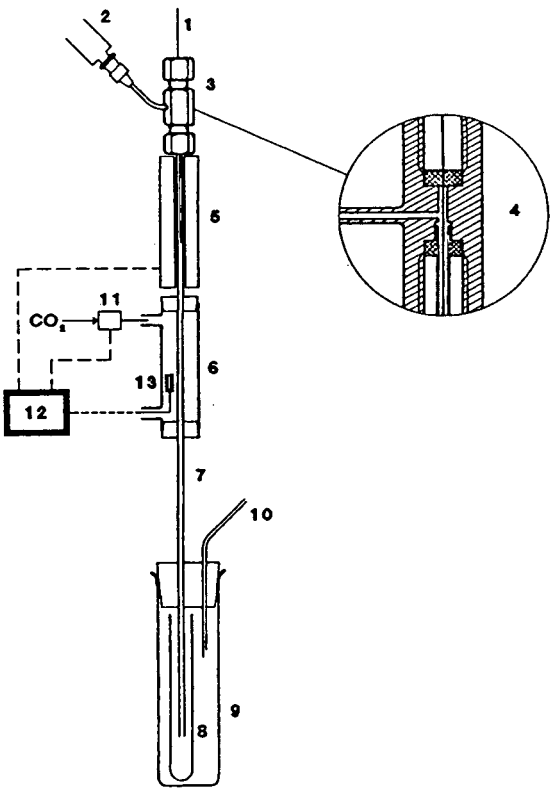

Fig. 1. Schematic representation of the trapping system. 1 = Restrictor; 2 = syringe; 3 = connecting union; 4 = detailed inner configuration of the connecting union; 5 = heater; 6 = trapping capillary; 7 = cryofocuser; 8, 9 = vials; 10 = output of CO_2; 11 = solenoid valve; 12 = control unit; 13 = thermistor.

by a solenoid valve and a temperature controller, which also regulated the extraction cell and restrictor heater temperature. A 30-μl sample of a 0.8 mg ml^{-1} flufenoxuron standard in 1,4-dioxane was spiked onto glass beads in an extraction cell of internal volume 0.6 ml. The solvent was allowed to evaporate prior to extraction. A series of extractions were carried out for various experimental conditions. Each extraction was performed at 40 MPa and 60°C; the other extraction conditions and parameters are summarized in Tables 1 and 2.

The flow-rate of gaseous CO_2–methanol was measured using a bubble flow meter coupled to the collection microvial. The volume of methanol collected from the 500-μm capillary was

Table 1
Flufenoxuron recovery (spike experiments)

Experiment No.	Recovery (%) in		Total recovery (%)
	Condensed modifier	Rinsing solvent	
1	75.6	19.8	95.4
2	92.2	3.5	95.7
3	87.6	2.9	90.5
4	85.6	3.8	89.4
5	76.2	10.2	86.4
6	80.2	15.9	96.1
Mean	82.9	9.4	92.3
R.S.D. (%)	7.3		4.0

Flow-rate of CO_2 100 ml min^{-1} (at ambient conditions), cryofocusing temperature −30°C.

determined by mass and density calculations. After each extraction the trapping capillary was rinsed with 100 μl of methanol (HPLC grade, Fisons Chemicals, Loughborough, UK). An additional rinse with methanol was carried out to determine whether any analytes are retained in the trapping capillary after the initial wash.

The collected methanol and methanol-rinse fractions were analysed by reversed-phase HPLC. The HPLC system consisted of a Merck–Hitachi L6000 reciprocating pump, a Rheodyne 6-port injection valve with a 10-μl sample loop, a 25 cm × 4.5 mm I.D. S10 ODS2 packed column (Spherisorb), a Merck–Hitachi L4000 UV detector and a Hewlett-Packard 3395 integrator. The mobile phase was acetonitrile–water–propan-2-ol (60:35:5, v/v/v). Analyte recoveries were calculated by absolute calibration. A calibration curve was prepared by analysis of a set of standard flufenoxuron solutions.

Table 2
Flufenoxuron recovery (spike experiments)

Experiment No.	Recovery (%) in		Total recovery (%)
	Condensed modifier	Rinsing solvent	
1	75.6	14.5	90.1
2	73.8	7.7	81.5
3	79.2	7.5	86.7
4	81.0	7.0	88.0
5	73.1	10.7	83.8
6	72.9	11.0	83.9
Mean	75.9	9.7	85.7
R.S.D. (%)	4.1		3.4

Flow-rate of CO_2 180 ml min^{-1} (at ambient conditions), cryofocusing temperature −30°C.

3. Results and discussion

Flufenoxuron has been quantitatively recovered from spiked soil samples in previous studies [2]. Extraction was found to be quantitative after 20 min at 60°C and 40 MPa with carbon dioxide modified with 10% of methanol. The aim of this study was not to examine the extraction efficiency, but to evaluate the trapping procedure.

An extraction time of 15 min was found to be sufficient for quantitative extraction at flow-rates of approximately 100 ml min^{-1} (flow of CO_2 at ambient conditions) with the 20-μm restrictor. After an initial extraction a repeated extraction gave no further flufenoxuron recovery. Glass beads were found to be a good inert support for flufenoxuron and allowed efficient and fast extraction. Since the vapour pressure of pure methanol under ambient conditions is ca. 88 mmHg (1 mmHg = 133.322 Pa), only a very small amount of methanol condenses in the capillary when the system is operated without cooling. Because of restrictor heating methanol is not condensed, but swept out in gaseous state from the trapping capillary in a stream of carbon dioxide. For the cooling operation, a cryofocusing device was located immediately after the restrictor heater. At constant measured flow-rate of expanding CO_2 the total amount of collected condensed methanol during 15 min was determined for different temperatures of the cryofocusing device.

It can be seen from Fig. 2 that practically linear dependence of collected methanol volume on the cryofocusing temperature was obtained at temperature interval from −30°C to 25°C. The experimental work was split into two sections to

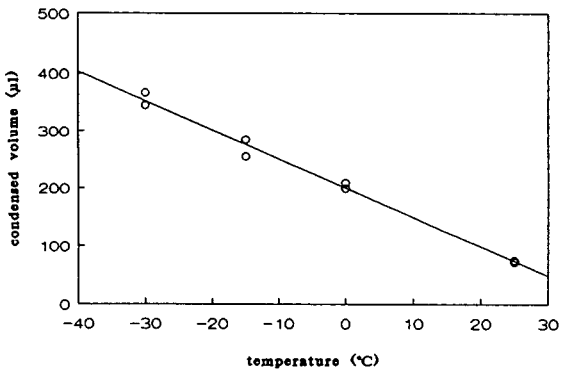

Fig. 2. Dependence of volume of condensed methanol on cryofocusing temperature for 10% methanol-modified CO_2. Pressure 40 MPa, restrictor 20 μm I.D., flow-rate of CO_2 100 ml min^{-1} at ambient conditions.

evaluate the effect of flow-rate of expanding carbon dioxide.

All experiments were performed at a cryofocusing temperature of −30°C to obtain approximately 300 μl of liquid phase for repeated analysis by liquid chromatography. The results are summarized in Tables 1 and 2. Flufenoxuron has a high solubility in methanol and therefore only a small amount of methanol is required to dissolve the flufenoxuron extracted. The flow-rates of CO_2 measured at ambient conditions were 90–110 ml min^{-1} for a restrictor of 20 μm I.D. and 170–190 ml min^{-1} for one of 25 μm I.D.

In both cases an average analyte recovery around 10% in methanol wash was obtained as a result of analyte precipitation on the part of capillary wall between the restrictor tip and the point of appearance of methanol condensation. The analyte recovery in the methanol collected with the 25-μm restrictor was lower than for a 20-μm restrictor, 75 and 83%, respectively. The value of total flufenoxuron recovery also reflects this fact.

Higher flow-rates produced larger amounts of condensed methanol by virtue of a larger amount of methanol being passed through the system but reduced recovery of analyte in the methanol fraction condensed. Lower R.S.D. values for total flufenoxuron recovery provide evidence of better reproducibility of the overall trapping process than of individual steps. A more rigorous investigation of the analyte recovery in the collected methanol versus the amount of methanol collected would be to extract an analyte that is less soluble in methanol than flufenoxuron. A more definite relationship between amount of extracted analyte in the collected modifier and the amount of collected modifier could be established.

4. Conclusions

A new approach to trapping into liquid solvent for off-line SFE with a modified extracting fluid was investigated. The flufenoxuron recovery from an idealised matrix was found to be quantitative and reproducible. Recoveries for the trapping device, when operated with cooling were 85.7% (R.S.D. 3.4%) for the 25-μm restrictor and 92.3% (R.S.D. 4.0%) for the 20-μm restrictor. The trapping efficiencies obtained with this device appear dependent on the flow-rate of expanding CO_2 through the trapping capillary: the higher the flow-rate the lower the analyte recovery. An analyte with a lower solubility in methanol than flufenoxuron could be used to verify the relationship between the amount of collected methanol and the trapping efficiency.

Acknowledgement

J.V. thanks the Commission of the European Community for a visiting fellowship at the University of Leeds.

References

[1] J. Vejrosta, A. Ansorgová, M. Mikešová and K.D. Bartle, *J. Chromatogr. A*, 659 (1994) 209–212.
[2] D.G. Breen, K.D. Bartle and A.A. Clifford, personal communication.

ELSEVIER

Journal of Chromatography A, 683 (1994) 411–412

JOURNAL OF CHROMATOGRAPHY A

Book review

Advances in Lipid Methodology —2, edited by W.W. Christie, Oily Press, Dundee, 1993, VI + 335 pp., price US$ 62.00, ISBN 0-9514171-3-4.

This book contains eight chapters of review topics each providing extensive coverage of recent developments in particular lipid analyses. The book serves well as a convenient, excellent reference for lipid methodology, containing over 1100 individual references. An appendix of the book comprises additional categorized sections of important literature citations for the years 1991 and 1992. As leaders in specialized fields, the authors present the critical reviews under the general formats of background introduction, analytical methods, tabular complications of experimental data, conclusions, and references. This volume in the series includes much of interest to diverse groups of lipid scientists.

The first chapter, entitled High resolution ^{13}C NMR spectroscopy of lipids, focuses on studies of (i) individual molecular species, (ii) mixtures and (iii) individual oil seeds and physical properties. The descriptions of qualitative and quantitative NMR techniques in structural analyses are thorough and sound. The spectral data for various lipids as compiled in 59 tables are well-organized. Chapter 2, entitled Preparation of ester derivatives of fatty acids for chromatographic analysis, deals with different derivatization methods for fatty acid analysis. Faced with numerous available methods, the review provides a very useful guideline for the choice of reagents. Chapter 3, entitled Size-exclusion chromatography (SEC) in the analysis of lipids, is concerned with (i) SEC of polymers, partial glycerides and oxidized compounds in organic media and (ii) SEC of lipoproteins and vesicles and micelles in aqueous media. This is a unique comprehensive documentation of the application of the SEC technique for the analysis of high-molecular-mass lipids of interest. Chapter 4, entitled Mercury adduct formation (MAF) in the analysis of lipids, describes in detail major applications of the MAF techniques in the lipid field. This chapter concisely illustrates the preparation of unsaturated fatty acid concentrates, analyses of oils, fatty acids and related compounds, and structural elucidation of unsaturated fatty acids. Chapters 5 and 8 are devoted to methodological efforts that have played a pivotal role in methods development for the clinical analysis of lipoproteins and acylcarnitines. Following general principles of capillary isotachophoresis (cITP) (Chapter 5), the focus turns to practical aspects of cITP analyses with detailed discussions of subclass resolution of lipoproteins in metabolic and diagnostic samples. The potential applicability of analytical cITP techniques for fast and reliable automated analyses of lipoproteins is also discussed. For acylcarnitine analyses (Chapter 8), the review embodies published chromatographic, NMR and mass spectrometric techniques and the chapter ends with the authors' authoritative comments on the various methods. Chapter 6, entitled Preparation of lipid extracts from tissues, covers specific subjects in the areas of sample pretreatment/storage, sam-

SSDI 0021-9673(94)00666-0

ple extraction, contaminant removal, artefacts of extraction procedures, practical extraction procedures and some difficult cases requiring special treatments. This chapter is rich in sample-processing materials that are a "must be read" by technicians, researchers and novices. Chapter 7, entitled Tandem mass spectrometry in the structural analysis of lipids, concentrates on the key elements of tandem MS, general concepts/principles and MS–MS instrumentation. This is followed by enlightening essays on applications of the techniques in the analysis of a broad spectrum of lipid structures in complex sample matrices. The chapter provides up-to-date coverage of published work on the powerful tandem MS techniques used in lipid structural analyses. Overall, this book would be a valuable resource for anyone engaging in lipid research and would be a valuable addition to clinical, university and industrial research libraries.

Peoria, IL, USA S.L. Abidi

Author Index

CALL FOR PAPERS

1995 International Symposium & Exhibit on
PREPARATIVE CHROMATOGRAPHY
June 11-14, 1995
Washington, DC, USA

Abstract Deadline -- NOVEMBER 8, 1994

Organized by Professor Georges Guiochon
University of Tennessee and Oak Ridge National Laboratory

LECTURE & POSTER PRESENTATIONS
WORKSHOPS
SEMINARS
ROUNDTABLE DISCUSSIONS
CASE STUDIES
INSTRUMENTATION EXHIBIT

Sponsored by the Washington Chromatography Discussion Group

For more information contact: Janet Cunningham, c/o Barr Enterprises
P.O. Box 279, Walkersville, Maryland 21793 USA
(tele. 301-898-3772, fax 301-898-5596)

PUBLICATION SCHEDULE FOR THE 1995 SUBSCRIPTION

Journal of Chromatography A and *Journal of Chromatography B: Biomedical Applications*

MONTH	O 1994	N 1994	D 1994	
Journal of Chromatography A	683/1 683/2 684/1	684/2 685/1 685/2 686/1	686/2 687/1 687/2 688/1 + 2	The publication schedule for further issues will be published later.
Bibliography Section				
Journal of Chromatography B: Biomedical Applications				

INFORMATION FOR AUTHORS

(Detailed *Instructions to Authors* were published in *J. Chromatogr. A*, Vol. 657, pp. 463–469. A free reprint can be obtained by application to the publisher, Elsevier Science B.V., P.O. Box 330, 1000 AH Amsterdam, Netherlands.)

Types of Contributions. The following types of papers are published: Regular research papers (full-length papers), Review articles, Short Communications and Discussions. Short Communications are usually descriptions of short investigations, or they can report minor technical improvements of previously published procedures; they reflect the same quality of research as full-length papers, but should preferably not exceed five printed pages. Discussions (one or two pages) should explain, amplify, correct or otherwise comment substantively upon an article recently published in the journal. For Review articles, see inside front cover under Submission of Papers.

Submission. Every paper must be accompanied by a letter from the senior author, stating that he/she is submitting the paper for publication in the *Journal of Chromatography A* or *B*.

Manuscripts. Manuscripts should be typed in **double spacing** on consecutively numbered pages of uniform size. The manuscript should be preceded by a sheet of manuscript paper carrying the title of the paper and the name and full postal address of the person to whom the proofs are to be sent. As a rule, papers should be divided into sections, headed by a caption (*e.g.*, Abstract, Introduction, Experimental, Results, Discussion, etc.). All illustrations, photographs, tables, etc., should be on separate sheets.

Abstract. All articles should have an abstract of 50–100 words which clearly and briefly indicates what is new, different and significant. No references should be given.

Introduction. Every paper must have a concise introduction mentioning what has been done before on the topic described, and stating clearly what is new in the paper now submitted.

Experimental conditions should preferably be given on a *separate* sheet, headed "Conditions". These conditions will, if appropriate, be printed in a block, directly following the heading "Experimental".

Illustrations. The figures should be submitted in a form suitable for reproduction, drawn in Indian ink on drawing or tracing paper. Each illustration should have a caption, all the *captions* being typed (with double spacing) together on a *separate sheet*. If structures are given in the text, the original drawings should be provided. Coloured illustrations are reproduced at the author's expense, the cost being determined by the number of pages and by the number of colours needed. The written permission of the author and publisher must be obtained for the use of any figure already published. Its source must be indicated in the legend.

References. References should be numbered in the order in which they are cited in the text, and listed in numerical sequence on a separate sheet at the end of the article. Please check a recent issue for the layout of the reference list. Abbreviations for the titles of journals should follow the system used by *Chemical Abstracts*. Articles not yet published should be given as "in press" (journal should be specified), "submitted for publication" (journal should be specified), "in preparation" or "personal communication".

Vols. 1–651 of the *Journal of Chromatography*; *Journal of Chromatography, Biomedical Applications* and *Journal of Chromatography, Symposium Volumes* should be cited as *J. Chromatogr.* From Vol. 652 on, *Journal of Chromatography A* (incl. Symposium Volumes) should be cited as *J. Chromatogr. A* and *Journal of Chromatography B: Biomedical Applications* as *J. Chromatogr. B.*

Dispatch. Before sending the manuscript to the Editor please check that the envelope contains four copies of the paper complete with references, captions and figures. One of the sets of figures must be the originals suitable for direct reproduction. Please also ensure that permission to publish has been obtained from your institute.

Proofs. One set of proofs will be sent to the author to be carefully checked for printer's errors. Corrections must be restricted to instances in which the proof is at variance with the manuscript.

Reprints. Fifty reprints will be supplied free of charge. Additional reprints can be ordered by the authors. An order form containing price quotations will be sent to the authors together with the proofs of their article.

Advertisements. The Editors of the journal accept no responsibility for the contents of the advertisements. Advertisement rates are available on request. Advertising orders and enquiries can be sent to the Advertising Manager, Elsevier Science B.V., Advertising Department, P.O. Box 211, 1000 AE Amsterdam, Netherlands; courier shipments to: Van de Sande Bakhuyzenstraat 4, 1061 AG Amsterdam, Netherlands; Tel. (+31-20) 515 3220/515 3222, Telefax (+31-20) 6833 041, Telex 16479 els vi nl. *UK*: T.G. Scott & Son Ltd., Tim Blake, Portland House, 21 Narborough Road, Cosby, Leics. LE9 5TA, UK; Tel. (+44-533) 753 333, Telefax (+44-533) 750 522. *USA and Canada*: Weston Media Associates, Daniel S. Lipner, P.O. Box 1110, Greens Farms, CT 06436-1110, USA; Tel. (+1-203) 261 2500, Telefax (+1-203) 261 0101.